

CHARM LESS INCLUSIVE B DECAYS AND THE
EXTRACTION OF $V(UB)$

A Dissertation

Presented to the Faculty of the Graduate School

of Cornell University

in Partial Fulfillment of the Requirements for the Degree of

Doctor of Philosophy

by

Gil Paz

August 2006

c 2006 GilPaz

ALL RIGHTS RESERVED

CHARM LESS INCLUSIVE B DECAYS AND THE EXTRACTION OF V_{ub}

Gil Paz, Ph.D.

Cornell University 2006

This work discusses charm less inclusive B decays and its application to the extraction of $|V_{ub}|$. Starting from first principles we relate the differential decay rate to the hadronic tensor in terms of optimal choice of kinematical variables. We review the traditional methods of calculating the hadronic tensor, expansion in s and HQET, and discuss their shortcomings. In the kinematical region relevant for experiment ("shape function" region), the hadronic tensor can be factorized, at each order in $1/m_b$, as a product of calculable hard functions and a convolution of calculable jet functions with non perturbative shape functions.

Using SCET, we calculate the leading order hard and jet function to first order in s . Large logarithms are resummed in RG improved perturbation theory. Local OPE is used to relate moments of the renormalized shape function to HQET parameters, defined in the "shape function scheme". Beyond leading order in $1/m_b$, several subleading shape functions arise. We derive them at tree level, where they can be expressed as forward matrix elements of bi-local light-cone operators.

Based on these theoretical calculations we present two applications. In the first, we present the "state-of-the-art" expressions for the triple differential $B \rightarrow X_u l$ decay rate and the $B \rightarrow X_s \gamma$ photon spectrum. These expressions include all known contributions and smoothly interpolate between the "shape-function" and "OPE region". Based on these an event generator can be constructed, from which the theoretical prediction for any experimental cut can be extracted. In the second, a weight function is constructed that relates the P_+ spectrum in $B \rightarrow X_u l$ to the

normalized $B \rightarrow X_s$ photon spectrum. This weight function is independent of the leading order shape function. At leading power the weight function contains two loop corrections at the scale $\mu = m_b$. Power corrections from phase space are included exactly, while the remaining subleading contributions are included at first order in $1/m_b$.

B I O G R A P H I C A L S K E T C H

G ilPaz was born in H aifa, Israel. In 1999, he completed his undergraduate study at the Technion – Israel Institute of Technology, receiving a B A . in Physics and a B A . in M athem atics both sum m a cum laude. In 2001 he received a M .Sc. in Physics, also from the Technion, under the supervision of P rofessor M ichael G ronau. The sam e year he cam e to C ornell university. H e then completed a M .Sc. in 2004 and a P h D . in 2006 under the supervision of P rofessor M atthias N eubert.

ACKNOWLEDGEMENTS

First, I would like to thank my collaborators: Stefan Bosch, Björn Lange and Matthias Neubert. The work presented here was done in collaboration with them over the last few years.

I would like to thank my advisor Matthias Neubert for his help, encouragement and for teaching me to always try to improve the work that we do.

I would like to thank the members of my special committee Csaba Csaki and Lawrence Gibbons for their help and advice. Special thanks to Maxim Perelstein for being a proxy on my B exam and for his comments on the dissertation.

I would like to thank the Institute for Advanced Study, Princeton, NJ, and the Institute of Nuclear Theory at the University of Washington, where part of this research was performed.

This research was supported by the National Science Foundation under Grant PHY-0098631 and Grant PHY-0355005.

TABLE OF CONTENTS

1	Introduction	1
1.1	Preface	1
1.2	Chapter outline	2
1.3	Kinematics made easy	2
1.4	From the optical theorem to the hadronic tensor	6
1.5	Free quark approximation – tree level and α_s corrections	11
1.6	Effective field theories I: HQET	14
1.7	Effective field theories II: SCET	20
2	Perturbative Corrections	24
2.1	Chapter outline	24
2.2	Factorization theorem for inclusive decay rates	24
2.3	Matching calculations	27
2.3.1	Hard functions	27
2.3.2	Jet function	30
2.3.3	Renormalized shape function	31
2.4	Renormalization-group resummation	33
2.4.1	Evolution of the hard functions	34
2.4.2	Evolution of the shape function	35
2.5	Properties of the shape function	38
2.5.1	Shape-function moments in the pole scheme	38
2.5.2	Shape-function moments in a physical scheme	41
2.5.3	Moments of the scheme-independent function $\hat{S}(\not{n}; \mu)$	43
2.5.4	Asymptotic behavior of the shape function	44
2.6	Conclusions	45
3	Non-Perturbative Corrections	47
3.1	Introduction	47
3.2	Short-distance expansion of the hadronic tensor	47
3.3	Definition of subleading shape functions	53
3.4	Moment relations and comparison with the literature	57
3.5	Contributions from four-quark operators	57
3.6	Applications	60
3.7	Conclusions	61
4	Applications: Event Generator	63
4.1	Introduction	63
4.2	Inclusive radiative decays	65
4.2.1	Leading-power factorization formula	66
4.2.2	Kinematical power corrections	68
4.2.3	Subleading shape-function contributions	69
4.2.4	Residual hadronic power corrections	71

4.3	Inclusive semileptonic decays	73
4.3.1	Leading-power factorization formula	75
4.3.2	Kinematical power corrections	75
4.3.3	Subleading shape-function contributions	78
4.3.4	Residual hadronic power corrections	78
4.3.5	Weak annihilation contributions	79
4.4	Shape-function parameterizations	81
4.4.1	Models for the leading shape function	81
4.4.2	Models for subleading shape functions	86
4.4.3	Illustrative studies	88
4.5	Predictions and error estimates for partial rates	88
4.5.1	Total decay rate	92
4.5.2	Cut on charged-lepton energy	93
4.5.3	Cut on hadronic P_+	95
4.5.4	Cut on hadronic invariant mass and q^2	95
4.5.5	Cut on s_H^{max} and E_1	98
4.5.6	Eliminating weak annihilation contributions	99
4.5.7	Dependence on m_b and shape-function sensitivity	101
4.6	Conclusions	102
5	Applications: Weight Function	104
5.1	Introduction	104
5.2	Calculation of the weight function	107
5.2.1	Leading power	107
5.2.2	Subleading power	110
5.3	Results	112
5.3.1	Leading power	113
5.3.2	Subleading power	114
5.3.3	Normalization	116
5.4	Numerical results	117
5.4.1	Studies of the perturbative expansion	118
5.4.2	Comments on the normalization of the photon spectrum	120
5.4.3	Comments on $\mathcal{O}(s^2)$ terms and scale separation	122
5.4.4	Subleading corrections from hadronic structures	123
5.5	Conclusions	125
6	Conclusions	127
A	The hadronic tensor	130
B	Perturbative Expressions	132
B.1	Anomalous dimensions	132
B.2	Evolution factor	133

C Partially integrated decay rates	134
Bibliography	136

LIST OF TABLES

1.1	Number of kinematic variables for inclusive B decays. Using the constraints on the right column we can eliminate some of the variables on the left column.	3
1.2	Different modes in SCET-I. We define $\mu = Q_{CD} = m_b$ and write the light cone components of vector a as $(n \cdot a; n \cdot \bar{a})a$	20
4.1	Partial decay rate $\Gamma_u(E_0)$ for a cut on charged-lepton energy $E_1 > E_0$ in the B-meson rest frame, given in units of fb ps^{-1} . Predictions are based on the shape-function parameter values $m_b = 4.61 \text{ GeV}$, $\mu^2 = 0.2 \text{ GeV}^2$ (top) and $m_b = 4.55 \text{ GeV}$, $\mu^2 = 0.3 \text{ GeV}^2$ (bottom).	93
4.2	Same as Table 4.1, but for the partial decay rate $\Gamma_u^{(\prime)}(E_0)$ for a cut on lepton energy $E_1 > E_0$ in the (4S) rest frame.	94
4.3	Partial decay rate $\Gamma_u(P_+; E_0)$ for a cut on the hadronic variable P_+ and lepton energy $E_1 > E_0$, given in units of fb ps^{-1} . Predictions are based on the shape-function parameter values $m_b = 4.61 \text{ GeV}$, $\mu^2 = 0.2 \text{ GeV}^2$ (top) and $m_b = 4.55 \text{ GeV}$, $\mu^2 = 0.3 \text{ GeV}^2$ (bottom).	96
4.4	Partial decay rate $\Gamma_u(M_X; q_0^2)$ for combined cuts $M_X > M_0$ on hadronic invariant mass, $q^2 > q_0^2$ on leptonic invariant mass, given in units of fb ps^{-1} . Predictions are based on the shape-function parameter values $m_b = 4.61 \text{ GeV}$, $\mu^2 = 0.2 \text{ GeV}^2$ (top) and $m_b = 4.55 \text{ GeV}$, $\mu^2 = 0.3 \text{ GeV}^2$ (bottom).	97
4.5	Partial decay rate $\Gamma_u(M_X; q_0^2; E_0)$ for combined cuts $M_X > M_0$ on hadronic invariant mass, $q^2 > q_0^2$ on leptonic invariant mass, and $E_1 > E_0$ on charged-lepton energy, given in units of fb ps^{-1} . Predictions are based on the shape-function parameter values $m_b = 4.61 \text{ GeV}$, $\mu^2 = 0.2 \text{ GeV}^2$ (top) and $m_b = 4.55 \text{ GeV}$, $\mu^2 = 0.3 \text{ GeV}^2$ (bottom).	97
4.6	Partial decay rate $\Gamma_u(s_0; E_0)$ for combined cuts $s_H^{\text{max}} > s_0$ and $E_1 > E_0$, given in units of fb ps^{-1} . Predictions are based on the shape-function parameter values $m_b = 4.61 \text{ GeV}$, $\mu^2 = 0.2 \text{ GeV}^2$ (top) and $m_b = 4.55 \text{ GeV}$, $\mu^2 = 0.3 \text{ GeV}^2$ (bottom).	99
4.7	Examples of partial decay rates with a cut on $q^2 > (M_B - M_D)^2$ imposed to eliminate the weak annihilation contribution. We consider an additional cut on the hadronic variable P_+ (top), or on the hadronic invariant mass $M_X > M_0$ (bottom). As before, decay rates are given in units of fb ps^{-1} . Predictions are based on the shape-function parameters $m_b = 4.61 \text{ GeV}$ and $\mu^2 = 0.2 \text{ GeV}^2$	100

4.8	Values of the exponent $a(m_b)$ for different kinematical cuts. The parameter $\tau^2 = 0.2 \text{ GeV}^2$ is kept fixed. Also quoted is the sensitivity of the partial decay rates to the functional form of the shape functions. See text for explanation.	101
-----	--	-----

LIST OF FIGURES

- 1.1 The $(P_+; P_-)$ phase space for $B \rightarrow X_u l$. The charm free region is the dark grey region below the black hyperbola, which correspond to $M_X^2 = P_+ P_- = M_D^2$. The solid blue line is $q^2 = (M_B - P_+)(M_B + P_-) = (M_B - M_D)^2$. The red dashed line is $P_+ = M_D^2/M_B$ 6
- 2.1 One-loop diagrams contributing to the current correlator in SCET. The effective current operators are denoted by crossed circles, and hard-collinear propagators are drawn as dashed lines. Mirror graphs obtained by exchanging the two currents are not shown. 29
- 2.2 Radiative corrections to the shape function. The bilocal HQET operator is denoted by the black square. A mirror copy of the first graph is not shown. 31
- 3.1 Representative examples of time-ordered products contributing to the current correlator T_{ij} in SCET. Double lines show heavy-quark fields, dashed ones hard-collinear fields, and wavy lines denote the external currents. Lagrangian insertions and higher-order effective current operators are exemplified by soft gluons. 51
- 4.1 The hadronic phase space in P_+ and P_- . The light gray region contains background from $B \rightarrow X_c l$ decays, while the dark gray region is only populated by $B \rightarrow X_u l$ events. The line separating the two regions is the contour where $M_X^2 = P_+ P_- = M_D^2$. Each point represents a $B \rightarrow X_u l$ event in a Monte-Carlo simulation using the results of this chapter. While the shape-function region of large P_- and small P_+ is highly populated, there is not a single event with P_+ larger than 3 GeV out of the 1300 events generated. 74
- 4.2 Top: Different functional forms for the leading shape function. We show $F^{(exp)}(\hat{s}; \hat{t}; 2)$ (solid), $F^{(gauss)}(\hat{s}; \hat{t}; 2)$ (dotted), and $F^{(hyp)}(\hat{s}; \hat{t}; 2)$ (dash-dotted) as functions of the ratio $\hat{t} = \hat{s}$. Bottom: The same functions with the parameters \hat{s} and \hat{t} tuned such that $m_b(\hat{s}; \hat{t}) = 4.61 \text{ GeV}$ and $\hat{t}^2(\hat{s}; \hat{t}) = 0.2 \text{ GeV}^2$. See text for explanation. 84
- 4.3 Nine models for the subleading shape function $\hat{u}(\hat{t})$ obtained by adding or subtracting one of the four functions $h_n(\hat{t})$ to the default model in (4.47), shown as a thick line. See text for explanation. 87

- 4.4 Top: Theoretical prediction for the double differential decay rate. The light area represents a large decay rate. Black regions denote areas where the decay rate is close to zero. The dotted line is given by $P_+ P_- = M_D^2$, which means that charm background is located in the upper wedge. See text for further explanation. Bottom: The P_+ spectrum extended to large values of P_+ . The thin solid line denotes the leading-power prediction, the dashed line depicts first-order power corrections, the dash-dotted line shows second-order power corrections, and the thick solid line is their sum 89
- 5.1 Residual scale dependence of $\Gamma_u(\mu)$ for $\mu = 0.65 \text{ GeV}$. The dashed line depicts the variation of μ_h about its default value $\mu_b = \sqrt{2}$, the dash-dotted line the variation of μ_i about 1.5 GeV , and the dotted line the variation of μ also about 1.5 GeV . The highlighted area shows the combined perturbative uncertainty. 118
- 5.2 Convergence of the perturbative series and residual scale dependence. Left: RG-improved results at LO (dotted), NLO (dashed), and NNLO (solid) as a function of the scales μ_i, μ_h, μ , which are varied simultaneously about their default values. Right: Fixed-order results at tree-level (dotted) and one-loop order (dashed). . . 119
- 5.3 Perturbative uncertainties on $\Gamma_u(\mu)$ encountered when using the weight function $W(\mu; P_+)$ (dark gray) or $\tilde{W}(\mu; P_+)$ (light gray). In the latter case, the normalization of the photon spectrum is chosen such that the two predictions agree at $\mu = 0.65 \text{ GeV}$ for central values of the matching scales. 121
- 5.4 Estimates for the hadronic uncertainty $\Gamma_{\text{hadr}}(\mu)$ obtained from a scan over models for the subleading shape functions. The dashed lines correspond to the individual results for the four $h_i(\mu)$ functions suggested in [95]. The thick solid line, which covers one of the dashed lines, shows the maximum effect. 124

Chapter 1

Introduction

1.1 Preface

The standard model is a theory that describes our knowledge of three of the four fundamental forces in nature: the strong, the electromagnetic and the weak. The strong and the weak forces especially pose interesting challenges to theoretical physics.

The strong interaction can be described at high energies by the QCD Lagrangian, where the quarks couple to each other via an exchange of gluons. The coupling strength is universal, i.e. independent of the flavor of the quarks. At energies above roughly 1 GeV we can use perturbation theory to calculate the effects of the strong force. At lower energies the perturbative description, based on the use of the interaction Lagrangian, breaks down. As a result, at low energies one has to use either non perturbative methods such as lattice calculations and chiral perturbation theory, or extract information from experiment. The separation of scales and the perturbative from the non perturbative physics will be a major theme in this work.

The weak interaction is one of the richest parts of the standard model. As opposed to the strong interaction, the weak interaction is not universal and is different for different flavors. More specifically the strength of the interaction between quarks of different flavors is described by a unitary matrix known as the Cabibbo-Kobayashi-Maskawa (CKM) matrix. The CKM matrix elements are fundamental parameters of the standard model and therefore it is important to measure them as accurately as possible. Indeed, Measuring the CKM matrix elements has been one of the main goals of research in particle physics, both for theory and experiment.

This work aims at precision measurements of V_{ub} , one of the smallest CKM matrix elements. Currently the highest precision on $|V_{ub}|$ can be achieved through inclusive measurement of charmless decays of B mesons. By charmless we mean both semileptonic ($B \rightarrow X_u l$) and radiative ($B \rightarrow X_s \gamma$) decays. The former is used to actually measure $|V_{ub}|$ while the latter is used to extract, directly or indirectly, the main non perturbative object which is the shape function. Of course, better understanding of radiative decays is important by itself, as it has important implications for constraining physics beyond the standard model.

The outline of this work is as follows. We begin by an introduction, which takes the reader from "first principles" to the starting point of chapters 2 and 3. These two chapters are more theoretical, where in 2 and 3 the perturbative and non perturbative calculations are presented, respectively. The last two chapters are concerned with applying these calculations. Chapter 4 gives the necessary ingredients for a construction of an event generator, which allows experimenters to calculate any semileptonic spectrum they would like to measure. In chapter 5 a weight function is constructed, that directly relates the P_+ spectrum in $B \rightarrow X_u l$

to the photon spectrum in $B \rightarrow X_s \gamma$. We present our conclusions in chapter 6.

1.2 Chapter outline

In this chapter we begin our study of inclusive charmless B decays. We start with the description of the kinematics of these decays and discuss the optimal choice of kinematical variables. We then turn to the dynamics. The basic quantity we are trying to calculate is the hadronic tensor, which cannot be calculated exactly. We review the "traditional" approximation methods, namely, expansion in α_s and Heavy Quark Effective Theory (HQET) and discuss their shortcomings. In order to overcome these problems we introduce the appropriate effective field theory suitable for inclusive charmless B decays, the Soft Collinear Effective Theory (SCET). This effective field theory will be used in the following chapters to analyze both the perturbative (chapter 2) and non perturbative (chapter 3) corrections to the hadronic tensor. This introduction is meant to be pedagogical, so we present most of the derivations explicitly.

1.3 Kinematics made easy

In this work we focus on $B \rightarrow X_u \ell$ decays, but also discuss $B \rightarrow X_s \ell$ decays, both by itself and in relation to $B \rightarrow X_u \ell$. These decays are inclusive in a sense that one of the final states is something that contains a specific quark (u or s) but is otherwise unrestricted and can even be a group of particles.

We begin analyzing these decays by looking at the simple question, "How many kinematical variables are needed to describe an inclusive event?". We are looking at a decay of a B meson into n particles, where $n-1$ of them have known mass. The "particle" X has unspecified invariant mass. In general for a decay into n particles there are $3n-4$ kinematical variables, but not all of them are determined from the dynamics. Since we do not have information about the spin of the hadronic state X or the spin/polarization of the other decay products, the only four vectors we have at our disposal are P_B , the four momentum of the B meson, $p_1 \dots p_X$ the four momentum of X , and $p_2; \dots; p_n$. Lorentz invariance implies then that the possible variables are the $(n+1)(n+2)/2$ scalar products of these $n+1$ vectors. Since the masses of all the particles apart from p_1 are known, we have n constraints of the form $p_i^2 = m_i^2$; ($i = 2; \dots; n$). Conservation of momentum would allow us to eliminate all the pairs that contain P_B (since $P_B = \sum_{i=1}^n p_i$), i.e. eliminating $n+1$ variables. That leaves us with $n(n-1)/2$ independent variables. The rest of the variables are undetermined from the dynamics and can be integrated over. This argument holds for $n \geq 3$, since at 4 dimensions at most 4 vectors (corresponding to $n = 3$) can be linearly independent. For $n > 3$ the argument needs to be modified.

The decay mode $B \rightarrow X_s \gamma$ has $n = 2$ and therefore only one relevant variable. This variable is usually taken to be E_γ , the energy of the photon. As we shall see,

a related variable, $P_+ = M_B^2 - 2E_l$ will turn out be useful. For $B \rightarrow X_u l$ we have $n = 3$ and three relevant variables (see table 1.1). There are various choices in the literature for these variables, and in order to understand them we have to say a few words about the dynamics of these decays.

Table 1.1: Number of kinematic variables for inclusive B decays. Using the constraints on the right column we can eliminate some of the variables on the left column.

B ! X _s			
Scalar Products			Constraints
P _B ²	P _B P _X	P _B P	P _B = P + P
	P _X ²	P _X P	(P _X + P) ² = M _B ²
		P ²	P ² = 0

B ! X _{u l}			
Scalar Products			Constraints
P _B ²	P _B P _X	P _B P ₁	P _B = P + P ₁ + P
	P _X ²	P _X P ₁	(P _X + P ₁ + P) ² = M _B ² , P ₁ ² = 0
		P ₁ ²	
		P ₁ P	
		P ²	P ² = 0

First we need to distinguish between the hadronic level, which looks at the decay as a decay of hadrons, and the partonic level, which looks at the decay as a decay of quarks. At the hadronic level we have a B meson carrying momentum $P_B = M_B v$ decaying into a leptonic pair (the lepton and the anti-neutrino) carrying momentum total q , and a hadronic jet carrying momentum P_X . Conservation of momentum implies $M_B v = q + P_X$. At the partonic level we look at this decay as a decay of a b quark, carrying momentum $m_b v$, into a u quark, carrying momentum p (at tree level), and a virtual W carrying momentum q . The W in turn decays into a lepton l and an anti-neutrino $\bar{\nu}_l$. (More accurately we write the momentum of the b quark as $m_b v + k$ where k is $O(\Lambda_{QCD})$, and expand in powers of k). Conservation of momentum implies $m_b v = q + p$. If we define $M_B = m_b$ we find that $P_X = p + q$. Beyond tree level p would be the momentum of the jet of light partons created in the decay. We will elaborate on the exact definition of in chapter 2.

There are generically two common choices of variables:

Leptonic: The energy of the lepton E_l , the energy of the neutrino $E_{\bar{\nu}}$ and the invariant mass of virtual W boson q^2 , which is also the invariant mass of the lepton pair. This choice focuses on the leptons created in the decay and was used for example in [1]

Partonic: the energy of the lepton E_l , the energy of the partonic jet $v \cdot p$, and the invariant mass of the partonic jet p^2 . This choice focuses on the partons created in the decay and was used for example in [2].

We will use a different choice of variables, which in some sense is the optimal one. We start by noting the fact that any measurement of $B \rightarrow X_u l$ suffers from a large background from the decay $B \rightarrow X_c l$. The reason for the large background is that $|V_{cb}| \gg |V_{ub}|$, meaning that the b quark "likes" to decay to a c quark much more than to a u quark. In order to eliminate the background we have to look at regions of phase space where particles containing charm cannot be produced. For example we can only look at events for which $P_X^2 < M_D^2$. This fact implies that the "typical" X_u state will have large energy of order m_b , since it originates from a decay of a heavy quark and intermediate invariant mass, because of the experimental cut. Since $M_D \approx m_b + Q_{CD}$ we can write $P_X^2 \approx m_b + Q_{CD}$. This implies that some of the components of P_X are larger than others. We would like the choice of our variables to reflect that. In other words we look for two variables, one of which scales like m_b and one of which scales like Q_{CD} . A pair of variables which satisfy this condition is:

$$P_- = E_X + |\vec{P}_X|; \quad P_+ = E_X - |\vec{P}_X|; \quad (1.1)$$

where E_X and P_X are the energy and momentum of the hadronic jet, respectively. Note that $P_+ P_- = P^2$; $P_+ + P_- = 2E_X$ and $P_+ - P_- = 2|\vec{P}_X|$. The scaling of these variables will therefore be $P_- \sim m_b$ and $P_+ \sim Q_{CD}$. In order to complete our choice we should add another variable. Specifying P_+ and P_- would determine the energy and the invariant mass of the lepton pair, but not the individual energies of the lepton and the neutrino. We therefore have to add another variable that would distinguish between the two. We will choose:

$$P_1 = M_B - 2E_1; \quad (1.2)$$

where E_1 is the energy of the lepton. These three variables allow us to specify any $B \rightarrow X_u l$ event.

Having chosen the variables, the next task is to determine the phase space in terms of P_+ , P_1 , and P_- . In the rest frame of the B meson, conservation of energy and momentum gives us the following equations (the notation is self explanatory):

$$E_1 + E_\nu + E_X = M_B \quad (1.3)$$

$$\vec{P}_1 + \vec{P}_\nu + \vec{P}_X = 0; \quad (1.4)$$

We take the leptons to be massless, implying $E_1 = |\vec{P}_1|$ and $E_\nu = |\vec{P}_\nu|$. The limits of phase space are determined by the extremal values of the angles between the momenta. Because of conservation of momentum (1.4) we have only two independent angles.

Let θ be the angle between \vec{P}_1 and \vec{P}_X . Equation (1.4) then implies $|\vec{P}_X|^2 = E_1^2 + E_\nu^2 + 2E_1 E_\nu \cos \theta$. Since $-1 \leq \cos \theta \leq 1$, we have $(E_1 - E_\nu)^2 \leq |\vec{P}_X|^2 \leq (E_1 + E_\nu)^2$. Using $P_+ = P_- + 2E_X$, the upper limit gives us $P_- \leq M_B$, and the lower limit $P_+ \geq P_1 - P_-$.

Let θ be the angle between \vec{P}_1 and \vec{P}_X . Equation (1.4) then implies $E^2 = (M_B - E_1 - E_X)^2 = E_1^2 + \vec{P}_X^2 + 2E_1\vec{P}_X \cos \theta$. Since $-1 \leq \cos \theta \leq 1$, the upper limit gives $(M_B - P_+)(P_1 - P) = 0$, and the lower limit $(M_B - P)(P_1 - P_+) = 0$.

We have also an additional constraint from the QCD spectrum. The lightest state containing a u quark is the pion, so we must have $M^2 - P_X^2 = P_+ P_-$. (Without this constraint the lower limit of P_+ would be 0). Combining all of these constraints we finally have:

$$\frac{M^2}{P} - P_+ - P_1 - P = M_B : \quad (1.5)$$

One of the benefits of this choice of variables (apart from the easy derivation) is that phase space has an extremely simple form, probably the simplest form possible (compare for example the phase space limits in [2]). This has practical implications: since we ultimately integrate over phase space, some of the integrations can be done analytically. We note that a similar choice of variables would be useful also for $B \rightarrow X_c \gamma$.

What are the phase space limits for $B \rightarrow X_s \gamma$? Conservation of momentum and energy imply that $M_B - E_X = E_1$ and $E_1 = \sqrt{\vec{P}_X^2}$ or $P_- = M_B$ and $P_+ = M_B - 2E_1$. The limit of the phase space for P_+ are determined from $E_1 = 0$, and the QCD spectrum constraint $M_K^2 - P_X^2 = P_+ P_- = M_B P_+$, where $K(892)$ is the lightest strange meson that can be produced in this decay. Altogether we have:

$$\frac{M_K^2}{M_B} - P_+ = M_B \quad (1.6)$$

Notice the similarities between equation (1.5) and (1.6), especially if we take the heavy quark limit, which sets the lower limit of P_+ to be 0. In the following we will explore these similarities extensively.

Having discussed the kinematics let us say a few words on experimental cuts and the regions of phase space they probe. For measurement of the photon spectrum $B \rightarrow X_s \gamma$, experiments must impose a cut on the photon energy of about 1.8 GeV (measured in the rest frame of the B meson) [3, 4, 5]. This means that the typical values of $P_+ = M_B - 2E_1$ are of order Λ_{QCD} .

For $B \rightarrow X_u \gamma$, as we mentioned earlier, experimental cuts are imposed to eliminate the charm background (figure 1.1). Some of the cuts are:

Cut on the charged lepton energy E_1 . If $E_1 = (M_B^2 - M_D^2)/2M_B = 2.31$ GeV, the final hadronic state will have invariant mass smaller than M_D . For this cut $P_1 = 0.66$ GeV, which implies that P_+ is of order Λ_{QCD} .

Cut on the hadronic invariant mass M_X^2 . To eliminate the charm background we need $M_X^2 < M_D^2$. The cut $M_X^2 = M_D^2$ is depicted as a solid black hyperbola in figure 1.1.

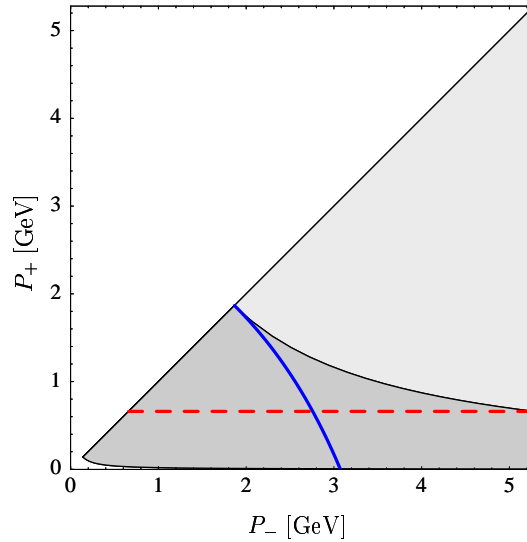


Figure 1.1: The (P_+, P_-) phase space for $B \rightarrow X_u l$. The charm free region is the dark grey region below the black hyperbola, which correspond to $M_X^2 = P_+ P_- = M_D^2$. The solid blue line is $q^2 = (M_B - P_+)(M_B - P_-) = (M_B - M_D)^2$. The red dashed line is $P_+ = M_D^2/M_B$.

Cut on the leptonic invariant mass q^2 . Any cut of the form $q^2 = (M_B - M_D)^2$ would not contain charm events. The cut $q^2 = (M_B - P_+)(M_B - P_-) = (M_B - M_D)^2$ is depicted as a solid blue line in figure 1.1

Cut on P_- will be discussed in chapter 2. The cut $P_+ = M_D^2/M_B$ is depicted as a red dashed line in figure 1.1

1.4 From the optical theorem to the hadronic tensor

The basis for the calculation of an inclusive rate is the optical theorem, which relates the decay rate to the imaginary part of the forward scattering amplitude. In terms of the \hat{T} matrix [6]

$$\text{hf} \hat{T} \text{fi} = (2\pi)^4 (P_i - P_f) M(i \rightarrow f); \quad (1.7)$$

the optical theorem states that

$$2 \text{Im} M(i \rightarrow i) = \sum_f \int \frac{d^3 P_f}{2E_f (2\pi)^3} M(i \rightarrow f)^\dagger (2\pi)^4 (P_i - P_f); \quad (1.8)$$

Using the optical theorem we obtain the following expression for the total rate

$$\begin{aligned}
&= \frac{1}{2M_B} \sum_f \int \frac{d^3 P_f}{2E_f (2\pi)^3} \text{Im} \langle i | T | f \rangle^2 (2\pi)^4 \delta^4(P_i - P_f) \\
&= \frac{1}{M_B} \text{Im} M \langle i | i \rangle
\end{aligned} \tag{1.9}$$

This formula holds both for $B \rightarrow X_u l$ and $B \rightarrow X_s$, but M is different in each case.

In order to proceed we need to find the matrix element of the \hat{T} matrix, which is determined by the Hamiltonian. The relevant general Hamiltonian contains both weak interactions and strong interactions (unless otherwise noted, we neglect contributions from electromagnetic interactions). For the weak interactions we can use perturbation theory. At the lowest order in the weak interaction coupling g_w (or alternatively G_F) we have for $B \rightarrow X_u l$ decays:

$$H_W = \frac{G_F}{2} V_{ub} \bar{u} (1 - \gamma_5) b + \text{h.c.} \tag{1.10}$$

This Hamiltonian can be thought of as an effective Hamiltonian, obtained (at tree level) after integrating out the heavy W bosons [7]. For $B \rightarrow X_s$ we have (see [7] for derivation)

$$H_W = \frac{G_F}{2} C_7^e V_{tb} V_{ts}^* \bar{b} \gamma_5 s + \text{h.c.} \tag{1.11}$$

There are other contributions from the weak Hamiltonian to $B \rightarrow X_s$, but their contribution to the rate is suppressed by g_s^2 and we will ignore them.

Using $\hat{S} = T e^{-i \int d^4 x H}$ (T is the time ordering symbol) and $\hat{S} = 1 + i\hat{T}$, the non vanishing lowest-order contribution to the \hat{T} matrix element is given by:

$$\langle B | \hat{T} | B \rangle = i \int \frac{d^4 x}{(2\pi)^4} \int d^4 x_1 d^4 x_2 T \langle B | H_W(x_1) H_W(x_2) | B \rangle \tag{1.12}$$

If we write $H_W = O + O^\gamma$, the only non vanishing contribution to the matrix element would come from $T \langle O^\gamma(0) O(x) \rangle$. Using the delta function in equation (1.7) we can eliminate one of the x_i integrals to obtain the result:

$$M = i \int d^4 x \langle B | T \langle O^\gamma(0) O(x) \rangle | B \rangle \tag{1.13}$$

This can be simplified further, by noting that up to a constant O can be written as a product of two "currents":

$$O = C \bar{q} b J_{NH} = C J_{\bar{q}H} \tag{1.14}$$

For $B \rightarrow X_u l$ transitions $J = \bar{l} (1 - \gamma_5) b$ and $J_{NH} = \bar{l} (1 - \gamma_5) l$, and for $B \rightarrow X_s$ we have $J = \bar{s} (1 + \gamma_5) b$ and $J_{NH} = 2 \bar{q} q$. In both cases the fields

in J_{NH} do not have any strong interactions, which would allow us to factorize M to a product of hadronic and non hadronic tensors. We insert a complete set of states in the form of

$$\sum_X \langle X | h_X | j \rangle_{NH} \langle j | h_{NH} | j \rangle_{NH} \frac{d^3 P_{NH}}{2E_{NH} (2\pi)^3} : \quad (1.15)$$

(The notation is such that the sum over the hadronic states includes the integration over the hadronic momenta) Thus we get:

$$\begin{aligned} M &= i \int d^4 x \langle j | \\ &\quad \left(\sum_{X_q, NH} \langle X | h_X | j \rangle_{NH} \langle j | h_{NH} | j \rangle_{NH} \frac{d^3 P_{NH}}{2E_{NH} (2\pi)^3} \right. \\ &\quad \left. + \sum_{X_{bbq}, NH} \langle X | h_X | j \rangle_{NH} \langle j | h_{NH} | j \rangle_{NH} \frac{d^3 P_{NH}}{2E_{NH} (2\pi)^3} \right) \\ &\quad \langle h_B | j^Y(0) | X_q \rangle \langle X_q | h_{NH} | j^Y(0) | j \rangle_{NH} \langle j | h_X | j(x) \rangle \langle j | h_{NH} | j_{NH}(x) \rangle \langle j | \\ &\quad \langle h_B | j(x) | X_{bbq} \rangle \langle X_{bbq} | h_{NH} | j_{NH}(x) \rangle \langle j | h_X | j^Y(0) \rangle \langle j | h_{NH} | j_{NH}^Y(0) \rangle \langle j | \end{aligned} \quad (1.16)$$

where X_q (X_{bbq}) is a complete set of hadronic states containing a q quark (two b quarks and a q). NH is a non hadronic state, i.e., a photon for $B \rightarrow X_s$ and a lepton pair for $B \rightarrow X_{ul}$. The second term in equation (1.16) would not contribute to B decays, since after taking the imaginary part one gets a factor of $\epsilon^4 (P_B \cdot P_{X_{bbq}} \cdot q)$ (see appendix A). For the first term we distinguish between $B \rightarrow X_s$ and $B \rightarrow X_{ul}$. For $B \rightarrow X_s$ we have:

$$\begin{aligned} \sum_{NH} \langle h_B | j_{NH}^Y(0) | j \rangle_{NH} \langle j | h_{NH} | j_{NH}(x) \rangle &= \sum_X \langle h_B | j^Y_A(0) | j(q) \rangle \langle j(q) | h^Y_A(x) | j \rangle \\ &= 4q \bar{q} g e^{iqx}; \end{aligned} \quad (1.17)$$

where q is the photon momentum. For $B \rightarrow X_{ul}$ we have:

$$\begin{aligned} \sum_{NH} \langle h_B | j_{NH}^Y(0) | j \rangle_{NH} \langle j | h_{NH} | j_{NH}(x) \rangle &= \\ \sum_{X_{NH}} \langle h_B | j_{\mu_1}(1/5) u_{\mu_1}(p^1) l(p^1) i h_{\mu_1}(p^1) l(p^1) j_{\mu_1}(1/5) v_{\mu_1} \rangle & \\ \text{spins} & \\ 8 P^1 P^1 + P^1 P^1 - g P^1 P^1 - i P_1 P_1 e^{iqx}; & \end{aligned} \quad (1.18)$$

where $q = P^1 + P^1$ and we take $\epsilon_{0123} = 1$.

Using this we write M as:

$$M = \sum_{NH} \frac{d^3 P_{NH}}{2E_{NH} (2\pi)^3} A_L \langle h_B | j^Y | j \rangle : \quad (1.19)$$

The current correlator T is defined as

$$T = i \int d^4x e^{iqx} T f J^Y(0); J(x)g; \quad (1.20)$$

where the currents are:

$$\begin{aligned} J_{b!u} &= \bar{u} (1 - \gamma_5) b \\ J_{b!s} &= \bar{s} \frac{1}{4} \gamma_\mu \gamma_5 (1 + \gamma_5) b; \end{aligned} \quad (1.21)$$

and we have written the photon momentum as $q = n \frac{1}{2}$ (see below). We have also defined:

$$\begin{aligned} A^{b!u} &= \frac{G_F^2}{2} J_{ub} J^2 \\ A^{b!s} &= \frac{G_F^2}{2} J_7^e J^2 J_{tb} V_{ts} J_{\bar{m}b}^2 \frac{em}{16^3}; \end{aligned} \quad (1.22)$$

and

$$\begin{aligned} L^{b!u} &= 8 P^1 P^1 + P^1 P^1 - g P^1 P^1 - i P_1 P_1 \\ L^{b!u} &= 4g (n^2 - \bar{q}^2) \end{aligned} \quad (1.23)$$

We should note that in writing M in this form we have used the fact that the second term in equation (1.16) does not contribute to B decays, so we have changed its phase factor to e^{iqx} .

It is customary to define the hadronic tensor W as:

$$W = \frac{1}{2M_B} \frac{\text{Im} h_B J^2 J^2 i}{2M_B}; \quad (1.24)$$

which allows us to write the differential rate as:

$$d = \sum_{N_H} \frac{d^3 P_{N_H}}{2E_{N_H} (2\pi)^3} 2 A L W; \quad (1.25)$$

In order to continue we separate the discussion of $B \rightarrow X_s \gamma$ and $B \rightarrow X_u \gamma$.

For $B \rightarrow X_s \gamma$ decays, we have a real photon ($q^2 = 0$) recoiling against the hadronic jet. In the rest frame of the B meson we can take the jet to be moving in the $+z$ direction and the photon to be moving in the $-z$ direction. The momentum of the B meson in its rest frame is then $P_B = M_B v$, where $v = (1; 0; 0; 0)$. We also introduce two conjugate light-like vectors $n = (1; 0; 0; 1)$ and $\bar{n} = (1; 0; 0; -1)$, which satisfy $n \cdot \bar{n} = 2$; $n \cdot v = \bar{n} \cdot v = 1$; $n + \bar{n} = 2v$. Any 4-vector can be decomposed as:

$$a = n \frac{a_-}{2} + \bar{n} \frac{a_+}{2} + a_\perp, \quad a = a_- + a_+ + a_\perp; \quad (1.26)$$

where a_x, a_y are the x, y components of a (for our choice of n and n'). In terms of these vectors we can write the photon 4-momentum as $q = n' \frac{E_1}{2} = 2E_1 \frac{n'}{2}$. We can also express P_+ and P_- as $P_+ = n \cdot P$; $P_- = n' \cdot P$.

For $B \rightarrow X_s$ the P_{NH} momentum in (1.25) is q . Integrating over the angles, we find that the photon spectrum in $B \rightarrow X_s$ is:

$$d = \frac{d^3 q}{2E_1 (2\pi)^3} 2 A L W = \frac{E_1^3 dE_1}{4\pi^4} G_F^2 \mathcal{F}_7^e \mathcal{F}_{tb} V_{ts} \mathcal{F}_{mb}^2 \epsilon_m W ; \quad (1.27)$$

We now turn to $B \rightarrow X_u$ decays. The P_{NH} momenta in (1.25) are P_1 and P_{-1} . As we saw before, of the 6 variables only 3 are relevant, which can be taken to be $E_1 = (M_B - P_1) = 2, E_- = (M_B + P_1, P_+ - P_-) = 2$ and $\cos \theta = (\vec{P}_X^2 - E_1^2 - E_-^2) = (2E_1 E_-)$ (θ is the angle between P_1 and P'). Integrating over the three irrelevant angles and changing variables to P_+, P_1, P_- . We find that

$$d = dP_+ dP_1 dP_- \frac{G_F^2 \mathcal{F}_{ub}^2 (P_+ - P_-)}{256\pi^3} L W ; \quad (1.28)$$

The hadronic tensor has the property (proved in appendix A) that $W = (W_i)$. Using this identity we can decompose the tensor as a sum of 5 possible Lorentz structures. Given an independent pair of 4-vectors a and b , the 5 structures are $a \cdot a; b \cdot b; (a \cdot b + a \cdot b); g$ and $i \cdot a \cdot b$. The coefficients of these structures are called structure functions, denoted as W_i .

Typical choices for a and b that appear in the literature are v and q [1], and v and p [2]. We will choose v and n , which has the benefit that the coefficients of the structure functions W_i in the triple decay rate are independent of m_b . Decomposing the hadronic tensor in this basis we write:

$$W = (n \cdot v + n \cdot v \cdot g \cdot i \cdot n \cdot v) \tilde{W}_1 + g \cdot \tilde{W}_2 + v \cdot v \tilde{W}_3 + (n \cdot v + n \cdot v) \tilde{W}_4 + n \cdot n \tilde{W}_5 \quad (1.29)$$

The reason for defining the coefficient of \tilde{W}_1 in this way is that then at tree level only \tilde{W}_1 is non zero. The structure functions \tilde{W}_i are (generalized) functions of P_+ and P_- (or $n \cdot p$ and $n' \cdot p$). Having decomposed the hadronic tensor, we can write the triple rate in terms of the structure functions \tilde{W}_i . In the expression $L W$ we have several scalar products: $v \cdot P, v \cdot P_1, n \cdot P, n \cdot P_1, P_1 \cdot P_1$. Using $P_1 = M_B v - P_X$ we can eliminate all the scalar products that contain P_1 . Of the remaining scalar products $v \cdot P = E_1$ and $n \cdot P$ can be obtained from $P_X \cdot P$ via $P_X \cdot P = P \cdot (n \cdot P + P_+ (2E_1 - n \cdot P) = 2$ (since P_X has no y components). After a little bit of algebra we find the following compact result:

$$\frac{d^3}{dP_+ dP_- dP_1} = \frac{G_F^2 \mathcal{F}_{ub}^2}{16\pi^3} (M_B - P_+)^h \left[(P_- - P_1) (M_B - P_+ + P_1 - P_+) \tilde{W}_1 + (M_B - P_-) (P_- - P_+) \frac{\tilde{W}_2}{2} + (P_- - P_1) (P_1 - P_+) \left(\frac{Y}{4} \tilde{W}_3 + \tilde{W}_4 + \frac{1}{Y} \tilde{W}_5 \right) \right] ; \quad (1.30)$$

where we have defined

$$Y = \frac{P_-}{M_B} \frac{P_+}{P_-} : \quad (1.31)$$

Notice that the triple rate only depends on one linear combination of W_3 , W_4 and W_5 . The reason is that in the limit $M_1 \rightarrow 0$ (justified for electrons and muons) we have the two constraints $q_L = q_{\bar{L}} = 0$.

Equations (1.27) and (1.30) are the main results of this section. Of course they are not useful without the knowledge of W . The (approximate) calculation of the hadronic tensor will be one of the main topics of this work. In the rest of the chapter we discuss mostly $B \rightarrow X_u l$ and mention in passing what are the equivalent formulas for $B \rightarrow X_s$.

1.5 Free quark approximation – tree level and α_s corrections

In calculating the hadronic tensor, the simplest approximation we can make is to look at the b quark as a free quark, ignoring the spectator quark in the B meson and the non perturbative interactions that binds them together. As we shall see in the next section, this approximation would be the zeroth order term in an HQET based local Operator Product Expansion (OPE).

In this approximation the B meson states can be written as $|B\rangle = |b(m_b v)\rangle$. Writing the current as $J = \bar{q} \gamma_\mu b$, the matrix element of T is:

$$\begin{aligned} \langle b(m_b v) | T | b(m_b v) \rangle &= i \int d^4 x e^{iqx} \langle b | \bar{q} \gamma_\mu J^\nu(0) ; J^\mu(x) g | b \rangle \\ &= \frac{i}{2} \sum_{\text{b quark spin}} \int d^4 x e^{i(q - m_b v) \cdot x} \langle b | \bar{q} \gamma_\mu(0) ; q(x) g | b \rangle \\ &= \frac{1}{m_b} \int d^4 p \delta^4(m_b v - q - p) \text{Tr} \left[\frac{\not{p}}{p^2 + i} \frac{1 + \not{v}}{2} \right] ; \end{aligned} \quad (1.32)$$

where in the second line we have averaged over the b quark spins and $\int d^4 x = \int_0^\infty dy^0 \int d^3 y$.

Using the identity [8]

$$\text{Im} \frac{1}{(x - i)^n} = \frac{(-1)^{n-1}}{(n-1)!} \delta^{(n-1)}(x); \quad (1.33)$$

we find that

$$W = \frac{(\not{p}^2)}{2} \text{Tr} \left[\not{p} \frac{1 + \not{v}}{2} \right] : \quad (1.34)$$

(Notice that for the free quark approximation $m_b \rightarrow M_B$). For $B \rightarrow X_u l$ decays we can write (\not{p}^2) as $(n - p) = (n - p)$. Since

$$(n - p) \not{p} = (n - p) \frac{n}{2} + n \frac{n}{2} = (n - p) n \frac{n}{2} ; \quad (1.35)$$

and $\mathbf{A} = (1 \quad 5)$ we find

$$W = (n \quad p) (n \quad v \quad g \quad i \quad n \quad v) \quad \tilde{W}_1 = (n \quad p): \quad (1.36)$$

This simple result is the reason that \tilde{W}_1 is defined as it is.

As a quick check let us plug this result into (1.30). Since $P_+ = n - p_+$, we can integrate over the total phase space to find the well known result, that total rate at tree level is $G_F^2 N_{ub} f_m^2 = (192^{-3})$.

For $B \rightarrow X_s$ decays we have $\Gamma = \frac{1}{4} [\dots] (1 - \epsilon)$ and $\Gamma = \frac{1}{4} [\dots] (1 + \epsilon)$. Calculating the trace in equation (1.34) we find that

$$W = 2(n-p): \quad (1.37)$$

Using $n_p = n_b \sqrt{m_q} = m_b \sqrt{2E}$, we can plug this result in equation (1.27) and find that the total $B \rightarrow X_s$ rate at tree level is $G_F^2 V_{tb}^2 V_{ts}^2 |C_7^e|^2 m_b^5 = (32 \pm 4)$

A much more complicated calculation is to find the $O(\alpha_s)$ corrections to the structure functions W_i , in the free quark approximation. Such a calculation was performed by DeFazio and Neubert in [2]. The hadronic tensor in [2] was decomposed using the vectors p and v :

$$W = (p_v + p_v - g_v - p_i - p_v)W_1 + gW_2 + v_vW_3 + (p_v + p_v)W_4 + p_pW_5 \quad (1.38)$$

The relation to our basis is:

$$\begin{aligned} \tilde{W}_1 &= \frac{n}{2} \frac{p}{2} \frac{n}{2} W_1^p & \tilde{W}_2 &= W_2 + n \frac{p}{2} W \\ \tilde{W}_3 &= W_3 + 2n \frac{p}{2} (W + W_4 + n \frac{p}{2} W) & (1.39) \\ \tilde{W}_4 &= \frac{n}{2} \frac{p}{2} \frac{n}{2} (W_4 + n \frac{p}{2} W) & \tilde{W}_5 &= \frac{n}{2} \frac{p}{2} \frac{n}{2} W_5^2 \end{aligned}$$

The kinematical variables $z; t; p^2$ and x in [2] are related to ours via:

$$z = (n \quad p + n \quad p)_{\frac{1}{b}} = (n \quad p \quad n \quad p) = (n \quad p + n^2 = p)(n \quad p)_{\frac{1}{b}} \text{ and}$$

$$x = (M_B \quad P_+)_{\frac{1}{b}}, \text{ where again } P_+ = n \quad p + ; P_- = n \quad p + .$$

We will not transform the complete $O(s)$ result from [2] to our basis. Instead, we would like to illustrate the well known problem with the QCD calculation, namely the appearance of double and single logarithms that might spoil the convergence of the perturbative expansion. Let us look on one of the terms of W_1 :

$$W_1 = \frac{2}{m_b^2} \left(p^2 + \frac{C_F s}{4} \right) - 4 \frac{\ln p^2}{p^2} + \dots; \quad (1.40)$$

where the \star distribution is defined in chapter 2 and the \vdots denote other $O(s)$ terms. In terms of our basis we have:

$$\tilde{W}_1 = (n-p) + \frac{C_F s}{4} \frac{n-p}{n-p} \frac{\ln(n-p)}{n-p} + \dots; \quad (1.41)$$

The star distribution has two parts. The second part, which is proportional to a delta function, is the source of the double log. Inserting equation (1.41) into (1.30) we have:

$$\frac{d^3}{dP_+ dP_- dP_1} = \frac{G_F^2 \mathcal{Y}_{ub} f^2}{16 \pi^3} (M_B - P_+) (P_- - P_1) (M_B - P - P_1 - P_+) \times (n - p) \frac{C_F s}{4} - \frac{(n - p)}{2} \ln^2 \frac{u}{m_b} + \dots : \quad (1.42)$$

In a somewhat implicit notation, u is the upper limit of $n - p$ in the P integration and depends on the specific experimental cut. As an example, let us find the P_1 spectrum. The integral over P_- is automatic. For the P_+ integral we note that the upper limit of $n - p$ is $u = P_-$. Changing variables to $x = (M_B - P_1)/m_b$ we find that:

$$\frac{d}{dx} = \frac{G_F^2 \mathcal{Y}_{ub} f^2 m_b^5}{192 \pi^3} 2x^2 (3 - 2x) - 1 - \frac{C_F s}{2} \ln^2 (1 - x) + \dots : \quad (1.43)$$

which was first derived in [9]. It means that for high values of E_1 , i.e. $x \rightarrow 1$, the so called "endpoint region", the double log gets large. Notice that equation (1.42) implies that this is a generic problem. Anytime the value of u is not of order m_b , the double log would not be small. But, because of the experimental cuts the values of u are never of order m_b ! A similar situation arises for the single logarithms. Since these logarithms are multiplied with s , we might question the convergence of the perturbative series.

The same double logarithms appear for $B \rightarrow X_s \gamma$. From [10] and earlier references cited there, we find that the decay rate for $B \rightarrow X_s \gamma$ with a lower cut on the photon spectrum $E_\gamma > (1 - \epsilon)m_b/2$ is:

$$B \rightarrow X_s \gamma_{E_\gamma > (1 - \epsilon)m_b/2} = \frac{G_F^2 \alpha_{em}}{32 \pi^4} \mathcal{Y}_{tb} V_{ts}^2 f^2 \mathcal{F}_7^e f^2 m_b^5 - 1 - \frac{C_F s}{2} \ln^2 + \dots : \quad (1.44)$$

Because of the experimental cut $Q_{CD} \approx m_b$, so we encounter large logarithms again. (The universality of the double logarithms is not a coincidence and has its origin in the properties of soft Wilson loops, see below).

Having large logarithms is of course a well known problem, encountered, for example, when one takes into account the QCD corrections to weak decays [7]. The solution to the problem is to "resum" these logarithms. This is done by matching to an appropriate effective field theory and then solving the RG equations. As we shall see, the appropriate effective field theory is SCET.

One more comment before we conclude this section. Usually when one talks about "large logarithms" the question arises "how large are the logarithms? do we need resummation?" In order to answer this question we should note that the scale dependence of $s(\mu)$ is unspecified at this order. Some prefer to set m_b , but as we shall see, the more appropriate scale for these logarithms

is $\frac{p}{m_b} \frac{1}{Q_{CD}} \approx 1.5 \text{ GeV}$. Recall that because of QCD running $\alpha_s(M_Z) = 0.112$; $\alpha_s(m_b) = 0.22$; $\alpha_s(1.5 \text{ GeV}) = 0.375$. So we have the effect of logarithms multiplied by large value of α_s . This further motivates the need for resummation.

1.6 Effective field theories I: HQET

Effective field theory (EFT) is a very useful tool in general and in particular for B physics. It allows us to extract as much perturbative physics as possible from the matrix elements, and to break down the problem of "solving QCD" into manageable pieces, that we can try to model or extract from experiment.

For our specific goal, the calculation of the hadronic tensor, given an effective field theory the procedure is as follows:

A QCD current J is matched onto a series of the form $J_{CD} = C_0 J_0 + C_1 J_1 + \dots$, where the Wilson coefficients C_i are calculable as an expansion in α_s and each J_i is suppressed by i -th powers of a large scale.

The QCD Lagrangian is matched onto a series of the form $L = L_0 + L_1 + \dots$.

The Bjimeson states are matched onto eigenstates of L_0 , called B_{i0} .

T can then be written as a series

$$T = \sum_i C_i J_i^Y; \quad \sum_i C_i J_i^Y; e^{i \int d^4 y L_1 + \dots} = T C_0 J_0^Y; C_0 J_0^Y + \sum_i C_1 J_1^Y; C_0 J_0^Y + T C_0 J_0^Y; C_1 J_1^Y + T C_0 J_0^Y; C_0 J_0^Y; i \int d^4 y L_1 + \dots$$

W is then written as a series of non perturbative matrix elements with calculable coefficients.

The effective field theories that we will use HQET and SCET, are based on an expansion in inverse powers of the b quark mass. Since the hadronic matrix elements scale like Q_{CD} and $Q_{CD} \ll m_b$, our expansion parameter will be $Q_{CD}/m_b \approx 0.1$.

We start by looking at HQET and review its predictions for the hadronic tensor. In order to do so we go over some of the elements HQET that are important for our purpose. For an extensive review of HQET see [11, 12]. We start by writing the b field as:

$$b(x) = e^{i m_b v \cdot x} [h_v(x) + H_v(x)]; \quad (1.45)$$

where

$$h_v(x) = e^{i m_b v \cdot x} \frac{1 + \not{v}}{2} b(x); \quad H_v(x) = e^{i m_b v \cdot x} \frac{1 - \not{v}}{2} b(x); \quad (1.46)$$

In terms of these fields the QCD Lagrangian for the b quark is

$$L = b(i \not{D} - m_b) b \\ = h_v i \not{D} h_v + H_v i \not{D} H_v + h_v i \not{D} H_v + H_v i \not{D} h_v; \quad (1.47)$$

where $\tilde{D} = D - \not{v} \not{v} D$. From equation (1.47) it is clear that the field ψ is to be integrated out. In zeroth order we find that

$$L_0 = h_v i \bar{\psi} \not{D} \psi \quad (1.48)$$

For the light quarks and gluons there is no change, so we can write the leading order current as:

$$q \rightarrow b(x) : J_0 = e^{-i m_b v \cdot x} q \rightarrow h_v(x) : \quad (1.49)$$

Armed with this information we can calculate W at tree level:

$$\begin{aligned} T &= i \int d^4 x e^{i q x} T f J^Y(0); J(x) g \\ &= i \int d^4 x e^{i(q - m_b v) \cdot x} T f h_v \rightarrow q(0); q \rightarrow h_v(x) g \\ &= \int d^4 p \delta^4(m_b v - q) \bar{u}_v \frac{\not{p}}{p^2 + i} u_v \end{aligned} \quad (1.50)$$

In order to find the matrix element of T we need [11]:

$$\langle B | \bar{h}_v h_v \not{B} | B \rangle = M_B \text{Tr} \frac{1 + \not{v}}{2} : \quad (1.51)$$

Proceeding as before we find that the zeroth order HQET result is identical to the free quark result, namely:

$$\tilde{W}_1 = (n \cdot p); \quad W = 2 (n \cdot p) \quad (1.52)$$

The $\mathcal{O}(1/m_b)$ corrections to this zeroth order result would give us the De Fazio-Neubert hadronic tensor.

The reason for using HQET is to calculate the $1/m_b$ corrections to the hadronic tensor. Such a calculation was performed in [1, 13] for $B \rightarrow X_c l$. We will present the results as they appear in [12] after taking the limit $m_c \rightarrow 0$. These corrections are known only at $\mathcal{O}(1/m_b)$.

First let us look at the $1/m_b$ term in the HQET Lagrangian:

$$L_1 = h_v \frac{\tilde{D}^2}{2m_b} h_v - g_h \frac{G}{4m_b} h_v \quad (1.53)$$

The matrix elements of the operators in L_1 define two HQET parameters:

$$\begin{aligned} \langle B | \bar{h}_v \tilde{D}^2 h_v | B \rangle &= 2M_{B-1} \\ \langle B | \bar{h}_v G h_v | B \rangle &= 12M_{B-2} \end{aligned} \quad (1.54)$$

Intuitively we can think of M_{B-1} as measuring the kinetic energy of heavy quark inside the B meson and of M_{B-2} measuring its chromomagnetic interaction. Both parameters have mass dimension 2 and a priori we expect $M_{B-1} \sim \Lambda_{QCD}^2$.

Instead of matching the current J onto HQET current, the current correlator T itself can be matched onto HQET. Doing so one finds that the zeroth order term is identical to the free quark result. The $1/m_b$ correction to T vanishes. The reason is that the only operator that can appear at this order is $v \cdot h_v i \not{D} \cdot h_v$. At order $O(1/m_b^2)$ the matrix element of this operator would vanish because of HQET equations of motion [14]. This implies that the first non zero correction appears at order $1/m_b^2$.

The hadronic tensor in [12] is defined slightly different from ours:

$$W = \frac{1}{2M_B} \text{Im} \int d^4x \langle 0 | e^{iqx} h_B^\dagger J^\dagger(x) J(0) g \bar{\beta} i \rangle \quad (1.55)$$

where $J = u \gamma_5 (1 - \gamma_5) b/2$. This hadronic tensor is decomposed using the vectors q and v :

$$W = g W_1 + v \cdot v W_2 + i v \cdot q W_3 + q \cdot q W_4 + (v \cdot q + v \cdot q) W_5 \quad (1.56)$$

The relation to our basis is:

$$\begin{aligned} \tilde{W}_1 &= 4 \frac{n \cdot p}{2} \tilde{W}_3 & \tilde{W}_2 &= 4 \tilde{W}_1 - \frac{n \cdot p}{2} \tilde{W}_3 \\ \frac{y}{4} \tilde{W}_3 + \tilde{W}_4 + \frac{1}{y} \tilde{W}_5 &= (n \cdot p - \frac{n \cdot p}{m_b}) \frac{W_2}{n \cdot p} - 2 W_3 \end{aligned} \quad (1.57)$$

After the change of basis we find, including the zeroth order result $\tilde{W}_1 = (n \cdot p)$,

$$\begin{aligned} \tilde{W}_1 &= (n \cdot p) \left[1 + \frac{2}{3} \frac{1}{n \cdot \beta} \frac{3}{2} \right] + O(n \cdot p) \frac{2}{3n \cdot p} \frac{3}{2} - \frac{5}{6m_b} \frac{1}{n \cdot p} \frac{1}{6} ; \\ \tilde{W}_2 &= (n \cdot p) \frac{4}{3} \frac{1}{n \cdot \beta} \frac{6}{2} ; \\ \frac{y}{4} \tilde{W}_3 + \tilde{W}_4 + \frac{1}{y} \tilde{W}_5 &= \frac{(n \cdot p)}{n \cdot p} \frac{2}{3n \cdot p} \frac{1 + 12}{2} - \frac{4}{3m_b} \frac{1 + 9}{2} \\ &+ \frac{O(n \cdot p)}{n \cdot p} \frac{2}{3} \frac{1}{3} + 4 \frac{2}{2} : \end{aligned} \quad (1.58)$$

As we now show this calculation poses a problem when applied for charm less semileptonic decays. Define $\alpha_{QCD} = m_b$; using this small parameter we can define a systematic power counting. For example m_b would be an order 1 quantity, while the HQET parameters $1/m_b^2$ are order 2 .

For $B \rightarrow X_c l$ both $n \cdot p$ and $n \cdot \beta$ scale like m_b . This means that $(n \cdot p)$ and its derivatives are order 1 quantities. Considering the scaling of the HQET parameters, we have an expansion of the form $\tilde{W}_i = 1 + 1/m_b^2 + \dots$. We can imagine extending this calculation to higher order in $1/m_b^2$, by introducing more HQET

parameters. Each term in the expansion would be suppressed by more powers of

The situation is fundamentally different for $B \rightarrow X_u l$. We recall that because of the kinematical cuts enforced on us due to the large charm background, $n \cdot p$ never really scales like m_b . In fact, it scales like Q_{CD} . The appropriate power counting for $B \rightarrow X_u l$ is therefore $n \cdot p$ and $n \cdot p \ll 1$. Since the n -th derivative of $\langle x \rangle$ scales like $1=x^{n+1}$ we have three types of terms in (1.58): terms which scale like 1 , e.g. $(n \cdot p)^0 (n \cdot p)_1$; terms which scale like 0 , e.g. $0(n \cdot p)_1$; and terms which scale like 1 , e.g. $(n \cdot p)_1$. It follows that the expansion in (1.58) must be rearranged as:

$$\begin{aligned}
W_1 &= (n \cdot p)^0 (n \cdot p)_1^1 + \dots \\
&+ 0(n \cdot p) \frac{2 \cdot 1}{3n \cdot p} \frac{3 \cdot 2}{6m_b} + \dots \\
&+ (n \cdot p) \frac{2 \cdot 1}{3(n \cdot p)} \frac{3 \cdot 2}{p} + \dots ; \\
W_2 &= 0 + 0 + (n \cdot p) \frac{4 \cdot 1}{3(n \cdot p)} \frac{6 \cdot 2}{p} + \dots ; \\
\frac{y}{4} W_3 + W_4 + \frac{1}{y} W_5 &= 0 + \frac{0(n \cdot p)}{n \cdot p} \frac{2 \cdot 1}{3} + 4 \cdot 2 \dots \\
&+ \frac{(n \cdot p)}{n \cdot p} \frac{2 \cdot 1 + 12 \cdot 2}{3n \cdot p} \frac{4 \cdot 1 + 9 \cdot 2}{3m_b} + \dots : (1.59)
\end{aligned}$$

Our notation is such that in each square bracket we group terms which scale the same way. (Notice that in W_2 , for example, the lowest order terms are of order 0). Even after this rearranging we have a problem. By matching to higher orders in the HQET expansion and by introducing more HQET parameters, some of the terms might not be suppressed at all and will contribute to lower orders. In fact, in each order in $1/m_b$ we have to sum in infinite number of terms that contribute at that order. (We have included \dots in each square bracket to reflect this fact). This problem was first observed in [15, 16, 17] and is often referred to as "breaking down" of the OPE. A more accurate description would be to say that we have tried to use an HQET based OPE in a kinematical region where it is not valid. This OPE assumes that all the components of p are large compared to Q_{CD} , which is true for $B \rightarrow X_c l$ but not for $B \rightarrow X_u l$.

Let us look at the lowest order in $1/m_b$, i.e. the order 1 in equation (1.59). The infinite number of terms that are summed give us a new non perturbative object which is no longer just a matrix element of an HQET operator, but a function of the variable $n \cdot p$. This function is known as the leading order shape function, denoted as S . Beyond leading order there are more than one shape function and one would talk about several subleading shape functions. This analysis is the subject of chapter 3.

The fact that we had to do this resummation implies that HQET is not the most appropriate effective field theory to describe charm less inclusive B decays. We will introduce the more appropriate theory (SCET) in the next section. As chapters 2 and 3 will show, in this effective field theory the various shape functions arise naturally as non local matrix elements and there is no need to resum the HQET OPE. For the rest of this section let us talk a little more about the leading order calculation.

At $O(1/s)$ the leading order shape function can be defined as the sum of a series of distributions:

$$S(!) = (!) - \frac{1}{6} \delta(!) + \dots \quad (1.60)$$

(When no confusion can arise we will refer to the leading order shape function simply as the "shape function"). Moments of this function would then be related to HQET parameters. In order to find the relation, let us write a function $f(x)$ as a sum of infinite series of the form $f(x) = \sum_i a_i \delta^{(i)}(x)$. Using "integration by parts" [8] we find that the n -th moment is $\int dx x^n f(x) = (-1)^n n! a_n$. Equation (1.60) implies that the first three moments of the leading order shape function are $1; 0$, and $-1/3$.

In [16] it was shown that we can write the leading order shape function as:

$$\frac{\langle B | \bar{\psi}_v (!) \gamma_5 \psi | D \rangle}{2M_B} = S(!) \quad (1.61)$$

Notice that the shape function is defined as a matrix element of a non local operator. Another important property derived in [16] is the support of the shape function. In the absence of radiative corrections (see chapter 2) we can think of the shape function as a probability distribution for the b quark to have residual light cone momentum $! = n \cdot k$. For the total b quark light cone momentum fraction we have

$$\frac{n \cdot p}{n \cdot P} = \frac{n \cdot (q + k)}{M_B} = \frac{m_b + n \cdot k}{M_B} \quad (1.62)$$

Since $0 \leq \frac{n \cdot p}{n \cdot P} \leq 1$, (the limits corresponding to the b quark carrying none or all of the B meson light cone momentum), we have $m_b \leq n \cdot k \leq M_B - m_b$. In the $m_b \rightarrow 1$ limit this correspond to $1 - n \cdot k$, where at tree level $= \lim_{m_b \rightarrow 1} (M_B - m_b)$. In chapter 2 we will define beyond tree level.

So far we have ignored the $1/s$ corrections. How does the picture change when we include them? The answer was given by Korchemsky and Sterman in [18] who argued that at leading order a factorization formula holds. The factorization formula states that the differential rate can be written as a product of "hard" function and a convolution of a "jet" function with the leading order shape function, where both the hard and the jet function are calculable in perturbation theory. We will prove this factorization formula using SCET in chapter 2. At this stage we can illustrate this formula by using, yet again, the free quark approximation. Let us

write \tilde{W}_1 as:

$$\tilde{W}_1^{(0)} = \int_0^1 (n \cdot p) = 1 - d! \int_0^1 n \cdot p [n \cdot p (n \cdot p + 1)] S(1) \quad (1.63)$$

We now identify the term $S(1)$ with the first term in the moment expansion of $S(1)$. We also define a hard function as $H_{u1}(n \cdot p) = 1 + O(\epsilon_s)$ and a jet function as $J(u) = (u) + O(\epsilon_s)$. The factorization formula is then:

$$\tilde{W}_1 = H_{u1} \int_0^1 d! \int_0^1 n \cdot p J[n \cdot p (n \cdot p + 1)] S(1); \quad (1.64)$$

or symbolically $\tilde{W}_1 = H_u \cdot J \cdot S$.

We can motivate this procedure in the following way. At tree level we can think of the jet function as related to the imaginary part of the u quark propagator. Not neglecting the residual momentum k of the b quark, the light quark propagator is:

$$\text{in } \frac{n}{2} \frac{1}{n \cdot p (n \cdot p + n \cdot k) + i} \quad (1.65)$$

Expanding this propagator as a power series in $n \cdot k$ would generate the leading order shape function $S(n \cdot k)$. Following this procedure we can "implement" the shape function in any parton level calculation as:

$$\tilde{W}_1 = f(n \cdot p; n \cdot p) \int_0^1 d! f(n \cdot p; n \cdot p + 1) S(1) \quad (1.66)$$

Such procedure was used for example in [2]. We should stress though, that this procedure is justified at $O(\epsilon_s^0)$ only. A rigorous implementation of the shape function at $O(\epsilon_s)$ appears in chapter 2.

For $B \rightarrow X_s$ we find similar features. The HQET calculation performed in [19] gives:

$$W = 2 \int_0^1 (n \cdot p) \frac{1}{6} \omega(n \cdot p) + \frac{1}{2m_b} \frac{3}{2} \omega^2(n \cdot p) : \quad (1.67)$$

Because of the experimental cuts $n \cdot p$ scales like \sqrt{s} (see section 1.3). We therefore have to group the terms according to their scaling in an analogous way to $B \rightarrow X_{u1}$. We also see that at leading order the hadronic tensor is proportional to the leading order shape function S . Including radiative effects the W (and therefore the photon spectrum) can be factorized at leading order as

$$W = H \int_0^1 d! m_b J[m_b (n \cdot p + 1)] S(1); \quad (1.68)$$

Comparing equation (1.64) to (1.68), we see that the factorization formulas are very similar. The shape and jet function are the identical, but the argument of the jet function is different, since for $B \rightarrow X_s$, $n \cdot p = m$ (this is a result of the fact the kinematics is simpler for radiative decays). The hard functions are different, with H turning out to be more complicated. We will utilize these similarities in chapters 4 and 5.

Table 1.2: Different modes in SCET-I. We define $\mu = \Lambda_{\text{QCD}} = m_b$ and write the light cone components of vector a as $(n \cdot a; n_\perp \cdot a; \bar{n} \cdot a)$

Mode name	Momentum scaling	Examples
Hard	$(1; 1; 1)$	hard gluons
Hard-Collinear	$(\lambda; 1; \lambda^{\frac{1}{2}})$	hard-collinear quarks (q) hard-collinear gluons (A_{hc})
Soft	$(\lambda; \lambda; \lambda)$	heavy quarks (h_v), spectator quarks (q_s) soft gluons (A_s)

1.7 Effective field theories II: SCET

In the previous sections we have encountered two problems in trying to calculate the hadronic tensor. On the perturbative side we had large double and single logarithms that threaten the convergence of the perturbative expansion. On the non perturbative side we had to sum infinite numbers of HQET matrix elements into non perturbative functions, called shape functions, which are matrix elements of non local operators. This summation procedure is defined at tree level and it is unclear how to include radiative correction in a systematic fashion. Both of these problems can be solved by using SCET, which we now introduce.

We will present a brief review of SCET, focusing again on its application for charmless B decays. For a more complete discussion see [20, 21, 22]. The relevant effective field theory is known in the literature as SCET-I. Our presentation of SCET-I is based on the "position space" formalism first presented in [23, 24]. In SCET-I we distinguish between three type of modes according to the scaling of their momenta: hard, hard-collinear, and soft. Two of these modes, namely hard and soft, are familiar from HQET. The new mode, hard-collinear, is designed to describe the light quark produced in the b quark decay. The various modes are listed in table 1.2.

In constructing SCET, we first integrate out the hard modes, which leaves us with hard-collinear and soft modes only. For the soft quark modes the Lagrangian is the regular QCD Lagrangian for the soft quarks and the HQET Lagrangian for the heavy quarks. (The Yang-Mills Lagrangian for the soft and hard-collinear modes can be found in [23, 24]). We will therefore focus on the Lagrangian for hard-collinear quarks. In order to construct it we decompose the hard-collinear elds as:

$$\psi(x) = \frac{\not{n}\not{n}}{4} \psi + \frac{\not{n}_\perp \not{n}}{4} \psi + \dots; \quad (1.69)$$

where $\not{n}\not{n}=4$ and $\not{n}_\perp \not{n}=4$ are projection operators and $n; n_\perp$ are the light like vectors introduced before. In terms of ψ and $\bar{\psi}$ the QCD Lagrangian for massless hard-

collinear quarks is

$$L_{hc} = i\bar{\psi} \not{D} \psi = \frac{\not{n}}{2} \text{in } D + \frac{\not{n}}{2} \text{in } D + i\bar{\psi} \not{D}_\perp \psi + i\bar{\psi} \not{D}_\perp \psi : \quad (1.70)$$

(The covariant derivative in (1.70) contains both hard-collinear and soft gluons).

In order to decide which field is to be integrated out, let us look at the two point function for :

$$\langle 0 | \bar{\psi}(x) \psi(0) | 0 \rangle = \int \frac{d^4 p}{(2\pi)^4} e^{ip \cdot x} \frac{\not{n}}{p^2 + i\epsilon} : \quad (1.71)$$

Since p is hard-collinear momentum we have $d^4 p \sim p_\perp^2, p^2$, and $n \cdot p \sim 1$, which implies that scales like $1=2$. In a similar way we can show that scales like and it should be "integrated out". Once this is done equation (1.70) becomes:

$$L_{hc} = \frac{\not{n}}{2} \text{in } D + i\bar{\psi} \frac{1}{\text{in } D} i\bar{\psi} : \quad (1.72)$$

This Lagrangian contains terms of different orders in and we will expand it to the lowest order, shortly.

What about the currents? Our naive expectation is that the current $\bar{\psi}(x) \psi(x)$ would be matched, at tree level and leading order in , onto $e^{im_b v \cdot x} \langle x | h_v(x)$. The problem is that when a soft field interacts with a hard collinear field only one component of the momentum is conserved, namely $n \cdot p$. As a result, in position space, the soft fields need to be "multipole expanded" [23]. At leading order this amounts to placing at x while h_v is at $x = \frac{1}{2} n \cdot x n$. As soon as we put the two fields at different points the current is not gauge invariant. In order to make it gauge invariant we introduce a Wilson line:

$$W = P \exp \left(ig \int_1^0 dt n \cdot A(x + tn) \right) \quad (1.73)$$

The Wilson line has the right transformation properties such that the current $e^{im_b v \cdot x} W(x) h_v(x)$ is gauge invariant. We can think of this Wilson line as summing infinite number of hard-collinear gluons that can interact with the hard-collinear quark at leading order. (Of course each interaction "costs" us one power of g which is perturbative at the hard collinear scale). Apart from this hard-collinear Wilson line it is also convenient to introduce a soft Wilson line:

$$S = P \exp \left(ig \int_1^0 dt n \cdot A(x + tn) \right) \quad (1.74)$$

Using this Wilson line we redefine the hard-collinear fields according to

$$\psi(x) = S(x) \psi^{(0)}(x); \quad A_{hc} = S(x) A_{hc}^{(0)}(x) S^\dagger(x) : \quad (1.75)$$

The fields $\psi^{(0)}$ and $A_{hc}^{(0)}$ are "sterile" in the sense that they do not interact with soft gluons. In terms of the $A_{hc}^{(0)}$, the hard-collinear Wilson line can be written as $W(x) = S(x)W^{(0)}(x)S^\dagger(x)$, where

$$W^{(0)} = P \exp \left[ig \int_1^Z dt n \cdot A_{hc}^{(0)}(x + tn) \right] : \quad (1.76)$$

Thus the QCD current $q(x) \bar{b}(x)$ is matched onto $e^{im_b v \cdot x} J^{(0)}$, where

$$J^{(0)} = W \not{h}_v = \psi^{(0)} S^\dagger W \not{h}_v = \psi^{(0)} W^{(0)} S^\dagger \not{h}_v \quad X S^\dagger \not{h}_v = X(x) H(x); \quad (1.77)$$

and $X = \psi^{(0)} W^{(0)} = W S$. Beyond tree level and at leading order in ϵ the current would be matched onto [23]

$$q(x) \bar{b}(x) \rightarrow e^{im_b v \cdot x} \int_0^X ds C_i(s) X(x + sn) \psi_H(x); \quad (1.78)$$

Notice that non local currents arise naturally in SCET.

We can now go back to the hard-collinear Lagrangian, equation (1.72), which we want to expand to the lowest order in ϵ . By looking at the two point function for the hard-collinear and soft gluons, one can show that they scale like their momentum. That is, $A_{hc} \sim (\epsilon; 1; \epsilon)$ and $A_s \sim (\epsilon; \epsilon; \epsilon)$. Since $iD = i\partial + gA_{hc} + gA_s$. We find that to the lowest order in

$$\begin{aligned} \text{in } D &\rightarrow \text{in }_{hc} D = \text{in } \partial + g n_{hc} A \\ iD &\rightarrow iD_{hc} = i\partial + g A_{hc} \\ \text{in } D &\rightarrow \text{in }_{hc} D + g n_{hc} A = \text{in } \partial + g n_{hc} A + g n_{hc} A_s \end{aligned} \quad (1.79)$$

The leading order collinear Lagrangian is therefore:

$$L_{hc}^{(0)} = \frac{\not{D}}{2} \text{ in }_{hc} D + g n_{hc} A(x) + iD_{hc} \frac{1}{\text{in }_{hc} D} iD_{hc} : \quad (1.80)$$

Note that we have multipole expanded the soft gluon since it interacts with collinear quarks. We now introduce the "sterile" fields into the leading order Lagrangian. Using the identity

$$S^\dagger (\text{in } \partial + g n_s A) S = \text{in } \partial \quad (1.81)$$

the Lagrangian becomes:

$$L_{hc}^{(0)} = \psi^{(0)} \frac{\not{D}}{2} \text{ in }_{hc} D^{(0)} + iD_{hc}^{(0)} \frac{1}{\text{in }_{hc} D^{(0)}} iD_{hc}^{(0)} \psi^{(0)} : \quad (1.82)$$

Thus at leading order there are no interactions between soft gluons and hard-collinear quarks.

This concludes the leading order "derivation" of the SCET-I Lagrangian and currents. Equation (1.78) will be used in chapter 2 to derive the factorization formula $W_i = H \cdot J \cdot S$. Renormalization group equations will be used to resum the large logarithms, solving our first problem. In chapter 3 we will use higher order corrections to the currents and Lagrangians to calculate the subleading shape function contributions. The shape functions will be described as matrix elements of non local operators that arise naturally in the process of integrating out hard-collinear modes, so we do not need to sum in finite number of HQET parameters. Since SCET is an effective field theory it is clear how to carry on this procedure to any order and include radiative corrections, leading to a well defined double expansion in s and m_b .

Chapter 2

Perturbative Corrections

2.1 Chapter outline

In this chapter we analyze the perturbative corrections to $B \rightarrow X_u \ell$ hadronic tensor at leading order in $1/m_b$. We begin by presenting a derivation of the factorization formula for inclusive rates in the shape-function region using the position-space formulation of SCET. We then perform a two step matching calculation $QCD \rightarrow SCET \rightarrow HQET$ at next-to-leading order in perturbation theory, extracting the hard (H) and jet (J) functions. We then derive renormalization-group equations governing the dependence of the functions H , J , and the shape function S on the renormalization scale, and solve these equations analytically in momentum space. Next, we derive several model-independent properties of the shape function S . In particular, we present the precise form of the relations between renormalized shape-function moments and HQET parameters such as \bar{m}_b and α_s , and we give an analytical formula for the asymptotic behavior of the shape function. An unexpected outcome of this analysis is the finding that the shape function is not positive definite, but acquires a negative radiative tail at large values of $|j|$.

2.2 Factorization theorem for inclusive decay rates

Recall that

$$W = \frac{1}{2M_B} \text{Im} \frac{h_B(jT) \beta_i}{2M_B}; \quad T = i \int d^4x e^{iq \cdot x} T f J^\gamma(0); J(x) g; \quad (2.1)$$

where for $B \rightarrow X_u \ell$ decays $J = u \gamma (1 - \gamma_5) b$.

Below a matching scale $\mu_h = m_b$, the semileptonic current can be expanded as

$$u(x) \gamma (1 - \gamma_5) b(x) = e^{im_b v \cdot x} \sum_{i=1}^3 \int ds \mathcal{C}_i(s) X(x + sn) \tilde{H}(x) + \dots; \quad (2.2)$$

where the dots denote higher-order terms in the SCET expansion, which can be neglected at leading power in $QCD = m_b$. The position-space Wilson coefficient functions $\mathcal{C}_i(s)$ depend on the variables defining the position of the hard-collinear field. Here and below we denote functions in position space with a tilde, which is omitted from the corresponding Fourier-transformed functions in momentum space. A convenient basis of Dirac structures in (2.2) is

$$\gamma_1 = \gamma (1 - \gamma_5); \quad \gamma_2 = \gamma v \cdot (1 + \gamma_5); \quad \gamma_3 = n \cdot (1 + \gamma_5); \quad (2.3)$$

The current correlator in (2.1) then becomes

$$T = i \int d^4x e^{ip \cdot x} \sum_{i,j=1}^3 \int ds dt \mathcal{C}_j(t) \mathcal{C}_i(s) T H(0) \gamma_j X(x + tn); X(x + sn) \gamma_i H(x) + \dots; \quad (2.4)$$

In a second step, the hard-collinear fluctuations associated with the light-quark jet can be integrated out by matching SCET onto HQET at an intermediate scale $\mu_b \sim m_b \sim Q_{CD}$. At leading order the SCET Lagrangian (when written in terms of the gauge-invariant fields such as X) does not contain interactions between hard-collinear and soft fields. Since the external B -meson states only contain soft constituents, we can take the vacuum matrix element over the hard-collinear fields, defining a jet function

$$\langle h | j_T(X_k(tn); X_l(x + sn)) | j \rangle = \delta_{kl} \mathcal{J}(x + (s - t)n) + \dots; \quad (2.5)$$

where k, l are color indices, and we have used translational invariance to determine the dependence on the coordinate vectors. At higher orders in SCET power counting, additional jet functions would arise, but their contributions can be neglected at leading power. Shifting the integration variable from x to $z = x + (s - t)n$, with $z \cdot n = x \cdot n$, and introducing the Fourier-transformed Wilson coefficient functions

$$C_i(n, p) = \int_0^Z ds e^{isn} \mathcal{C}_i(s); \quad (2.6)$$

we then obtain

$$T = i \sum_{i,j=1}^3 C_j(n, p) \mathcal{C}(n, p) \int_0^Z d^4 z e^{ip \cdot z} H(0) \cdot j \mathcal{J}(z) \cdot i H(z) + \dots; \quad (2.7)$$

In the next step, we rewrite the bilocal heavy-quark operator as [15, 16]

$$\begin{aligned} H(0) \cdot H(z) &= \int_0^Z (h S_s)(0) \cdot e^{z \cdot \partial} (S_s^\dagger h)(0) = h(0) \cdot e^{z \cdot D} h(0) \\ &= d! e^{\frac{1}{2}! n \cdot \partial} h(0) \cdot (! \cdot \text{in } D) h(0); \end{aligned} \quad (2.8)$$

where m may be an arbitrary (even z -dependent) Dirac structure, and we have used the property $\text{in } D S = S_s \text{in } \partial$ of the soft Wilson line S , where $iD = i\partial + g_s A_s$ is the covariant derivative with respect to soft gauge transformations. When this expression is used in (2.7), the resulting formula for the correlator involves the Fourier transform of the jet function,

$$\int_0^Z d^4 z e^{ip \cdot z} \mathcal{J}(z) = \not{p} J(p^2); \quad (2.9)$$

however with p replaced by the combination $p_\perp = p + \frac{1}{2}! n$. In defining the momentum-space jet function $J(p^2)$ we have taken into account that the matrix element in (2.5) vanishes when multiplied by \not{n} from either side, since $\not{n} X = 0$. Using that $p_\perp \cdot n = p \cdot n$, we now obtain

$$T = i \sum_{i,j=1}^3 H_{ij}(n, p) d! J(p_\perp^2) h_j \not{p}_i (! \cdot \text{in } D) h + \dots; \quad (2.10)$$

where $H_{ij}(n, p) = \zeta(n, p) \zeta(n, p)$ are called the hard functions.

In order to compute the hadronic tensor we take the discontinuity of the jet function,

$$J(p^2) = \frac{1}{2} \text{Im} [iJ(p^2)]; \quad (2.11)$$

and evaluate the B-meson matrix element of the soft operator using the HQET trace formalism, which allows us to write [11]

$$\frac{\langle B | \bar{h} \gamma_\mu (1 - \gamma_5) h | D \rangle}{2M_B} = S(\mu) \frac{1}{2} \text{tr} \left[\frac{1 + \not{v}}{2} \right] + \dots \quad (2.12)$$

at leading power in the heavy-quark expansion. The soft function $S(\mu)$ coincides with the shape function $f(k_+)$ introduced in [15, 16]. This gives the factorization formula

$$W = \sum_{i,j=1}^3 H_{ij}(n, p) \text{tr} \left[\frac{\not{p}}{2} \gamma_i \frac{1 + \not{v}}{2} \right] \int_0^Z d\lambda J(p_i^2) S(\mu) + \dots \quad (2.13)$$

At leading power one could replace $\not{p} \rightarrow \not{p}$ and $n \cdot p = 2v \cdot p - 2v \cdot p$ in this result.

In the final expressions (2.10) and (2.13) the dependence on the three scales $n \cdot p$, p_i^2 , m_b , Q_{CD} and μ has been factorized into the hard, jet, and shape functions, respectively. Large logarithms associated with ratios of these scales can be resummed by solving renormalization-group equations for the scale dependence of these component functions. The factorization formula (2.13) was derived at tree level in [15, 16, 17], and was generalized to all orders in perturbation theory in [18, 25]. The derivation presented above is equivalent to a proof of this formula presented in [22] (see also [20]). The limits of integration in the convolution integral are determined by the facts that the jet function defined in (2.11) has support for $p_i^2 \geq 0$, and the shape function defined in (2.12) has support for $1 < \mu$ with $\mu = M_B - m_b$, where m_b is the heavy-quark pole mass. The argument p_i^2 of the jet function can be rewritten as

$$p_i^2 = p^2 + n \cdot p = n \cdot p (P \cdot \hat{n}) = n \cdot p (P \cdot \hat{n}); \quad (2.14)$$

where the variable $\hat{n} = \frac{1}{\sqrt{2}}(1, 0, 0, 1)$. We shall see below that expressing the convolution integral in terms of the new variable \hat{n} eliminates any spurious dependence of the decay spectra on the b-quark pole mass.

Using the fact that the Wilson coefficients C_i are real and hence H_{ij} is symmetric in its indices, we find

$$\begin{aligned} \sum_{i,j=1}^3 H_{ij} \text{tr} \left[\frac{\not{p}}{2} \gamma_i \frac{1 + \not{v}}{2} \right] &= H_{11} (n \cdot v + n \cdot v) + H_{22} v \cdot v + (H_{12} + H_{23}) (n \cdot v + n \cdot v) \\ &\quad + (2H_{13} + H_{33}) n \cdot n : \end{aligned} \quad (2.15)$$

This result may be compared with the general Lorentz decomposition of the hadronic tensor:

$$W = (\not{n} \not{v} + \not{n} \not{v} - g_{\mu\nu} \not{n} \not{v}) \tilde{W}_1 + g_{\mu\nu} \tilde{W}_2 + \not{v} \not{v} \tilde{W}_3 + (\not{n} \not{v} + \not{n} \not{v}) \tilde{W}_4 + \not{n} \not{n} \tilde{W}_5 \quad (2.16)$$

We see that the structure function \tilde{W}_2 is not generated at leading order in the SCET expansion. Since only the Wilson coefficient C_1 is non-zero at tree-level, the structure function \tilde{W}_1 receives leading-power contributions at tree level, whereas \tilde{W}_4 and \tilde{W}_5 receive leading-power contributions at $\mathcal{O}(\alpha_s(m_b))$. The function \tilde{W}_3 receives leading-power contributions only at $\mathcal{O}(\alpha_s^2(m_b))$, which is beyond the accuracy of a next-to-leading order calculation.

In the next section we will calculate the H_{ij} from [2]. This paper uses the decomposition

$$W = (\not{p} \not{v} + \not{p} \not{v} - g_{\mu\nu} \not{p} \not{v} - i \not{p} \not{v}) W_1 + g_{\mu\nu} W_2 + \not{v} \not{v} W_3 + (\not{p} \not{v} + \not{p} \not{v}) W_4 + \not{p} \not{p} W_5: \quad (2.17)$$

Equation (2.13) then implies that:

$$\begin{aligned} W_1 &= 2H_{11} \int_0^Z d! J(p_i^2) S(!) + \dots \\ W_4 &= 2H_{12} \int_0^Z d! J(p_i^2) S(!) + \dots \\ W_5 &= \frac{8H_{11}}{n \cdot p} \int_0^Z d! J(p_i^2) S(!) + \dots \end{aligned} \quad (2.18)$$

2.3 Matching calculations

In this section we derive perturbative expressions for the hard functions $H_{ij}(n \cdot p)$ and the jet function $J(p_i^2)$ in (2.13) at next-to-leading order in α_s . To this end, we match expressions for the hadronic tensor obtained in full QCD, SCET, and HQET, using for simplicity on-shell external b-quark states. We also present results for the renormalized shape function in the parton model, which are needed in the matching calculation. Throughout this chapter we use the $\overline{\text{MS}}$ subtraction scheme and work in $d = 4 - 2\epsilon$ space-time dimensions.

2.3.1 Hard functions

Perturbative expressions at $\mathcal{O}(\alpha_s)$ for the structure functions W_i in the decomposition (2.17) have been obtained in [2] by evaluating one-loop Feynman graphs for the current correlator T using on-shell external quark states with residual momentum k (satisfying $v \cdot k = 0$) in full QCD. The leading terms in the region of

hard-collinear jet momenta are

$$\begin{aligned}
\frac{1}{2}W_1 &= (C_F) \left[1 - \frac{C_F s}{4} \left(8 \ln^2 y - 10 \ln y + \frac{2 \ln y}{1-y} + 4L_2(1-y) + \frac{4}{3} \right) + 5 \right. \\
&\quad \left. + \frac{C_F s}{4} \frac{\ln(p_k^2 - m_b^2)}{p_k^2} + (8 \ln y - 7) \frac{1}{p_k^2} + \dots \right]; \\
\frac{1}{2}W_4 &= (C_F) \frac{C_F s}{4} \frac{2}{1-y} \frac{y \ln y}{1-y} + 1 + \dots; \\
\frac{m_b}{4}W_5 &= (C_F) \frac{C_F s}{4} \frac{2}{1-y} \frac{1}{1-y} \frac{2y}{y} \ln y - 1 + \dots;
\end{aligned} \tag{2.19}$$

whereas W_2 and W_3 do not receive leading-power contributions at this order, in accordance with our general observations made above. Here $s = s(\mu)$, $p_k^2 = p^2 + n \cdot p - k$, and in the shape function region, where $P \ll P$, we have $y \approx n \cdot p - m_b$. We have used that $2v \cdot p - m_b = n \cdot p - m_b + O(\mu)$ in the hard-collinear region. The star distributions are generalized plus distributions defined as [2]

$$\begin{aligned}
\int_0^z dx F(x) \frac{1}{x}^{[u]} &= \int_0^z dx \frac{F(x) - F(0)}{x} + F(0) \ln \frac{z}{u}; \\
\int_0^z dx F(x) \frac{\ln(x=u)}{x}^{[u]} &= \int_0^z dx \frac{F(x) - F(0)}{x} \ln \frac{x}{u} + \frac{F(0)}{2} \ln^2 \frac{z}{u};
\end{aligned} \tag{2.20}$$

where $F(x)$ is a smooth test function. For later purposes, we note the useful identities

$$\begin{aligned}
\frac{1}{x}^{[u]} &= \frac{1}{x}^{[u=]} = \frac{1}{x}^{[u]} + (x) \ln; \\
\frac{\ln(x=u)}{x}^{[u]} &= \frac{\ln(x=u)}{x}^{[u=]} = \frac{\ln(x=u)}{x}^{[u]} + \frac{1}{x}^{[u]} \ln + \frac{(x)}{2} \ln^2;
\end{aligned} \tag{2.21}$$

In order to find the hard functions H_{ij} , we calculate the discontinuity of the current correlator (2.4) between on-shell heavy-quark states in momentum space. We work to one-loop order in SCET, keeping i, j fixed and omitting the Wilson coefficient functions. The corresponding tree diagram yields

$$D^{(0)} = K (C_F); \quad \text{with } K = u_b(v) \not{p}_j \not{p}_i u_b(v); \tag{2.22}$$

where $u_b(v)$ are on-shell HQET spinors normalized to unity, and the quantity K corresponds to the Dirac trace in (2.13). The interpretation of this result in terms of hard, jet, and soft functions is that, at tree level, $J^{(0)}(p_i^2) = (C_F)$ and $S_{\text{parton}}^{(0)}(!) = (! - n \cdot k)$. (The second result is specific to the free-quark decay picture.) Then the convolution integral $d! J(p_i^2) S(!)$ in (2.13) produces (C_F) ,

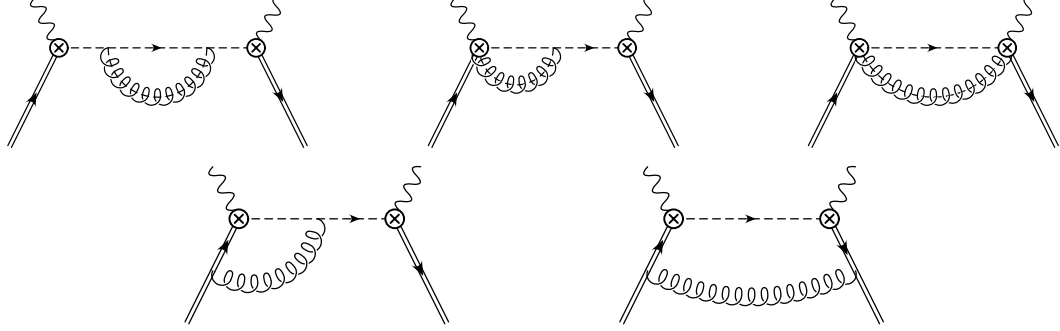


Figure 2.1: One-loop diagrams contributing to the current correlator in SCET. The effective current operators are denoted by crossed circles, and hard-collinear propagators are drawn as dashed lines. Mirror graphs obtained by exchanging the two currents are not shown.

and comparison with (2.19) shows that $H_{11}^{(0)} = 1$, while all other hard functions vanish at tree level.

The diagrams contributing at one-loop order are shown in Figure 2.1. They are evaluated using the Feynman rules of SCET. The first three graphs contain hard-collinear gluon exchanges, while the last two diagrams contain soft exchanges. The wave-function renormalization factors of the external heavy quarks equal 1 on-shell. For the sum of all hard-collinear exchange graphs, we find

$$D_{hc}^{(1)} = K \frac{C_F s}{4} \left[\frac{4}{2} + \frac{3}{2} + 7 \frac{1}{p_k^2} \right] (p_k^2) + 4 \frac{\ln(p_k^2 = 2)}{p_k^2} \left[\frac{4}{2} + 3 \frac{1}{p_k^2} \right] \# \quad (2.23)$$

The sum of the soft contributions is given by

$$D_s^{(1)} = K \frac{C_F s}{4} \left[\frac{2}{2} \frac{4}{2} L + \frac{2}{2} (4L^2 + 4L) \frac{1}{6} \right] (p_k^2) + 8 \frac{\ln(p_k^2 = 2)}{p_k^2} \left[\frac{4}{2} + 8L \right] \frac{1}{p_k^2} \# ; \quad (2.24)$$

where $L = \ln(n/p)$. The $1/p$ poles in the sum of the hard-collinear and soft contributions are subtracted by a multiplicative renormalization factor Z_J^2 applied to the bare current correlator in (2.4), where

$$Z_J = 1 + \frac{C_F s}{4} \left[\frac{1}{2} + \frac{2}{2} L \right] \frac{5}{2} \quad (2.25)$$

is the (momentum-space) current renormalization constant in SCET [21]. Taking the sum of (2.23) and (2.24) after subtraction of the pole terms, and matching it

with the results in (2.19), we find that at one-loop order

$$\begin{aligned}
H_{11}(n, p) &= 1 + \frac{C_F s}{4} (4L^2 + 10L - 4 \ln y - \frac{2 \ln y}{1-y} - 4L_2(1-y) - \frac{2}{6}) ; \\
H_{12}(n, p) &= \frac{C_F s}{4} \frac{2}{1-y} \frac{y \ln y}{1-y} + 1 ; \\
H_{13}(n, p) &= \frac{C_F s}{4} \frac{y}{1-y} \frac{1-2y}{1-y} \ln y - 1 :
\end{aligned} \tag{2.26}$$

In deriving these results we have used the identities (2.21) to rearrange the various star distributions. The remaining hard functions start at $O(\frac{2}{s})$. Using the relation $H_{ij} = C_i C_j$, one can derive from these results expressions for the Wilson coefficients in the expansion of the semileptonic current in (2.2). We confirm the expressions for these coefficients given in [21].

2.3.2 Jet function

After the hadronic tensor is matched onto HQET as shown in (2.13), the SCET loop graphs in Figure 2.1 determine the one-loop contributions to the product of the jet function and the shape function in (2.13). We may write this product symbolically as $J^{(1)} \otimes S^{(0)} + J^{(0)} \otimes S^{(1)}$, where the \otimes symbol means a convolution in $!$. Whereas the jet function is a short-distance object that can be calculated in perturbation theory, the shape function is defined in terms of a hadronic matrix element and cannot be properly described using Feynman diagrams with on-shell external quark states. In a second step, we must therefore extract from the results (2.23) and (2.24) the one-loop contribution $J^{(1)}$ to the jet function. To this end, we must compute the renormalized shape function at one-loop order in the parton model. This will be done in the next subsection. We may, however, already anticipate the result for the jet function at this point, because at one-loop order the graphs in Figure 2.1 can be separated into diagrams with hard-collinear (first line) or soft (second line) gluon exchange. (This separation would be non-trivial beyond one-loop order.) The hard-collinear contribution in (2.23) thus determines the convolution $J^{(1)} \otimes S^{(0)} = J^{(1)}(p_k^2)$, whereas the soft contribution in (2.24) corresponds to $J^{(0)} \otimes S^{(1)}$. It follows that the renormalized jet function is given by the distribution

$$J(p_i^2) = \delta(p_i^2) + \frac{C_F s}{4} (7 - 2\epsilon) \delta(p_i^2) + 4 \frac{\ln(p_i^2 = s)}{p_i^2} \delta(p_i^2) - 3 \frac{1}{p_i^2} \delta(p_i^2) : \tag{2.27}$$

This result disagrees with a corresponding expression obtained in [35]. It will often be useful to separate the dependence on $n \cdot p$ and P in this result by means of the substitution $p_i^2 = y p_i'^2$, where $p_i'^2 = m_b(P + \not{n})$ according to (2.14). Using the

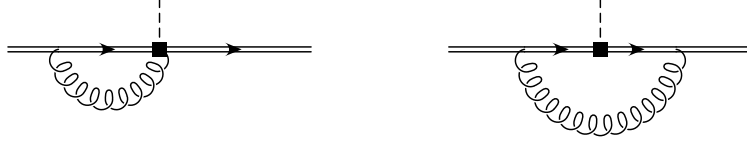


Figure 2.2: Radiative corrections to the shape function. The bilocal HQET operator is denoted by the black square. A mirror copy of the first graph is not shown.

identities (2.21), we find

$$\begin{aligned}
 y J(\vec{p}_i^2) - \hat{J}(\vec{p}_i^2; y) = & \left(\frac{C_F}{4} \right) \left(\frac{s}{\vec{p}_i^2} \right) \left(2 \ln^2 y - 3 \ln y + 7 \right) \left(\frac{1}{\vec{p}_i^2} \right) \\
 & + 4 \frac{\ln(\vec{p}_i^2 = 2)}{\vec{p}_i^2} + (4 \ln y - 3) \frac{1}{\vec{p}_i^2} : \quad (2.28)
 \end{aligned}$$

The jet function is non-zero only if $y > 0$ and $P_+ > 0$, which ensures that $\vec{p}_i^2 > 0$.

2.3.3 Renormalized shape function

Having calculated the short-distance objects H_{ij} and J in the factorization formula (2.13) at one-loop order, we now turn to a study of radiative corrections to the shape function $S(!)$. There is considerable confusion in the literature about the renormalization properties of the shape function, and several incorrect results for its anomalous dimension have been published. We therefore present our calculation in some detail in this subsection and the following section.

According to (2.12), the shape function is defined in terms of a hadronic matrix element in HQET and thus cannot be calculated perturbatively. However, the renormalization properties of this function can be studied using perturbation theory. To this end, we evaluate the matrix element (2.12) in HQET using external heavy-quark states with residual momentum k . For the time being, we keep $v \cdot k$ non-zero to regularize infra-red singularities. The relevant one-loop graphs are depicted in Figure 2.2. Adding the tree contribution, we obtain for the matrix element of the bare shape-function operator $O(!) = \bar{h}(! \text{ in } D) h$ (expressed in terms of renormalized fields)

$$\begin{aligned}
 S_{\text{bare}}(!) = & Z_h(! \text{ in } k) \frac{4C_F g_s^2}{(4\pi)^2} (1 + \dots) \\
 & - \frac{1}{0} \int_0^1 d\ell \ell^{-1/2} \bar{h}(! \text{ in } k) \left(\frac{1}{k+1\ell} - \frac{1}{1} \right) \\
 & + (n-k-!) (n-k) \left(\frac{1}{k} - \frac{1}{k+1} \right) ; \quad (2.29)
 \end{aligned}$$

where $\mu = 2v - k$, and

$$Z_h = 1 + \frac{4C_F g_s^2}{(4\pi)^2} (2 - \epsilon) (1 - \epsilon)^{-2} \quad (2.30)$$

is the on-shell wave-function renormalization constant of a heavy quark in HQET. The next step is to extract the ultra-violet poles from this result, which determine the anomalous dimension of the shape function. We define a renormalization factor through

$$\begin{aligned} S_{\text{ren}}(!) &= \int_0^{\Lambda} d!^0 Z_S(!; !^0) S_{\text{bare}}(!^0); \\ Z_S(!; !^0) &= (! - !^0) + \frac{C_F s}{4} Z_S(!; !^0) + \dots \end{aligned} \quad (2.31)$$

The result for Z_S following from (2.29) must be interpreted as a distribution on test functions $F(!^0)$ with support on the interval $1 < !^0$. We obtain

$$\begin{aligned} Z_S(!; !^0) &= \frac{2}{2} + \frac{4}{\epsilon} \ln \frac{2}{!} - \frac{2}{\epsilon} (! - !^0) - \frac{4}{\epsilon} \frac{(!^0 - !)}{!^0 - !} + \\ &= \frac{2}{2} - \frac{2}{\epsilon} (! - !^0) - \frac{4}{\epsilon} \frac{1}{!^0 - !} : \end{aligned} \quad (2.32)$$

Note the peculiar dependence on the parameter ϵ setting the upper limit on the integration over $!^0$ in (2.31), which combines with the plus distribution to form a star distribution in the variable $(!^0 - !)$.

We can now determine the renormalized shape function from (2.31). The result must once again be interpreted as a distribution, this time on test functions $F(!)$ integrated over a finite interval $_{\text{had}} < !$. In practice, the value of $_{\text{had}}$ is set by kinematics or by virtue of some experimental cut. The result is

$$\begin{aligned} S_{\text{parton}}(!) &= (! - n - k) \left(1 - \frac{C_F s}{24} + L_2 \frac{1}{_{\text{had}} + n - k} \right. \\ &\quad + \frac{C_F s}{n - k} \frac{(n - k - !)}{!} \ln \frac{n - k - !}{n - k} + \ln \frac{n - k - !}{n - k} + \\ &\quad + (n - k - !)^2 \ln \frac{_{\text{had}} + n - k}{n - k - !} + \frac{(n - k - !)}{n - k - !} \\ &\quad \left. + (n - k - !) \ln : \right) \end{aligned} \quad (2.33)$$

While it was useful to keep the heavy quark on-shell in the calculation of the ultra-violet renormalization factor, the limit $\mu = 2v - k \rightarrow 0$ can be taken in the result for the renormalized shape functions without leading to infra-red singularities.

This gives

$$S_{\text{parton}}(!) = (! - n - k)! \frac{C_F s}{24} \frac{2}{n - k} \ln \frac{n - k}{!} + \frac{1}{n - k} \frac{!^{\#}}{!}; \quad (2.34)$$

where the star distributions must now be understood as distributions in the variable $(n - k - !)$.

We stress that these results for the renormalized shape function are obtained in the parton model and can in no way provide a realistic prediction for the functional form of $S(!)$. This should be obvious from the fact that our results depend on a single hadronic parameter $n - k$, corresponding to a fixed residual momentum of the heavy quark. Only the dependence on the ultra-violet renormalization scale can be trusted. However, the one-loop result in (2.34) is needed to complete the matching calculation of the jet function described in the previous subsection, which can legitimately be performed with on-shell external b -quark states. Given the expression for the renormalized shape function, we obtain

$$\begin{aligned} d! J^{(0)}(p_i^2) S^{(1)}(!) &= \frac{1}{n} S^{(1)}(p^2 = n - p) \\ &= \frac{C_F s}{24} \frac{2}{p_k^2} + \frac{2}{n} \frac{n - p}{p} \ln \frac{p_k^2}{n - p} + \frac{1}{n} \frac{n - p}{p} \frac{p^{\#}}{p_k^2}; \end{aligned} \quad (2.35)$$

With the help of the identities (2.21) this can be shown to be equal to the finite part of (2.24), as we claimed above.

2.4 Renormalization-group resummation

Equations (2.26) and (2.27) determine the short-distance objects H_{ij} and J in the factorization formula (2.13) at one-loop order in perturbation theory. However, there is no common choice of the renormalization scale that would eliminate all large logarithms from these results. Likewise, the shape function, being a hadronic matrix element, is naturally renormalized at some low scale, whereas the short-distance objects contain physics at higher scales. The problem of large logarithms arising from the presence of disparate mass scales can be dealt with using renormalization-group equations. Proceeding in three steps, our strategy will be as follows:

i) At a high scale $\mu_h \gg m_b$ we match QCD onto SCET and extract matching conditions for the hard functions H_{ij} . The corresponding one-loop expressions have been given in (2.26). At that scale, they are free of large logarithms and so can be reliably computed using perturbation theory. We then evolve the hard functions down to an intermediate hard-collinear scale $\mu_i \sim m_b$ by solving

the renormalization-group equation

$$\frac{d}{d \ln} H_{ij}(n, p; \mu) = \gamma_J(n, p; \mu) H_{ij}(n, p; \mu); \quad (2.36)$$

where γ_J is the anomalous dimension of the semileptonic current in SCET.

ii) Next, we start from a model for the shape function $S(!; \mu_0)$ at some low scale $\mu_0 = \text{few } Q_{CD}$ large enough to trust perturbation theory. Such a model could be provided by a QCD-inspired approach such as QCD sum rules or lattice QCD, or it could be tuned to experimental data. We then solve the integro-differential evolution equation

$$\frac{d}{d \ln} S(!; \mu) = \int d!^0 \gamma_S(!; !^0; \mu) S(!^0; \mu) \quad (2.37)$$

to obtain the shape function at the intermediate scale μ_i .

iii) Finally, at the scale μ_i we combine the results for the hard functions and for the shape function with the jet function J in (2.27), which at that scale is free of large logarithms and so has a reliable perturbative expansion. The dependence on the matching scales μ_h and μ_i cancels in the final result (to the order at which we are working).

We now discuss these three steps in detail.

2.4.1 Evolution of the hard functions

At one-loop order, the anomalous dimension γ_J for the SCET current is twice the coefficient of the $1/\epsilon$ pole in the renormalization factor Z_J in (2.25). More generally [21, 26],

$$\gamma_J(n, p; \mu) = \gamma_{\text{cusp}}(\mu) \ln \frac{\mu}{n \cdot p} + \gamma^0(\mu) = \frac{C_F}{\mu} \ln \frac{\mu}{n \cdot p} \frac{5}{4} + \dots; \quad (2.38)$$

where $\gamma_{\text{cusp}} = C_F \mu = + \dots$ is the universal cusp anomalous dimension governing the ultra-violet singularities of Wilson lines with light-like segments [27, 28]. The exact solution to the evolution equation (2.36) can be written as

$$H_{ij}(n, p; \mu) = H_{ij}(n, p; \mu_h) U_Y(\mu_h; \mu_i); \quad (2.39)$$

where

$$U_Y(\mu_h; \mu_i) = U(\mu_h; \mu_i) Y^{2a(\mu_h; \mu_i)}; \quad (2.40)$$

The exact expression for the evolution factor reads

$$\ln U(\mu_h; \mu_i) = 2S(\mu_h; \mu_i) - 2a(\mu_h; \mu_i) \ln \frac{\mu_b}{\mu_h} - 2a_0(\mu_h; \mu_i); \quad (2.41)$$

where the functions of the right-hand side are solutions to the renormalization-group equations

$$\begin{aligned}\frac{d}{d\ln} S(\mu; \mu_s) &= \gamma_{\text{cusp}}(\mu_s) \ln \frac{\mu}{\mu_s}; \\ \frac{d}{d\ln} a(\mu; \mu_s) &= \gamma_{\text{cusp}}(\mu_s); \quad \frac{d}{d\ln} a_0(\mu; \mu_s) = \gamma_0(\mu_s); \end{aligned} \quad (2.42)$$

with boundary conditions $S(\mu; \mu) = 0$ etc. at $\mu = \mu_s$. These equations can be integrated using that $d = d\ln \mu = (\mu_s/\mu) d = d_s$. The solutions are

$$S(\mu; \mu_s) = \int_{\mu_s(\mu)}^{\mu_s(\mu)} d \frac{\gamma_{\text{cusp}}(\mu_s)}{(\mu_s)} \frac{d \ln \mu}{(\mu_s)}; \quad a(\mu; \mu_s) = \int_{\mu_s(\mu)}^{\mu_s(\mu)} d \frac{\gamma_{\text{cusp}}(\mu_s)}{(\mu_s)}; \quad (2.43)$$

and similarly for a_0 . Explicit results for the Sudakov exponent S and the functions a and a_0 in (2.41) at next-to-leading order in renormalization-group improved perturbation theory are given in Appendix B.

2.4.2 Evolution of the shape function

At one-loop order, the anomalous dimension for the shape function is twice the coefficient of the $1/\epsilon$ pole in the renormalization factor Z_S . From (2.32), we obtain

$$\gamma_S(\epsilon; \epsilon^0; \mu) = \frac{C_F}{\epsilon} \left(2 \ln \frac{\mu}{\mu_s} - 1 \right) + \mathcal{O}(\epsilon^0) = 2 \frac{(\epsilon^0)}{(\epsilon^0)} : \quad (2.44)$$

The evolution equation (2.37) can be solved analytically using a general method developed in [29]. It is convenient to change variables from ϵ to $\hat{\epsilon} = \epsilon/2 \ln \mu/\mu_s$ and denote $\hat{S}(\hat{\epsilon}) = S(\epsilon; \mu_s)$. The renormalization-group equation then reads

$$\frac{d}{d\ln} \hat{S}(\hat{\epsilon}; \mu_s) = \int_0^{\hat{\epsilon}} d\hat{\epsilon}' \gamma_S(\hat{\epsilon}'; \mu_s) \hat{S}(\hat{\epsilon} - \hat{\epsilon}'); \quad (2.45)$$

where the anomalous dimension can be written in the general form

$$\gamma_S(\hat{\epsilon}; \hat{\epsilon}^0; \mu_s) = 2 \gamma_{\text{cusp}}(\mu_s) \frac{(\hat{\epsilon} - \hat{\epsilon}^0)}{\hat{\epsilon} \hat{\epsilon}^0} + 2 \gamma(\mu_s) \gamma_{\text{cusp}}(\mu_s) \ln \frac{\hat{\epsilon}}{\hat{\epsilon}^0} + \mathcal{O}(\hat{\epsilon}^0); \quad (2.46)$$

The logarithmic term containing the cusp anomalous dimension has a geometric origin. Since the heavy-quark field $h(x)$ in HQET can be represented as a Wilson line along the v direction, the field $H(x)$ entering the SCET formalism contains the product of a light-like Wilson line (along n) and a time-like Wilson line (along v), which form a cusp at point x . The shape function contains two such cusps. According to the renormalization theory of Wilson lines with light-like segments,

each cusp produces a contribution to the anomalous dimension proportional to $\ln \mu_{\text{cusp}}$ [27, 28].

The general solution of (2.45) can be obtained using the fact that

$$\int_0^Z \frac{d\Gamma^0(\Gamma^0)^a}{\Gamma^0} \mu_{\text{cusp}}(s) = \Gamma^a \mu_{\text{cusp}}(s)^h (1+a) + \frac{i}{E} \quad (2.47)$$

where $\gamma(z)$ is the logarithmic derivative of the Euler function and the integral on the left-hand side is convergent as long as $\text{Re } a > -1$.

Relation (2.47) implies that the ansatz [29]

$$f(\Gamma; \mu; \mu_0) = \frac{\Gamma^{2a(\mu; \mu_0)}}{\mu_0} U_2(\mu; \mu_0) U_3(\mu; \mu_0) \quad (2.48)$$

with

$$\begin{aligned} \ln U_2(\mu; \mu_0) &= 2S(\mu; \mu_0) + 2a(\mu; \mu_0); \\ \ln U_3(\mu; \mu_0) &= 2 \int_{s(\mu_0)}^{\mu} \frac{d}{ds} \mu_{\text{cusp}}(s) \left[1 + 2a(\mu; \mu_0) \right] + \frac{i}{E}; \end{aligned} \quad (2.49)$$

provides a solution to the evolution equation (2.45) with initial condition, $f(\Gamma; \mu_0; \mu_0) = \Gamma^0$ at some scale μ_0 . Here $s(\mu)$ is defined such that $s(\mu) = \mu$, a is defined as in equation (2.43) with μ_{cusp} replaced by μ , and i can be an arbitrary complex parameter. Note that $a(\mu; \mu_0) < 0$ if $\mu > \mu_0$.

We now assume that the shape function $\hat{S}(\Gamma; \mu_0)$ is given at the low scale μ_0 and define its Fourier transform with respect to $\ln(\Gamma = \mu_0)$ through

$$\hat{S}(\Gamma; \mu_0) = \frac{1}{2} \int_{-1}^Z dt S_0(t) \frac{\Gamma^{it}}{\mu_0}; \quad (2.50)$$

The exact result for the shape function at a different scale μ is then given by

$$\hat{S}(\Gamma; \mu) = \frac{1}{2} \int_{-1}^Z dt S_0(t) f(\Gamma; \mu_0; it); \quad (2.51)$$

With the help of this formula, it is straightforward to derive explicit expressions for the evolution of the shape function from the hadronic scale μ_0 up to the intermediate scale μ_i at any order in renormalization-group improved perturbation theory:

$$f(\Gamma; \mu_i; \mu_0; it) = U_2(\mu_i; \mu_0) e^{2a(\mu_0; \mu_i)E} \frac{\Gamma^{it} \mu_0^{2a(\mu_0; \mu_i)}}{\mu_0} \frac{(1+it)}{[1+it - 2a(\mu_0; \mu_i)]} : \quad (2.52)$$

The leading-order result presented above can be simplified further. When (2.52) is inserted into (2.51), the integration over t can be performed analytically. Setting $\mu = 2a(\mu_0; \mu_1)$, the relevant integral is

$$I = \frac{1}{2} \int_{-1}^1 dt S_0(t) \int_0^{\mu} \frac{it}{(1+it+\mu)}; \quad (2.53)$$

where

$$S_0(t) = \int_0^{\mu} \frac{d\mu^0}{\mu^0} \hat{S}(\mu^0; \mu_0) \int_0^{\mu^0} \frac{it}{\mu^0} \quad (2.54)$$

is the Fourier transform of the shape function as defined in (2.50). The integrand of the t -integral has poles on the positive imaginary axis located at $t = i\mu^0/n$ with $n \geq 1$ an integer. For $\mu < \mu^0$ the integration contour can be closed in the lower half-plane avoiding all poles, hence yielding zero. For $\mu > \mu^0$ we use the theorem of residues to obtain

$$I = \int_0^{\mu} d\mu^0 R(\mu; \mu^0) \hat{S}(\mu^0; \mu_0); \quad (2.55)$$

where

$$R(\mu; \mu^0) = \frac{1}{\mu} \sum_{j=0}^{\infty} \frac{\mu^0{}^j}{\mu^0} \frac{1}{(j+1)(-\mu^0)^j} = \frac{1}{(-\mu^0)} \frac{1}{\mu(\mu - \mu^0)^1}; \quad (2.56)$$

Note that $R(\mu; \mu^0) \rightarrow (\mu - \mu^0)^{-1}$ in the limit $\mu \rightarrow 0$, corresponding to $\mu_1 \rightarrow 0$, as it should be. Our final result for the shape function at the intermediate hard-collinear scale, valid at leading order in renormalization-group improved perturbation theory, can now be written in the simple form (valid for $\mu_1 > 0$, so that $\mu > 0$)

$$\hat{S}(\mu; \mu_1) = U_2(\mu; \mu_0) \frac{e^{-\mu}}{(-\mu)} \int_0^{\mu} d\mu^0 \frac{\hat{S}(\mu^0; \mu_0)}{\mu^0(\mu - \mu^0)^1}; \quad (2.57)$$

From the above equation one can derive scaling relations for the asymptotic behavior of the shape function for $\mu \rightarrow 0$ and $\mu \rightarrow 1$ (corresponding to $\mu_1 \rightarrow 0$ and $\mu_1 \rightarrow 1$). If the function $\hat{S}(\mu^0; \mu_0)$ at the low scale μ_0 vanishes proportional to μ^0 near the endpoint, the shape function at a higher scale $\mu_1 > \mu_0$ vanishes faster, proportional to $\mu^{1+\epsilon}$. Similarly, if $\hat{S}(\mu^0; \mu_0)$ falls off like μ^0 for $\mu^0 \rightarrow 1$, the shape function renormalized at a higher scale vanishes like $\mu^{m \ln(1/\mu) + \epsilon}$. Irrespective of the initial behavior of the shape function, evolution effects generate a radiative tail that falls off slower than $1/\mu$. This fact implies that the normalization integral of $\hat{S}(\mu; \mu_1)$ as well as all positive moments are ultra-violet divergent. The field-theoretic reason is that the bilocal shape-function operator in (2.8) contains ultra-violet singularities as $z \rightarrow 0$, which are not subtracted in the renormalization of the shape function. The situation is analogous to the case of the B-meson light-cone distribution amplitude discussed in [29, 30]. These divergences are never an obstacle in practice. Convolution integrals with the shape function are always cut off at some finite value of μ by virtue of phase-space or some experimental cut.

2.5 Properties of the shape function

In this section we discuss how moments of the shape function are related with HQET parameters. This will lead us to propose a new, physical scheme for defining a running heavy-quark mass, which is most appropriate for the study of inclusive spectra in the shape-function region. We will also present a model-independent result for the asymptotic behavior of the renormalized shape function (defined in the \overline{MS} scheme), finding that it is not positive definite.

Most of our discussion in this section is phrased in terms of the original (unhatted) shape function $S(!;)$. At the end, we formulate the resulting constraints on the function $\hat{S}(!;)$.

2.5.1 Shape-function moments in the pole scheme

Naively, ignoring renormalization effects, the moments $M_N = \int_0^R d! !^N S(!)$ are given by hadronic parameters defined in terms of B-meson matrix elements of local HQET operators [15]. In particular, $M_0 = 1$ fixes the normalization of the shape function, $M_1 = 0$ vanishes by the HQET equation of motion, and $M_2 = \frac{1}{3}$ is determined by the matrix element of the kinetic-energy operator. The vanishing of the first moment is connected with the implicit definition of the heavy-quark pole mass built into the HQET Lagrangian via the equation of motion $i \not{D} h = 0$. These moment constraints have been implemented in various model parameterizations for the shape function suggested in the literature [31, 32, 33]. Typically, one makes an ansatz for the shape function depending on a few HQET parameters such as α_s and μ_1 , and determines the values of these parameters from a fit to experimental data.

Beyond tree level, all moments M_N with $N \geq 0$ receive ultra-violet divergences from the region $! \rightarrow 1$ (or $! \rightarrow 1$). However, as we have mentioned above, the values of $!$ needed for the description of physical decay rates are always restricted to a finite interval. It is thus sufficient for all purposes to define the moments of the renormalized shape function as

$$M_N(\mu_{UV};) = \int_0^Z d! !^N S(!;) : \quad (2.58)$$

The dependence of these moments on the renormalization scale μ is controlled by the evolution equation (2.37). In addition, the moments depend on the lower cutoff on the $!$ integral. The choice of μ_{UV} is a matter of convenience, and so we are free to pick a value that is numerically (if not parametrically) large compared with μ_{QCD} . In this case, as we will now show, the dependence on μ_{UV} can also be controlled using short-distance methods.

For sufficiently large values of μ_{UV} it is possible to expand the moments $M_N(\mu_{UV};)$ in a series of B-meson matrix elements of local HQET operators. If for simplicity we set $\alpha_s = 1$ in the shape-function operator (which is legitimate,

since the Dirac structure is unaltered in HQET), the operators in question are Lorentz-scalar, "leading-twist" operators containing $\bar{h}::h$ [15, 17]. These are the operators that mix with $\bar{h}(\text{in } D^N)h$ under renormalization. It is straightforward to find the corresponding operators of a given dimension. The unique dimension-3 operator is $\bar{h}h$. The two operators of dimension 4 are $\bar{h}\text{in } D h$ (class-1) and $\bar{h}\text{iv } D h$ (class-2). The class-2 operator vanishes by the HQET equation of motion. The possible dimension-5 operators are

$$\begin{aligned} \text{class-1: } & \bar{h}(\text{in } D^2 h; \bar{h}(\text{id } \gamma) ^2 h; \\ \text{class-2: } & \bar{h}(\text{iv } D^2 h; \bar{h}\text{in } D \text{iv } D h, \bar{h}\text{iv } D \text{in } D h; \end{aligned} \quad (2.59)$$

where again the class-2 operators vanish by the equation of motion. Moreover, it follows from the Feynman rules of HQET that the two class-1 operators do not mix under renormalization, so the operator $\bar{h}(\text{id } \gamma) ^2 h$ can be ignored. From dimension 6 on the situation is more complicated, because several class-1 operators exist that can mix with $\bar{h}(\text{in } D^N)h$. For $N = 3$ these are of the form $\bar{h}\text{id } G h$ or $\bar{h}\text{id } q::qq::h$, where we omit Lorentz and color indices. We will restrict our discussion to operators of dimension less than 6.

For the operator product expansion of the moments in (2.58) we need the forward matrix elements

$$\langle h | i = \frac{\bar{h}B(v)\gamma_0 \beta(v)i}{2M_B} \quad (2.60)$$

of the leading-twist operators between B-meson states in HQET. Using the equation of motion, it can be shown that $\langle \bar{h}h | i = 1$, $\langle \bar{h}\text{in } D h | i = 0$, and $\langle \bar{h}(\text{in } D^2)h | i = 1/3$ [15]. We can thus write an expansion of the form

$$M_N(\bar{u}v; i) = \sum_{UV} K_0^{(N)}(\bar{u}v; i) + K_2^{(N)}(\bar{u}v; i) \left(\frac{1}{3} \frac{1}{\bar{u}v} + O\left(\frac{QCD}{\bar{u}v}\right) \right) : \quad (2.61)$$

This expansion is useful as long as the cutoff $\bar{u}v$ is chosen much larger than the typical hadronic scale characterizing the matrix elements of the local operators. The matching coefficients $K_n^{(N)}$ in this relation can be calculated using on-shell external b-quark states with residual momentum k . For operators of dimension up to 5 it suffices to calculate two-point functions. (Three and four-point functions would have to be considered at dimension 6.) We first evaluate the moments of the renormalized shape function in (2.34), finding at one-loop order

$$\begin{aligned} M_N^{\text{parton}}(\bar{u}v; i) & \quad (2.62) \\ &= (n - K) \frac{1}{2} \left[\frac{C_F}{s} \ln^2 \frac{\bar{u}v + n}{k} + \ln \frac{\bar{u}v + n}{k} + \frac{2}{24} \right. \\ & \quad \left. + \frac{C_F}{s} \sum_{j=1}^N \frac{1}{j} \left(1 + 2 \ln \frac{\bar{u}v + n}{k} \right) \frac{2}{1} \left(\frac{\bar{u}v}{n} \right)^j \frac{1}{k} \right] : \end{aligned}$$

We then expand this result in powers of $n = k_{UV}$. Keeping the first three terms in the expansion, we obtain

$$\begin{aligned}
M_0^{\text{parton}}(UV; k) &= 1 - \frac{C_F s}{24} \ln^2 \frac{UV}{k^2} + \ln \frac{UV}{k^2} + \frac{1}{24} \\
&\quad - \frac{C_F s}{24} \frac{n}{UV} k^2 \ln \frac{UV}{k^2} + 1 + \frac{(n-k^2)}{24 UV} \ln \frac{UV}{k^2} + \frac{1}{24} + \dots; \\
M_1^{\text{parton}}(UV; k) &= n - k^2 \left[-\frac{C_F s}{24} \ln^2 \frac{UV}{k^2} - \ln \frac{UV}{k^2} + \frac{1}{24} \right] \\
&\quad - \frac{C_F s}{24} \frac{n}{UV} \left[2 \ln \frac{UV}{k^2} + 1 \right] + \frac{(n-k^2)}{24 UV} \left[2 \ln \frac{UV}{k^2} + 1 \right] + \dots; \\
M_2^{\text{parton}}(UV; k) &= (n-k^2) \left[-\frac{C_F s}{24} \ln^2 \frac{UV}{k^2} - 2 \ln \frac{UV}{k^2} + \frac{1}{24} \right] \\
&\quad - \frac{C_F s}{24} \frac{n}{UV} \left[\ln \frac{UV}{k^2} + n - k_{UV} \left[2 \ln \frac{UV}{k^2} + 3 \right] + \dots \right];
\end{aligned} \tag{2.63}$$

In the next step, we calculate the one-loop matrix elements of the local operators h (in D^N) h between heavy-quark states with residual momentum k . The relevant diagrams are the same as in Figure 2.2, where now the black square represents the local operators. Keeping $v = k$ non-zero to regularize infra-red singularities, we obtain for the bare matrix elements

$$\begin{aligned}
\langle h | (in D^N) h | i \rangle &= (n-k^2) \left[1 - \frac{4C_F g_s^2}{(4\pi)^2} \left(\sum_{j=1}^{X^N} \frac{N}{j} \frac{2v \cdot k^j}{n \cdot k} \right) \right] \\
&\quad (j=1) \quad (j=2) \quad (2-j) \tag{2.64}
\end{aligned}$$

While the individual diagrams are infra-red divergent, taking the limit $v = k \rightarrow 0$ in the sum of all contributions is possible without encountering singularities. Then the one-loop contributions vanish, and the matrix elements simply reduce to their tree-level values. In other words, the one-loop contributions correspond to a mixing with class-2 operators, whose hadronic matrix elements vanish by the equations of motions. It follows that in (2.63) we must identify $(n-k^2) \rightarrow \langle h | (in D^N) h | i \rangle$. Substituting the results for the HQET matrix elements given earlier, we obtain for the Wilson coefficients of the first three moments

$$\begin{aligned}
K_0^{(0)} &= 1 - \frac{C_F s}{24} \ln^2 \frac{UV}{k^2} + \ln \frac{UV}{k^2} + \frac{1}{24}; \quad K_2^{(0)} = \frac{C_F s}{24} \ln \frac{UV}{k^2} - \frac{1}{24}; \\
K_0^{(1)} &= \frac{C_F s}{24} \left[2 \ln \frac{UV}{k^2} - 1 \right]; \quad K_2^{(1)} = -2 \frac{C_F s}{24} \ln \frac{UV}{k^2}; \\
K_0^{(2)} &= \frac{C_F s}{24} \ln \frac{UV}{k^2}; \quad K_2^{(2)} = 1 - \frac{C_F s}{24} \ln^2 \frac{UV}{k^2} - 2 \ln \frac{UV}{k^2} + \frac{1}{24} - \frac{1}{24};
\end{aligned} \tag{2.65}$$

At tree level, this reproduces the naive moment relations mentioned at the beginning of this section. Beyond tree level, the moments get corrected by calculable short-distance effects, which can be controlled using fixed-order perturbation theory as long as the ratio $\mu_{UV} = \mu/\mu_{UV}$ is of $O(1)$. In particular, the renormalized first moment no longer vanishes, but is proportional to the cutoff μ_{UV} up to small power corrections.

As mentioned earlier, the value of the first moment is connected with the definition of the heavy-quark mass (see also [34, 35]). The first moment of the renormalized shape function can be made to vanish to all orders in perturbation theory by choosing an appropriate scheme for the definition of m_b . So far our calculations have assumed the definition of the heavy-quark mass as a pole mass, m_b^{pole} , which is implied by the HQET equation of motion $\bar{D}h = 0$. Results such as (2.65) are valid in this particular scheme. A more general choice is to allow for a residual mass term m in HQET, such that $\bar{D}h = mh$ with $m = O_Q(\text{CD})$ [36]. It is well known that the pole mass is an ill-defined concept, which suffers from infra-red renormalon ambiguities [37, 38]. The parameter $\mu_{\text{pole}} = M_B - m_b^{\text{pole}}$, which determines the support of the shape function in the pole-mass scheme, inherits the same ambiguities. It is therefore advantageous to eliminate the pole mass in favor of some short-distance mass. For the analysis of inclusive B -meson decays, a proper choice is to use a so-called low-scale subtracted heavy-quark mass $m_b(\mu_f)$ [39], which is obtained from the pole mass by removing a long-distance contribution proportional to a subtraction scale $\mu_f = \mu_{\text{CD}}$,

$$m_b^{\text{pole}} = m_b(\mu_f) + \mu_f g_s(\mu_f); \quad \mu_{\text{pole}} = m_b(\mu_f) + m; \quad (2.66)$$

As long as $m_b(\mu_f)$ is defined in a physical way, the resulting perturbative expressions after elimination of the pole mass are well-behaved and not plagued by renormalon ambiguities. Replacing the pole mass by the physical mass shifts the values of n , k and $!$ by an amount m , since $n_b^{\text{pole}}(m\nu + k) = m_b(\mu_f) + (n - k + m)$, and because the covariant derivative in the definition of the shape function in (2.12) must be replaced by $\bar{D} \rightarrow \bar{D} - m$ [36]. At the same time $\mu_{\text{pole}} = (\mu_f) - m$, where $(\mu_f) = M_B - m_b(\mu_f)$ is a physical parameter. Note that this leaves the parameter $\hat{\mu} = \mu_{\text{pole}}/!$ and hence the shape function $\hat{S}(\hat{\mu}; \nu)$ invariant. This follows since $\mu_{\text{pole}}/!_{\text{pole}} = (\mu_f)/(!_{\text{pole}} + m)$, where $!_{\text{pole}}$ denotes the value in the pole-mass scheme used so far.

2.5.2 Shape-function moments in a physical scheme

From now on we will adopt a mass scheme defined by some specific choice of m . Let us denote by $! = !_{\text{pole}} + m$ the value of the light-cone momentum variable in that scheme and define "physical" moments M_N^{phys} as in (2.58), but with all parameters replaced by their values in the new scheme, in particular $\mu = (\mu_f)$. Then the expressions for the moments in (2.62) and (2.63) change according to the replacements $n - k \rightarrow n - k + m$ and $! \rightarrow !_{\text{pole}} + m$ everywhere. We now choose

such that the first moment vanishes, thereby defining a low-scale subtracted heavy-quark mass (with $\mu_f = \mu_{UV}$) to all orders in perturbation theory. We will refer to this mass as the "shape-function mass" m_b^{SF} . This is a "physical", short-distance mass in the sense that it is free of renormalon ambiguities. (However, the definition of the shape-function mass depends on the renormalization scheme used to define the shape function.) From (2.63) and (2.66), it follows that at one-loop order

$$m_b^{\text{pole}} = m_b^{SF}(\mu_f; \mu_f) + \mu_f \frac{C_F s(\mu_f)}{3} \left[1 - 2 \ln \frac{\mu_f}{\mu_{UV}} + \frac{2}{3} \left(\frac{1}{\mu_f^2} \right) \ln \frac{\mu_f}{\mu_{UV}} + \dots \right] : \quad (2.67)$$

Note that after introduction of the shape-function mass the coefficients $K_n^{(1)}$ in the operator-product expansion for the moments in (2.61) vanish by definition. However, to first order in μ_s the values for the coefficients $K_n^{(0)}$ and $K_n^{(2)}$ of the zeroth and second moments given in (2.65) remain unchanged, since $m = O(\mu_s)$. This would no longer be true for the coefficients of higher moments.

The shape-function mass can be related to any other short-distance mass using perturbation theory. For instance, at one-loop order its relations to the potential-subtracted mass introduced in [40] and to the kinetic mass defined in [41, 42] read

$$m_b^{SF}(\mu_f; \mu_f) = m_b^{PS}(\mu_f) = m_b^{\text{kin}}(\mu_f) + \mu_f \frac{C_F s(\mu_f)}{3} : \quad (2.68)$$

Note that, in addition to the dependence on the subtraction scale μ_f , the shape-function mass depends on the scale at which the shape function is renormalized. While it is natural to set $\mu = \mu_f$, as we did here, this is not necessary. Given a value for the shape-function mass for some choice of scales, we can solve (2.67) to obtain its value for any other choice, using the fact that the pole mass is scale independent.

Proceeding in an analogous way, we can use the second moment to define a physical kinetic-energy parameter, commonly called μ^2 . This quantity can be used to replace the HQET parameter μ_1 , which like the pole mass suffers from infra-red renormalon ambiguities [43, 44]. At one-loop order, we obtain

$$\begin{aligned} \frac{\mu^2(\mu_{UV}; \mu_f)}{3} &= \frac{M_2^{\text{phys}}(\mu_{UV}; \mu_f)}{M_0^{\text{phys}}(\mu_{UV}; \mu_f)} \\ &= \frac{C_F s(\mu_f)}{3} \frac{2}{\mu_{UV}} \ln \frac{\mu_{UV}}{\mu_f} + \frac{1}{3} \left(\frac{1}{\mu_f^2} \right) \left[1 + \frac{C_F s(\mu_f)}{3} \ln \frac{\mu_{UV}}{\mu_f} + \frac{1}{2} \right] + \dots : \end{aligned} \quad (2.69)$$

Taking the ratio of M_2^{phys} and M_0^{phys} has the advantage of eliminating the double logarithmic radiative corrections from this expression. Our definition is similar to the running parameter μ^2 defined in the kinetic scheme [41, 42]. At one-loop order, the two parameters are related by

$$\mu^2(\mu_f; \mu_f) = \frac{2}{\mu_f} \frac{C_F s(\mu_f)}{3} + [\mu^2(\mu_f)]_{\text{kin}} \left[1 + \frac{C_F s(\mu_f)}{2} \right] : \quad (2.70)$$

Given a value for the kinetic energy in the shape-function scheme for some choice of scales, we can solve (2.69) to obtain its value for any other choice, using that μ_1 is scale independent.

Similarly, each new moment of the renormalized shape function can be used to define a new physical, scale-dependent parameter

$$A_N(\mu_{UV};) = M_N^{\text{phys}}(\mu_{UV};) = M_0^{\text{phys}}(\mu_{UV};);$$

which coincides with the corresponding HQET parameter $A_N = \langle h(\mu_{UV})^N \rangle$ at tree level, and which beyond tree level is related to HQET parameters through well-controlled perturbative expressions. Obviously, the presence of power divergences implies that higher moments are progressively less sensitive to HQET parameters, since they are dominated by the perturbative terms of order $\mu_s^N \mu_{UV}^N$.

2.5.3 Moments of the scheme-independent function $\hat{S}(\mu;)$

It will be useful to rewrite the moment relations derived above in terms of the variable $\mu = \mu_s$, which is invariant under redefinitions of the heavy-quark mass. Defining a new set of scheme-independent moments

$$\hat{M}_N(\mu;)=\int_0^{\mu_s+\mu_{UV}}d\mu\mu^N\hat{S}(\mu;); \quad (2.71)$$

we obtain

$$\begin{aligned} \hat{M}_0(\mu;)&=1-\frac{C_F\mu_s(\mu)}{2}\ln^2\frac{\mu}{\mu_s}+\ln\frac{\mu}{\mu_s}+\frac{\mu^2}{24} \\ &+\frac{C_F\mu_s(\mu)}{2}\ln\frac{\mu}{\mu_s}-\frac{1}{2}\frac{\mu^2(\mu;)}{3\mu_s^2}+:::; \\ \frac{\hat{M}_1(\mu;)}{\hat{M}_0(\mu;)}&=\mu(\mu;); \quad \frac{\hat{M}_2(\mu;)}{\hat{M}_0(\mu;)}=\frac{\mu^2(\mu;)}{3}+\mu(\mu;)^2; \end{aligned} \quad (2.72)$$

where the parameters $\mu(\mu;)=M_B-m_b^{\text{SF}}(\mu;)$ and $\mu^2(\mu;)$ should be considered as known physical quantities. Using the relations in the previous subsection, we have

$$\begin{aligned} m_b^{\text{SF}}(\mu;)&=m_b^{\text{SF}}(\mu;)+\frac{C_F\mu_s(\mu)}{2}\ln^2\frac{\mu}{\mu_s}+\ln\frac{\mu}{\mu_s}+\frac{\mu^2}{24} \\ &+\frac{C_F\mu_s(\mu)}{2}\ln\frac{\mu}{\mu_s}-\frac{1}{2}\frac{\mu^2(\mu;)}{3\mu_s^2}+\mu(\mu;)^2; \\ \mu^2(\mu;)&=\mu^2(\mu;)-\frac{C_F\mu_s(\mu)}{2}+\frac{C_F\mu_s(\mu)}{2}\ln^2\frac{\mu}{\mu_s}+\ln\frac{\mu}{\mu_s} \\ &+\frac{1}{2}\frac{\mu^2(\mu;)}{3\mu_s^2}+\mu(\mu;)^2; \end{aligned} \quad (2.73)$$

where μ_f denotes the scale at which initial values for the two parameters are obtained, for instance using relations such as (2.68) and (2.70). These relations are particularly simple if one chooses $\mu_f = \mu_s$.

In the relations above we have eliminated the unphysical HQET parameter μ_1 in favor of the physical parameter μ_s defined in the shape-function scheme. At first sight, this seems to threaten the convergence of the operator product expansion. For instance, the term proportional to μ_s^{-2} in the expression for the zeroth moment \hat{M}_0 in (2.72) contains a leading-power perturbative contribution of order $\alpha_s^2(\mu_s)$, and similar contributions would arise from all other terms in the expansion. These contributions would have to be subtracted from the Wilson coefficient of the first term, if this coefficient were computed to two-loop order. The overall convergence of the operator product expansion is unaffected by this reorganization of perturbative corrections.

2.5.4 Asymptotic behavior of the shape function

The fact that for sufficiently large values of the cutoff the moments of the shape function can be calculated using an operator-product expansion implies that a similar expansion can be used to obtain a model-independent description of the asymptotic behavior of the shape function. Taking the derivative of the zeroth moment \hat{M}_0 in (2.71) with respect to μ_f , one obtains

$$\hat{S}(\mu_f; \mu_s) = 1 - \frac{d \ln b^{SF}(\mu_f; \mu_s)}{d \ln \mu_f} \hat{M}_0(\mu_f; \mu_s) : \quad (2.74)$$

This relation can be trusted as long as $\mu_f \gg \mu_{QCD}$. It allows us to determine the behavior of the shape function for large values of μ_f . From (2.72) we find at one-loop order

$$\begin{aligned} \hat{S}(\mu_f; \mu_s) = & \frac{C_F \alpha_s(\mu_s)}{\mu_f} \frac{1}{\mu_f} - 2 \ln \frac{\mu_f}{\mu_s} + 1 \\ & + \frac{2}{3} \frac{\alpha_s^2(\mu_s)}{(\mu_f)^2} \ln \frac{\mu_f}{\mu_s} - 1 + \dots : \end{aligned} \quad (2.75)$$

The precise definitions of μ_s and μ_f are not specified at this order. (Note that the shape function cannot depend on the value of the cutoff μ_f .) We have checked that this asymptotic behavior of the shape function is consistent with the evolution equation (2.57) when expanded to first order in α_s .

Relation (2.75) is a model-independent result as long as $\mu_f \gg \mu_{QCD}$. We stress the remarkable fact that this radiative tail of the shape function is negative, in contrast with the naive expectation based on a probabilistic interpretation of the shape function as a momentum distribution function. The point is that the definition of the renormalized shape function requires scheme-dependent ultra-violet subtractions. From (2.75) it follows that the shape function must have a zero, which for sufficiently large μ_s is located at a value $\mu_{f0} = \mu_s e^{-\frac{3}{2C_F}}$.

2.6 Conclusions

The hadronic physics governing the inclusive semileptonic decay $B \rightarrow X_u l$ is encoded in the structure functions \tilde{W}_i appearing in the Lorentz decomposition of the hadronic tensor W in (2.16). In the shape-function region, only two combinations of these functions are required at leading order in $Q_{CD} = m_b$. They follow from the factorization formula (2.13) using the explicit results for the hard functions H_{ij} and the jet function J derived in this chapter. Explicitly, we obtain at next-to-leading order in renormalization-group improved perturbation theory

$$\begin{aligned} \tilde{W}_1 &= U_Y(\mu_h; \mu_i) \left[1 + \frac{C_F \alpha_s(\mu_h)}{4} \left(4 \ln^2 \frac{\mu_b}{\mu_h} + 10 \ln \frac{\mu_b}{\mu_h} - 4 \ln y - \frac{2 \ln y}{1-y} \right) \right. \\ &\quad \left. + 4 L_2(1-y) - \frac{2}{6} \int_0^1 d\hat{t} \mu_b J(\mu_b(P_+ - \hat{t}); \mu_i) \hat{S}(\hat{t}; \mu_i) + \dots \right] \\ \tilde{W}_4 + \frac{1}{y} \tilde{W}_5 &= U_Y(\mu_h; \mu_i) \frac{C_F \alpha_s(\mu_h)}{4} \frac{2 \ln y}{1-y} \\ &\quad + \int_0^1 d\hat{t} \mu_b J(\mu_b(P_+ - \hat{t}); \mu_i) \hat{S}(\hat{t}; \mu_i) + \dots; \end{aligned} \quad (2.76)$$

where the dots represent power corrections in $Q_{CD} = m_b$.

In all our results, m_b denotes the heavy-quark mass defined in the "shape-function scheme" introduced in Section 2.5. The jet function $J(\mu_b(P_+ - \hat{t}); \mu_i)$ at an intermediate hard-collinear scale $\mu_i = m_b / Q_{CD}$ can be calculated in fixed-order perturbation theory. The relevant expression valid at one-loop order is given in (2.27). The above results contain the renormalization-group function $U_Y(\mu_h; \mu_i)$, which arises in the solution of evolution equations discussed in Section 2.4. Our results are formally independent of the precise choice of high-energy matching scale $\mu_h = m_b$. The numerical effect of the residual μ_h dependence remaining after truncation of the perturbative expansion has been studied in [26] and was found to be small.

The function $\hat{S}(\hat{t}; \mu_i)$ in (2.76) is the shape function after the transformation of variables from z to $\hat{t} = \mu_b z$. The limits of integration for the variable \hat{t} (i.e., $0 \leq \hat{t} \leq P_+$) are set by hadronic kinematics and are independent of the definition of the heavy-quark mass. The shape function is a non-perturbative object, which at present cannot be predicted from first principles. It enters our results (2.76) renormalized at the intermediate hard-collinear scale μ_i . In (2.57), we have presented an analytic formula (valid at all orders in renormalization-group improved perturbation theory) that relates the shape function at a high scale to the shape function renormalized at a low hadronic scale. Many properties of the shape function that were so far unknown have been derived in Section 2.5. In particular, we have given explicit formulae relating the moments of the shape function to HQET parameters, and we have proved that the shape function has a negative tail for large values of \hat{t} , whose explicit form can be calculated using

an operator product expansion. These new insights about the shape function will be very helpful in constructing a realistic model for the function $\hat{S}(\not{p}; \not{v})$, which can then be refined by tuning it to experimental data such as the photon energy spectrum in inclusive $B \rightarrow X_s \gamma$ decays.

Chapter 3

Non-Perturbative Corrections

3.1 Introduction

In the previous chapter we have seen how to incorporate leading order perturbative corrections to $B \rightarrow X_u l$. Corrections suppressed by a power of $\alpha_{\text{QCD}} = m_b$ are considered the second largest source of uncertainty for inclusive charmless B decays. The present chapter is devoted to a more thorough study of power corrections to inclusive B decays distributions in the shape-function region, using the two-step matching procedure.

In a first step, hard fluctuations are integrated out by matching the QCD currents onto soft-collinear effective theory (SCET) [21, 23]. The current correlator is then expanded in terms of light-cone operators in heavy-quark effective theory (HQET) [11], thereby integrating out fluctuations at the hard-collinear scale. The fact that the relevant HQET operators live on the light cone follows from the structure of the multipole expansion of soft fields in SCET. We carry out the matching procedure at tree level and to order $\alpha_{\text{QCD}} = m_b$ in the heavy-quark expansion. We indicate how our results would change if loop corrections were included.

3.2 Short-distance expansion of the hadronic tensor

SCET is the appropriate effective field theory for the description of the interactions among soft and hard-collinear degrees of freedom. Its Lagrangian is organized in an expansion in powers of $\frac{1}{p_-}$. The leading-order Lagrangian is

$$\begin{aligned} L_{\text{SCET}}^{(0)} = & \frac{\not{v}}{2} \text{tr} \left[\bar{\psi}_{\text{hc}} + g n \cdot A_s(x) + i \not{D}_{\text{hc}} \frac{1}{i \not{D}_{\text{hc}}} i \not{D}_{\text{hc}} \right. \\ & \left. + q i \not{D}_s q + h i \not{v} \cdot D_h + L_{\text{YM}}^{(0)} \right]; \end{aligned} \quad (3.1)$$

where ψ_{hc} is a hard-collinear quark field, q is a soft, massless quark field, h is a heavy-quark field defined in HQET, A_s is a soft gluon field, and $i \not{D}_{\text{hc}} = i \not{\partial} + g A_{\text{hc}}$ is the covariant derivative containing a hard-collinear gluon field. All fields in the above Lagrangian are evaluated at point x , except for the soft gluon field in the first term, which is evaluated at $x = \frac{1}{2}(n \cdot x)n$. The explicit form of the leading-order Yang-Mills Lagrangian can be found in [23, 24].

The terms up to second order in the expansion in $\frac{1}{p_-}$ are

$$\begin{aligned} L_{\text{SCET}}^{(1)} &= L^{(1)} + L_q^{(1)} + L_{\text{YM}}^{(1)}; \\ L_{\text{SCET}}^{(2)} &= L^{(2)} + L_q^{(2)} + L_h^{(2)} + L_{\text{YM}}^{(2)}; \end{aligned} \quad (3.2)$$

where

$$L_h^{(2)} = \frac{1}{2m_b} \text{tr} \left[(i \not{D}_s)^2 h + \frac{C_{\text{mag}}}{2} h \not{G}_s h \right] \quad (3.3)$$

is the next-to-leading term in the expansion of the HQET Lagrangian [11]. Expressions for the remaining Lagrangian corrections have been presented in [23].

While it is consistent to apply a perturbative expansion at the hard and hard-collinear scales, the soft-gluon couplings to hard-collinear fields are non-perturbative and must be treated to all orders in the coupling constant. For instance, the hard-collinear quark propagator derived from (3.1) should be taken to be the propagator in the background of the soft gluon field, summing up arbitrarily many insertions of the field A_s . The most convenient way of achieving this summation is to decouple the leading-order interactions between the soft gluon field and hard-collinear fields in (3.1) with the help of a field redefinition, under which [21, 45]

$$\psi(x) = S(x) \psi^{(0)}(x); \quad A_{hc}(x) = S(x) A_{hc}^{(0)}(x) S^\dagger(x); \quad (3.4)$$

where

$$S(x) = P \exp \left[ig \int_0^1 dt n \cdot A(x + tn) \right] \quad (3.5)$$

is a soft Wilson line along the n direction. Introducing the new fields into the Lagrangian yields

$$\mathcal{L}^{(0)} = \bar{\psi}^{(0)} \left[\not{D}_{hc}^{(0)} + i \not{D}_{?hc}^{(0)} \frac{1}{\not{D}_{hc}^{(0)}} i \not{D}_{?hc}^{(0)} \right] \psi^{(0)}; \quad (3.6)$$

and similarly all interactions between soft and hard-collinear gluon fields are removed from the Yang-Mills Lagrangian $\mathcal{L}_{YM}^{(0)}$. The propagator of the new hard-collinear quark field is now given by the simple expression

$$\langle \psi(x) \bar{\psi}(y) \rangle = \not{n} \int \frac{d^4 p}{(2\pi)^4} \frac{1}{p^2 + i0} e^{-ip \cdot (x-y)}; \quad (3.7)$$

The effect of soft-gluon attachments is taken into account by factors of the Wilson line S in the results below.

We now list the expressions for the subleading corrections to the SCET Lagrangian in terms of the redefined fields, using the formalism of gauge-invariant building blocks [46]. We define

$$X = W^\dagger \psi^{(0)}; \quad A_{hc} = W^\dagger (i D_{hc}^{(0)} W); \quad (3.8)$$

where

$$W = P \exp \left[ig \int_0^1 dt n \cdot A_{hc}^{(0)}(x + tn) \right] \quad (3.9)$$

is a hard-collinear Wilson line. These "calligraphic" fields are invariant under both hard-collinear and soft gauge transformations. Note that in the light-cone gauge,

in $A_{hc}^{(0)} = 0$, we simply have $X = A_{hc}^{(0)}$ and $A_{hc} = gA_{hc}^{(0)}$. In terms of these fields, the results compiled in [23] take the form

$$\begin{aligned}
L^{(1)} &= X \frac{\not{D}}{2} x_? n \cdot S^y g G \cdot S_x X ; \\
L^{(2)} &= X \frac{\not{D}}{2} \frac{n \cdot x}{2} n \cdot S^y g G \cdot S_x + \frac{x_? x_?}{2} n \cdot S^y \not{D} ; g G \cdot S_x X \\
&+ X \frac{\not{D}}{2} i \not{D}_{?hc} \frac{1}{in} \frac{x_?}{2} \cdot S^y g G \cdot S_x \\
&+ \frac{x_?}{2} \cdot S^y g G \cdot S_x \frac{1}{in} i \not{D}_{?hc} X ; \\
L_q^{(1)} &= (qS)_x i \not{D}_{?hc} X + h.c. ; \tag{3.10}
\end{aligned}$$

where $i \not{D}_{hc} = i \not{D} + A_{hc}$, and we have dropped the subscript "s" on the soft covariant derivative and field strength. The expression for $L_q^{(2)}$ will not be needed for our analysis. The notation $(:::)_x$ indicates that, in interactions with hard-collinear fields, soft fields are multipole expanded and live at position x , whereas hard-collinear fields are always evaluated at position x . Because the SCET Lagrangian is not renormalized [23], the above expressions are valid to all orders in perturbation theory.

Next, we need the expressions for heavy-light current operators in SCET. In general, a QCD current $q \cdot b$ matches onto

$$q(x) \cdot b(x) = e^{im_b v \cdot x} J_A^{(0)} + J_A^{(1)} + J_A^{(2)} + J_B^{(1)} + J_B^{(2)} + ::: ; \tag{3.11}$$

where we distinguish between type-A "two-particle" operators and type-B "three-particle" operators [47]. The operators arising at tree level are [23, 47, 48]

$$\begin{aligned}
J_A^{(0)} &= X \cdot S^y h_x ; \\
J_A^{(1)} &= X \cdot x_? \cdot S^y \not{D} \cdot h_x + X \frac{\not{D}}{2} i \not{D}_{?} \frac{1}{in} \not{D} \cdot S^y h_x ; \\
J_A^{(2)} &= X \cdot \frac{n \cdot x}{2} S^y n \cdot \not{D} h_x + \frac{x_? x_?}{2} S^y \not{D} \cdot \not{D} h_x + S^y \frac{i \not{D}}{2m_b} h_x \\
&+ X \frac{\not{D}}{2} i \not{D}_{?} \frac{1}{in} \not{D} \cdot x_? \cdot S^y \not{D} \cdot h_x ; \tag{3.12}
\end{aligned}$$

and

$$\begin{aligned}
J_B^{(1)} &= X \frac{\not{n}}{2} \not{A}_{?hc} \frac{1}{\text{in } \mathcal{Q}} S^y h_x X \frac{\not{n}}{2m_b} \not{A}_{?hc} S^y h_x ; \\
J_B^{(2)} &= X \left[\frac{1}{\text{in } \mathcal{Q}} + \frac{\not{n}}{2m_b} n \cdot \not{A}_c \right] S^y h_x \\
&\quad X \frac{\not{n}}{2} \not{A}_{?hc} \frac{1}{\text{in } \mathcal{Q}} + \frac{\not{n}}{2m_b} \not{A}_{?hc} x_{?} S^y D h_x \\
&\quad X \frac{1}{\text{in } \mathcal{Q}} \frac{(i \not{D}_{?hc} \not{A}_{?hc})}{m_b} S^y h_x \\
&\quad + X \frac{i \not{D}_{?hc}}{m_b} \frac{1}{\text{in } \mathcal{Q}} \frac{\not{n}}{2} \frac{\not{n}}{2} \not{A}_{?hc} S^y h_x :
\end{aligned} \tag{3.13}$$

The expressions for the currents beyond tree level are more complicated, primarily because several new Dirac structures appear. The relevant formulae are known at leading [21] and next-to-leading order [47] in the power expansion. The corresponding results for the currents $J_A^{(2)}$ and $J_B^{(2)}$ have not yet been derived. They would be needed if the analysis in this chapter should be extended beyond tree level.

If perturbative corrections at the hard-collinear scale are neglected, the hard-collinear gluon fields can be dropped, and the above expressions for the effective Lagrangians and currents simplify. In this approximation $X \rightarrow 1^{(0)}$, $A_{hc} \rightarrow 0$, $iD_{hc} \rightarrow i\mathcal{Q}$, and $J_B^{(n)} \rightarrow 0$. While this leads to great simplifications in the calculation, we stress that the structures of soft fields that arise do not simplify. We find operators containing $S^y g G_S, S^y D_{?g} G_S, S^y h, S^y D h$, and $S^y D D h$, and the same operators would arise if the calculation was extended beyond the tree approximation. The only exception is that we no longer retain Lagrangian corrections containing the soft quark field, because $L_q^{(1)} \rightarrow 0$ in the limit where the hard-collinear gluon field is neglected. (The term $qS i \not{D}_{?}^{(0)}$ is forbidden by momentum conservation.) In Section 3.5, we analyze the subleading shape functions introduced at $O(\Lambda_s)$ by two insertions of $L_q^{(1)}$.

With all the definitions in place, we are now ready to evaluate the current correlator T_{ij} including terms of up to second order in Λ_s , working at lowest order in Λ_b at the hard and hard-collinear scales. The leading term is readily found to be

$$T_{ij}^{(0)} = \int d^4x e^{i(q - m_b v) \cdot x} \int \frac{d^4p}{(2\pi)^4} e^{ip \cdot \frac{n}{p^2 + i} p} h S_0 \cdot i \frac{\not{n}}{2} j S^y h_x : \tag{3.14}$$

First-order corrections in Λ_s vanish by rotational invariance in the transverse plane (provided we choose the coordinate system such that $v_{?} = 0$ and $q_{\perp} = 0$), i.e., $T_{ij}^{(1)} = 0$. At second order in the expansion the correlator receives several contributions, which can be represented symbolically as

$$J^{y(2)} J^{(0)} ; J^{y(1)} J^{(1)} ; J^{y(0)} J^{(2)} ; \tag{3.15}$$

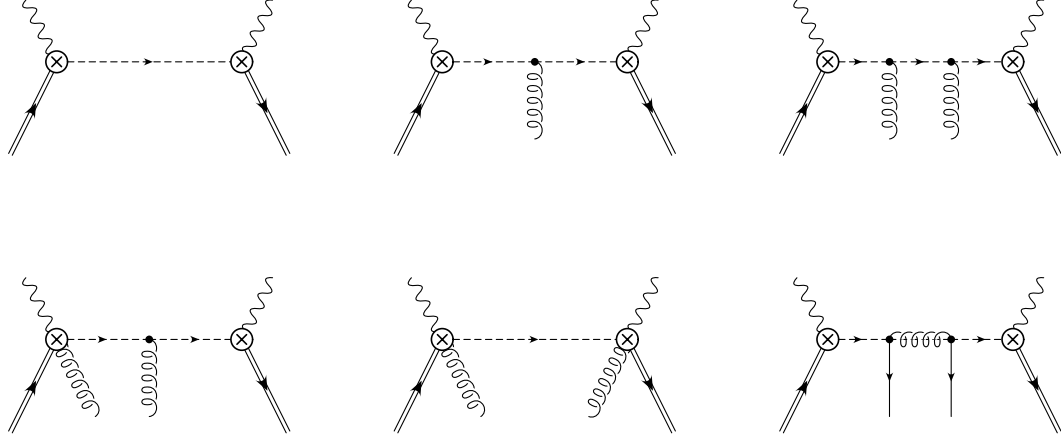


Figure 3.1: Representative examples of time-ordered products contributing to the current correlator T_{ij} in SCET. Double lines show heavy-quark fields, dashed ones hard-collinear fields, and wavy lines denote the external currents. Lagrangian insertions and higher-order effective current operators are exemplified by soft gluons.

$$J^{Y(1)} J^{(0)} \int d^4 z L^{(1)}; \quad J^{Y(0)} J^{(1)} \int d^4 z L^{(1)}; \quad J^{Y(0)} J^{(0)} \int d^4 z L^{(2)} + L_h^{(2)}; \quad (3.16)$$

and

$$J^{Y(0)} J^{(0)} \int d^4 z L^{(1)} \int d^4 w L^{(1)}; \quad (3.17)$$

where at tree level only the type-A current operators appear. Examples of these time-ordered products are depicted in Figure 3.1. At $O(\alpha_s)$, one must include a tree-level contribution of the form

$$J^{Y(0)} J^{(0)} \int d^4 z L_q^{(1)} \int d^4 w L_q^{(1)}; \quad (3.18)$$

shown by the last diagram in the figure. Beyond tree level, one would also have to include the contributions from the type-B current operators.

Because the external B-meson states in the definition of the hadronic tensor contain only soft constituents, and because the hard-collinear fields have been decoupled from the soft fields in the leading-order SCET Lagrangian (3.6), it is possible to contract all hard-collinear fields in the time-ordered products. At tree level, all we need is the hard-collinear quark propagator (3.7). Derivatives acting on hard-collinear fields give powers of p in momentum space, whereas components of x appearing in the multipole-expanded expressions for the effective Lagrangians and currents can be turned into derivatives $\partial = \partial/p$ acting on the momentum-space amplitudes. Each insertion of a SCET Lagrangian correction introduces an integral over soft fields located along the light-cone. Consequently, the time-ordered products in (3.15) lead to expressions involving bi-local operators as in (3.14), while those in (3.16), (3.17), and (3.18) also lead to tri- and quadri-local operators. At

At first sight, this would seem to require the introduction of complicated subleading shape functions depending on up to three momentum variables $!_i$, defined in terms of the Fourier transforms of the matrix elements of the non-local operators. However, the non-localities can be reduced using partial-fraction identities for the resulting hard-collinear quark propagators. At tree level, it suffices to define shape functions of a single variable $!_+$.

To see how this works, consider the effect of an insertion of the Lagrangian $L^{(1)}$ in (3.10). Since all hard-collinear fields must be contracted, we may consider without loss of generality the expression

$$L(Y_1; Y_2) = i \int d^4 z \int \frac{d^4 z'}{2} (Y_1 - z) \not{z}' \not{z} \int \frac{d^4 z''}{2} S^Y G S_{z''} (z - \underline{y}) : \quad (3.19)$$

The fact that the soft fields live at position z implies that the two hard-collinear quark propagators carry the same momentum components n_+ and p_+ . In analogy with the definition of the hard-collinear calligraphic gluon field, we now introduce the soft field [46]

$$A_s(x) = S^Y(x) (iD - S)(x) = \int \frac{d^4 t}{2} \not{t} n_+ S^Y G S_{x+t} ; \quad (3.20)$$

which allows us to write $(S^Y G S)_{z''}$ as a derivative, $n_+ \not{z} A_s(z)$. Integrating by parts in (3.19), we find

$$L(Y_1; Y_2) = i \int d^4 z \int \frac{d^4 z'}{2} (Y_1 - z) \not{z}' A_s(z) n_+ \not{z} A_s(z - \underline{y}) \\ + i \int d^4 z \int \frac{d^4 z'}{2} \not{z} A_s(z) (Y_1 - z) \not{z}' A_s(z - \underline{y}) : \quad (3.21)$$

The hard-collinear propagator is a Green's function obeying the differential equation

$$n_+ \not{z} \left(\frac{\partial^2}{\partial z'^2} - \frac{\partial^2}{\partial z^2} \right) A_s(x) = \frac{\not{z}'}{2} \delta^{(4)}(x) : \quad (3.22)$$

This allows us to write

$$L(Y_1; Y_2) = i \int d^4 z \int \frac{d^4 z'}{2} A_s(Y_2) \not{z}' A_s(Y_1) (Y_1 - \underline{y}) \\ + i \int d^4 z \int \frac{d^4 z'}{2} (Y_1 - z) \not{z}' A_s(z) \frac{\partial^2}{\partial z'^2} A_s(z - \underline{y}) \\ + i \int d^4 z \int \frac{d^4 z'}{2} \not{z} A_s(z) (Y_1 - z) \not{z}' A_s(z - \underline{y}) : \quad (3.23)$$

The terms involving transverse derivatives vanish at tree level, because they provide powers of transverse momenta of external lines, which are zero (recall that $v_+ = 0$ and $q_+ = 0$). This leaves the terms shown in the first line, in which the z integral

has been eliminated, and in which the product of two propagators has been reduced to a single propagator. In momentum space, these manipulations correspond to the partial-fraction identity

$$\frac{1}{n-pn-p^2} = \frac{1}{p(n-p+!)^2} = \frac{1}{n-p!} \frac{1}{pn-p^2} \frac{1}{p(n-p+!)^2} ; \quad (3.24)$$

valid for two momenta that differ only in their $n-p$ components.

In the sum of all terms many cancellations and simplifications take place, and we find the rather simple result

$$T_{ij}^{(2)} = \int d^4x e^{i(q-m_b v) \cdot x} \frac{d^4p}{(2\pi)^4} e^{ip \cdot x} \frac{n \cdot p}{p^2 + i} \sum_{n=1}^Z O_n(x); \quad (3.25)$$

where

$$\begin{aligned} O_1(x) &= i \int d^4z T f h S_0 \cdot i \frac{\not{n}}{2} \cdot j S^y h_x L_h^{(2)}(z) g; \\ O_2(x) &= \frac{1}{2m_b} h S_0 \cdot i \frac{\not{n}}{2} \cdot j S^y i \not{D} h_x + h(\not{D}) S_0 \cdot i \frac{\not{n}}{2} \cdot j S^y h_x; \\ O_3(x) &= \frac{1}{n \cdot p} h S_0 \cdot i \frac{\not{n} \not{n}}{4} \cdot j S^y i \not{D} h_x \\ &\quad + h i \not{D} S_0 \cdot i \frac{\not{n} \not{n}}{4} \cdot j S^y h_x; \\ O_4(x) &= \frac{i}{n \cdot p} \int_0^{\infty} dt h S_0 \cdot i S^y i \not{D} \cdot \frac{\not{n}}{2} i \not{D} S_{tn} \cdot j S^y h_x; \end{aligned} \quad (3.26)$$

In deriving these expressions, we have made use of the identity $i \not{D} = S(i \not{\partial} + A_s) S^y$ with A_s as defined in (3.20). Note that on the space of forward matrix elements the result for $T_{ij}^{(2)}$ is hermitean, because we can integrate by parts and use translational invariance.

In the last step, we can simplify the operator O_2 by noting that the HQET equation of motion, $i \not{D} h = 0$, along with $\not{v} h = h$, implies

$$S^y i \not{D} h = S^y i \not{D} h + (\not{v} - \not{n}) \cdot i S^y h; \quad (3.27)$$

It follows that all gauge-covariant derivatives of the heavy-quark fields are perpendicular derivatives. This fact restricts the number of subleading shape functions.

3.3 Definition of subleading shape functions

The Dirac structure of the operators O_n can be simplified noting that the heavy-quark fields h of HQET are two-component spinor fields, so that between $h :: h$

the Dirac basis collapses to a set of four basis matrices $(1; \gamma_5)$. In four-component notation, these are the upper-left 2×2 blocks of $(1; \gamma_5)$ (in the Dirac representation). Instead of γ_5 , we are free to take the matrices γ_5 and γ_5 . It follows that, between the $P_v = \frac{1}{2}(1 + \gamma_5)$ projectors supplied by the heavy-quark fields, any Dirac matrix can be decomposed as

$$= \frac{1}{2} \text{tr}(P_v) 1 + \frac{1}{2} \text{tr}[P_v (\gamma_5 \gamma_\mu) \gamma_5] \gamma_\mu + \frac{1}{2} \text{tr}(P_v \gamma_5) \gamma_5 : \quad (3.28)$$

We denote by

$$h h :: h i = \frac{h B(v) j h :: h B(v) i}{2m_B} \quad (3.29)$$

the forward B-meson matrix element of any HQET operator. Rotational invariance in the transverse plane implies that transverse indices can only be contracted using the symmetric and anti-symmetric tensors (we set $\epsilon_{0123} = 1$)

$$g_\mu = g \frac{n_\mu n_\nu + n_\nu n_\mu}{2}; \quad \gamma_\mu = \gamma_\mu n_\nu : \quad (3.30)$$

It follows that the only non-vanishing matrix elements are

$$\begin{aligned} \int_0^Z h h S_0 S^y h_x i &= \int_0^Z d! e^{\frac{i}{2}!n} x s(!); \\ \int_0^Z h i d^4 z T f h S_0 S^y h_x L_h^{(2)}(z) g i &= \frac{1}{m_b} \int_0^Z d! e^{\frac{i}{2}!n} x s(!); \\ \int_0^Z h h S_0 \gamma_5 S^y i D_\mu h_x i &= \frac{i \gamma_\mu}{2} \int_0^Z d! e^{\frac{i}{2}!n} x t(!); \\ \int_0^Z i d t h h S_0 S^y i D_\mu i D_\mu S_{tn} S^y h_x i &= \frac{g_\mu}{2} \int_0^Z d! e^{\frac{i}{2}!n} x u(!); \\ \int_0^Z i d t h h S_0 \gamma_5 S^y i D_\mu i D_\mu S_{tn} S^y h_x i &= \frac{i \gamma_\mu}{2} \int_0^Z d! e^{\frac{i}{2}!n} x v(!); \end{aligned} \quad (3.31)$$

If radiative corrections at the hard scale are included, it would be more appropriate to split up $s(!) = s_{\text{kin}}(!) + C_{\text{mag}} s_{\text{mag}}(!)$, where C_{mag} is the Wilson coefficient of the chromo-magnetic operator in the subleading HQET Lagrangian. This ensures that the shape functions remain independent of the heavy-quark mass. The definitions

of the functions t, u, v are chosen such that

$$\begin{aligned}
\int_{x=2}^Z dh(0) \not{D}[0;x] (i \not{D}_? h)(x) i &= \int_0^Z d! e^{\frac{i}{2}!n} t(!); \\
\int_{x=2}^Z i \, dthh(0) [0;tn] (i \not{D}_?)^2 (tn) [tn;x] h(x) i &= \int_0^Z d! e^{\frac{i}{2}!n} u(!); \\
\int_{x=2}^0 i \, dthh(0) \frac{\not{D}}{2} [0;tn] ? gG_? (tn) [tn;x] h(x) i &= \int_0^Z d! e^{\frac{i}{2}!n} v(!);
\end{aligned} \tag{3.32}$$

where $[x;y] = S(x)S^y(y)$ is a product of two finite-length soft Wilson lines, which on the light cone (i.e., for $x;y \propto n$) collapses to a straight Wilson line of finite length connecting x and y .

We also need a variation of the first matrix element in (3.32), in which the derivative is located at position 0. Using hermitean conjugation, translational invariance, and the reality of $t(!)$, which follows from parity and time-reversal invariance of the strong interactions, we find that

$$h(h i \not{D}_?)(0) \not{D}[0;x] h(x) i = hh(0) \not{D}[0;x] (i \not{D}_? h)(x) i; \tag{3.33}$$

implying that all terms containing a single insertion of $D_?$ can be related to the function $t(!)$. From this relation, it follows that

$$\begin{aligned}
\int_0^Z d! e^{\frac{i}{2}!n} t(!) &= h h S_0 \frac{\not{D}}{2} h_{s?}(x) h_{s?}(0) S^y h_x i \\
&= \int_{x=2}^Z dthh(0) \frac{\not{D}}{2} [0;tn] ? n gG_? (tn) [tn;x] h(x) i;
\end{aligned} \tag{3.34}$$

which defines the function $t(!)$ in terms of a matrix element of the field-strength tensor.

It is now straightforward to express the forward matrix element of the current correlator T_{ij} in terms of shape functions. The resulting traces of Dirac matrices can be simplified using identities for the $?$ tensor derived in [49]. Taking the imaginary part, we obtain for the hadronic tensor

$$\begin{aligned}
W_{ij}^{(0)} &= \int_0^Z d! (n \cdot p + !) S(!)_1 T_2 \quad W_{ij}^{(1)} = 0; \\
W_{ij}^{(2)} &= \int_0^Z d! (n \cdot p + !) \frac{! S(!) + t(!)}{m_b} T_2 + \frac{s(!)}{m_b} T_1 \\
&\quad + \frac{t(!)}{n \cdot p} T_3 + \frac{u(!)}{n \cdot p} T_1 - \frac{v(!)}{n \cdot p} T_4;
\end{aligned} \tag{3.35}$$

where now $p = m_b v - q$, and

$$\begin{aligned} T_1 &= \frac{1}{4} \text{tr} \left[\not{\epsilon}_i \not{\epsilon}_j \frac{1 + \not{v}}{2} \right]; & T_3 &= \frac{1}{4} \text{tr} \left[\not{\epsilon}_i \not{\epsilon}_5 \not{v} \not{p} \frac{1 + \not{v}}{2} \right]; \\ T_2 &= \frac{1}{8} \text{tr} \left[\not{\epsilon}_i \not{\epsilon}_j (\not{v} \not{p}) \right]; & T_4 &= \frac{1}{4} \text{tr} \left[\not{\epsilon}_i \not{\epsilon}_5 \not{v} \not{p} \frac{1 + \not{v}}{2} (\not{v} \not{p}) \right]; \end{aligned} \quad (3.36)$$

It follows from (3.35) that the subleading shape functions $s(!)$ and $u(!)$ always come with the same trace as the leading shape function $S(!)$. However, $u(!)$ is divided by the kinematic variable $n \cdot p$, and so it does not enter in a universal (i.e., process-independent) combination with $S(!)$.

We can now specialize our result to the case of semileptonic decay, for which $i = (1 \dots 5)$ and $j = (1 \dots 5)$. This yields

$$\begin{aligned} W &= \int d! (n \cdot p + !)^{-1} n \cdot v + n \cdot v \cdot g \cdot i \cdot n \cdot v \\ &\quad \left(1 + \frac{!}{m_b} S(!) + \frac{s(!) + t(!)}{m_b} + \frac{u(!)}{n \cdot p} \frac{v(!)}{p} \right) \\ &\quad 2(n \cdot v + n \cdot v) \frac{t(!)}{n \cdot p} + 2n \cdot n \cdot \left(\frac{! S(!)}{m_b} \frac{t(!)}{m_b} + \frac{t(!) + v(!)}{n \cdot p} \right) : \end{aligned} \quad (3.37)$$

Similarly, for the contribution of the dipole operator Q_7 to $B \rightarrow X_s$ decay, the Dirac structures are (up to prefactors) $i = \frac{1}{4} [\not{\epsilon}; \not{\epsilon}] (1 \dots 5)$ and $j = \frac{1}{4} [\not{\epsilon}; \not{\epsilon}] (1 \dots 5)$, where the indices ϵ are contracted with the transverse polarization vector of the photon. In this case we obtain

$$\begin{aligned} W &= (i \cdot \epsilon \cdot \epsilon) \int d! (n \cdot p + !)^{-1} \left(1 + \frac{!}{m_b} S(!) \right. \\ &\quad \left. + \frac{s(!) + t(!)}{m_b} + \frac{u(!)}{n \cdot p} \frac{v(!)}{p} \right) : \end{aligned} \quad (3.38)$$

We stress, however, that while at leading power in $Q_{CD} = m_b$ the dipole operator gives the only tree-level contribution to the $B \rightarrow X_s$ decay rate, this is no longer the case when power corrections are included. For instance, interference terms of the dipole operator with current-current operators can lead to new subleading shape functions even at lowest order in perturbation theory. To derive these structures, it would be necessary to match the entire effective weak Hamiltonian for $B \rightarrow X_s$ decay onto SCET operators [50]. This task still has to be completed beyond the leading order in α_s . Contrary to claims in [51, 52], a complete description of tree-level subleading shape-function effects in $B \rightarrow X_s$ decay is therefore still lacking.

3.4 Moment relations and comparison with the literature

Moments of the shape functions can be related to forward B-meson matrix elements of local HQET operators [15]. In particular, setting $x = 0$ in the defining relations (3.31) yields expressions for the normalization integrals of the shape functions. They are

$$\int_0^1 d! S(!) = 1; \quad \int_0^1 d! f_S(!); t(!); u(!); v(!) g = 0; \quad (3.39)$$

The vanishing of the norm of all subleading shape functions is a consequence of Luke's theorem [53], and it ensures that there are no first-order $\alpha_{\text{QCD}} = m_b$ corrections to total inclusive decay rates. For the functions t, u, v this is an obvious consequence of the fact that the integration domain in (3.34) and (3.32) shrinks to zero in the limit $x \rightarrow 0$. The interpretation of (3.39) is that subleading shape functions lead to local distortions of inclusive spectra, which cancel out when the spectra are integrated over a sufficiently large region in phase space. The first moments characterize the strength of the distortions, while higher moments determine their shape.

Taking a derivative in x in the definitions (3.31) brings down a factor of $!$ under the integrals on the right-hand side. Setting then $x \rightarrow 0$ yields a set of relations for the first moments of the shape functions. The resulting matrix elements can be evaluated by means of the relations [54]

$$\langle h | \bar{u} \gamma_\mu \gamma_5 u | h \rangle = \frac{1}{2} \text{tr} \left[\frac{1 + \not{v}}{2} \not{g} \not{v} \not{v} \left(\frac{1}{3} + i \frac{2}{2} \frac{1 + \not{v}}{2} \right) \right]; \quad (3.40)$$

and [1]

$$\int_0^1 d! z T f(h | \bar{u} \gamma_\mu \gamma_5 u | h)(0) L_h^{(2)}(z) g i = \int_0^1 d! z L_h^{(2)}(0) i = \int_0^1 d! z \frac{1 + 3 C_{\text{mag}}^2}{2 m_b}; \quad (3.41)$$

where c_1 and c_2 are the familiar HQET parameters arising in the parameterization of second-order power corrections to inclusive decay spectra, and $C_{\text{mag}} = 1$ at tree level. We obtain

$$\begin{aligned} \int_0^1 d! S(!) &= \frac{1 + 3 c_2}{2}; & \int_0^1 d! S(!) u(!) &= \frac{2 c_1}{3}; \\ \int_0^1 d! S(!) t(!) &= c_2; & \int_0^1 d! S(!) v(!) &= c_2; \end{aligned} \quad (3.42)$$

We also recall that the first two moments of the leading shape function are $\int_0^1 d! S(!) = 0$ and $\int_0^1 d! S(!)^2 = \frac{1}{3}$ [15].

3.5 Contributions from four-quark operators

The last diagram in Figure 3.1 shows a tree-level contribution to the hadronic tensor involving two insertions of the subleading SCET Lagrangian $L_q^{(1)}$. The

exchange of a hard-collinear gluon implies that this graph is of order g^2 , and so it vanishes in the limit where α_s is set to zero. The fact that the suppression factor is α_s instead of α_s^2 reflects the phase-space enhancement of four-quark tree-level graphs compared with loop diagrams [55]. One might therefore expect that the four-quark contribution is numerically as important as the other tree-level subleading shape-function contributions.

Applying the partial-fraction identity (3.24) twice, we find that the resulting contribution to the correlator $T_{ij}^{(2)}$ can be written as in (3.25), adding a fifth operator to the sum. It reads

$$O_5(x) = \frac{\alpha_s}{n} \int_0^x \int_0^{x-t_1} dt_1 dt_2 \text{tr} [S_{0i}(t_1) \not{t}_a S_{t_1n}^y(q) S_{t_2n} \not{t}_j S_{t_2x}^y] ; \quad (3.43)$$

where t_a are the generators of color $SU(N_c)$. Note that the field insertions are ordered according to "light-cone time" x^+ , just as they appear in the Feynman diagram in Figure 3.1. This is a general result. Because the minus components n^- of hard-collinear momenta are large, of order m_b , hard-collinear fields always propagate forward in light-cone time. Turning, for instance, a forward-moving hard-collinear quark into a backward-moving hard-collinear anti-quark would require a hard quantum fluctuation, which is already integrated out in SCET. As a result, Feynman amplitudes in SCET are ordered with respect to light-cone time, and that ordering is preserved in the matching onto HQET. This discussion explains why all our operators have the property that the coordinates z of soft fields range from 0 to x in an ordered fashion. The results can therefore always be expressed in terms of bi-local operators depending only on 0 and x . However, at present we cannot exclude the possibility of non-trivial weight functions under these integrals, which could arise at higher orders in perturbation theory. If present, they may require a generalization of our definitions of subleading shape functions.

Returning to the case of the four-quark operator in (3.43), we note that its contribution vanishes in the vacuum-insertion approximation due to the color-octet structure of the heavy-light quark bilinears. While this approximation is admittedly naive, phenomenological evidence based on studies of B -meson lifetimes [55, 56, 57] and theoretical arguments based on lattice calculations [58, 59] and QCD sum rules [60] support the notion that matrix elements which vanish in the vacuum-insertion approximation are numerically suppressed, typically by an order of magnitude. It is thus very unlikely that the four-quark operator in (3.43) could give a larger contribution than loop-suppressed $O(\alpha_s)$ corrections, which we have neglected. Note also that the contribution of the corresponding local operator to total inclusive rates, which is what remains when the corresponding shape functions are integrated over a sufficiently large domain, is bound to be tiny. The effect is of order $(\alpha_{QCD}/m_b)^3$, and it is α_s -suppressed with respect to a four-quark contribution discussed by Voloshin [61], whose effect on the total decay rate is believed to be at most 3%.

Nevertheless, it is interesting to study the structure of the operator $O_5(x)$ in more detail and define corresponding subleading shape functions. The decomposition (3.28) implies that the Dirac structure can be rearranged in the form (omitting factors of S , S^γ and color indices for simplicity)

$$i \not\sim j = \frac{1}{2} \left(\frac{1}{\not\sim_5} A_{ij} + \frac{1+\gamma}{2} \left(\frac{1}{\not\sim_5} A_{ij} \right) \right) \quad (3.44)$$

Note that the definitions (3.47) imply that the normalization integrals as well as the first moments of the functions $f_u(!)$ and $f_v(!)$ vanish (because the integration domain is of second order in $n - x$), and therefore the new functions \mathfrak{u} and \mathfrak{v} have the same first moments as the original ones, see (3.42).

While the shape functions S, s, t, u, v are expected to be identical for charged and neutral B mesons up to tiny isospin-breaking corrections, this is no longer the case for the four-quark shape functions f_u and f_v . The values of these functions will depend crucially on whether the light-quark flavor q in the four-quark operators matches that of the B -meson spectator quark. In the semileptonic decay $B \rightarrow X_u l \bar{\nu}$, the difference between the subleading shape functions f_u and f_v for B and B^0 mesons is likely to be one of the dominant sources of isospin-breaking effects on the decay distributions.

3.6 Applications

We are now ready to summarize our results. We absorb the contributions from four-quark operators into the functions $\mathfrak{u}(!)$ and $\mathfrak{v}(!)$ defined in (3.49). The moment constraints on the shape functions can be summarized by their expansions in distributions [15], which read

$$\begin{aligned} S(!) &= (!) - \frac{1}{6} \langle ! \rangle + \dots; & s(!) &= \frac{1+3\langle ! \rangle}{2} \langle ! \rangle + \dots; \\ t(!) &= \langle ! \rangle^2 + \dots; & \mathfrak{u}(!) &= \frac{2}{3} \langle ! \rangle + \dots; & \mathfrak{v}(!) &= \langle ! \rangle^2 + \dots \end{aligned} \quad (3.50)$$

These expressions allow us to test our results against existing predictions for inclusive spectra obtained using a conventional heavy-quark expansion.

The analytic properties of the shape functions are such that they have support for $1 - \langle ! \rangle < ! < 1$, where 1 is the asymptotic value of the mass difference $(m_B - m_b)_{m_b \rightarrow 1}$ in the heavy-quark limit. This parameter differs from the physical value of 1 by power-suppressed terms,

$$m_B - m_b = 1 - \frac{1+3\langle ! \rangle}{2m_b} + \dots \quad (3.51)$$

We would like the support in $!$ to extend over the physical interval $1 - \langle ! \rangle < ! < 1$, since this will ensure that the kinematic boundaries for decay distributions take their physical values set by the true B -meson mass. This can be achieved by shifting the arguments of all shape functions by a small amount $! = \frac{1}{2}(1 + 3\langle ! \rangle) = m_b$. For the subleading shape functions this changes nothing to the order we are working, since $t(! + !) = t(!) + \dots$ etc., where the dots represent terms of higher order in $1 - m_b$. For the leading-order shape function, however, this shift produces a new $1 - m_b$ correction: $S(!) = S(! + !) - ! S'(! + !) + \dots$, where the prime denotes a derivative with respect to the argument. Using the fact that

$S(!)$ and $s(!) = m_b$ always appear together, we can absorb the extra term into a redefinition of the subleading shape function s , defining a new function

$$s_0(!) = s(!) - \frac{1}{2}(\alpha_1 + 3\alpha_2)S^0(!): \quad (3.52)$$

From (3.42), it follows that the first moment of the function s_0 vanishes. In terms of these definitions,

$$S(! + !) = S(! + !) + \frac{s_0(! + !)}{m_b} = S(!) + \frac{s(!)}{m_b} + \dots: \quad (3.53)$$

In other words, our expressions for the hadronic tensors in (3.37) and (3.38) remain valid when in all shape functions the argument is shifted from $!$ to $! + !$, except that the subleading shape function s must be replaced with the redefined function s_0 , whose norm and first moment vanish. Once this is done, the integrals over $!$ extend from -1 up to the physical value of $!$.

It is now convenient to express the shape functions as functions of $\hat{!}$ [63]. They have support in this variable for $0 \leq \hat{!} < 1$. The $\hat{!}$ -functions in the tree-level expressions (3.37) and (3.38) for the hadronic tensors set $\hat{!} = P_+$. We denote functions of $\hat{!}$ by a hat, e.g. $\hat{S}(\hat{!}) = S(\hat{!} + !)$, $\hat{t}(\hat{!}) = t(\hat{!} + !)$, and similarly for the other functions. In the equations below, $!$ always refers to the physical parameter defined with the true B -meson mass.

Based on equation (3.37), we can write the structure functions W_i for $B \rightarrow X_{u1}$ decays as:

$$\begin{aligned} W_1 &= 1 + \frac{P_+}{m_b} \hat{S}(P_+) + \frac{\hat{t}(P_+)}{m_b} + \frac{\hat{u}(P_+) - \hat{v}(P_+)}{n - p}; \\ W_4 + \frac{1}{y} W_5 &= \frac{2}{y} \left(\frac{(P_+)}{m_b} \hat{S}(P_+) - \frac{2\hat{t}(P_+)}{m_b} + \frac{\hat{t}(P_+) + \hat{v}(P_+)}{n - p} \right); \end{aligned} \quad (3.54)$$

where $y = n - p$.

For $B \rightarrow X_s$ we have from equation (3.38):

$$W = 2 - 1 - \frac{P_+}{m_b} \hat{S}(P_+) + \frac{\hat{t}(P_+) + \hat{u}(P_+) - \hat{v}(P_+)}{m_b}; \quad (3.55)$$

where for radiative decays $n = p = 0$.

3.7 Conclusions

In this chapter, we have used the formalism of SCET to perform a systematic study of power-suppressed effects to charmless inclusive B decays. At tree level, the results can be expressed in terms of a set of subleading shape functions defined via the Fourier transforms of forward matrix elements of bi-local light-cone operators

in heavy-quark effective theory. We have identified a new contribution arising from four-quark operators, which was not considered previously. We have shown that, when shape functions appearing in process-independent combinations are combined into single functions, then a total of three subleading shape functions are required to describe arbitrary current-induced decay distributions of B mesons into light final-state particles.

In the last part of this chapter, we have presented analytical expressions for the hadronic tensor of semileptonic and radiative charmless B decays. While this concludes the problem of tree-level power corrections in semileptonic decay, we have stressed that no complete (tree-level) analysis of power-suppressed corrections to the $B \rightarrow X_s$ decay exists to date. The formalism developed in this chapter can, however, readily be extended to this case.

Chapter 4

Applications: Event Generator

4.1 Introduction

The theoretical tools for the calculation of inclusive B decays are QCD factorization on the one hand [15, 16, 17, 18, 25, 50, 62, 63, 64], and local operator product expansions (OPE) on the other [1, 13]. Both approaches perform a systematic separation of long-distance hadronic quantities from short-distance perturbative ones, while organizing the calculation in inverse powers of the heavy b -quark mass m_b . The OPE is an appropriate tool for the calculation of total inclusive rates (for example in $B \rightarrow X_c l$ decay) or for partial rates integrated over sufficiently large regions in phase space, where all components of the final-state hadronic momentum P_X are large compared to Λ_{QCD} . QCD factorization, on the other hand, is better suited for the calculation of partial rates and spectra near kinematical boundaries, where typically some components of P_X are large, while the invariant hadronic mass $M_X = \sqrt{P_X^2}$ is small.

It is important to note that the heavy-quark expansions valid in these two kinematical regions are not identical, because the power counting rules differ in the two regimes. Also the nature of the non-perturbative inputs is different. In the OPE region, non-perturbative physics is encoded in a few hadronic parameters, and the heavy-quark expansion is the usual Wilsonian expansion in local operators. In the endpoint (or shape-function) region, the presence of multiple scales complicates the power counting, and the interplay between soft and collinear modes gives rise to large non-localities. As a result, non-perturbative physics is described by hadronic structure functions called "shape functions", and the heavy-quark expansion is an expansion in non-local string operators defined on the light-cone. The connections between the two regimes is that moments of the shape functions can be expressed in terms of local operators.

In this chapter we develop a formalism that smoothly interpolates between the two kinematical regimes (see [65] for a related discussion, which is however restricted to the tree approximation). This is essential for building an event generator for inclusive $B \rightarrow X_u l$ and $B \rightarrow X_s$ decays, which can be used to study partial and differential decay rates in different kinematical domains. In the shape-function region, our approach relies on exact QCD factorization theorems, which exist in every order of power counting. They allow us to systematically disentangle short- and long-distance physics and, in the process, resum parametrically large logarithms order by order in perturbation theory. This factorization can be done with high accuracy for the terms of leading power in $1/m_b$, and with somewhat less sophistication for the first-order power corrections. For the second-order power corrections, we only include contributions that do not vanish when integrated over all phase space. This is a safe approximation; the effects of the remaining $1/m_b^2$ terms can to a large extent be absorbed by a redefinition of the subleading shape functions arising at order $1/m_b$.

Our formalism is "optimized" for the shape-function region in the sense that sophisticated theoretical technology is applied in this regime. However, when our expressions for the differential decay rates are integrated over sufficiently wide domains, they automatically reduce to the simpler results that can be derived using the OPE approach, up to yet unknown terms of $O(\Lambda_{\text{QCD}}^2)$. The moment relations for the shape functions are crucial in this context. Note that local $1=m_b^2$ corrections in the OPE receive contributions from terms of leading power ($1=m_b^0$), subleading power ($1=m_b$), and sub-subleading power ($1=m_b^2$) in the shape-function region, so the transition is highly non-trivial. In implementing the program outlined here, we include all presently known information on the triple differential $B \rightarrow X_{u1}$ decay rate and on the differential $B \rightarrow X_s$ decay rate in a single, unified framework. We neglect, for simplicity, hadronic power corrections of order $1=m_b^3$ and higher, which are known to have a negligible effect on the observables considered here. The only possible exception is contributions from "weak annihilation", which are estimated as part of our error analysis. We also ignore the existing results on $O(\Lambda_{\text{QCD}}^2)$ radiative corrections for some single-differential distributions, because the corresponding corrections are not known for the double or triple differential $B \rightarrow X_{u1}$ decay spectra. While these $O(\Lambda_{\text{QCD}}^2)$ terms are sometimes found to be large when naive perturbation theory in $\Lambda_{\text{QCD}}(m_b)$ is used, their effects are expected to be small in our scheme, which is based on a complete scale separation using QCD factorization. We see no reason why the Λ_{QCD}^2 terms should be enhanced compared to other, unknown corrections of $O(\Lambda_{\text{QCD}}^2)$.

A technical complication in realizing the approach described here has to do with the treatment of phase-space factors. The heavy-quark expansion of the hadronic tensor for $B \rightarrow X_{u1}$ decay gives rise to expressions that are singular at certain points in phase space. One way to avoid these singularities is to also expand phase-space factors order by order in $1=m_b$ (see, e.g., the treatment in [66]). However, since this expansion depends on the kinematical cuts of any given analysis, it cannot be implemented in a straightforward way in an event generator. An alternative is to reorganize the heavy-quark expansion in such a way that the expansion parameter is related to hadronic (as opposed to partonic) kinematical variables, in which case kinematical singularities are always canceled by exact phase-space factors. Following this strategy, we obtain expressions for decay distributions and partial decay rates which are free of explicit reference to partonic quantities such as the b-quark mass. A dependence on m_b enters only implicitly via the first moment of the leading-order shape function $\hat{S}(\hat{s})$. The philosophy of our approach is that this function¹ is extracted experimentally from a fit to the $B \rightarrow X_s$ photon spectrum, which has been measured with good precision in the region where $P_+ = M_B - 2E_{\text{QCD}}$. This is analogous to the extraction of parton distribution functions from deep inelastic scattering. The photon spectrum

¹More precisely, we define a new shape function $\hat{S}(\hat{s})$ by the combination of leading and subleading shape functions contributing to $B \rightarrow X_s$ decay, and we will use the same function to make predictions for $B \rightarrow X_{u1}$ decay distributions.

is experimentally accessible to energies as low as 1.8 GeV, which corresponds to a sampling of the shape function for values of \hat{s} up to about 1.7 GeV. Once the shape function has been extracted over this range, we can use it to obtain predictions for arbitrary partial $B \rightarrow X_u l$ decay rates with cuts. In doing so, the residual hadronic uncertainties in the extraction of $\langle V_{ub} \rangle$ only enter at the level of power corrections.

We emphasize that the program outlined above is equivalent to an approach put forward in [16] and later refined in [67, 68, 69], in which $\langle V_{ub} \rangle$ is extracted with the help of shape-function independent relations between weighted integrals over differential decay distributions in $B \rightarrow X_s$ and $B \rightarrow X_u l$. The experimental error in the results for these weighted integrals corresponds, in our approach, to the error in the prediction of $B \rightarrow X_u l$ partial rates resulting from the experimental uncertainty in the extraction of the shape function from the $B \rightarrow X_s$ photon spectrum. While the shape-function independent relations are very elegant, it is more convenient for the construction of a generator to have a formulation where the shape function is used as an input. In this way, it is possible to impose arbitrary cuts on kinematical variables without having to recompute the weight functions in each case.

The chapter is structured as follows: In Section 4.2 we collect the relevant formulae for the calculation of the $B \rightarrow X_s$ photon spectrum. These expressions can be used to extract the leading non-perturbative structure function from experiment. An analogous presentation for the triple differential decay rate in $B \rightarrow X_u l$ decays is presented in Section 4.3. In order to perform a numerical analysis one needs to rely on parameterizations of the shape functions. A collection of several useful functional forms is given in Section 4.4. In Section 4.5 we present a full error analysis of partial $B \rightarrow X_u l$ decay rates for a variety of experimental cuts. We also explore the sensitivity of the results to the b-quark mass and to the functional forms adopted for the shape functions. Section 4.6 contains our conclusions.

4.2 Inclusive radiative decays

The decay process $B \rightarrow X_s$, while more complex in its short-distance physics, is considerably simpler in its kinematics than the semileptonic process $B \rightarrow X_u l$. Since the radiated photon is on-shell, the hadronic variables P that describe the momentum of the X_s system are trivially related to the photon energy E by $P_+ = M_B^2 - 2E$ and $P_- = M_B^2$. In the crudest approximation, namely at tree level and leading power, the photon-energy spectrum is directly proportional to the leading shape function, $d_s = dE / \hat{S}(P_+)$. In this section we collect all relevant formulae needed to compute the $B \rightarrow X_s$ photon spectrum or, equivalently, the invariant hadronic mass distribution. It is implicitly assumed that these spectra are sufficiently "smeared" (e.g., by experimental resolution) to wash out any sharp hadronic structures. In cases where the resolution is such that the K resonance

peak is observed, it can be accounted for by combining the formulae in this section with the prescription for subtracting the K peak proposed in [32].

The differential $B \rightarrow X_s$ decay rate can be written as

$$\frac{d\Gamma_s}{dE} = \frac{G_F^2}{2^4} E^3 V_{tb} V_{ts}^2 \overline{m}_b^2(\mu_h) (C_7^e(\mu_h))^2 U(\mu_h; \mu_i) F(P_+); \quad (4.1)$$

where the structure function F depends on the photon energy via $P_+ = M_B - 2E$. The prefactor contains the electromagnetic α -structure constant normalized at $q^2 = 0$, two powers of the running b -quark mass (defined in the \overline{MS} scheme) originating from the electromagnetic dipole operator Q_7 in the effective weak Hamiltonian, and the square of the corresponding Wilson coefficient C_7^e , which is needed at next-to-leading order in renormalization-group improved perturbation theory [10]. Renormalization-group running from the hard scale $\mu_h = m_b$ to the intermediate scale $\mu_i = m_b / Q_{CD}$ gives rise to the evolution factor $U(\mu_h; \mu_i)$, whose explicit form is discussed in Appendix B. We keep U and $(C_7^e)^2$ outside of the structure function F ; it is understood that when combining the various terms in (4.1) all perturbative quantities should be expanded for consistency to the required order in α_s .

4.2.1 Leading-power factorization formula

At leading order in $1/m_b$ the structure function F factorizes as [50]

$$F^{(0)}(P_+) = H_s(\mu_h) \int_0^{Z_{P_+}} d\mu_b J(\mu_b(P_+ - \mu); \mu_i) \hat{S}(\mu; \mu_i); \quad (4.2)$$

At this order a single non-perturbative parton distribution function arises, called the leading shape function [16] and denoted by $\hat{S}(\mu; \mu_i)$. Our notation is adopted from [63, 66]: hatted shape functions have support for $\mu \geq 0$. The function \hat{S} is defined in terms of a non-local matrix element in heavy-quark effective theory (HQET). Renormalization-group running between the intermediate scale and a low hadronic scale is avoided when using the shape functions renormalized at the intermediate scale μ_i . Evolution effects below this scale are universal (i.e., process independent) and so can be absorbed into the renormalized shape function. Short-distance contributions from scales above $\mu_h = m_b$ are included in the hard function H_s , which in practice is obtained by matching the effective weak Hamiltonian onto a current operator in soft-collinear effective theory (SCET). At next-to-leading

order in perturbation theory, the result reads

$$\begin{aligned}
H_s(\mu_h) = & 1 + \frac{C_F s(\mu_h)}{4} \left(2 \ln^2 \frac{m_b}{\mu_h} + 7 \ln \frac{m_b}{\mu_h} - 6 \frac{\mu_h^2}{12} + \alpha_{ew} + \alpha_{peng} \right) \\
& + \frac{C_{8g}^e(\mu_h) C_F s(\mu_h)}{C_7^e(\mu_h) 4} \left(\frac{8}{3} \ln \frac{m_b}{\mu_h} + \frac{11}{3} \frac{\mu_h^2}{9} + \frac{2}{3} i \right) \\
& + \frac{C_1(\mu_h) C_F s(\mu_h)}{C_7^e(\mu_h) 4} \left(\frac{104}{27} \ln \frac{m_b}{\mu_h} + g(z) \frac{V_{ub} V_{us}}{V_{tb} V_{ts}} g(0) - g(z) \right); \quad (4.3)
\end{aligned}$$

where the variable $z = (\mu_c/\mu_b)^2$ denotes the ratio of quark masses relevant to charm-loop penguin diagrams, and the penguin function $g(z)$ can be approximated by the first few terms of its Taylor expansion,

$$\begin{aligned}
g(z) = & \frac{833}{162} - \frac{20}{27} i + \frac{8}{9} z^{3/2} \\
& + \frac{2z}{9} \left(48 - 5z^2 - 36z + (30 - 2z^3)i + (36 - 9z^2 + 6i) \ln z \right) \\
& + (3 + 6i) \ln^2 z + \ln^3 z \\
& + \frac{2z^2}{9} \left(18 + 2z^2 - 2z^3 i + (12 - 6z^2) \ln z + 6i \ln^2 z + \ln^3 z \right) \\
& + \frac{z^3}{27} \left(9 - 14z^2 + 112i + (182 - 48i) \ln z - 126 \ln^2 z + \dots \right); \quad (4.4)
\end{aligned}$$

The Wilson coefficients C_1 and C_{8g}^e in (4.3) multiply the current-current operators Q_1^{uc} and the chromomagnetic dipole operator Q_{8g} in the effective weak Hamiltonian. The quantities $\alpha_{ew} \approx 1.5\%$ and $\alpha_{peng} \approx 0.6\%$ account for small electroweak corrections and the effects of penguin contractions of operators other than Q_1^{uc} , respectively. The differential decay rate (4.1) is formally independent of the matching scales μ_h and μ_i . The μ_h dependence of the evolution factor $U(\mu_h; \mu_i)$ cancels the scale dependence of the product $\overline{m}_b^2(\mu_h) [C_7^e(\mu_h)]^2 [H_s(\mu_h)]^2$, while its μ_i dependence compensates the scale dependence of the convolution integral $J(\mu_i) \hat{S}(\mu_i)$.

Finally let us discuss the jet function J , which appears as the hard-scattering kernel in the convolution integral in (4.2). It can be written in terms of distributions that act on the shape function \hat{S} . At one-loop order, the jet function is given by [62, 63]

$$J(p^2; \mu) = (p^2) \left(1 + \frac{C_F s(\mu)}{4} (7 - 2\gamma_E) + \frac{C_F s(\mu)}{4} \frac{1}{p^2} \left(4 \ln \frac{p^2}{2} - 3 \right) \right)^{[2]}; \quad (4.5)$$

where the star distributions have the following effect on a function f when inte-

grated over a domain $Q^2 \in [0, Q^2]$:

$$\begin{aligned} \int_0^{Q^2} dp^2 \frac{1}{p^2} f(p^2) &= \int_0^{Q^2} dp^2 \frac{f(p^2) - f(0)}{p^2} + f(0) \ln \frac{Q^2}{2}; \\ \int_0^{Q^2} dp^2 \frac{1}{p^2} \ln \frac{p^2}{2} f(p^2) &= \int_0^{Q^2} dp^2 \frac{f(p^2) - f(0)}{p^2} \ln \frac{p^2}{2} + \frac{f(0)}{2} \ln^2 \frac{Q^2}{2}; \end{aligned} \quad (4.6)$$

4.2.2 Kinematical power corrections

There exists a class of power corrections to (4.2) that do not involve new hadronic quantities. Instead, the power suppression results from the restriction of certain variables (P_+ in the present case) to a region where they are kinematically suppressed (here $P_+ \leq M_B$). The corresponding terms are known in fixed-order perturbation theory, without scale separation and renormalization-group resummation [70, 71] (see also [32]). To perform a complete RG analysis of even the first-order terms in $1/m_b$ is beyond the scope of this work. Since, as we will see later, power corrections only account for small corrections to the decay rates, an approximate treatment will suffice. To motivate it, we note the following two facts [50]: First, while the anomalous dimensions of the relevant subleading SCET and HQET operators are only known for a few cases [47], the leading Sudakov double logarithms are the same as for the terms of leading power, because they have a geometric origin in terms of Wilson lines [72]. The leading Sudakov double logarithms are therefore the same as those resummed into the function U in (4.1). Secondly, the kinematical power corrections in $B \rightarrow X_s$ decay are associated with gluon emission into the hadronic final state X_s . Because of the kinematical restriction to low-mass final states, i.e. $M_X^2 \leq M_B^2 - Q_{CD}^2$, we associate a coupling $\alpha_s(\mu)$ with these terms, where typically $\mu \sim m_b$. Strictly speaking, however, the scale ambiguity associated with the choice of μ could only be resolved by computing the relevant anomalous dimensions.

Within this approximation, the kinematical power corrections to the structure function F can be extracted from [32, 50]. We find it convenient to express the result in terms of the variable

$$x = \frac{P_+}{M_B} \frac{\mu}{P_+}; \quad (4.7)$$

which in the shape-function region scales like $Q_{CD} = m_b$. We obtain

$$\begin{aligned} F^{\text{kin}}(P_+) &= \frac{1}{M_B} \frac{C_F \alpha_s(\mu)}{P_+} \sum_{i,j=1,7,8}^X \frac{C_i(\mu) C_j(\mu)}{C_7^e(\mu)^2} \int_0^{P_+} d\mu \hat{S}(\mu; \mu) h_{ij}(x) \\ &\quad + \frac{2}{9m_c^2} \frac{C_1(\mu)}{C_7^e(\mu)} \hat{S}(P_+; \mu); \end{aligned} \quad (4.8)$$

The coefficient functions $h_{ij}(x)$ are

$$\begin{aligned}
h_{77}(x) &= 3(5 + 2x) + 2(8 + 9x + 3x^2) \ln \left(1 + \frac{1}{x}\right); \\
h_{88}(x) &= \frac{2}{9}(1 + 3x + 4x^2 + 2x^3) - 2 \ln \frac{m_b}{m_s} \ln \left(1 + \frac{1}{x}\right) \\
&\quad - \frac{1}{9}(3 + 9x + 16x^2 + 8x^3); \\
h_{78}(x) &= \frac{2}{3}(5 + 8x + 4x^2) - \frac{8}{3}x(1+x)^2 \ln \left(1 + \frac{1}{x}\right); \\
h_{11}(x) &= \frac{16}{9} \int_0^1 du (1+x-u) \frac{z(1+x)}{u} G \left(\frac{u}{z(1+x)}\right) + \frac{1}{2}; \\
h_{17}(x) &= 3h_{18}(x) = \frac{8}{3} \int_0^1 du u \operatorname{Re} \frac{z(1+x)}{u} G \left(\frac{u}{z(1+x)}\right) + \frac{1}{2};
\end{aligned} \tag{4.9}$$

where as before $z = (m_c/m_b)^2$, and

$$\begin{aligned}
G(t) &= \frac{8}{t^2} \arctan^2 \sqrt{\frac{t}{4-t}}; \quad t < 4; \\
&= \frac{1}{2} \ln^2 \left(\frac{t}{4-t}\right) - \frac{i}{2} \frac{1}{t-4}; \quad t > 4;
\end{aligned} \tag{4.10}$$

In the shape-function region the expressions for $h_{ij}(x)$ could, if desired, be expanded in a power series in $x = O(\alpha_{\text{QCD}}/m_b)$, and this would generate a series of power-suppressed terms $F^{\text{kin}(n)}(P_+)$ with $n \geq 1$, where the superscript " n " indicates the order in the $1/m_b$ expansion. Note that this expansion would contain single logarithms $\ln x = \ln(\alpha_{\text{QCD}}/m_b)$. These are precisely the logarithms that would be resummed in a more proper treatment using effective field-theory methods.

Outside the shape-function region the variable x can take on arbitrarily large positive values, and $F^{\text{kin}}(P_+)$ is no longer power suppressed. Note that for $P_+ \rightarrow M_B$ (corresponding to $x \rightarrow 1$ and $E \rightarrow 0$) most functions $h_{ij}(x)$ grow like x^2 or weaker, so that the spectrum tends to a constant. The only (well known) exception is $h_{88}(x)$, which grows like x^3 , giving rise to a $1=E$ soft-photon singularity [71]. The main effect of the kinematical power corrections (4.8) to the photon spectrum is to add a radiative tail extending into the region of small photon energies. These corrections therefore become the more significant the larger the integration domain over E is.

4.2.3 Subleading shape-function contributions

At order $1/m_b$ in power counting, different combinations of subleading shape functions enter the $B \rightarrow X_s \gamma$ and $B \rightarrow X_u \gamma$ decay distributions [51, 52, 73, 74].

They provide the dominant hadronic power corrections, which must be combined with the kinematical power corrections discussed in the previous section. We include their effects using the results of recent calculations in [66, 75, 76]. Little is known about the subleading shape functions apart from expressions for their first few moments. In particular, the norms of these functions vanish at tree level, while their first moments are determined by the HQET parameters α_1 and α_2 , which are defined via the forward B-meson matrix elements of the kinetic-energy and the chromomagnetic operators, respectively [54].

For the case of $B \rightarrow X_s$ decay, subleading shape-function contributions are currently only known for the matrix elements of the dipole operator Q_7 , and the corresponding hard and jet functions have been computed at tree level. Adopting the notations of [66], the relevant subleading shape functions are $\hat{t}(\not{n})$, $\hat{u}(\not{n})$, and $\hat{v}(\not{n})$. An additional function, called s_0 , has been absorbed by a redefinition of the leading shape function, and it is included in our definition of $\hat{S}(\not{n})$. Roughly speaking, $\hat{u}(\not{n})$ is the "light-cone generalization" of the local HQET kinetic-energy operator. The functions $\hat{v}(\not{n})$ and $\hat{t}(\not{n})$ are both generalizations of the local chromomagnetic HQET operator, but $\hat{t}(\not{n})$ contains also a light-cone chromoelectric operator, which has no equivalent in the local OPE expansion. (Such a contribution arises since there are two external 4-vectors in the SCET expansion, n and v , while there is only v in the HQET expansion.) The contribution of subleading shape functions to the $B \rightarrow X_s$ photon spectrum is

$$F^{\text{hadr}(1)}(P_+) = \frac{1}{M_B - P_+} \int_0^1 dx \left((1-x) \hat{S}(P_+) + \hat{t}(P_+) + \hat{u}(P_+) + \hat{v}(P_+) \right) : \quad (4.11)$$

Compared to [66], we have replaced $1=m_b$ with $1=(M_B - P_+)$ in the prefactor, which is legitimate at this order. (The form of the shape functions restricts P_+ to be of order Q_{CD} .) The appearance of the HQET parameter $\alpha_1 = (M_B - m_b)/m_b$ is peculiar to the subleading shape-function contributions. This quantity is defined via the first moment of the leading-order shape function [63].

The formula given above can be modified to suit the purpose of extracting the shape function from the photon spectrum better. To this end, we absorb a linear combination of the subleading shape functions into a redefinition of the leading shape function, in such a way that the moment relations for this function remain unchanged to the order we are working. This is accomplished by defining

$$\hat{S}(\not{n}) = \hat{S}(\not{n}) + \frac{2 \left(\alpha_1 \hat{S}(\not{n}) + \hat{t}(\not{n}) + \hat{u}(\not{n}) + \hat{v}(\not{n}) \right)}{m_b} : \quad (4.12)$$

When using \hat{S} instead of \hat{S} in the leading-power formula (4.2), the subleading shape-function contribution becomes

$$F^{\text{hadr}(1)}(P_+) = \frac{3 \left(\frac{P_+}{M_B - P_+} \right)}{M_B - P_+} \hat{S}(P_+) : \quad (4.13)$$

The hatted shape functions used in this chapter are related to the original definitions in [66] by

$$\begin{aligned}\hat{S}(\hat{r}) &= S(\hat{r}) + \frac{s_0(\hat{r})}{m_b}; \\ \hat{t}(\hat{r}) &= t(\hat{r}); \quad \hat{u}(\hat{r}) = u(\hat{r}); \quad \hat{v}(\hat{r}) = v(\hat{r});\end{aligned}\quad (4.14)$$

where the unhatted functions have support on the interval between -1 and 1 . It is convenient to rewrite $\hat{r} = ! + !$, where

$$! = (M_B - m_b) = \frac{1 + 3/2}{2m_b} + \dots \quad (4.15)$$

accounts for the mismatch between the HQET parameter m_b and the difference $(M_B - m_b)$ due to power-suppressed terms in the $1/m_b$ expansion [11]. It follows that the variable $! = (M_B - m_b) \hat{r}$ runs from -1 to $(M_B - m_b)$. The moment relations for the leading and subleading shape functions derived in [16] and [51, 66] can be summarized as

$$\begin{aligned}\hat{S}(\hat{r}) &= S(! + !) + \frac{s_0(! + !)}{m_b} = (!) - \frac{1}{6} {}^0(!) + \frac{1 + 3/2}{2m_b} {}^0(!) + \dots; \\ \hat{t}(\hat{r}) &= t(! + !) = {}^2 {}^0(!) + \dots; \\ \hat{u}(\hat{r}) &= u(! + !) = \frac{2}{3} {}^1 {}^0(!) + \dots; \\ \hat{v}(\hat{r}) &= v(! + !) = {}^2 {}^0(!) + \dots;\end{aligned}\quad (4.16)$$

The function \hat{S} has the same moment expansion as \hat{S} . The hadronic parameter α_2 determines the leading contribution to the hyperfine splitting between the masses of B and B mesons through $m_B^2 - m_B^2 = 4\alpha_2 + O(1/m_b)$ [54], from which it follows that $\alpha_2 = 0.12 \text{ GeV}^2$. The value of the parameter α_1 is more uncertain. In much the same way as the b -quark pole mass, it is affected by infrared renormalization ambiguities [43, 44]. It is therefore better to eliminate α_1 in favor of some observable, for which we will choose the width of the leading shape function.

4.2.4 Residual hadronic power corrections

At order $1/m_b^2$ a new set of sub-subleading shape functions enter, which so far have not been classified completely in the literature. Since the functional form of even the subleading shape functions is rather uncertain, there is no need to worry too much about the precise form of sub-subleading shape functions. Most of their effects can be absorbed into the subleading functions. An exception, however, are terms that survive when the sub-subleading shape functions are integrated over a wide domain. Whereas the norms of all subleading ($1/m_b$) shape functions vanish, the norms of the sub-subleading shape functions ($1/m_b^2$) are in general non-zero and given in terms of the heavy-quark parameters α_1 and α_2 . (At tree

level, the class of functions with non-zero norm has been studied in [65].) Our strategy in this chapter will be as follows: We start from the well-known expressions for the (tree-level) second-order power corrections to the $B \rightarrow X_s$ photon spectrum [19] (and similarly for the triple-differential $B \rightarrow X_{u1}$ decay distribution [13, 1], see Section 4.3.4). They are of the form $\sim m_b^{-2}$ times one of the singular distributions $\delta(p^2)$, $\delta'(p^2)$, or $\delta''(p^2)$, where $p^2 = (m_b v - q)^2$ is the invariant partonic mass squared of the final-state jet. As mentioned earlier, the power counting in the shape-function region is different from the one used in OPE calculations, and indeed a good portion of the $\sim m_b^{-2}$ terms in the OPE is already accounted for by the contributions proportional to the leading and subleading shape functions in (4.2) and (4.11). We identify the corresponding terms using the momentum relations for the shape functions in (4.16). In particular, this reproduces all terms at order $\sim m_b^{-2}$ in the OPE which contain derivatives of $\delta(p^2)$. We include the remaining terms of the form $\sim m_b^{-2} \delta(p^2)$ by replacing

$$\begin{aligned} \delta(p^2) &= \delta(p \cdot p) = \frac{1}{p \cdot p} \int_0^\infty d\lambda \delta(p + \lambda) \delta(\lambda) \\ &\rightarrow \frac{1}{P \cdot P_+} \int_0^\infty d\lambda \delta(P_+ - \lambda) \hat{S}(\lambda) = \frac{\hat{S}(P_+)}{P \cdot P_+} : \end{aligned} \quad (4.17)$$

Here p are the light-cone projections of the partonic momentum p , which are related to the hadronic quantities P by $P = p + (M_B - m_b)$. Similarly, $\lambda = (M_B - m_b) \lambda'$.

The result of these manipulations is

$$F^{\text{hadr}(2)} = \frac{1}{(M_B - P_+)^2} \hat{S}(P_+) : \quad (4.18)$$

Together with (4.2) and (4.11) this accounts for all known first- and second-order power corrections to the $B \rightarrow X_s$ photon spectrum, both in the shape-function region and in the OPE region. The redefinition (4.12) of the leading shape function from \hat{S} to \hat{S}' leaves the form of the second-order power corrections unaffected.

In Section 4.5 we study the numerical impact of second-order power corrections on various $B \rightarrow X_{u1}$ partial rates and find their effects to be tiny. It is therefore a safe approximation to neglect hadronic power corrections of order $\sim m_b^{-3}$ or higher. The only possible exception to this conclusion relates to the so-called weak annihilation terms in $B \rightarrow X_{u1}$ decay, which will be included in our error analysis.

4.3 Inclusive semileptonic decays

In terms of the \tilde{W}_i functions introduced in chapter 1, the triple differential decay rate for $B \rightarrow X_u l$ reads

$$\begin{aligned} \frac{d^3 \Gamma_u}{dP_+ dP_- dP_1} &= \frac{G_F^2 \tilde{Y}_{ub}^2}{16\pi^3} U_Y(h; i) (M_B - P_+) \\ &\quad (P_- - P_1) (M_B - P_+ + P_1 - P_+) F_1 \\ &\quad + (M_B - P_-) (P_- - P_+) F_2 + (P_- - P_1) (P_1 - P_+) F_3 ; \end{aligned} \quad (4.19)$$

where we have collected the relevant combinations of \tilde{W}_i into the three functions

$$\begin{aligned} U_Y(h; i) F_1 &= \tilde{W}_1 ; \quad U_Y(h; i) F_2 = \frac{\tilde{W}_2}{2} ; \\ U_Y(h; i) F_3 &= \frac{Y}{4} \tilde{W}_3 + \tilde{W}_4 + \frac{1}{Y} \tilde{W}_5 \end{aligned} \quad (4.20)$$

and defined a new kinematical variable

$$Y = \frac{P_- - P_+}{M_B - P_+} ; \quad (4.21)$$

which can take values $0 \leq Y \leq 1$. The leading evolution factor $U(h; i)$ has been factored out in (4.19) for convenience, as we have done earlier in (4.1). The function $U_Y(h; i)$ differs from the corresponding function in $B \rightarrow X_s$ decay by a Y -dependent factor,

$$U_Y(h; i) = U(h; i) Y^{2a(h; i)} ; \quad (4.22)$$

where the function a in the exponent is related to the cusp anomalous dimension and is given in Appendix B.

Eq. (4.19) for the triple differential rate is exact. Note that there is no reference to the b -quark mass at this point. The only dependence on m_b is through the structure functions $F_i(P_+; Y)$ (via hard matching corrections and via the momentum constraints on the shape function \hat{S}), which are independent of the leptonic variable P_1 . The fact that the total decay rate Γ_u is proportional to m_b^5 is not in contradiction with (4.19). It is instructive to demonstrate how these five powers of m_b are recovered in our approach. At tree level and leading power the functions F_2 and F_3 vanish, while $F_1 = \hat{S}(P_+)$. Integrating over the full range of P_1 and P_- builds up five powers of $(M_B - P_+)$. For the purpose of illustration, let us rename the P_+ variable to $!$ in the last integration, so that the total decay rate is given as

$$\begin{aligned} \Gamma_u &= \frac{G_F^2 \tilde{Y}_{ub}^2}{192\pi^3} \int_0^{M_B} d! (M_B - !)^5 \hat{S}(!) = \frac{G_F^2 \tilde{Y}_{ub}^2}{192\pi^3} \int_{m_b}^{M_B - m_b} d! (m_b + !)^5 S(!) \\ &= \frac{G_F^2 \tilde{Y}_{ub}^2}{192\pi^3} (m_b + h!)^5 [1 + O(\frac{1}{m_b^2})] : \end{aligned} \quad (4.23)$$

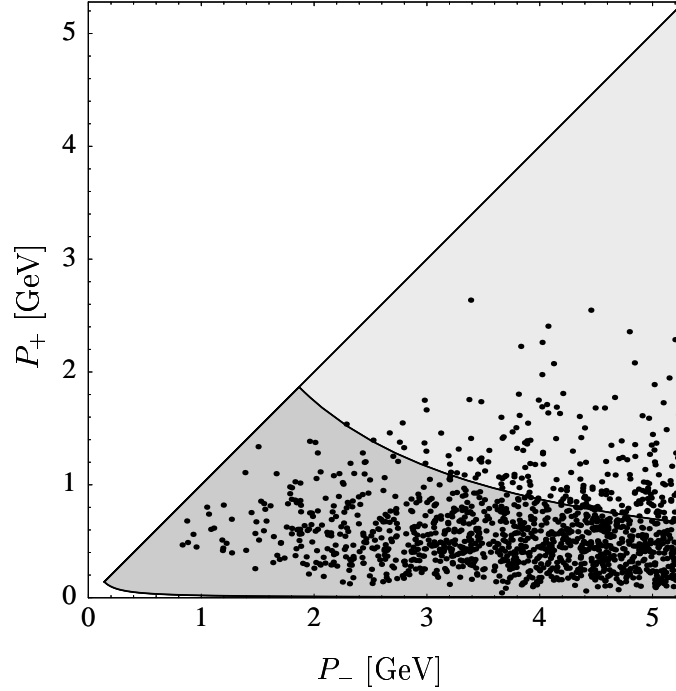


Figure 4.1: The hadronic phase space in P_+ and P_- . The light gray region contains background from $B \rightarrow X_c l$ decays, while the dark gray region is only populated by $B \rightarrow X_u l$ events. The line separating the two regions is the contour where $M_X^2 = P_+ P_- = M_D^2$. Each point represents a $B \rightarrow X_u l$ event in a Monte-Carlo simulation using the results of this chapter. While the shape-function region of large P_- and small P_+ is highly populated, there is not a single event with P_+ larger than 3 GeV out of the 1300 events generated.

At tree level, the first moment of the shape function $S(!)$ vanishes. Beyond tree level this is no longer the case, and the average $h(!)$ depends on the size of the integration domain. The above observation motivates the use of the shape-function scheme [63], in which the b-quark mass is defined as $m_b^{SF} = m_b^{\text{pole}} + h(!) + O(1=m_b)$. After this is done, (4.23) recovers the form of the conventional OPE result.

Eq. (4.19) and the above argument tell us that the differential rate is a priori rather insensitive to the b-quark mass in the endpoint region, where P_+ (and therefore $h(!)$) is a small quantity. Only when the rates are integrated over a sufficiently wide domain, so that shape-function integrals can be approximated using a moment expansion, a dependence on m_b enters indirectly via the first moment of the leading-order shape function. Likewise, a dependence on other HQET parameters such as α_s enters via the sensitivity to higher moments.

In the remainder of this section we present the various contributions to the structure functions F_i , following the same line of presentation as we did in the case of $B \rightarrow X_s$ decay in Section 4.2. As before, while the resulting expressions are

"optimized" for the shape-function region, they can be used over the entire phase space and give the correct result for the total decay rate up to corrections of $O(\frac{2}{s})$. In the shape-function region, where P_+ is a small quantity, one may organize each F_i as a series in inverse powers of $1=(M_B - P_+)$. No assumption about the variable y is made, which is treated as an $O(1)$ quantity.² A preview of the results of our calculation is depicted in Figure 4.1, which shows an illustration of our prediction for the distribution of events in the plane $(P_+; P_-)$.

4.3.1 Leading-power factorization formula

The leading-power expressions for the hadronic structure functions W_i have been calculated in [63] at one-loop order in renormalization-group improved perturbation theory. At this level F_2 does not obtain a contribution, whereas F_1 and F_3 do. Symbolically, they take the factorized form $H_{ui} J \hat{S}$, consisting of hard functions H_{ui} and the convolution of the jet function J with the leading shape function \hat{S} . More precisely,

$$F_i^{(0)}(P_+; y) = H_{ui}(y; \mu_h) \int_0^{P_+} dy_b J(y_b(P_+ - y); \mu_b) \hat{S}(y; \mu_b); \quad (4.24)$$

where the hard functions are given by

$$\begin{aligned} H_{u1}(y; \mu_h) &= 1 + \frac{C_F s(\mu_h)}{4} \left[4 \ln^2 \frac{y \mu_b}{\mu_h} + 10 \ln \frac{y \mu_b}{\mu_h} \right. \\ &\quad \left. + 4 \ln y \frac{2 \ln y}{1 - y} - 4 I_2(1 - y) - \frac{2}{6} \right]; \\ H_{u3}(y; \mu_h) &= \frac{C_F s(\mu_h)}{4} \frac{2 \ln y}{1 - y}; \end{aligned} \quad (4.25)$$

and $H_{u2} = 0$. As before, the differential decay rate is independent of the matching scales μ_h , μ_b and μ_i at $\mu_b \ll Q \ll \mu_h$. The jet function J has already been given in (4.5). Note that the b -quark mass appears only as the argument of logarithms, where it plays the role of setting the renormalization scale.

4.3.2 Kinematical power corrections

As in the case of $B \rightarrow X_s$ decay, there is a class of power corrections to the $B \rightarrow X_{u1}$ decay distributions which are small only because of the restriction to certain regions in phase space, but which are not associated with new hadronic parameters. In the present case, these terms can be extracted from the one-loop expressions derived in [2]. They are then convoluted with the leading shape function. As previously, the scale separation that can be achieved for these power-suppressed

²In the shape-function region, where $P_+ \ll P_-$, we have $y \approx \mu_b$, which is the variable used in the leading-power analysis in [63].

terms is only approximate, and we thus assign a coupling $\alpha_s(\mu)$ with them, where the scale μ is expected to be of order $\sqrt{s} \approx m_b \sqrt{QCD}$.

The resulting expressions for the structure functions can be written in a compact form in terms of the variables x and y defined in (4.7) and (4.21). We find

$$\begin{aligned}
F_1^{kin}(P_+; y) &= \frac{1}{M_B} \frac{C_F \alpha_s(\mu)}{P_+} \int_0^{Z_{P_+}} d\tau \hat{S}(\tau; y) \\
&\quad \frac{f_1(x; y)}{(1+x)^2 y (x+y)} - \frac{2g_1(x; y)}{x(1+x)^2 y^2 (x+y)} \\
&\quad \ln \left(1 + \frac{y}{x} \right) - \frac{4}{x} \ln \left(y + \frac{y}{x} \right) ; \\
F_2^{kin}(P_+; y) &= \frac{1}{M_B} \frac{C_F \alpha_s(\mu)}{P_+} \int_0^{Z_{P_+}} d\tau \hat{S}(\tau; y) \\
&\quad \frac{f_2(x; y)}{(1+x)^2 y^2 (x+y)} - \frac{2x g_2(x; y)}{(1+x)^2 y^3 (x+y)} \ln \left(1 + \frac{y}{x} \right) ; \\
F_3^{kin}(P_+; y) &= \frac{1}{M_B} \frac{C_F \alpha_s(\mu)}{P_+} \int_0^{Z_{P_+}} d\tau \hat{S}(\tau; y) \\
&\quad \frac{f_3(x; y)}{(1+x)^2 y^3 (x+y)} + \frac{2g_3(x; y)}{(1+x)^2 y^4 (x+y)} \ln \left(1 + \frac{y}{x} \right) ;
\end{aligned} \tag{4.26}$$

where the functions f_i, g_i are given by

$$\begin{aligned}
f_1(x; y) &= 9y + 10y^2 + x(16 + 12y + 6y^2) + x^2(13y - 12) ; \\
g_1(x; y) &= 2y^3 - 2xy^2(4+y) - x^2y(12 + 4y + y^2) - 4x^3(y+2) + 3x^4(y-2) ; \\
f_2(x; y) &= y^2 + xy(8 + 4y + y^2) + 3x^2y(10 + y) + x^3(12 + 19y) + 10x^4 ; \\
g_2(x; y) &= 2y^2 + 4xy(1 + 2y) + x^2y(18 + 5y) + 6x^3(1 + 2y) + 5x^4 ; \\
f_3(x; y) &= 2y^3(2y - 11) + xy^2(94 + 29y + 2y^2) + 2x^2y(72 + 18y + 13y^2) \\
&\quad + x^3(72 - 42y + 70y^2 - 3y^3) - 10x^4(6 - 6y + y^2) ; \\
g_3(x; y) &= 4y^4 - 6x(y - 5)y^3 - 4x^2y^2(20 + 6y + y^2) \\
&\quad + x^3y(90 - 10y - 28y^2 + y^3) + x^4(36 + 36y - 50y^2 + 4y^3) \\
&\quad + 5x^5(6 - 6y + y^2) ;
\end{aligned} \tag{4.27}$$

The above formulae are the exact $O(\alpha_s)$ corrections to the leading-power expression. This means that, when integrated over the entire phase space, they will give rise to the correct result for the total rate up to that order. In the shape-function region (where $P_+ \ll P$) the integrands in (4.26) can be expanded in powers of $1/m_b$ by counting $y = O(1)$ and $x = O(1/m_b)$. Note that this organizes the $1/m_b$ expansion as an expansion in powers of the hadronic variable $1/(M_B - P_+)$. The

leading terms read

$$\begin{aligned}
F_1^{\text{kin}(1)}(P_+; y) &= \frac{1}{M_B P_+} \frac{C_F s(\cdot)}{4} \int_0^{Z_{P_+}} d\tau \hat{S}(\tau; i) \left[6 \frac{5}{y} + \frac{12}{y} - 4 \ln \frac{y}{x} \right]; \\
F_2^{\text{kin}(1)}(P_+; y) &= \frac{1}{M_B P_+} \frac{C_F s(\cdot)}{4} \int_0^{Z_{P_+}} d\tau \hat{S}(\tau; i) \frac{1}{y}; \\
F_3^{\text{kin}(1)}(P_+; y) &= \frac{1}{M_B P_+} \frac{C_F s(\cdot)}{4} \int_0^{Z_{P_+}} d\tau \hat{S}(\tau; i) \left[4 \frac{22}{y} + \frac{8}{y} \ln \frac{y}{x} \right] : \quad (4.28)
\end{aligned}$$

Further accuracy can be achieved by adding the next-order corrections, for which we obtain

$$\begin{aligned}
F_1^{\text{kin}(2)}(P_+; y) &= \frac{1}{(M_B P_+)^2} \frac{C_F s(\cdot)}{4} \int_0^{Z_{P_+}} d\tau (P_+ - \tau) \hat{S}(\tau; i) \\
&\quad \left[12 + \frac{16}{y} + \frac{3}{y^2} + \frac{12}{y^2} \frac{20}{y} + 6 \ln \frac{y}{x} \right]; \\
F_2^{\text{kin}(2)}(P_+; y) &= \frac{1}{(M_B P_+)^2} \frac{C_F s(\cdot)}{4} \int_0^{Z_{P_+}} d\tau (P_+ - \tau) \hat{S}(\tau; i) \\
&\quad \left[1 + \frac{2}{y} + \frac{7}{y^2} - \frac{4}{y^2} \ln \frac{y}{x} \right]; \\
F_3^{\text{kin}(2)}(P_+; y) &= \frac{1}{(M_B P_+)^2} \frac{C_F s(\cdot)}{4} \int_0^{Z_{P_+}} d\tau (P_+ - \tau) \hat{S}(\tau; i) \\
&\quad \left[6 + \frac{69}{y} - \frac{64}{y^2} + \frac{52}{y^2} \frac{28}{y} \ln \frac{y}{x} \right] : \quad (4.29)
\end{aligned}$$

In the various phase-space regions of interest to the determination of \mathcal{N}_{ub} , the above terms (4.28) and (4.29) approximate the full result (4.26) very well (see Section 4.5 below).

Let us comment here on a technical point already mentioned in section 4.1. When combined with the phase-space factors in (4.19), the exact expressions for F_i^{kin} in (4.26) are regular in the limit $P_- \rightarrow P_+$, corresponding to $y \rightarrow 0$. However, this feature is not automatically ensured when the structure functions, but not the phase-space factors, are expanded about the heavy-quark limit. With our choice of the variables x and y , we encounter terms as singular as $1=y^n$ at n -th order in the expansion, as is obvious from the explicit expressions above. Phase space scales like y^2 in the limit $y \rightarrow 0$ (note that $P_- \rightarrow P_+$ as $P_- \rightarrow P_+$ because of (1.5)), so that the results (4.28) and (4.29) can be applied without encountering any kinematical singularities. In order to achieve this, it was crucial to define the variable y in the way we did in (4.21). We emphasize this point because straightforward application of the technology of SCET and HQET developed in [66, 75, 76] would give an expansion of the structure functions F_i in powers of $1=y^n$, whereas phase space is proportional to $4p^2 = (p_- - p_+)^2 / y^2$. In the kinematical region where $p_+ < 0$, which is allowed due to off-shell effects in the B meson, this

leads to singularities as $p \rightarrow 0$. In order to avoid these singularities, we have reorganized the SCET expansion as an expansion in $1=(p_+ - p_-)$ instead of $1=p_-$, where $p_+ = p_-$ in the shape-function region.

4.3.3 Subleading shape-function contributions

The contributions from subleading shape functions to arbitrary $B \rightarrow X_u 1$ decay distributions have been derived (at tree level) in [66, 75, 76]. The results involve the same set of subleading shape functions as previously discussed in Section 4.2.3. Again, the structure function F_2 does not obtain a contribution, while

$$\begin{aligned} F_1^{\text{hadr}(1)}(p_+; y) &= \frac{1}{M_B - p_+} \left((p_+) \hat{S}(p_+) + \hat{\ell}(p_+) + \frac{\hat{u}(p_+) - \hat{v}(p_+)}{y} \right); \\ F_3^{\text{hadr}(1)}(p_+; y) &= \frac{1}{M_B - p_+} \frac{2}{y} \left((p_+) \hat{S}(p_+) - \hat{\mathcal{X}}(p_+) + \frac{\hat{\ell}(p_+) + \hat{v}(p_+)}{y} \right); \end{aligned} \quad (4.30)$$

At this point we recall the discussion of Section 4.2.3, where we have argued that the $B \rightarrow X_s$ photon spectrum should be used to fit the function \hat{S} of (4.12), which is defined to be a linear combination of the leading shape function \hat{S} and the subleading shape functions $\hat{\ell}$, \hat{u} , \hat{v} . When the above results are rewritten in terms of the new function \hat{S} nothing changes in the expressions for $F_i^{(0)}$ except for the simple replacement $\hat{S} \rightarrow \hat{S}$, which we from now on assume. At the level of subleading shape functions $F_2^{\text{hadr}(1)} = 0$ and $F_3^{\text{hadr}(1)}$ remain unchanged, while

$$\begin{aligned} F_1^{\text{hadr}(1)}(p_+; y) &= \frac{1}{M_B - p_+} \left((p_+) \hat{S}(p_+) + 2\hat{\ell}(p_+) \right. \\ &\quad \left. + [\hat{u}(p_+) - \hat{v}(p_+)] \frac{1}{y} \right); \end{aligned} \quad (4.31)$$

It follows that there reside some linear combinations of subleading shape functions in the triple differential decay rate that cannot be extracted from information on the photon spectrum in $B \rightarrow X_s$ decays. In the end, this dependence gives rise to a theoretical uncertainty.

4.3.4 Residual hadronic power corrections

In analogy with our treatment for the case of $B \rightarrow X_s$ decay, we start from the expressions for the $1=m_b^2$ corrections to the triple differential $B \rightarrow X_u 1$ decay rate obtained by applying the OPE to the hadronic tensor [1, 13]. We saw in

chapter 1 that:

$$\begin{aligned}
W_1^{(2)} &= (p_+) \left[1 + \frac{2}{3p^2} \frac{1}{2} \frac{3}{2} \right] + {}^0(p_+) \left[\frac{2}{3p} \frac{1}{2} \frac{3}{2} + \frac{5}{6m_b} \frac{1}{2} \frac{15}{2} \right] \\
&\quad {}^0(p_+) \frac{1}{6} ; \\
W_2^{(2)} &= (p_+) \left[\frac{4}{3p^2} \frac{1}{2} \frac{6}{2} \right] ; \\
\frac{y}{4} W_3^{(2)} + W_4^{(2)} + \frac{1}{y} W_5^{(2)} &= \frac{(p_+)}{p} \left[\frac{2}{3p} \frac{1}{2} \frac{12}{2} + \frac{4}{3m_b} \frac{1}{2} \frac{9}{2} \right] \\
&\quad + \frac{{}^0(p_+)}{p} \left[\frac{2}{3} \frac{1}{2} + 4 \frac{2}{2} \right] : \tag{4.32}
\end{aligned}$$

The desired $1=(M_B - P_+)^2$ corrections to the structure functions F_i can then be extracted by expanding the leading and subleading contributions $F_i^{(0)}$ and $F_i^{\text{hadr}(1)}$ in terms of their moments in (4.16), and by subtracting the results from (4.32). Following the same procedure as in Section 4.2.4 to express the remaining power corrections in terms of the leading shape function, we obtain

$$\begin{aligned}
F_1^{\text{hadr}(2)}(P_+; y) &= \frac{1}{(M_B - P_+)^2} \left[\frac{4}{3y^2} \frac{1}{2} \frac{6}{2} + \frac{1}{3} \frac{1}{2} \frac{3}{2} \right] \hat{S}(P_+); \\
F_2^{\text{hadr}(2)}(P_+; y) &= \frac{1}{(M_B - P_+)^2} \left[\frac{2}{3y^2} \frac{1}{2} \frac{3}{2} \right] \hat{S}(P_+); \\
F_3^{\text{hadr}(2)}(P_+; y) &= \frac{1}{(M_B - P_+)^2} \left[\frac{4}{3y^2} \frac{1}{2} \frac{24}{2} + \frac{4}{3y} \frac{1}{2} \frac{9}{2} \right] \hat{S}(P_+) : \tag{4.33}
\end{aligned}$$

These expressions remain unchanged when the shape function \hat{S} is used instead of $\hat{\hat{S}}$.

4.3.5 Weak annihilation contributions

In the OPE calculation several contributions appear at third order in the power expansion: $1=m_b$ corrections to the kinetic and chromomagnetic operators, the Darwin and spin-orbit terms, and weak annihilation contributions. The Darwin and spin-orbit terms correspond to the forward B-meson matrix elements of (light) flavor-singlet operators [77]. The corresponding HQET parameters $\hat{3}_D$ and $\hat{3}_{LS}$ can in principle be extracted from moments of inclusive $B \rightarrow X_c l$ decay spectra. They are insensitive to the flavor of the spectator quark inside the B-meson. The weak annihilation contribution, on the other hand, results from four-quark operators with flavor non-singlet structure. Graphically, this contribution corresponds to a process in which the b and u quark annihilate into a W^- . Weak annihilation terms come with a phase-space enhancement factor of 16^{-2} and so are potentially more important than other power corrections of order $1=m_b^3$. Because of the flavor

dependence, these contributions can affect neutral and charged B mesons differently [78]. One choice of basis for the corresponding four-quark operators is [55]

$$\langle B | \bar{d}_L u_L u_L b_L | B \rangle = \frac{f_B^2 M_B^2}{4} B_1; \quad \langle B | \bar{d}_R u_L u_L b_R | B \rangle = \frac{f_B^2 M_B^2}{4} B_2; \quad (4.34)$$

where f_B is the B meson decay constant, and B_i are hadronic parameters. In the vacuum saturation approximation they are given by $B_1 = B_2 = 1$ for charged B mesons and $B_1 = B_2 = 0$ for neutral ones. The total semileptonic rate is proportional to the difference ($B_2 - B_1$), which implies that the weak annihilation contribution would vanish in this approximation. Currently, only rough estimates are available for the magnitude of the deviation of this difference from zero. The resulting effect on the total branching ratio is [61]

$$\mathcal{B}(B \rightarrow X_u \ell^+ \ell^-) \approx 3.9 \frac{f_B^2}{(0.2 \text{ GeV})^2} \frac{B_2 - B_1}{0.1} \mathcal{V}_{ub}^2; \quad (4.35)$$

Again, we expect this effect to be different for charged and neutral B mesons. The most important feature of weak annihilation is that it is formally concentrated at the kinematical point where all the momentum of the heavy quark is transferred to the lepton pair [78]. At the parton level this implies that the corresponding contribution is proportional to $(q^2 - m_b^2)$. It is therefore included in every cut that includes the q^2 endpoint, and its effect is independent of the specific form of the cut.

We suggest two different strategies to control this effect. The first is to include it in the error estimate as a constant contribution proportional to the total rate. A recent study [79] puts a limit on this effect of $\sim 1.8\%$ on the total rate (at 68% confidence level) by analyzing CLEO data. The second one is to impose a cut $q^2 \geq q_{\text{max}}^2$, thus avoiding the region where the weak annihilation contribution is concentrated. The maximal value of q^2 is $(M_B - M)^2$, but one must exclude a larger region of phase space, such that the excluded contribution to the decay rate at large q^2 (corresponding to a region near the origin in the $(P_-; P_+)$ plane) can be reliably calculated. In our numerical analysis, we will study the effect of a cut $q^2 \geq (M_B - M_D)^2$, which satisfies this criterion.

For completeness, we note that even after the weak annihilation contribution near maximum q^2 has been removed, there could in principle exist other, flavor-specific contributions to the semileptonic decay amplitudes that are different for charged and neutral B mesons. The leading terms of this kind contribute at order $1/m_b$ in the shape-function region and are parameterized by a set of four-quark subleading shape functions [66, 75, 76]. Model estimates of these contributions show that they are very small for all observables considered for an extraction of \mathcal{V}_{ub} [76, 80]. If only flavor-averaged decay rates are measured, the effects of four-quark subleading shape functions can be absorbed entirely by a redefinition of the functions $\hat{u}(\hat{s})$ and $\hat{v}(\hat{s})$ [66], without affecting the momentum relations in (4.16).

4.4 Shape-function parameterizations

Hadronic-physics effects enter the description of inclusive decay rates via non-perturbative shape functions. Perturbation theory cannot tell us much about the local form of these functions, but moments of them are calculable provided that the domain of integration is much larger than Λ_{QCD} . Since the shape functions contain information about the internal structure of the B meson, knowledge of them relates directly to the determination of the b-quark mass m_b , the kinetic-energy parameter μ_1 , and in principle the matrix elements of higher-dimensional operators. Improved measurements of the shape of the $B \rightarrow X_s \gamma$ photon spectrum will therefore lead directly to a more precise determination of HQET parameters. This argument can be turned around to constrain the leading shape function using knowledge of m_b and μ_1 from other physical processes such as a $b \rightarrow c$ moment analysis [81]. We emphasize, however, that there are obviously infinitely many locally different functions that have identical first few moments. In this section we present a few functional forms that can be used to model the shape functions and to fit the current experimental data.

To achieve stringent constraints on the leading shape function a precise definition of the HQET parameters is required. It is a well-known fact that the pole-mass scheme introduces uncontrollable ambiguities. To avoid these uncertainties several short-distance definitions have been proposed, such as the $\overline{\text{MS}}$ scheme, the potential-subtraction scheme [40], the $(1S)$ scheme [82], the kinetic scheme [39], or the shape-function scheme [63]. While the decay rates are of course independent of the particular choice, it is advantageous to use a mass scheme that is designed for the physics problem at hand. In the case of inclusive B decays into light particles, this is the shape-function scheme.

4.4.1 Models for the leading shape function

Model-independent constraints on the shape function $\hat{S}(\tau; i)$ can be derived by analyzing moments defined with an upper limit of integration τ_0 , i.e.

$$M_N(\tau_0; i) = \int_0^{\tau_0} d\tau \tau^N \hat{S}(\tau; i) : \quad (4.36)$$

For practical applications, τ_0 should be taken of order the size of the window where the $B \rightarrow X_s \gamma$ photon spectrum is experimentally accessible, $\tau_0 = M_B - 2E_{\text{min}}^{\text{in}}$ with $E_{\text{min}}^{\text{in}} = 1.8 \text{ GeV}$. These moments can be expanded in terms of matrix elements of local operators as long as τ_0 is large compared to Λ_{QCD} . In the shape-function scheme, HQET parameters are defined to all orders in perturbation theory through ratios of such moments, e.g. [63]

$$\begin{aligned} \frac{M_1(\tau_0 + (\tau_0; i); i)}{M_0(\tau_0 + (\tau_0; i); i)} &= (\tau_0; i); \\ \frac{M_2(\tau_0 + (\tau_0; i); i)}{M_0(\tau_0 + (\tau_0; i); i)} &= \frac{2(\tau_0; i)}{3} + (\tau_0; i); \end{aligned} \quad (4.37)$$

Here, the factorization scale μ_f is related to the size of the integration domain via the implicit equation $\mu_0 = \mu_f + \mathcal{O}(\mu_f; \mu_i)$. In practice μ_f is close to the intermediate scale μ_i . At tree level, the relations between parameters in the shape-function scheme and the pole scheme are $\mu_f(\mu_i) = \mu_i^{\text{pole}}$ and $\mu_0^2(\mu_f; \mu_i) = \mu_i^2$. The corresponding relations at one- and two-loop order have been worked out in [63] and [83], respectively. These relations allow us to obtain precise determinations of $\mu_f(\mu_i)$ and $\mu_0^2(\mu_f; \mu_i)$ from other physical processes.

For reference purposes, it is helpful to quote values for μ_f and μ_0^2 using only a single scale μ_i instead of two independent scales μ_f and μ_i . To one-loop order, these parameters can be related to those determined from the moments via [63]

$$\begin{aligned} \mu_f(\mu_i) &= \mu_i \left(1 + \frac{C_F}{2} \frac{\mu_i^2}{\mu_f^2} \right) + \frac{C_F}{2} \frac{\mu_i^2}{\mu_f^2} \ln \frac{\mu_f}{\mu_i}; \\ \mu_0^2(\mu_f; \mu_i) &= \mu_i^2 \left(1 + \frac{C_F}{2} \frac{\mu_i^2}{\mu_f^2} \right) + \frac{C_F}{2} \frac{\mu_i^2}{\mu_f^2} \ln \frac{\mu_f}{\mu_i} \\ &\quad + 3 \frac{C_F}{2} \frac{\mu_i^2}{\mu_f^2} \ln \frac{\mu_f}{\mu_i}; \end{aligned} \quad (4.38)$$

where we have neglected higher-dimensional operator matrix elements that are suppressed by inverse powers of μ_f . A typical choice for the scale μ_i is 1.5 GeV, which we will use as the reference scale throughout this chapter. It will be convenient to connect the parameter μ_i extracted from the first moment of the shape function with a low-scale subtracted quark-mass definition referred to as the "shape-function" mass. Following [63], we define

$$m_b(\mu_f; \mu_i) = M_B(\mu_f; \mu_i); \quad (4.39)$$

The general procedure for modeling the leading shape function $\hat{S}(\mu_f; \mu_i)$ from a given functional form $F(\mu_f)$ is as follows. The shape of $F(\mu_f)$ is assumed to be tunable so that it can be used to fit the $B \rightarrow X_s$ photon spectrum. Only the norm of the shape function is fixed theoretically. Note that the moment relations (4.37) are insensitive to the norm, so that formulae for μ_f and μ_0^2 follow directly from the functional form of $F(\mu_f)$. Examples of such formulae will be given below. We define moments $M_N^{[\mathbb{F}]}(\mu_0)$ of F in analogy with (4.36). The first relation in (4.37) implies that for a given μ_0 the factorization scale is

$$\mu_f = \mu_0 \frac{M_1^{[\mathbb{F}]}(\mu_0)}{M_0^{[\mathbb{F}]}(\mu_0)}; \quad (4.40)$$

Now that μ_f is known, the norm is determined by requiring that the zeroth moment

of the shape function is [63]

$$\begin{aligned} M_0(\hat{\mu}_0; \hat{\mu}_i) = 1 & - \frac{C_{Fs}(\hat{\mu}_i)}{C_{Fs}(\hat{\mu}_0)} \ln^2 \frac{\hat{\mu}_i}{\hat{\mu}_0} + \ln \frac{\hat{\mu}_i}{\hat{\mu}_0} + \frac{\hat{\mu}_i^2}{24} \\ & + \frac{C_{Fs}(\hat{\mu}_i)}{C_{Fs}(\hat{\mu}_0)} \ln \frac{\hat{\mu}_i}{\hat{\mu}_0} \frac{1}{2} - \frac{\hat{\mu}_i^2}{3} \frac{C_{Fs}(\hat{\mu}_i)}{\hat{\mu}_i^2} + \dots \end{aligned} \quad (4.41)$$

It follows that $M_0(\hat{\mu}_0; \hat{\mu}_i) = M_0^{[F]}(\hat{\mu}_0) F(\hat{\mu})$ serves as a model of $\hat{S}(\hat{\mu}; \hat{\mu}_i)$ or $\hat{S}(\hat{\mu}; \hat{\mu}_i)$.

We now suggest three two-parameter models for the leading-order shape function based on an exponential-type function $F^{(\text{exp})}$, a gaussian-type function $F^{(\text{gauss})}$, and hyperbolic-type function $F^{(\text{hyp})}$. We use two parameters that can be tuned to fit the photon spectrum: a dimensionful quantity which coincides with the position of the average $h\hat{\mu}_i$, and a positive number b which governs the behavior for small $\hat{\mu}$. The functions we propose are

$$\begin{aligned} F^{(\text{exp})}(\hat{\mu}; \hat{\mu}_i; b) &= \frac{N^{(\text{exp})}}{d_{(\text{exp})}^b} \exp \left(-\frac{\hat{\mu}_i}{d_{(\text{exp})}} \right); \\ F^{(\text{gauss})}(\hat{\mu}; \hat{\mu}_i; b) &= \frac{N^{(\text{gauss})}}{d_{(\text{gauss})}^b} \exp \left(-\frac{\hat{\mu}_i^2}{d_{(\text{gauss})}^2} \right); \\ F^{(\text{hyp})}(\hat{\mu}; \hat{\mu}_i; b) &= \frac{N^{(\text{hyp})}}{d_{(\text{hyp})}^b} \cosh^{-1} \left(\frac{\hat{\mu}_i}{d_{(\text{hyp})}} \right); \end{aligned} \quad (4.42)$$

For convenience, we normalize these functions to unity. The parameters $d_{(i)}$ are determined by the choice $\hat{\mu} = h\hat{\mu}_i$. We find

$$\begin{aligned} N^{(\text{exp})} &= \frac{d_{(\text{exp})}^b}{(b)}; & d_{(\text{exp})} &= b; \\ N^{(\text{gauss})} &= \frac{2d_{(\text{gauss})}^{b-2}}{(b=2)}; & d_{(\text{gauss})} &= \frac{\left(\frac{1+b}{2}\right)^{1/2}}{\left(\frac{b}{2}\right)}; \\ N^{(\text{hyp})} &= \frac{[4d_{(\text{hyp})}]^b}{2(b)(b; \frac{1}{4})(b; \frac{3}{4})}; & d_{(\text{hyp})} &= \frac{b}{4} \frac{(1+b; \frac{1}{4})(1+b; \frac{3}{4})}{(b; \frac{1}{4})(b; \frac{3}{4})}; \end{aligned} \quad (4.43)$$

where $(b; a) = \prod_{k=0}^{P-1} (k+a)^{-b}$ is the generalized Riemann zeta function. An illustration of the different functional forms is given on the left-hand side in Figure 4.2. We show a plot with the choice $b=2$, corresponding to a linear onset for small $\hat{\mu}$.

For the first two models, analytic expressions for the HQET parameters $\hat{\mu}_0$ and $\hat{\mu}_i$ are available. Following the discussion above, we compute the moments on the interval $[0; \hat{\mu}_0]$ and find for the exponential form $F^{(\text{exp})}(\hat{\mu}; \hat{\mu}_i; b)$

$$\begin{aligned} \langle \hat{\mu}; \hat{\mu}_i \rangle &= \frac{(1+b)}{b} \frac{(1+b; \frac{b\hat{\mu}_0}{b})}{(b)(b; \frac{b\hat{\mu}_0}{b})}; \\ \langle \hat{\mu}^2; \hat{\mu}_i \rangle &= \frac{2}{b^2} \frac{(2+b)}{(b)} \frac{(2+b; \frac{b\hat{\mu}_0}{b})}{(b; \frac{b\hat{\mu}_0}{b})} \langle \hat{\mu}; \hat{\mu}_i \rangle^2; \end{aligned} \quad (4.44)$$

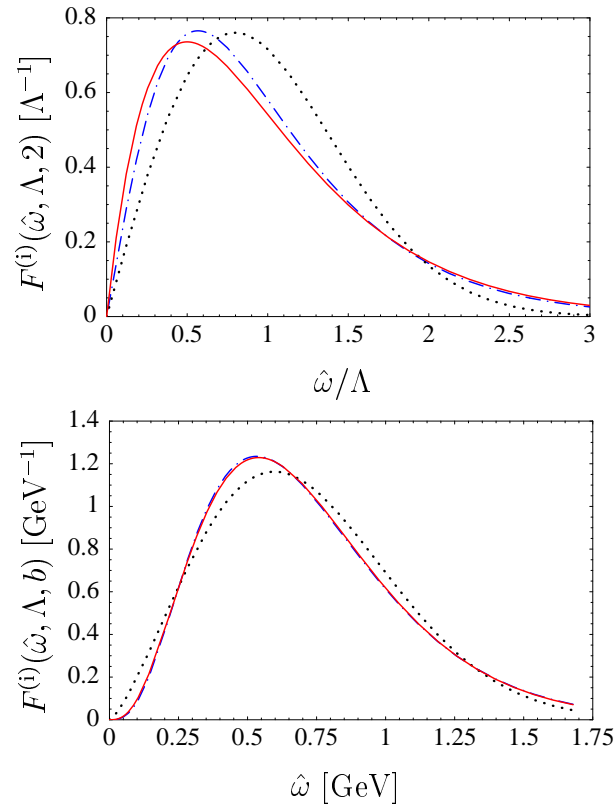


Figure 4.2: Top: Different functional forms for the leading shape function. We show $F^{(\text{exp})}(\uparrow; ; 2)$ (solid), $F^{(\text{gauss})}(\uparrow; ; 2)$ (dotted), and $F^{(\text{hyp})}(\uparrow; ; 2)$ (dash-dotted) as functions of the ratio $\uparrow =$. Bottom: The same functions with the parameters Λ and b tuned such that $m_b(\uparrow; ;) = 4.61 \text{ GeV}$ and $\Lambda^2(\uparrow; ;) = 0.2 \text{ GeV}^2$. See text for explanation.

where $f = \hat{\Gamma}_0$ ($f; i$).

A similar calculation for the gaussian form $F^{(gauss)}(\hat{\Gamma}; b)$ yields

$$\begin{aligned} (f; i) &= \frac{1}{d_{(gauss)}} \frac{\left(\frac{1+b}{2}\right) \left(\frac{1+b}{2}; \frac{d_{(gauss)} \hat{\Gamma}_0^2}{2}\right)}{\left(\frac{b}{2}\right) \left(\frac{b}{2}; \frac{d_{(gauss)} \hat{\Gamma}_0^2}{2}\right)}; \\ \hat{\Gamma}^2 (f; i) &= 3 \frac{1}{d_{(gauss)}} \frac{\left(1 + \frac{b}{2}\right) \left(1 + \frac{b}{2}; \frac{d_{(gauss)} \hat{\Gamma}_0^2}{2}\right)}{\left(\frac{b}{2}\right) \left(\frac{b}{2}; \frac{d_{(gauss)} \hat{\Gamma}_0^2}{2}\right)} (f; i)^2 : (4.45) \end{aligned}$$

The corresponding relations for $F^{(hyp)}(\hat{\Gamma}; b)$ must be obtained numerically.

Ultimately the shape function should be fitted to the $B \rightarrow X_s$ photon spectrum, and the above equations then determine $\hat{\Gamma}$ and $\hat{\Gamma}^2$. On the other hand, these formulae can be inverted to determine $\hat{\Gamma}$ and b from the current values of the HQET parameters. For example, if we adopt the values $m_b(\hat{\Gamma}) = 4.61 \text{ GeV}$ and $\hat{\Gamma}^2(\hat{\Gamma}) = 0.20 \text{ GeV}^2$ for the parameters in (4.38) at $\hat{\Gamma} = 1.5 \text{ GeV}$, then we find the parameter pair $\hat{\Gamma} = 0.72 \text{ GeV}$, $b = 3.95$ for the exponential model, $\hat{\Gamma} = 0.71 \text{ GeV}$, $b = 2.36$ for the gaussian model, and $\hat{\Gamma} = 0.73 \text{ GeV}$, $b = 3.81$ for the hyperbolic model. On the right-hand side of Figure 4.2 we show these three different functions plotted on the interval $[0; \hat{\Gamma}_0]$ over which themoment constraints are imposed. While the exponential (solid) and hyperbolic (dash-dotted) curves are barely distinguishable, the gaussian model has quite different characteristics. It is broader, steeper at the onset, faster to fall off, and the maximum is shifted toward larger $\hat{\Gamma}$.

An important comment is that, once a two-parameter ansatz is employed, the shape-function parameters (i.e., m_b and $\hat{\Gamma}^2$) can either be determined from a fit to the entire photon spectrum, or to the first two moments of the spectrum. Both methods are equivalent and should yield consistent results. If they do not, it would be necessary to refine the ansatz for the functional form of the shape function.

In most applications shape functions are needed for arguments $\hat{\Gamma}$ of order Q_{CD} . However, in some cases, like the ideal cut on hadronic invariant mass, $\hat{\Gamma}$ is required to be as large as M_D , which is much larger than Q_{CD} . The large- $\hat{\Gamma}$ behavior of the shape functions can be computed in a model-independent way using short-distance methods. For the leading shape function, one finds [63]

$$\hat{S}(\hat{\Gamma} \gg Q_{CD}; i) = \frac{C_F s(i)}{\hat{\Gamma}} \frac{1}{2 \ln \frac{\hat{\Gamma}}{i}} + 1 + \dots : (4.46)$$

Note that this radiative tail is negative, implying that the shape function must go through zero somewhere near $\hat{\Gamma} \sim \text{few } Q_{CD}$. For practical purposes, we "glue" the above expression onto models of the non-perturbative shape function starting at $\hat{\Gamma} = \hat{\Gamma}_+ = \sqrt{2} \bar{e} = 1.6 \text{ GeV}$, where the tail piece vanishes. In this way we obtain a continuous shape-function model with the correct asymptotic behavior. We stress that for applications with a maximal P_+ not larger than about 1.6 GeV the radiative tail of the shape function is never required. This includes all methods for extracting \mathcal{V}_{ub} discussed later in this chapter, except for the case of a cut on hadronic invariant mass, $M_X \leq M_0$, if M_0 is above 1.6 GeV .

4.4.2 Models for subleading shape functions

In the last section we have been guided by the fact that the $B \rightarrow X_s$ photon spectrum is at leading power directly determined by the leading shape function. This helped in finding models that have roughly the same shape as the photon spectrum. At the subleading level considered here, however, no such guidance is provided to us. The available information is limited to the tree-level moment relations (4.16), stating that the norms of the subleading shape functions vanish while their first moments do not. In [66], two classes of models have been proposed, in which the subleading shape functions are "derived" from the leading shape function. A particularly simple choice is

$$\hat{f}(\tau) = \frac{1}{2} \hat{S}^0(\tau); \quad \hat{u}(\tau) = \frac{2}{3} \hat{S}^0(\tau); \quad \hat{v}(\tau) = \frac{1}{2} \hat{S}^0(\tau); \quad (4.47)$$

Below, we will sometimes refer to this set of functions as the "default choice". We choose the parameter τ_0 in the expression for $\hat{u}(\tau)$ (as well as in the expressions for the second-order hadronic power corrections) to coincide with the quantity $\tau_0^2(\tau; \tau_0)$ given in (4.44) and (4.45). However, for consistency with the tree-level moment relations, we identify the parameter τ_0 in (4.13) and (4.31) with the quantity $\tau_0(\tau; \tau_0)$ evaluated in the limit where $\tau_0 \rightarrow 1$. This implies $\tau_0 = 0$ for all three types of functions and ensures that the subleading shape functions have zero norm when integrated over $0 \leq \tau < 1$.

There are of course infinitely many possibilities to find models for subleading shape functions that are in accordance with (4.16). Any function with vanishing norm and first moment can be arbitrarily added to any model for a subleading shape function without violating them moment relations. Several such functions have been proposed in recent work on subleading shape functions, see e.g. [66, 74, 76, 80]. Specifically, we define the functions

$$\begin{aligned} h_1(\tau) &= \frac{M_2}{N_0^3} \frac{a^{a+1}}{2(a)} z^{a-1} e^{az} \frac{a-1}{z} a(2-z); \\ h_2(\tau) &= \frac{M_2}{N_0^3} \frac{a^3}{2} e^{az} \left(1 - 2az + \frac{a^2 z^2}{2} \right); \\ h_3(\tau) &= \frac{M_2}{N_0^3} \frac{2^p a}{2} e^{az^2} \left(1 - 2z \frac{a}{2} \right) 2e^z + 2ze^{2z} \text{Ei}(z); \\ h_4(\tau) &= \frac{M_2}{N_0^3} \frac{2^p a}{4} \frac{2}{2} e^{az^2} \left(1 - 2z \frac{a}{2} \right) \\ &\quad + \frac{8}{(1+z^2)^4} z \ln z + \frac{z}{2} (1+z^2) - \frac{1}{4} (1-z^2); \end{aligned} \quad (4.48)$$

where $z = \tau - \tau_0$, and the reference quantity $\tau_0 = 0$ (τ_{CD}) depends on the type of function, namely $\tau_0 = 0$ for h_1 and h_2 , $\tau_0 = \frac{2}{3}$ for h_3 , and $\tau_0 = \frac{8}{3}$ for h_4 . The quantity a is a free parameter. The functions (4.48) have by construction vanishing

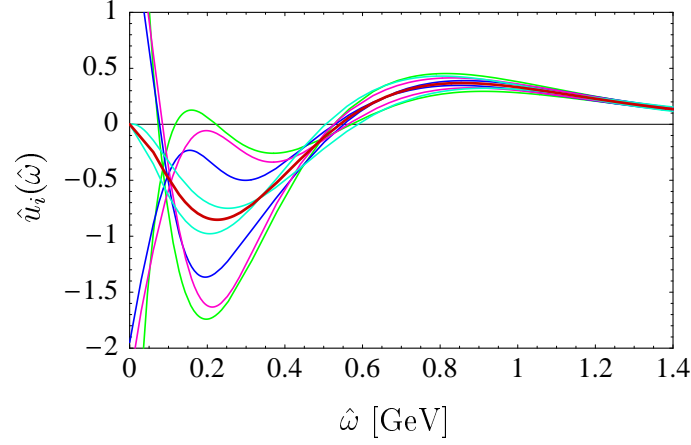


Figure 4.3: Nine models for the subleading shape function $\hat{u}(\hat{\omega})$ obtained by adding or subtracting one of the four functions $h_n(\hat{\omega})$ to the default model in (4.47), shown as a thick line. See text for explanation.

norm and first moment. Their second moments are given by the parameter M_2 , provided the normalization constants are chosen as $N = 1$ for h_1 and h_2 , and

$$N = 1 - \frac{4}{2} \left(\frac{1}{2} \right) \frac{1}{a}; \quad N = 1 - \frac{2}{8} \left(\frac{4}{2} \right) \frac{1}{a} \quad (4.49)$$

for h_3 and h_4 , respectively. The values for the parameters a and M_2 should be chosen such that the following characteristics of subleading shape functions are respected: First, they are dimensionless functions, so that their values are naturally of $O(1)$ for $\hat{\omega} \sim \Lambda_{\text{QCD}}$. Secondly, when integrated over a sufficiently large domain, their contributions are determined in terms of their first few moments. In particular, this implies that for values of $\hat{\omega} \sim \Lambda_{\text{QCD}}$ the integrals over the subleading shape functions must approach zero. Taking these considerations into account, we use $M_2 = (0.3 \text{ GeV})^3$ in all cases and choose $a = 3.5$ for h_1 , $a = 5$ for h_2 , and $a = 10$ for h_3 and h_4 .

Given the four functions (4.48), we can construct several new models for the subleading shape functions $\hat{t}(\hat{\omega})$, $\hat{u}(\hat{\omega})$, and $\hat{v}(\hat{\omega})$. For each function, we construct a set of 9 models by adding or subtracting any of the functions $h_n(\hat{\omega})$ to the default choice in (4.47). Together, this method yields $9^3 = 729$ different sets $f\hat{t}_i(\hat{\omega}); \hat{u}_j(\hat{\omega}); \hat{v}_k(\hat{\omega})$ with $i, j, k = 1; \dots; 9$. This large collection of functions will be used to estimate the hadronic uncertainties in our predictions for partial decay rates. Note that for most of these sets we no longer have $\hat{t}_i(\hat{\omega}) = -\hat{v}_i(\hat{\omega})$, which was an "accidental" feature of the default model (4.47). The fact that the two functions have equal (but opposite in sign) first moments does not imply that their higher moments should also be related to each other.

For the case of $\hat{u}(\hat{\omega})$ the resulting functions are shown in Figure 4.3, where we have used the exponential model (4.42) with parameters $\omega_0 = 0.72 \text{ GeV}$ and

$b = 3.95$ for the leading shape function. In the region $\sqrt{s} \sim \Lambda_{\text{QCD}}$ they differ dramatically from each other, while the large \sqrt{s} dependence is dominated by the moment relations (4.16).

4.4.3 Illustrative studies

We stressed several times that the calculation of the hadronic tensor is "optimized" for the shape-function region of large P_- and small P_+ , while it can smoothly be extended over the entire phase space. The notions "large P_- " and "small P_+ " are to be understood as the sizes of integration domains for P_- and P_+ . Only when the differential distributions are integrated over a sufficiently large region in phase space, global quark-hadron duality ensures that the partonic description used in the present chapter matches the true, hadronic distributions with good accuracy. A more ambitious goal would be to calculate the differential decay rate point by point in the (P_+, P_-) plane. This can be done invoking local quark-hadron duality, as long as there is a sufficiently large number of hadronic final states contributing to the rate at any given point in phase space.

It is instructive to integrate the triple differential decay rate (4.19) over the leptonic variable P_1 in the range $P_+ \leq P_1 \leq P_-$, which yields the exact formula

$$\frac{d^2 \Gamma_u}{dP_+ dP_-} = \frac{G_F^2 |V_{ub}|^2}{96 \pi^3} U_Y(h; i) (M_B - P_+) (P_- - P_+)^2 \times \\ (3M_B^2 - 2P_-^2 - P_+^2) F_1 + 6(M_B - P_-) F_2 + (P_- - P_+) F_3 : \quad (4.50)$$

Our theoretical prediction for the double differential decay rate (4.50) is shown on the left-hand side of Figure 4.4. We use the exponential model for the leading shape function with parameters $m_b(\mu) = 4.61 \text{ GeV}$ and $\alpha_s(\mu) = 0.2 \text{ GeV}^{-2}$, as well as the default choice (4.47) for the subleading shape functions. For very small P_- values the rate turns negative (to the left of the gray line in the figure), signaling a breakdown of quark-hadron duality. It is reassuring that the only region where this happens is the "resonance region", where the hadronic invariant mass is of order Λ_{QCD} , and local duality breaks down.

Another useful quantity to consider is the differential P_+ rate, which is obtained by integrating the double differential rate over P_- in the range $P_+ \leq P_- \leq M_B$. The resulting P_+ spectrum is shown on the right-hand side of Figure 4.4. In the plot we also disentangle the contributions from different orders in power counting.

4.5 Predictions and error estimates for partial rates

Before discussing predictions for partial $B \rightarrow X_u \ell$ rates for various kinematical cuts, let us recapitulate the ingredients of the calculation and general procedure. We have presented expressions for the triple differential decay rate, which can be

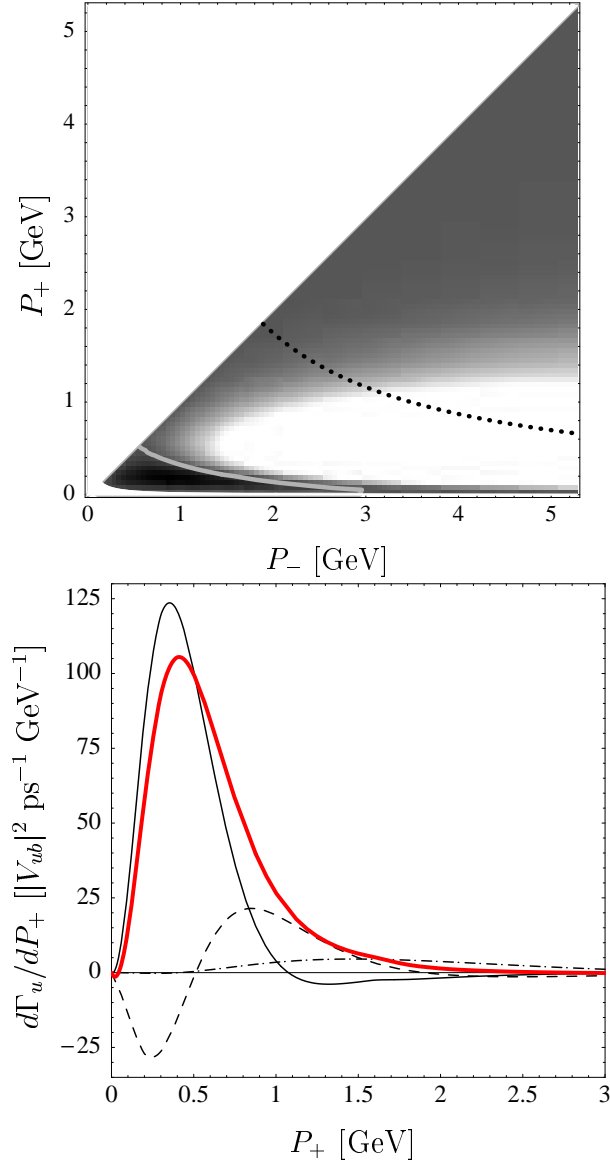


Figure 4.4: Top: Theoretical prediction for the double differential decay rate. The light area represents a large decay rate. Black regions denote areas where the decay rate is close to zero. The dotted line is given by $P_+ P_- = M_D^2$, which means that charm background is located in the upper wedge. See text for further explanation. Bottom: The P_+ spectrum extended to large values of P_+ . The thin solid line denotes the leading-power prediction, the dashed line depicts first-order power corrections, the dash-dotted line shows second-order power corrections, and the thick solid line is their sum.

organized in an expansion in inverse powers of $(M_B - P_+)$. The leading-power contribution is given at next-to-leading order in renormalization-group improved perturbation theory. At first subleading power two contributions arise. The first type involves subleading shape functions and is included at tree level, while the second type contributes perturbative corrections of order α_s that come with the leading shape function. Further contributions enter at second subleading power and are again of the two types: perturbative corrections of order α_s and non-perturbative structures at tree level. In summary, then, partial rates can be computed term by term in an expansion of the form

$$\Gamma_u = \Gamma_u^{(0)} + (\Gamma_u^{\text{kin}(1)} + \Gamma_u^{\text{hadr}(1)}) + (\Gamma_u^{\text{kin}(2)} + \Gamma_u^{\text{hadr}(2)}) + \dots \quad (4.51)$$

The goal of this section is to test the convergence of this series expansion and to perform a thorough analysis of uncertainties. For the kinematical corrections $\Gamma_u^{\text{kin}(n)}$ the sum of all terms is known and given by the expressions in (4.26), while the first two terms in the series correspond to the expanded results in (4.28) and (4.29). We will find that in all cases of interest the first two terms give an excellent approximation to the exact result for Γ_u^{kin} .

For the purpose of illustration, we adopt the exponential model for the shape function and present numerical results for two sets of input parameters, which are biased by the results deduced from fits to $B \rightarrow X_c \ell$ moments [83]. Specifically, we use $m_b(\mu_b) = 4.61 \text{ GeV}$, $\alpha_s^2(\mu_b) = 0.2 \text{ GeV}^2$ (set 1) and $m_b(\mu_b) = 4.55 \text{ GeV}$, $\alpha_s^2(\mu_b) = 0.3 \text{ GeV}^2$ (set 2). The values of the b-quark mass coincide with those obtained at two-loop and one-loop order in [83] (see also the discussion below), while the values of α_s^2 are close to the corresponding values in that reference. As was mentioned before, in the future the leading shape function $\hat{S}(\ell; \mu_i)$ should be extracted from a fit to the $B \rightarrow X_s \gamma$ photon spectrum, in which case the uncertainty in its shape becomes an experimental error, which can be systematically reduced with improved data. In the process, the "theoretically preferred" parameter values used in the present work will be replaced with the "true" values extracted directly from data. While this will change the central values for the partial rates, our estimates of the theoretical errors will only be affected marginally.

The different sources of theoretical uncertainties are as follows: First, there are uncertainties associated with the functional forms of the subleading shape functions. To estimate them, we take the spread of results obtained when using the large set of different models described in Section 4.4.2, while the central value for a partial decay rate corresponds to the default model (4.47). Secondly, there are perturbative uncertainties associated with the choice of the matching scales μ_h , μ_i , and μ_b . Decay rates are formally independent of these scales, but a residual dependence remains because of the truncation of the perturbative series. Our error analysis is as follows:

The hard scale μ_h is of order m_b . In perturbative logarithms the scale appears in the combination $(\gamma_{m_b} = \mu_h)$, see e.g. (4.25). To set a central value for μ_h we are guided by the average $\mu_{\text{hy}} m_b$. The leading term for the double differential

decay rate $d^2 \Gamma_u/dP_+ dy$ is proportional to $2y^2(3-2y)$. It follows that the average y on the interval $[0;1]$ is 0.7. However, in some applications y is not integrated over the full domain. Also, there are large negative constants in the matching correction H_{u1} in (4.25), whose effect can be ameliorated by lowering the scale further. In the error analysis we use the central value of $\mu_h = m_b = 2.3 \text{ GeV}$ and vary the scale by a factor between $1/\sqrt{2}$ and $\sqrt{2}$. For the central value $s(\mu_h) = 0.286$.

The intermediate scale $\mu_i = \frac{P_+}{m_b Q_{CD}}$ serves as the renormalization point for the jet and shape functions. We fix this scale to $\mu_i = 1.5 \text{ GeV}$. Variations of μ_i would affect both the normalization and the functional form of the shape function, as determined by the solution to the renormalization-group equation for the shape function discussed in [63, 50]. In practice, effects on the shape are irrelevant because the shape function is fitted to data. The only place where the intermediate scale has a direct impact on the extraction of \mathcal{N}_{ub} is through the normalization of the shape function (4.41). In the analysis we therefore estimate the uncertainty by assigning the value $(\frac{s(\mu_i)}{s(\mu_h)})^2$ as a relative error, where $s(\mu_i) = 0.354$.

The scale μ_u appears as the argument of s in the perturbative contributions Γ_u^{kin} . We vary from $\mu_i/\sqrt{2}$ to $\mu_i\sqrt{2}$ with the central value $\mu_u = \mu_i = 1.5 \text{ GeV}$.

These three errors are added in quadrature and assigned as the total perturbative uncertainty. Finally, we need to estimate the effects from higher-dimensional operators at third and higher-order in power counting. If the considered cut includes the region of phase space near the origin $(P_+ \rightarrow P_+, P_{CD} \rightarrow 0)$, then the dominant such contributions are weak annihilation effects, which we have discussed in Section 4.3.5. From the analysis in [79] one can derive a bound on the weak annihilation contribution that is 1.8% of the total decay rate, for which we take $\Gamma_u = 70 \mathcal{N}_{ub}^2 \text{ ps}^{-1}$ (see below). The resulting uncertainty $\frac{\Gamma_u^{\text{WA}}}{\Gamma_u} = 1.3 \mathcal{N}_{ub}^2 \text{ ps}^{-1}$ affects all partial rates which include the region near the origin in the $(P_+; P_-)$ plane. The uncertainty from weak annihilation can be avoided by imposing a cut $q^2 \geq q_{\text{max}}^2$ (see Section 4.5.6). For all observables considered in the present work, other power corrections of order $1/m_b^3$ can be safely neglected. This can be seen by multiplying the contributions from second-order hadronic power corrections to the various decay rates (called $\Gamma_u^{\text{hadr}(2)}$) by an additional suppression factor $Q_{CD}/m_b = 0.1$.

The following subsection contains a discussion of the total decay rate. In the remainder of this section we then present predictions for a variety of kinematical cuts designed to eliminate (or reduce) the charm background. These partial rates can be computed either numerically or, in many cases, semi-analytically. In Appendix C we discuss how to perform the integrations over the kinematical variables P_1 and P_- analytically.

4.5.1 Total decay rate

Before presenting our predictions for the various partial decay rates, it is useful to have an expression for the total $B \rightarrow X_u l$ decay rate expressed in terms of the heavy-quark parameters defined in the shape-function scheme. We start from the exact two-loop expression for the total rate derived in [84], add the second-order hadronic power corrections, which are known at tree level [13, 1], and finally convert the parameters m_b and s_1 from the pole scheme to the shape-function scheme. The relevant replacements at two-loop order can be taken from [83] and read

$$\begin{aligned} m_b^{\text{pole}} &= m_b + 0.424 s_1(\mu) + 1.357 + 1.326 \ln \frac{\mu}{m_b} + 0.182 \frac{s_1^2(\mu)}{2} \\ &\quad + \frac{3 s_1^2(\mu)}{2 m_b} + \frac{0.330 s_1^2(\mu)}{2 m_b} + \dots; \\ s_1 &= s_1^2 + 0.330 s_1^2(\mu) + \dots; \end{aligned} \quad (4.52)$$

where here and from now on $m_b = m_b(\mu; \alpha_s)$ and $s_1^2 = s_1^2(\mu; \alpha_s)$ are defined in the shape-function scheme. At a reference scale $\mu = 1.5 \text{ GeV}$ the values of these parameters have been determined to be $m_b = (4.61 \pm 0.08) \text{ GeV}$ and $s_1^2 = (0.15 \pm 0.07) \text{ GeV}^2$ [83],³ where we account for the small $1/m_b$ correction to the relation for the pole mass in the above formula (corresponding to a shift of about 0.02 GeV in m_b), which was not included in that paper.

The resulting expression for the total decay rate is

$$\begin{aligned} \Gamma_u &= \frac{G_F^2 |V_{ub}|^2 m_b^5}{192 \pi^3} \left(1 + s_1(\mu) \left(0.768 + 2.122 \frac{1}{m_b} \right) \right. \\ &\quad + s_1^2(\mu) \left(2.158 + 1.019 \ln \frac{m_b}{\mu} + 1.249 + 2.814 \ln \frac{\mu}{m_b} + 0.386 \frac{s_1^2(\mu)}{2} \frac{1}{m_b} \right. \\ &\quad \left. \left. + 0.811 \frac{s_1^2(\mu)}{m_b^2} + \frac{3(s_1^2(\mu) - s_1^2)}{m_b^2} + \dots \right) \right) \end{aligned} \quad (4.53)$$

We observe that for $\mu = 1.5 \text{ GeV}$ and $s_1 = 0$ (m_b), the perturbative expansion coefficients are strongly reduced compared to their values in the pole scheme (0.768 and 2.158 , respectively), indicating a vastly improved convergence of the perturbative expansion. For $m_b = \mu = 4.61 \text{ GeV}$, and $s_1^2 = 0.15 \text{ GeV}^2$ we obtain for the one-loop, two-loop, and power corrections inside the brackets in (4.53): 0.17 , 0.030 , 0.004 . All of these are very small corrections to the leading term.

Including the uncertainties in the values of m_b and s_1^2 quoted above, and varying the renormalization scale between m_b and $m_b = 2$ (with a central value of $m_b = \mu$),

³The values obtained from a one-loop analysis are $m_b = (4.55 \pm 0.08) \text{ GeV}$ and $s_1^2 = (0.34 \pm 0.07) \text{ GeV}^2$.

Table 4.1: Partial decay rate $\Gamma_u(E_0)$ for a cut on charged-lepton energy $E_1 > E_0$ in the B-meson rest frame, given in units of fb ps^{-1} . Predictions are based on the shape-function parameter values $m_b = 4.61 \text{ GeV}$, $\mu^2 = 0.2 \text{ GeV}^2$ (top) and $m_b = 4.55 \text{ GeV}$, $\mu^2 = 0.3 \text{ GeV}^2$ (bottom).

$E_0 [\text{GeV}]$	Mean	Subl. SF	Pert.	Total
1.9	24.79	0.53	+1.90 -1.66	+2.34 -2.15
2.0	18.92	0.60	+1.35 -1.20	+1.95 -1.84
2.1	13.07	0.71	+0.82 -0.75	+1.66 -1.63
2.2	7.59	0.81	+0.38 -0.34	+1.55 -1.54
2.3	3.12	0.89	+0.15 -0.16	+1.55 -1.55
2.4	0.42	1.05	+0.16 -0.22	+1.65 -1.65
1.9	21.10	0.53	+1.57 -1.35	+2.08 -1.92
2.0	15.83	0.60	+1.08 -0.94	+1.77 -1.68
2.1	10.73	0.68	+0.64 -0.55	+1.57 -1.54
2.2	6.12	0.74	+0.31 -0.23	+1.50 -1.48
2.3	2.47	0.84	+0.17 -0.22	+1.53 -1.53
2.4	0.29	0.99	+0.18 -0.24	+1.61 -1.62

we get

$$\begin{aligned}
 \frac{\Gamma_u}{\text{fb ps}^{-1}} &= 68.0^{+5.9}_{-5.5} [m_b] \quad 0.7 [^2]^{+0.6}_{-0.9} [] \\
 &= 68.0 \quad 0.7 [^2]^{+0.6}_{-0.9} [] \quad \frac{m_b}{4.61 \text{ GeV}}^{4.81} : \quad (4.54)
 \end{aligned}$$

Here and below, we quote values for decay rates in units of fb ps^{-1} . To convert these results to partial branching fractions the numbers need to be multiplied by the average B-meson lifetime. Without including the two-loop corrections, the central value in the above estimate increases to 70.6. For comparison, with the same set of input parameters our new approach based on (4.19) predicts a total decay rate of $\Gamma_u = (71.4^{+6.2}_{-5.0} \pm 0.5) \text{ fb ps}^{-1}$, where the first error accounts for perturbative uncertainties while the second one refers to the modeling of subleading shape functions (to which there is essentially no sensitivity at all in the total rate). The fact that this is in excellent agreement with the direct calculation using (4.53) supports the notion that the formalism developed in this chapter can be used to describe arbitrary $B \rightarrow X_u l$ decay distributions, both in the shape-function region and in the OPE region of phase space.

4.5.2 Cut on charged-lepton energy

Traditionally, the most common variable to discriminate against the charm background is the charged-lepton energy E_1 . As long as one requires that E_1 is bigger

Table 4.2: Same as Table 4.1, but for the partial decay rate $\Gamma_u^{(0)}(E_0)$ for a cut on lepton energy $E_1 > E_0$ in the $(4S)$ rest frame.

E_0 [GeV]	Mean	Subl. SF	Pert.	Total
1.9	24.82	0.54	+1.91 -1.66	+2.35 -2.15
2.0	19.00	0.61	+1.37 -1.21	+1.96 -1.85
2.1	13.25	0.71	+0.85 -0.76	+1.68 -1.63
2.2	7.99	0.78	+0.42 -0.37	+1.54 -1.53
2.3	3.83	0.86	+0.18 -0.13	+1.54 -1.53
2.4	1.31	0.99	+0.10 -0.14	+1.61 -1.61
1.9	21.16	0.54	+1.58 -1.35	+2.09 -1.93
2.0	15.94	0.60	+1.10 -0.95	+1.78 -1.69
2.1	10.94	0.68	+0.66 -0.57	+1.58 -1.54
2.2	6.49	0.74	+0.34 -0.26	+1.50 -1.48
2.3	3.05	0.84	+0.17 -0.18	+1.53 -1.53
2.4	0.98	0.92	+0.13 -0.18	+1.56 -1.57

than $(M_B^2 - M_D^2) = 2M_B \cdot 2.31 \text{ GeV}$, the final hadronic state cannot have an invariant mass larger than M_D . For this ideal cut, and using the default set of subleading shape functions, we find

$$\begin{aligned} & \Gamma_u^{(0)} + (\Gamma_u^{\text{kin}(1)} + \Gamma_u^{\text{hadr}(1)}) + (\Gamma_u^{\text{kin}(2)} + \Gamma_u^{\text{hadr}(2)}) \\ = & 6.810 + (0.444 + 3.967) + (0.042 + 0.555) \text{ fb ps}^{-1} : \end{aligned} \quad (4.55)$$

The corrections from subleading shape functions are quite sizable, in accordance with the findings in [52, 73, 74]. Note that the sum $\Gamma_u^{\text{kin}(1)} + \Gamma_u^{\text{kin}(2)} = 0.486$ is an excellent approximation to the exact result $\Gamma_u^{\text{kin}} = 0.482$ (all in units of fb ps^{-1}) obtained using (4.26), indicating that the expansion of the kinematical power corrections is converging rapidly. The same will be true for all other observables considered below.

In practice, the cut on E_1 can be relaxed to some extent because the background is well understood, thereby increasing the efficiency and reducing the impact of theoretical uncertainties. Our findings for different values of the cut E_0 are summarized in Table 4.1. Here and below, the columns have the following meaning: "Mean" denotes the prediction for the partial decay rate, "Subl. SF" the uncertainty from subleading shape functions, and "Pert." the total perturbative uncertainty. In the column "Total" we add the stated errors plus the uncertainty from weak annihilation in quadrature.

Experiments often do not measure the partial rates in the B -meson rest frame, but in the rest frame of the $(4S)$ resonance produced in e^+e^- collisions. Boosting to the $(4S)$ frame with $\beta = v/c = 0.064$ has a small effect on the spectrum and

rates. The exact formula for this boost is [32]

$$\Gamma_u^{(B)}(E_0) = \frac{1}{1 + \frac{Z_{M_B=2}}{E_0} \frac{d\Gamma_u^{(B)}}{dE}} + \max \left\{ \frac{E_0}{E} \right\}; \quad (4.56)$$

where $\Gamma_u^{(B)} = \frac{p}{1} \frac{p}{1}$, and the factor $\frac{p}{1} \frac{p}{1} = 1.002$ on the left-hand side takes the time dilation of the B -meson lifetime $\tau_B^0 = \tau_B$ into account. (In other words, branching fractions are Lorentz invariant.) The above formula can be accurately approximated by the first term in an expansion in β^2 , which yields [32]

$$\Gamma_u^{(B)}(E_0) = \Gamma_u^{(B)}(E_0) - \frac{2}{6} E_0^3 \frac{d}{dE} \frac{1}{E} \frac{d\Gamma_u^{(B)}}{dE} + O(\beta^4); \quad (4.57)$$

$E = E_0$

as long as E_0 is not too close to the kinematical endpoint (i.e., $E_0 \ll M_B = 2.47 \text{ GeV}$). The numerical results for the partial decay rate $\Gamma_u^{(B)}(E_0)$ in the rest frame of the $(4S)$ resonance are given in Table 4.2.

4.5.3 Cut on hadronic P_+

Cutting on P_+ samples the same hadronic phase space as a cut on the charged-lepton energy, but with much better efficiency [63, 85]. The phase space $P_+ = P_-$ with the ideal separator $P_+ = M_D^2 - M_B^2 = 0.66 \text{ GeV}$ contains well over half of all $B \rightarrow X_{u1} \ell^+ \nu_\ell$ events. Here we end with the default settings

$$\begin{aligned} & \Gamma_u^{(0)} + \left(\Gamma_u^{\text{kin}(1)} + \Gamma_u^{\text{hadr}(1)} \right) + \left(\Gamma_u^{\text{kin}(2)} + \Gamma_u^{\text{hadr}(2)} \right) \\ = & 53.225 + (4.646 + 11.862) + (0.328 + 0.227) \text{ fb} \text{ ps}^{-1}; \end{aligned} \quad (4.58)$$

We see a much better convergence of the power series than in the case of a cut on the charged-lepton energy, namely $53.225 \pm 7.216 \pm 0.100$ when grouping the above numbers according to their power counting. Once again, the sum $\Gamma_u^{\text{kin}(1)} + \Gamma_u^{\text{kin}(2)} = 4.973$ is very close to the full kinematical correction $\Gamma_u^{\text{kin}} = 4.959$ (in units of $\text{fb} \text{ ps}^{-1}$).

Often times it is required to impose an additional cut on the charged-lepton energy, as leptons that are too soft are difficult to detect. In Table 4.3 we list results for both $E_\ell = 0$ and $E_\ell = 1.0 \text{ GeV}$. For the ideal cut we find that the prediction is quite precise, as the total theoretical uncertainty is only about 6.8%. For comparison, the ideal cut for the lepton energy is uncertain by about 50%, but rapidly improving as the energy cut is relaxed.

4.5.4 Cut on hadronic invariant mass and q^2

The most efficient separator for the discrimination of $B \rightarrow X_{c1} \ell^+ \nu_\ell$ events is a cut on the invariant mass M_X of the hadronic final state, $M_X \ll M_D$ [86, 87]. It has

Table 4.3: Partial decay rate $\Gamma_u(p; E_0)$ for a cut on the hadronic variable P_+ and lepton energy $E_l = E_0$, given in units of fb ps^{-1} . Predictions are based on the shape-function parameter values $m_b = 4.61 \text{ GeV}$, $\sigma^2 = 0.2 \text{ GeV}^2$ (top) and $m_b = 4.55 \text{ GeV}$, $\sigma^2 = 0.3 \text{ GeV}^2$ (bottom).

p [GeV]	E_0 [GeV]	Mean	Subl. SF	Pert.	Total
0.70	0.0	48.90	1.15	+2.83 2.65	+3.30 3.15
0.65	0.0	45.34	1.46	+2.55 2.41	+3.20 3.09
0.60	0.0	41.34	1.76	+2.26 2.15	+3.13 3.05
0.55	0.0	36.91	2.01	+1.95 1.87	+3.08 3.02
0.50	0.0	32.09	2.34	+1.64 1.58	+3.12 3.09
0.70	1.0	43.36	1.02	+2.54 2.39	+3.01 2.88
0.65	1.0	40.18	1.30	+2.28 2.16	+2.92 2.82
0.60	1.0	36.59	1.59	+2.01 1.92	+2.86 2.80
0.55	1.0	32.61	1.86	+1.73 1.67	+2.84 2.80
0.50	1.0	28.29	2.19	+1.44 1.40	+2.91 2.89
0.70	0.0	39.95	1.19	+2.18 2.06	+2.79 2.70
0.65	0.0	36.94	1.42	+1.95 1.86	+2.72 2.66
0.60	0.0	33.67	1.65	+1.71 1.65	+2.69 2.65
0.55	0.0	30.15	1.88	+1.47 1.43	+2.70 2.68
0.50	0.0	26.40	2.09	+1.22 1.21	+2.73 2.72
0.70	1.0	35.42	1.13	+1.95 1.85	+2.59 2.51
0.65	1.0	32.73	1.34	+1.74 1.66	+2.53 2.48
0.60	1.0	29.81	1.55	+1.52 1.47	+2.51 2.48
0.55	1.0	26.65	1.76	+1.29 1.27	+2.52 2.51
0.50	1.0	23.29	1.95	+1.07 1.06	+2.56 2.55

Table 4.4: Partial decay rate $\Gamma_u(M_0; q_0^2)$ for combined cuts $M_X = M_0$ on hadronic invariant mass, $q^2 > q_0^2$ on leptonic invariant mass, given in units of fb ps^{-1} . Predictions are based on the shape-function parameter values $m_b = 4.61 \text{ GeV}$, $s^2 = 0.2 \text{ GeV}^2$ (top) and $m_b = 4.55 \text{ GeV}$, $s^2 = 0.3 \text{ GeV}^2$ (bottom).

$M_0 [\text{GeV}]$	$q_0^2 [\text{GeV}^2]$	$E_0 [\text{GeV}]$	Mean	Subl. SF	Pert.	Total
M_D	0.0	0.0	59.30	0.36	+4.22 3.73	+4.42 3.96
1.70	0.0	0.0	53.13	0.73	+3.67 3.31	+3.95 3.61
1.55	0.0	0.0	45.72	1.16	+3.11 2.84	+3.55 3.32
M_D	6.0	0.0	34.37	0.37	+2.97 2.58	+3.25 2.89
1.70	8.0	0.0	24.80	0.36	+2.24 1.98	+2.59 2.37
M_D	$(M_B - M_D)^2$	0.0	12.55	0.49	+1.41 1.24	+1.95 1.83
M_D	0.0	0.0	50.08	0.54	+3.52 3.11	+3.78 3.40
1.70	0.0	0.0	44.20	0.86	+2.98 2.69	+3.35 3.09
1.55	0.0	0.0	37.76	1.22	+2.46 2.26	+3.03 2.86
M_D	6.0	0.0	29.42	0.35	+2.50 2.16	+2.82 2.52
1.70	8.0	0.0	20.87	0.39	+1.84 1.61	+2.26 2.08
M_D	$(M_B - M_D)^2$	0.0	10.49	0.48	+1.16 1.00	+1.76 1.68

Table 4.5: Partial decay rate $\Gamma_u(M_0; q_0^2; E_0)$ for combined cuts $M_X = M_0$ on hadronic invariant mass, $q^2 > q_0^2$ on leptonic invariant mass, and $E_1 = E_0$ on charged-lepton energy, given in units of fb ps^{-1} . Predictions are based on the shape-function parameter values $m_b = 4.61 \text{ GeV}$, $s^2 = 0.2 \text{ GeV}^2$ (top) and $m_b = 4.55 \text{ GeV}$, $s^2 = 0.3 \text{ GeV}^2$ (bottom).

$M_0 [\text{GeV}]$	$q_0^2 [\text{GeV}^2]$	$E_0 [\text{GeV}]$	Mean	Subl. SF	Pert.	Total
M_D	0.0	1.0	53.49	0.36	+3.91 3.45	+4.13 3.69
1.70	0.0	1.0	48.25	0.63	+3.42 3.08	+3.70 3.38
1.55	0.0	1.0	41.81	1.03	+2.91 2.66	+3.34 3.12
M_D	6.0	1.0	33.88	0.37	+2.94 2.55	+3.22 2.87
1.70	8.0	1.0	24.74	0.36	+2.23 1.97	+2.59 2.37
M_D	$(M_B - M_D)^2$	1.0	12.55	0.49	+1.41 1.24	+1.95 1.83
M_D	0.0	1.0	45.29	0.50	+3.27 2.88	+3.54 3.18
1.70	0.0	1.0	40.22	0.77	+2.78 2.50	+3.15 2.90
1.55	0.0	1.0	34.55	1.09	+2.31 2.11	+2.85 2.69
M_D	6.0	1.0	28.99	0.34	+2.48 2.13	+2.80 2.50
1.70	8.0	1.0	20.82	0.39	+1.83 1.60	+2.26 2.08
M_D	$(M_B - M_D)^2$	1.0	10.49	0.48	+1.16 1.00	+1.78 1.68

also been argued [88] that a cut on q^2 can reduce the shape-function sensitivity, since it avoids the collinear region in phase space where $P \rightarrow P_+$. In order to optimize signal efficiency and theoretical uncertainties, it was suggested in [89] to combine a q^2 cut with a cut on hadronic invariant mass.

The theoretical predictions obtained in [88, 89] were based on a conventional OPE calculation, which was assumed to be valid for these cuts. The assessment of the shape-function sensitivity was based on convolving the tree-level decay rate with a "tree-level shape function", for which two models (a realistic model similar to the ones considered here, and an unrealistic δ -function model) were employed. The shape-function sensitivity was then inferred from the comparison of the results obtained with the two models. The sensitivity to subleading shape functions was not considered, since it was assumed to be very small. Since our formalism smoothly interpolates between the "shape-function" and "OPE" regions, and since we include radiative corrections as well as power corrections as far as they are known, we can estimate the sensitivity of a combined M_X (q^2 cut to the leading and subleading shape functions) much more accurately. Contrary to [89], we do not find a significant reduction of the shape-function sensitivity when adding the q^2 cut to a cut on hadronic invariant mass.

In Tables 4.4 and 4.5 we give results for typical cuts on M_X and q^2 , with and without including an additional cut on charged-lepton energy. Let us study the contributions for the optimal cut $M_X = M_D$ in detail. We end with the default settings

$$= \frac{u^{(0)}}{u} + \left(\frac{u^{\text{kin}(1)}}{u} + \frac{u^{\text{hadr}(1)}}{u} \right) + \left(\frac{u^{\text{kin}(2)}}{u} + \frac{u^{\text{hadr}(2)}}{u} \right) \mathcal{V}_{\text{ub}}^2 \text{ps}^{-1} : \quad (4.59)$$

Note the almost perfect (accidental) cancellation of the two terms at order $1/m_b$. The resulting power series, $58.541 - 1.022 + 1.782$, again exhibits good convergence. As previously, the sum $\frac{u^{\text{kin}(1)}}{u} + \frac{u^{\text{kin}(2)}}{u} = 10.127$ is a good approximation to the exact value $\frac{u^{\text{kin}}}{u} = 9.753$ (in units of $\mathcal{V}_{\text{ub}}^2 \text{ps}^{-1}$). The analogous analysis for a combined cut $M_X = 1.7 \text{ GeV}$ and $q^2 = 8.0 \text{ GeV}^2$ reads

$$= \frac{u^{(0)}}{u} + \left(\frac{u^{\text{kin}(1)}}{u} + \frac{u^{\text{hadr}(1)}}{u} \right) + \left(\frac{u^{\text{kin}(2)}}{u} + \frac{u^{\text{hadr}(2)}}{u} \right) \mathcal{V}_{\text{ub}}^2 \text{ps}^{-1} ; \quad (4.60)$$

which means that the power series is $25.880 - 2.309 + 1.228$. Here we have $\frac{u^{\text{kin}(1)}}{u} + \frac{u^{\text{kin}(2)}}{u} = 5.449$, which is close to $\frac{u^{\text{kin}}}{u} = 5.160$ (in units of $\mathcal{V}_{\text{ub}}^2 \text{ps}^{-1}$).

4.5.5 Cut on s_H^{max} and E_1

In [90], the BaBar collaboration employed a cut on both $E_1 = E_0$ and a new kinematical variable $s_H^{\text{max}} = s$, where the definition for s_H^{max} involves both hadronic and leptonic variables. In the B-meson rest frame, it is

$$s_H^{\text{max}} = M_B^2 + q^2 - 2M_B E_1 + \frac{q^2}{4E_1} : \quad (4.61)$$

Table 4.6: Partial decay rate $\Gamma_u(s_0; E_0)$ for combined cuts $s_H^{m\text{ax}} \leq s_0$ and $E_1 \leq E_0$, given in units of fb ps^{-1} . Predictions are based on the shape-function parameter values $m_b = 4.61 \text{ GeV}$, $\sigma^2 = 0.2 \text{ GeV}^2$ (top) and $m_b = 4.55 \text{ GeV}$, $\sigma^2 = 0.3 \text{ GeV}^2$ (bottom).

$s_0 [\text{GeV}^2]$	$E_0 [\text{GeV}]$	Mean	Subl. SF	Pert.	Total
3.5	1.8	17.39	0.62	+1.54 -1.36	+2.08 -1.96
3.5	1.9	15.86	0.63	+1.33 -1.18	+1.94 -1.84
3.5	2.0	13.70	0.66	+1.05 -0.94	+1.77 -1.71
3.5	2.1	10.78	0.73	+0.71 -0.64	+1.62 -1.59
3.5	1.8	14.57	0.60	+1.25 -1.09	+1.87 -1.77
3.5	1.9	13.18	0.61	+1.06 -0.92	+1.76 -1.68
3.5	2.0	11.28	0.64	+0.82 -0.71	+1.63 -1.58
3.5	2.1	8.77	0.69	+0.54 -0.46	+1.54 -1.51

Rewriting the phase space of this cut in the variables P_+ , P_- , P_1 , we find

$$\begin{aligned}
0 &\leq P_+ \leq m \text{ in } (M_B - 2E_0; \sqrt{s_0}) ; \\
P_+ &\leq P_- \leq m \text{ in } \frac{s_0}{P_+}; M_B - \sqrt{s_0} ; \\
P_+ &\leq P_1 \leq m \text{ in } (M_B - 2E_0; \sqrt{s_0}) ;
\end{aligned} \tag{4.62}$$

where it is understood that if $q^2 = (M_B - P_+)(M_B - P_-) \leq (M_B - \sqrt{s_0})^2$, then the interval $P_1^{m\text{in}} < P_1 < P_1^{m\text{ax}}$ must be excluded from the P_1 integration. Here

$$P_1^{m\text{ax}=m\text{in}}(P_+; P_-) = \frac{\frac{P_+ + P_-}{2} + \frac{s_0 - P_+ P_-}{2M_B}}{\sqrt{\frac{P_+ + P_-}{2} + \frac{s_0 - P_+ P_-}{2M_B}} - \sqrt{s_0}} : \tag{4.63}$$

A summary of our findings is given in Table 4.6. When compared to the pure charged-lepton energy cut in Table 4.1, the additional cut on $s_H^{m\text{ax}}$ eliminates roughly another 20{30% of events. However, the hope is that this cut also reduces the sensitivity to the leading shape function, which we expect to be sizable for the pure E_1 cut. The uncertainty from subleading shape functions, however, is almost unaffected by the $s_H^{m\text{ax}}$ cut.

4.5.6 Eliminating weak annihilation contributions

In Section 4.3.5 we have argued that a cut on high q^2 , i.e., $q^2 < q_0^2$, will eliminate the effect of weak annihilation and remove the uncertainty associated with this contribution. The cut q_0^2 should be small enough to exclude the region around

Table 4.7: Examples of partial decay rates with a cut on $q^2 = (M_B - M_D)^2$ imposed to eliminate the weak annihilation contribution. We consider an additional cut on the hadronic variable P_+ (top), or on the hadronic invariant mass $M_X = M_0$ (bottom). As before, decay rates are given in units of fb ps^{-1} . Predictions are based on the shape-function parameters $m_b = 4.61 \text{ GeV}$ and $\lambda^2 = 0.2 \text{ GeV}^2$.

$P_+ [\text{GeV}]$	Mean	SubL SF	Pert.	Total
0.70	39.96	1.27	+2.16 -2.01	+2.51 -2.38
0.65	37.18	1.50	+1.99 -1.85	+2.49 -2.38
0.60	34.05	1.71	+1.82 -1.69	+2.50 -2.41
0.55	30.61	1.89	+1.63 -1.52	+2.49 -2.42
0.50	26.86	1.97	+1.44 -1.33	+2.44 -2.38
$M_0 [\text{GeV}]$	Mean	SubL SF	Pert.	Total
M_D	46.75	0.65	+2.82 -2.50	+2.89 -2.58
1.70	40.70	1.12	+2.32 -2.11	+2.58 -2.39
1.55	33.69	1.56	+1.88 -1.73	+2.44 -2.32

$q^2 = m_b^2$, where this contribution is concentrated. It is instructive to assess the "cost" of such an additional cut in terms of the loss of efficiency and, more importantly, the behavior of the remaining uncertainties. In order to do this, we combine the cut $q^2 = (M_B - M_D)^2$ with either a cut on P_+ or on M_X . While this particular choice for q_0^2 still leaves some room to improve the efficiency by increasing q_0^2 , it is not desirable to raise the cut much further, since this would threaten the validity of quark-hadron duality.

The results are summarized in Table 4.7 and can be compared to the previous "pure" P_+ and M_X cuts in Tables 4.3, 4.4, and 4.5. As an example, let us consider the case $P_+ = 0.65 \text{ GeV}$, which is close to the charm threshold. Without the additional q^2 cut we found that the total theoretical uncertainty (including the weak annihilation error) is $+7.0\%$ _{-6.8%}. When cutting in addition on $q^2 = (M_B - M_D)^2$, the efficiency decreases by about 20% as expected. However, due to the absence of the weak annihilation uncertainty, the overall uncertainty decreases to $+6.7\%$ _{-6.4%}. Therefore both strategies result in comparable relative uncertainties, with a slight favor for imposing the additional cut from the theoretical point of view.

While the small reduction of theoretical errors hardly seems worth the effort of imposing the q^2 cut, performing an analysis of the type outlined here and comparing its results with those obtained without the additional cut may help to corroborate the expectation that the weak annihilation contribution is indeed not much larger than what has been found in [79].

Table 4.8: Values of the exponent $a(m_b)$ for different kinematical cuts. The parameter $s^2 = 0.2 \text{ GeV}^2$ is kept fixed. Also quoted is the sensitivity of the partial decay rates to the functional form of the shape functions. See text for explanation.

	$m_b [\text{GeV}]$	4.50	4.55	4.60	4.65	4.70
$M_X = M_D$	a	9.5	8.8	8.2	7.7	7.3
	FunctionalForm	1.4%	1.1%	0.8%	0.5%	0.4%
$M_X = 1.7 \text{ GeV}$	a	12.5	11.5	10.5	9.7	8.9
	FunctionalForm	2.9%	2.6%	2.2%	1.9%	1.6%
$M_X = 1.7 \text{ GeV}$ $q^2 = 8 \text{ GeV}^2$	a	10.3	9.8	9.3	9.0	8.7
	FunctionalForm	2.0%	1.7%	1.5%	1.4%	1.4%
$q^2 = (M_B - M_D)^2$	a	11.4	11.1	10.9	10.8	10.6
	FunctionalForm	5.0%	4.4%	4.0%	3.6%	3.2%
$P_+ = M_D^2 - M_B$	a	16.7	15.0	13.6	12.2	11.1
	FunctionalForm	5.3%	4.8%	4.4%	4.0%	3.6%
$E_1 = 2.2 \text{ GeV}$	a	22.6	21.0	19.7	18.5	17.4
	FunctionalForm	16.2%	13.1%	11.0%	9.3%	7.9%

4.5.7 Dependence on m_b and shape-function sensitivity

Non-perturbative hadronic physics enters in our approach via the form of the leading and subleading shape functions. The strongest sensitivity by far is to the first moment of the leading shape function, which determines the HQET parameter \bar{u} and with it the b-quark mass. Given that the value of $m_b = m_b(\bar{s})$ can be determined with good precision from other sources (such as moments of the leptonic or hadronic invariant mass spectra in $B \rightarrow X_c l \bar{\nu}$ decays), it is instructive to disentangle this dependence from the sensitivity to higher moments or, more generally, to the functional form of the shape functions for fixed m_b .

To explore the dependence on m_b we define the exponent

$$a(m_b) = \frac{d \ln \bar{u}}{d \ln m_b} = \frac{4}{\bar{u}} \frac{d \bar{u}}{d \ln m_b} = \frac{4 m_b}{\bar{u}} ; \quad (4.64)$$

which means that $\bar{u} \propto (m_b)^a$. Table 4.8 shows the values of this exponent over a wide range of values of m_b for a variety of experimental cuts. To estimate the sensitivity to the functional form we scan over a large set of models for the subleading shape functions, and we also study the difference between the results obtained using the exponential or the gaussian ansatz for the leading shape function. The corresponding variations are added in quadrature and given as a relative change in the corresponding partial decay rates (labeled "FunctionalForm"). In all cases, $s^2 = 0.2 \text{ GeV}^2$ is kept fixed. Because we restrict ourselves to only two functional forms for the leading shape function in this study, the resulting sensitivities should be interpreted with caution.

The entries in the table are listed in roughly the order of increasing sensitivity to m_b and to the functional form of the shape functions, with the hadronic invariant mass cut showing the least sensitivity and the lepton energy cut exhibiting the largest one. To some extent this reflects the different efficiencies (or "inclusiveness") of the various cuts. It is reassuring that $a \approx 10$ for the pure q^2 cut, in accordance with the findings of [91, 92]. Perhaps somewhat surprisingly, for this cut a substantial sensitivity to shape-function effects remains even for fixed m_b and q^2 . It is well known that the partial rate with a cut $q^2 \in (M_B - M_D)^2$ can be calculated using a local OPE in powers of $q_{CD} = m_c$ [88, 91], thereby avoiding the notion of shape-function sensitivity. Differences between the functional forms of the shape functions in our approach correspond to effects that are formally of order $1/m_c^3$ and higher. It is not unreasonable that these effects should be of order 3–5%.

We also checked that for much more relaxed cuts the value of $a(m_b)$ tends to 4.8, as stated in (4.54). For example, for a cut $P_+ \in [P_-]$ we find (with $m_b = 4.61 \text{ GeV}$ and $q^2 = 0.2 \text{ GeV}^2$):

$P_- [\text{GeV}]$	0.6	0.8	1.0	1.2	1.6	2.0	3.0	M_B
a	15.4	9.8	7.0	5.8	5.1	5.0	4.9	4.8

4.6 Conclusions

A high-precision measurement of the parameters of the unitarity triangle is an ongoing quest, which necessitates the close cooperation of theory and experiment. The determination of $|V_{ub}|$ from inclusive $B \rightarrow X_{u\ell}$ decay requires the measurement of partial decay rates with kinematical cuts that eliminate the large background from $B \rightarrow X_{c\ell}$ decay, as well as theoretical predictions for such quantities. To this end, it is desirable to have a theoretical description of the triple differential decay rate, which can be used for predicting arbitrary partial rates obtained after integrating over certain regions of phase space. One problem in providing such a description is that the power-counting rules of the heavy-quark expansion are different in different kinematical domains. In this chapter we have overcome this difficulty.

In the shape-function region, our results are in agreement with QCD factorization theorems, and perturbative effects have been separated from non-perturbative shape functions. When the allowed phase space extends over a large domain, our results smoothly reduce to the expressions obtained from the local operator product expansion. We have presented a formalism in which event distributions and partial decay rates are expressed without explicit reference to partonic quantities such as the b -quark mass. The sensitivity to such hadronic parameters enters indirectly, via the moments of shape functions. The most important non-perturbative object, namely the leading-order shape function, can be extracted from the photon spectrum in $B \rightarrow X_s$ decay. This is analogous to extractions of parton distribution functions from fits to data on deep inelastic scattering. In this way, the

dominant uncertainty from our ignorance about bound-state effects in the B meson is turned into an experimental uncertainty, which will reduce with increasing accuracy of the experimental data on the photon spectrum. Residual hadronic uncertainties are power suppressed in the heavy-quark expansion.

One goal of this chapter was to present a detailed framework in which this program can be carried out. We have given formulae that can be readily used for the construction of an event generator, as well as to estimate the remaining theoretical uncertainties in a robust and automated fashion.

In practice the leading shape function needs to be parameterized. We have suggested three different functional forms, which can be used to fit the data of the $B \rightarrow X_s \gamma$ photon spectrum. Once the data is accurately described by a choice of the shape functions, this function can be used in the predictions for partial $B \rightarrow X_u \ell$ rates and spectra. Subleading shape functions give rise to theoretical uncertainties starting at the level of $1/m_b$ power corrections. We have estimated these uncertainties using a large set of models, each of which obeys the known tree-level momentum relations, but which are very different in their functional form. A second error estimate is determined by the residual renormalization-scale dependence. We also considered uncertainties from weak annihilation effects, which in principle can be avoided by cutting away the region of phase space in which they contribute. We have suggested a cut on high leptonic invariant mass, which accomplishes just that.

The second half of this chapter contains detailed numerical predictions for a variety of partial $B \rightarrow X_u \ell$ decay rates with different kinematical cuts, including cuts on the charged-lepton energy (both in the rest frame of the B meson and of the $(4S)$ resonance), on the hadronic quantity $P_+ = E_X - \vec{p}_X \cdot \vec{j}$, on M_X , on q^2 , and on various combinations of these variables. Along with our predictions for the rates we have presented a complete analysis of theoretical uncertainties. Once the data on the $B \rightarrow X_s \gamma$ photon spectrum are sufficiently precise to accurately determine the leading-order shape function, a determination of $|V_{ub}|$ with theoretical uncertainties at the 5-10% level now seems feasible.

Applications: Weight Function

5.1 Introduction

The kinematical variable P_+ is common to semileptonic and radiative charmless inclusive B decays. In $B \rightarrow X_s \gamma$ decays P_+ is related to the B -meson mass and the photon energy, $P_+ = M_B^2 - 2E_\gamma$, and the measurement of its spectrum leads directly to the extraction of the leading hadronic structure function, called the shape function [15, 16, 17]. The P_+ spectrum in semileptonic $B \rightarrow X_u \ell$ decays, on the other hand, enables us to determine $\langle V_{ub} \rangle$ [34, 85, 93], but this requires a precise knowledge of the shape function. One approach for measuring $\langle V_{ub} \rangle$ is to first extract the shape function from the $B \rightarrow X_s \gamma$ photon spectrum, and then to use this information for predictions of event distributions in $B \rightarrow X_u \ell$. A comprehensive description of this program has been presented in chapter 4. Equivalently, it is possible to eliminate the shape function in $B \rightarrow X_u \ell$ decay rates in favor of the $B \rightarrow X_s \gamma$ photon-energy spectrum. This idea was first put forward in [16] and later refined in [67, 68, 69, 94]. Partial $B \rightarrow X_u \ell$ decay rates are then given as weighted integrals over the $B \rightarrow X_s \gamma$ photon-energy spectrum,

$$u(\cdot) = \frac{dP_+}{\exp.\text{input}} \Big|_{\{z\}}^0 = \mathcal{J}_{ub}^2 \frac{dP_+}{\text{theory}} \Big|_{\{z\}}^0 \frac{1}{\exp.\text{input}} \Big|_{\{z\}}^0 \frac{d_s}{dP_+} \Big|_{\{z\}}^0; \quad (5.1)$$

where the weight function $W(\sqrt{s}; P_+)$ is perturbatively calculable at leading power in α_{QCD} . A comparison of both sides of the equation determines the CKM matrix element V_{ub} directly. For the measurement of the left-hand side to be free of charm background, \sqrt{s} must be less than $M_D^2 = M_B^2 - 0.66 \text{ GeV}^2$. However, the P_+ spectrum in $B \rightarrow X_u \gamma$ decays displays many of the features of the charged-lepton energy spectrum, so that it is not inconceivable that the cut can be further relaxed for the same reasons that experimenters are able to relax the lepton cut beyond the charm threshold. We stress that for an application of relation (5.1) a measurement of the $B \rightarrow X_s \gamma$ photon spectrum is needed only for $E_\gamma \geq \frac{1}{2}(M_B - m_c) \approx 2.3 \text{ GeV}$ (or slightly lower, if the cut is relaxed into the charm region). This high-energy part of the spectrum has already been measured with good precision.

Previous authors [16, 67, 68, 69, 94] have considered relations such as (5.1) in the slightly different form

$$\begin{array}{c} \text{Z} \\ \frac{dP_+}{dP_+} \frac{d_u}{dP_+} = \frac{J_{ub} J_{ub}^2}{J_{tb} V_{ts} J_{ub}^2} \end{array} \quad \begin{array}{c} \text{Z} \\ \frac{dP_+}{dP_+} \frac{d_s}{dP_+} : \end{array} \quad (5.2)$$

Normalizing the photon spectrum by the total¹ rate $s(E)$ as done in (5.1) has

¹Due to an unphysical soft-photon singularity, the total decay rate is common only defined to include all events with photon energies above $E_\gamma = m_b = 20$ [32].

several advantages. Firstly, it is a known fact that event fractions in $B \rightarrow X_s$ decay can be calculated with better accuracy than partial decay rates (see [50] for a recent discussion), and likewise the normalized rate does not suffer from the relatively large experimental error on the total branching ratio. Secondly, relation (5.1) is independent of the CKM factor $|V_{tb}V_{ts}|$. Thirdly, unlike the total $B \rightarrow X_s$ decay rate, the shape of the photon spectrum is rather insensitive to possible New Physics contributions [32], which could distort the outcome of a $|V_{ub}|$ measurement via relation (5.2). Lastly, as we will see below, the weight function $W(\gamma; P_+)$ possesses a much better perturbative expansion than the function $\tilde{W}(\gamma; P_+) = |V_{tb}V_{ts}|^2 W(\gamma; P_+) =_s(E)$. This last point can be traced back to the fact that most of the very large contribution from the $O_1 - O_7$ operator mixing in the effective weak Hamiltonian cancels in the theoretical expression for the normalized photon spectrum.

In principle, any partial $B \rightarrow X_{u,l}$ decay rate can be brought into the form (5.1), with complicated weight functions. The relation between the two P_+ spectra is particularly simple, because the leading-power weight function is a constant at tree level. Experiments typically reject semileptonic B -decay events with very low lepton energy. The effect of such an additional cut can be determined from [95]. Alternatively, it is possible to modify the weight function so as to account for a lepton cut, however at the expense of a significant increase in complexity. We will not pursue this option in this chapter.

The weight function depends on the kinematical variable P_+ and on the size of the integration domain. It possesses integrable singularities of the form $\ln^k(\gamma) \ln^k[m_b(\gamma - P_+) =^2]$, with $k \leq n$, in perturbation theory. Different strategies can be found in the literature concerning these logarithms. Leibovich et al. resummed them by identifying $=^2$ with $m_b(\gamma - P_+)$ [67, 68]. The P_+ dependence of the weight function then enters via the running coupling $\alpha_s(\gamma - m_b(\gamma - P_+))$. This is a legitimate choice of scale as long as $(\gamma - P_+)$ has a generic value of order Q_{CD} ; however, it is not a valid choice in the small region where $m_b(\gamma - P_+) \sim Q_{CD}^2$. A key result underlying relation (5.1) is that, by construction, the weight function is insensitive to soft physics. Quark-hadron duality ensures that the region near the point $P_+ = 0$, which is without any physical significance, does not require special consideration after integration over P_+ . In the approach of [67, 68], the attempt to resum the above logarithms near the endpoint of the P_+ integral leads to integrals over unphysical Landau singularities of the running coupling in the nonperturbative domain. Hoang et al. chose to calculate the weight function in fixed-order perturbation theory at the scale $\mu = m_b$ [94]. This leads to parametrically large logarithms, since $P_+ \sim m_b$. In the present chapter we separate physics effects from two parametrically distinct scales, a hard scale $\mu_h \sim m_b$ and an intermediate scale $\mu_i \sim m_b / Q_{CD}$, so that we neither encounter Landau singularities nor introduce parametrically large logarithms. The shape of the weight function is then governed by a perturbative expansion at the intermediate scale, $\ln^k(\gamma) \ln^k[m_b(\gamma - P_+) =^2]$. As will be explained later, the coefficients in this series,

as well as the overall normalization, possess themselves an expansion in $s(h)$.

The calculation of the weight function starts with the theoretical expressions for the P_+ spectra in $B \rightarrow X_u l$ and $B \rightarrow X_s$ decays, which are given as [95]

$$\frac{d_u}{dP_+} = \frac{G_F^2 V_{ub}^2}{96 \pi^3} U(h; i) (M_B - P_+)^5 \int_0^1 dy y^{2a(h; i)} (3 - 2y) F_1(P_+; y) + 6(1 - y) F_2(P_+; y) + y F_3(P_+; y); \quad (5.3)$$

$$\frac{d_s}{dP_+} = \frac{G_F^2 V_{ts}^2}{32 \pi^4} U(h; i) (M_B - P_+)^3 \overline{m}_b^2(h) [C_7^e(h)]^2 F(P_+); \quad (5.4)$$

where

$$y = \frac{P_-}{M_B - P_+} \quad (5.5)$$

with $P_- = E_X + \vec{p}_X \cdot \vec{j}$ is a kinematical variable that is integrated over the available phase space. Expressions for the structure functions F_i valid at next-to-leading order (NLO) in renormalization-group (RG) improved perturbation theory and including first- and second-order power corrections can be found in [95] (see also [50, 62, 63]). Symbolically, they are written as $H(h) J(i) S(i)$, where $H(h)$ contains matching corrections at the hard scale μ_h . The jet function $J(i)$, which is a perturbative quantity at the intermediate scale μ_i , is convoluted with a non-perturbative shape function renormalized at that same scale. Separation of the two scales μ_h and μ_i allows for the logarithms in matching corrections to be small, while logarithms of the form $\ln \mu_h = \mu_i$, which appear at every order in perturbation theory, are resummed in a systematic fashion and give rise to the RG evolution functions $U(h; i)$ and $a(h; i)$ [63].

The leading-power jet function $J(p^2; i)$ entering the expressions for F_i is universal and has been computed at one-loop order in [62, 63]. The two-loop expression for J has been obtained apart from a single unknown constant in [96], which is the two-loop coefficient of the local (p^2) term. (This term was recently calculated in [97]). This constant does not enter in the two-loop result for the weight function $W(; P_+)$ in (5.1). Due to the universality of the leading-power jet function, it is possible to calculate the complete $O(s(i))$ corrections to the weight function. However, the extraction of hard corrections at two-loop order would require multi-loop calculations for both decay processes, which are unavailable at present. As a result, we will be able to predict the μ and P_+ dependence of the weight function $W(; P_+)$ at next-to-next-to-leading order (NNLO) in RG-improved perturbation theory, including exact two-loop matching contributions and three-loop running effects. However, the overall normalization of the weight function will have an uncertainty of $O(s(h))$ from yet unknown hard matching corrections.

The total rate $\Gamma_s(E)$ has been calculated in a local operator product expansion

and reads (including only the leading non-perturbative corrections) [50]

$$\Gamma_s(E) = \frac{G_F^2 V_{tb} V_{ts}^2}{32\pi^4} m_b^3 \bar{m}_b^2(\mu_h) [C_7^e(\mu_h)]^2 H_s(\mu_h) H(\mu_h) \left[1 - \frac{2}{9m_c^2} \frac{C_1(\mu_h)}{C_7^e(\mu_h)} \right]; \quad (5.6)$$

where H_s is the hard function of F , and H contains the remaining radiative corrections. We will present an explicit expression for this quantity at the end of Section 5.3 below. The hadronic correction proportional to $2/m_c^2$ cancels against an identical term in F . Apart from two powers of the running b -quark mass defined in the \overline{MS} scheme, which is part of the electromagnetic dipole operator O_7 in the effective weak Hamiltonian, three more powers of m_b emerge from phase-space integrations. To avoid the renormalization ambiguities of the pole scheme we use a low-scale subtracted quark-mass definition for m_b . Specifically, we adopt the shape-function mass $m_b^{SF}(\mu; \mu_h)$ [63, 83] defined at a subtraction scale $\mu_h = 1.5 \text{ GeV}$, which relates to the pole mass as

$$m_b^{\text{pole}} = m_b^{SF}(\mu; \mu_h) + \frac{C_F}{4} \frac{\alpha_s(\mu_h)}{\pi} + \dots \quad (5.7)$$

Throughout this chapter we will use $m_b^{SF}(\mu; \mu_h)$ as the b -quark mass and refer to it as m_b for brevity. The present value of this parameter is $m_b = (4.61 \pm 0.06) \text{ GeV}$ [96].

5.2 Calculation of the weight function

5.2.1 Leading power

The key strategy for the calculation of the weight function is to make use of QCD factorization theorems for the decay distributions on both sides of (5.1) and to arrange the resulting, factorized expressions such that they are both given as integrals over the shape function, $\int_0^1 dy y^{2a} H_u(y) \int_0^1 d\hat{s} \hat{S}(\hat{s}) g_i(\hat{s})$, with different functions g_i for the left-hand and right-hand sides. Relation (5.1) can then be enforced by matching g_{LHS} to g_{RHS} . Following this procedure, we find for the integrated P_+ spectrum in $B \rightarrow X_u l$ decay after a series of integration interchanges

$$\begin{aligned} \int_0^1 dP_+ \frac{d\Gamma_u}{dP_+} / \int_0^1 dy y^{2a} H_u(y) \int_0^1 d\hat{s} \hat{S}(\hat{s}) g_i(\hat{s}) &= \int_0^1 d\hat{s} \hat{S}(\hat{s}) \int_0^1 dq q^{2a} H_u(q) \int_0^1 dy y^{2a} H_u(y) \int_0^1 d\hat{s} \hat{S}(\hat{s}) g_i(\hat{s}) \\ &\quad \times \ln \frac{m_b(\mu_q)}{m_b(\mu_h)} + \ln y; \end{aligned} \quad (5.8)$$

where $q = m \ln(\mu_B/q)$, and [96]

$$j \ln \frac{Q^2}{\mu_i^2}; \mu_i = \int_0^{Q^2} dp^2 J(p^2; \mu_i) \quad (5.9)$$

is the integral over the jet function. For the sake of transparency, we often suppress the explicit dependence on μ_i and μ_h when it is clear at which scales the relevant quantities are defined. The function H_u is a linear combination of the hard functions entering the structures F_i in (5.3), which in the notation of [95] is given by

$$H_u(y; \mu_h) = 2y^2(3-2y)H_{u1}(y; \mu_h) + 12y^2(1-y)H_{u2}(y; \mu_h) + 2y^3H_{u3}(y; \mu_h); \quad (5.10)$$

RG resummation effects build up the factor y^{-2a} in (5.8), where $a = a(\mu_h; \mu_i)$ is the value of the RG-evolution function

$$a(\mu_h; \mu_i) = \int_{\mu_i}^{\mu_h} \frac{d\mu}{\mu} \gamma_{\text{cusp}}(\mu) = \int_{s(\mu_h)}^{s(\mu_i)} d\mu \frac{\gamma_{\text{cusp}}(\mu)}{\mu}; \quad (5.11)$$

which depends only on the cusp anomalous dimension [27, 28]. The quantity a has its origin in the geometry of time-like and light-like Wilson lines underlying the kinematics of inclusive B decays into light particles. Our definition is such that a is a positive number for $\mu_h > \mu_i$ and vanishes in the limit $\mu_h \rightarrow \mu_i$. We find it convenient to treat the function $a(\mu_h; \mu_i)$ as a running "physical" quantity, much like $\alpha_s(\mu)$ or $\overline{m}_b(\mu)$. Since the cusp anomalous dimension is known to three-loop order [98], the value of a can be determined very accurately. Note that three-loop accuracy in a (as well as in the running coupling α_s) is required for a consistent calculation of the weight function at NNLO. The corresponding expression is

$$\begin{aligned} a = a(\mu_h; \mu_i) = & \frac{0}{2} \ln \frac{s(\mu_i)}{s(\mu_h)} + \frac{1}{0} \frac{1}{0} \frac{s(\mu_i)}{4} \frac{s(\mu_h)}{s(\mu_h)} \\ & + \frac{2}{0} \frac{2}{0} \frac{1}{0} \frac{1}{0} \frac{1}{0} \frac{s^2(\mu_i)}{32} \frac{s^2(\mu_h)}{s^2(\mu_h)} + \dots; \end{aligned} \quad (5.12)$$

where the expansion coefficients c_n and d_n of the cusp anomalous dimension and γ -function can be found in appendix B.

Instead of the jet function J itself, we need its integral $j(\ln Q^2 = \mu_i^2; \mu_i)$ in the second line of (5.8). Since the jet function has a perturbative expansion in terms of "star distributions", which are logarithmically sensitive to the upper limit of integration [2], it follows that $j(L; \mu_i)$ is a simple polynomial in L at each order in perturbation theory. The two-loop result for this quantity has recently been computed by solving the integro-differential evolution equation for the jet function [96]. An unknown integration constant of $O(\mu_i^2 L^0)$ does not enter the expression for the weight function.

We now turn to the right-hand side of (5.1) and follow the same steps that lead to (5.8). It is helpful to make an ansatz for the leading-power contribution to the weight function, $W^{(0)}(\cdot; P_+)$, where the dependence on \cdot is solely given via an upper limit of integration. To this end, we define a function $f(k)$ through

$$W^{(0)}(\cdot; P_+) / \frac{1}{(M_B - P_+)^3} \int_0^{\cdot} dk f(k) (M_B - P_+ - k)^5 : \quad (5.13)$$

This allows us to express the weighted integral over the $B \rightarrow X_s$ photon spectrum as

$$\begin{aligned} & \int_0^{\cdot} dP_+ \frac{d_s}{dP_+} W^{(0)}(\cdot; P_+) / \\ & \int_0^{\cdot} dP_+ (M_B - P_+)^3 W^{(0)}(\cdot; P_+) \int_0^{\cdot} dm_b J(m_b(P_+ - \cdot)) \hat{S}(\cdot) \\ & / \int_0^{\cdot} d\cdot \hat{S}(\cdot) \int_0^{M_B - \cdot} dq 5q^4 \int_0^{\cdot} dk f(k) j \ln \frac{m_b(P_+ - \cdot - k)}{2} : \quad (5.14) \end{aligned}$$

Note that the jet function J (and with it j) is the same in semileptonic and radiative decays. The difference is that the argument of the jet function in (5.8) contains an extra factor of y , which is absent in (5.14). Comparing these two relations leads us to the matching condition

$$\int_0^{\cdot} dy y^{2a} H_u(y) j \ln \frac{m_b}{2} + \ln y = \int_0^{\cdot} dk f(k) j \ln \frac{m_b(P_+ - \cdot - k)}{2} ; \quad (5.15)$$

which holds to all orders in perturbation theory and allows for the calculation of $W^{(0)}(\cdot; P_+)$ via (5.13). The main feature of this important relation is that the particular value of \cdot is irrelevant for the determination of $f(k)$. It follows that, as was the case for the jet function J , the perturbative expansion of $f(k)$ in $s(\cdot)$ at the intermediate scale involves star distributions, and $W^{(0)}(\cdot; P_+)$ depends logarithmically on $(M_B - P_+)$. At two-loop order it suffices to make the ansatz

$$\begin{aligned} f(k) / & (k) + C_F \frac{s(\cdot)}{4} c_0^{(1)}(k) + c_1^{(1)} \frac{1}{k} \left[\frac{2}{i} m_b \right]^{\#} \\ & + C_F \frac{s(\cdot)}{4} c_0^{(2)}(k) + c_1^{(2)} \frac{1}{k} \left[\frac{2}{i} m_b \right]^{\#} + 2c_2^{(2)} \frac{1}{k} \ln \frac{m_b k}{2} \left[\frac{2}{i} m_b \right]^{\#} + \dots; \end{aligned} \quad (5.16)$$

where the star distributions have the following effect when integrated with some

smooth function $f(k)$ over an interval :

$$\begin{aligned} \int_0^Z dk \frac{1}{k} f(k) &= \int_0^Z dk \frac{f(k) - f(0)}{k} + f(0) \ln \frac{m_b}{\frac{2}{i}} ; \\ \int_0^Z dk \frac{1}{k} \ln \frac{m_b k}{\frac{2}{i}} f(k) &= \int_0^Z dk \frac{f(k) - f(0)}{k} \ln \frac{m_b k}{\frac{2}{i}} + \frac{f(0)}{2} \ln^2 \frac{m_b}{\frac{2}{i}} : \end{aligned} \quad (5.17)$$

A sensitivity to the hard scale μ_h enters into $f(k)$ via the appearance of $H_u(y; \mu_h)$ in (5.15). Because of the polynomial nature of $j(L; \mu_i)$, all we ever need are moments of the hard function with respect to $\ln y$. We thus define the master integrals

$$T_n(a; \mu_h) = \int_0^1 dy y^{-2a} H_u(y; \mu_h) \ln^n y; \quad h_n(a; \mu_h) = \frac{T_n(a; \mu_h)}{T_0(a; \mu_h)}; \quad (5.18)$$

which can be calculated order by order in $\alpha_s(\mu_h)$. Therefore, the coefficients $c_k^{(n)}$ of the perturbative expansion in (5.16) at the intermediate scale have the (somewhat unusual) feature that they possess themselves an expansion in $\alpha_s(\mu_h)$. This is a consequence of the fact that, unlike the differential decay rates (5.3) and (5.4), the weight function itself does not obey a simple factorization formula, in which the hard correction can be factored out. Rather, as can be seen from (5.15), it is a convolution of the type $W = H(\mu_h) \otimes J(\mu_i)$. To one-loop accuracy, the hard function H_u reads

$$\begin{aligned} H_u(y; \mu_h) &= 2y^2 (3 - 2y) \left[1 + \frac{C_F \alpha_s(\mu_h)}{4} \left(4 \ln^2 \frac{ym_b}{\mu_h} + 10 \ln \frac{ym_b}{\mu_h} - 4 \ln y \right) \right. \\ &\quad \left. + 4L_2(1-y) - \frac{2}{6} \right] + \frac{C_F \alpha_s(\mu_h)}{12} 3y^2 \ln y : \end{aligned} \quad (5.19)$$

Explicit expressions for the quantities T_0 , $c_k^{(n)}$, and h_n entering the distribution function $f(k)$ will be given below.

5.2.2 Subleading power

Power corrections to the weight function can be extracted from the corresponding contributions to the two P_+ spectra in (5.3) and (5.4). There exists a class of power corrections associated with the phase-space prefactors $(M_B - P_+)^n$ in these relations, whose effects are treated exactly in our approach, see e.g. (5.13). This is important, because these phase-space corrections increase in magnitude as the kinematical range over which the two spectra are integrated is enlarged. One wants to make μ_h as large as experimentally possible so as to increase statistics

and justify the assumption of quark-hadron duality, which underlies the theory of inclusive B decays.

The remaining power corrections fall into two distinct classes: kinematical corrections that start at order s and come with the leading shape function [32, 2], and hadronic power corrections that start at tree level and involve new, subleading shape functions [51, 52, 66, 73, 74, 75, 76, 99]. Because different combinations of these hadronic functions enter in $B \rightarrow X_u l$ and $B \rightarrow X_s$ decays, it is impossible to eliminate their contributions in relations such as (5.1). As a result, at $O(\Lambda_{QCD}/m_b)$ there are non-perturbative hadronic uncertainties in the calculation of the weight function $W(\cdot; P_+)$, which need to be estimated before a reliable extraction of $\langle V_{ub} \rangle$ can be performed. For the case of the charged-lepton energy spectrum and the hadronic invariant mass spectrum, this aspect has been discussed previously in [52, 74] and [99], respectively.

Below, we will include power corrections to first order in Λ_{QCD}/m_b . Schematically, the subleading corrections to the right-hand side of (5.1) are computed according to $\int_0^{(1)} W^{(0)} d_s^{(1)} = dP_+ + W^{(1)} d_s^{(0)} = dP_+$, where the superscripts indicate the order in Λ_{QCD}/m_b power counting. The power corrections to the weight function, denoted by $W^{(1)}$, are derived from the mismatch in the power corrections to the two decay spectra. The kinematical power corrections to the two spectra are known at $O(s)$, without scale separation. We assign a coupling $s(\cdot)$ to these terms, where the scale \cdot will be chosen of order the intermediate scale [95]. At first subleading power the leading shape function is convoluted with either a constant or a single logarithm of the form $\ln[(P_+ \cdot) = (M_B - P_+)]$, and we have (with $n = 0, 1$)

$$\begin{aligned} \int_0^Z dP_+ \frac{d_u}{dP_+} &= 3 \int_0^Z s(\cdot) dP_+ (M_B - P_+)^4 \int_0^{P_+} d\hat{s} \hat{S}(\hat{s}) \ln^n \frac{P_+ \cdot}{M_B - P_+} \\ &= s(\cdot) \int_0^Z d\hat{s} \hat{S}(\hat{s}) \int_0^{\hat{s}} dk (M_B - \hat{s} - k)^4 \ln^n \frac{k}{M_B - \hat{s} - k}; \end{aligned} \quad (5.20)$$

and similarly for the photon spectrum. On the other hand, the weighted integral in (5.1) also contains terms where the photon spectrum is of leading power and the weight function of subleading power,

$$\int_0^Z dP_+ \frac{d_s}{dP_+} W^{kin(1)}(\cdot; P_+) = 3 \int_0^Z dP_+ (M_B - P_+)^3 \hat{S}(P_+) W^{kin(1)}(\cdot; P_+); \quad (5.21)$$

Therefore the kinematical corrections to the weight function must have the form

$$\begin{aligned} W^{kin(1)}(\cdot; P_+) &= \frac{s(\cdot)}{(M_B - P_+)^3} \int_0^{P_+} dk (M_B - P_+ - k)^4 \\ &\quad A + B \ln \frac{k}{M_B - P_+ - k}; \end{aligned} \quad (5.22)$$

and a straightforward calculation determines the coefficients A and B . The hadronic power corrections to the weight function, $W^{\text{hadr}(1)}$, can be expressed in terms of the subleading shape functions $\hat{t}(\hat{P}_+)$, $\hat{u}(\hat{P}_+)$, and $\hat{v}(\hat{P}_+)$ defined in [66]. These terms are known at tree level only, and at this order their contribution to the weight function can be derived using the results of [95].

5.3 Results

Including the first-order power corrections and the exact phase-space factors, the weight function takes the form

$$\begin{aligned}
W(\hat{P}_+; P_+) &= \frac{G_F^2 m_b^3}{192 \pi^3} T_0(a; \eta) H(\eta) (M_B - P_+)^2 \\
&\left(1 + \frac{C_F}{4} \frac{s(\eta)}{s(\eta)} c_0^{(1)} + c_1^{(1)} \ln \frac{m_b(\hat{P}_+)}{2\hat{P}_+} \hat{P}(\hat{P}_+) \right. \\
&\quad + C_F \frac{s(\eta)}{4} c_0^{(2)} + c_1^{(2)} \ln \frac{m_b(\hat{P}_+)}{2\hat{P}_+} \hat{P}(\hat{P}_+) \\
&\quad \left. + c_2^{(2)} \ln^2 \frac{m_b(\hat{P}_+)}{2\hat{P}_+} 2\hat{P}(\hat{P}_+) \ln \frac{m_b(\hat{P}_+)}{2\hat{P}_+} + 2p_2(\hat{P}_+) \right) \\
&+ \frac{P_+}{M_B - P_+} \frac{C_F}{4} s(\eta) [A(a; \eta) I_A(\eta) + B(a; \eta) I_B(\eta)] \\
&+ \frac{1}{M_B - P_+} \frac{1}{2(1-a)(3-a)} 4(1-a)(\hat{P}_+) + 2(4-3a) \frac{\hat{t}(\hat{P}_+)}{\hat{S}(\hat{P}_+)} \\
&+ (4-a) \frac{\hat{u}(\hat{P}_+)}{\hat{S}(\hat{P}_+)} + (8-13a+4a^2) \frac{\hat{v}(\hat{P}_+)}{\hat{S}(\hat{P}_+)} + \frac{m_s^2}{M_B - P_+} \frac{\hat{S}^0(\hat{P}_+)}{\hat{S}(\hat{P}_+)} + \dots ;
\end{aligned} \tag{5.23}$$

where $\eta = M_B - m_b$ is the familiar mass parameter of heavy-quark effective theory, and $\hat{P}_+ = (P_+ - m_b) = (M_B - P_+)$. The first line denotes an overall normalization, the next three lines contain the leading-power contributions, and the remaining expressions enter at subleading power. The different terms in this result will be discussed in the remainder of this section.

For the leading-power terms in the above result we have accomplished a complete separation of hard and intermediate (hard-collinear) contributions to the weight function in a way consistent with the factorization formula $W = H \otimes J$ mentioned in the previous section. The universality of the shape function, which encodes the soft physics in both $B \rightarrow X_s$ and $B \rightarrow X_{u1}$ decays, implies that the weight function is insensitive to physics below the intermediate scale $\hat{P}_+ \sim m_b / Q_{CD}$. In particular, quark-hadron duality ensures that the small region in phase space where the argument $m_b(\hat{P}_+)$ of the logarithms scales as Q_{CD}^2 or smaller does not need special consideration. At a technical level, this can be seen by noting that the jet function is the discontinuity of the collinear quark

propagator in soft-collinear effective theory [22, 63], and so the P_+ integrals can be rewritten as a contour integral in the complex p^2 plane along a circle of radius m_b^2 .

5.3.1 Leading power

The leading-power corrections in the curly brackets in (5.23) are determined completely at NNLO in RG-improved perturbation theory, including three-loop running effects via the quantity a in (5.11), and two-loop matching corrections at the scale μ_i as indicated above. To this end we need expressions for the one-loop coefficients $c_n^{(1)}$ including terms of $\mathcal{O}(s(\mu_h))$, while the two-loop coefficients $c_n^{(2)}$ are needed at leading order only. We find

$$c_0^{(1)} = 3h_1(a; \mu_h) - 1 - \frac{C_F s(\mu_h)}{3m_b} + 2h_2(a; \mu_h); \quad c_1^{(1)} = 4h_1(a; \mu_h); \quad (5.24)$$

and

$$\begin{aligned} c_0^{(2)} = & C_F \left[\frac{3}{2} + 2s^2 - 24s_3 h_1(a; \mu_h) + \frac{9}{2} \frac{4s^2}{3} h_2(a; \mu_h) \right. \\ & \left. + 6h_3(a; \mu_h) + 2h_4(a; \mu_h) \right] \\ & + C_A \left[\frac{73}{9} + 40s_3 h_1(a; \mu_h) + \frac{8}{3} \frac{2s^2}{3} h_2(a; \mu_h) \right. \\ & \left. + \frac{247}{18} + \frac{2s^2}{3} h_1(a; \mu_h) + \frac{29}{6} h_2(a; \mu_h) + \frac{2}{3} h_3(a; \mu_h) \right]; \\ c_1^{(2)} = & C_F \left[12h_2(a; \mu_h) + 8h_3(a; \mu_h) \right] + C_A \left[\frac{16}{3} \frac{4s^2}{3} h_1(a; \mu_h) \right. \\ & \left. + \frac{29}{3} h_1(a; \mu_h) - 2h_2(a; \mu_h) \right]; \\ c_2^{(2)} = & 8C_F h_2(a; \mu_h) - 2s_0 h_1(a; \mu_h); \end{aligned} \quad (5.25)$$

As always $C_F = 4/3$, $C_A = 3$, and $s_0 = 11 - 2n_f/3$ is the first coefficient of the QCD β -function. The term proportional to s in the expression for $c_0^{(1)}$ arises because of the elimination of the pole mass in favor of the shape-function mass, see (5.7). Since the logarithms $\ln[m_b(P_+) = \frac{2}{s}]$ in (5.23) contain m_b , all coefficients except $c_n^{(1)}$ receive such contributions. However, to two-loop order only $c_0^{(1)}$ is affected.

Next, the corresponding expressions for the hard matching coefficients h_i are

calculated from (5.18). To the required order they read

$$\begin{aligned}
h_1(a; h) &= \frac{15}{2} \frac{12a + 2a^2}{(2-a)(3-a)(3-2a)} \\
&+ \frac{C_F}{4} \frac{s(h)}{4} \frac{2(189 - 318a + 192a^2 - 48a^3 + 4a^4)}{(2-a)^2(3-a)^2(3-2a)^2} \ln \frac{m_b}{h} \\
&+ \frac{2331}{4} \frac{5844a + 5849a^2 - 2919a^3 + 726a^4 - 72a^5}{(2-a)^3(3-a)^3(3-2a)^3} \\
&+ 4^{(2)}(3-2a) + \dots; \\
h_2(a; h) &= \frac{69}{2} \frac{90a + 36a^2 - 4a^3}{(2-a)^2(3-a)(3-2a)} \\
&+ \frac{C_F}{4} \frac{s(h)}{4} \frac{2(1692 - 3699a + 3138a^2 - 1272a^3 + 240a^4 - 16a^5)}{(2-a)^3(3-a)^2(3-2a)^2} \ln \frac{m_b}{h} \\
&+ \frac{46521}{2} \frac{140064a + 175479a^2 - 117026a^3 + 43788a^4 - 8712a^5 + 720a^6}{(2-a)^4(3-a)^2(3-2a)^4} \\
&+ \frac{4(15 - 12a + 2a^2)}{(2-a)(3-a)(3-2a)} 4^{(2)}(3-2a) + 4^{(3)}(3-2a) + \dots; \\
h_3(a; h) &= \frac{3(303 - 552a + 360a^2 - 96a^3 + 8a^4)}{4(2-a)^2(3-a)(3-2a)} + \dots; \\
h_4(a; h) &= \frac{3(1293 - 3030a + 2760a^2 - 1200a^3 + 240a^4 - 16a^5)}{2(2-a)^3(3-a)(3-2a)} + \dots;
\end{aligned} \tag{5.26}$$

where $^{(n)}(x)$ is the n -th derivative of the polygamma function. Because of the exact treatment of the phase space there are corrections to the logarithms in (5.23), which are finite-order polynomials in the small ratio $\mu_B = (P_+ - M_B)/P_+$. Explicitly,

$$\begin{aligned}
p_1(\mu_B) &= 5 - 5^2 + \frac{10}{3} \mu_B^3 - \frac{5}{4} \mu_B^4 + \frac{1}{5} \mu_B^5; \\
p_2(\mu_B) &= 5 - \frac{5}{2} \mu_B^2 + \frac{10}{9} \mu_B^3 - \frac{5}{16} \mu_B^4 + \frac{1}{25} \mu_B^5;
\end{aligned} \tag{5.27}$$

This concludes the discussion of the leading-power expression for the weight function.

5.3.2 Subleading power

The procedure for obtaining the kinematical power corrections to the weight function has been discussed in Section 5.2.2. For the coefficients A and B in (5.23) we

nd

$$\begin{aligned}
A(a; h) = & \frac{388 + 702a}{2(1-a)^2(2-a)(3-a)(3-2a)} - \frac{429a^2 + 123a^3}{2(1-a)^2(2-a)(3-a)(3-2a)} - \frac{34a^4 + 8a^5}{2(1-a)^2(2-a)(3-a)(3-2a)} \\
& + \frac{1}{3} - \frac{4}{9} \ln \frac{m_b}{m_s} - \frac{[C_{8g}^e(h)]^2}{[C_7^e(h)]^2} \\
& - \frac{10}{3} \frac{C_{8g}^e(h)}{C_7^e(h)} + \frac{8}{3} \frac{C_1(h)}{C_7^e(h)} - \frac{1}{3} \frac{C_1(h)C_{8g}^e(h)}{[C_7^e(h)]^2} g_1(z) \\
& - \frac{16}{9} \frac{[C_1(h)]^2}{[C_7^e(h)]^2} g_2(z); \\
B(a; h) = & \frac{2(8+a)}{(1-a)(3-a)} - \frac{2}{9} \frac{[C_{8g}^e(h)]^2}{[C_7^e(h)]^2}; \tag{5.28}
\end{aligned}$$

Here $C_i(h)$ denote the (effective) Wilson coefficients of the relevant operators in the effective weak Hamiltonian, which are real functions in the Standard Model. The variable $z = (m_c - m_b)^2$ enters via charm-loop penguin contributions to the hard function of the $B \rightarrow X_s \gamma$ photon spectrum [32], and

$$g_1(z) = \int_0^1 dx x \operatorname{Re} \left[\frac{z}{x} G\left(\frac{x}{z}\right) + \frac{1}{2} \right]; \quad g_2(z) = \int_0^1 dx (1-x) \left[\frac{z}{x} G\left(\frac{x}{z}\right) + \frac{1}{2} \right]; \tag{5.29}$$

with

$$G(t) = \begin{cases} \frac{8}{t^2} \arctan^2 \sqrt{\frac{t}{t-4}} & ; t < 4; \\ \frac{h}{2} \ln \left(\frac{t-4}{t} \right) + \frac{i}{2} \frac{1}{t-4} & ; t = 4; \\ \frac{i}{2} \frac{1}{t-4} & ; t > 4; \end{cases} \tag{5.30}$$

Furthermore we need the integrals over k in (5.22), which encode the phase-space corrections. They give rise to the functions

$$\begin{aligned}
I_A(h) = & 1 - 2 + 2^2 - 3 + \frac{1}{5} h^4; \\
I_B(h) = & I_A(h) \ln \frac{1}{1-h} + \frac{\ln(1-h)}{5} - \frac{4}{5} + \frac{3}{5} h - \frac{4}{15} h^2 + \frac{1}{20} h^3; \tag{5.31}
\end{aligned}$$

The hadronic power corrections come from subleading shape functions in the theoretical expressions for the two decay rates. We give their tree-level contributions to the weight function in the last two lines of (5.23), where \hat{S} denotes the leading shape function, and $\hat{t}; \hat{u}; \hat{v}$ are subleading shape functions as defined in [66]. For completeness, we also include a contribution proportional to m_s^2 resulting from finite-mass effects in the strange-quark propagator in $B \rightarrow X_s \gamma$ decays. For $m_s = O(\Lambda_{QCD})$ these effects are formally of the same order as other subleading shape-function contributions [100], although numerically they are strongly suppressed. The appearance of subleading shape functions introduces an irreducible

hadronic uncertainty to a $\sqrt{s_{\text{ub}}}$ determination via (5.1). In practice, this uncertainty can be estimated by adopting different models for the subleading shape functions. This will be discussed in detail in Section 5.4.4 below. Until then, let us use a "default model", in which we assume the functional forms of the subleading shape functions $\hat{t}(\hat{s})$, $\hat{u}(\hat{s})$, and $\hat{v}(\hat{s})$ to be particular linear combinations of the functions $\hat{S}^0(\hat{s})$ and $(\hat{s})\hat{S}(\hat{s})$. These combinations are chosen in such a way that the results satisfy the moment relations derived in [66], and that all terms involving the parameter a cancel in the expression (5.23) for the weight function for any value of a . These requirements yield

$$\hat{t}(\hat{s}) = \frac{3}{4} (\hat{s})\hat{S}(\hat{s}) + \frac{1}{4} \hat{S}^0(\hat{s}); \quad \hat{u}(\hat{s}) = \frac{1}{2} (\hat{s})\hat{S}(\hat{s}) + \frac{5}{6} \hat{S}^0(\hat{s}); \quad \hat{v}(\hat{s}) = \frac{1}{2} \hat{S}^0(\hat{s}); \quad (5.32)$$

and the last two lines inside the large bracket in the expression (5.23) for the weight function simplify to

$$\frac{\hat{S}^0(\hat{s})}{M_B^2} \frac{\hat{S}^0(\hat{s})}{P_+} \hat{S}(\hat{s}) \rightarrow \frac{\hat{S}^0(\hat{s})}{M_B^2} \frac{\hat{S}(\hat{s})}{P_+} \left(\frac{4}{M_B^2} \frac{\hat{S}^0(\hat{s})}{P_+} \right)^2; \quad (5.33)$$

where

$$\hat{S}^0(\hat{s}) = \frac{(2+a)}{3(1-a)} \frac{1}{(3-a)} + \frac{a(7-4a)}{2(1-a)(3-a)} m_s^2; \quad (5.34)$$

Here \hat{S}_1 and $\hat{S}_2 = \frac{1}{4} (M_B^2 - M_B^2)$ are hadronic parameters describing certain B -meson matrix elements in heavy-quark effective theory [54]. The strange-quark mass is a running mass evaluated at a scale typical for the final-state hadronic jet, for which we take 1.5 GeV. As mentioned above, the numerical effect of the strange-quark mass correction is small. For typical values of the parameters, it reduces the result for \hat{S}^0_{SSF} by about 10% or less. The expression on the right-hand side in (5.33) is equivalent to that on the left-hand side after the integration with the photon spectrum in (5.1) has been performed. It has been derived using the fact that the normalized photon spectrum is proportional to the shape function $\hat{S}(\hat{s})$ at leading order. Note that the second term in the final formula is power suppressed with respect to the first one. It results from our exact treatment of phase-space factors and thus is kept for consistency.

5.3.3 Normalization

Finally, let us present explicit formulae for the overall normalization factor in (5.23). The new ingredient here is the factor T_0 , which is defined in (5.18). At

one-loop order we find

$$\begin{aligned}
T_0(a; \mu_h) = & \frac{2(3-a)}{(2-a)(3-2a)} \left[1 - \frac{C_F s(\mu_h)}{4} 4 \ln^2 \frac{m_b}{\mu_h} \right. \\
& \frac{2(120-159a+69a^2-10a^3)}{(2-a)(3-a)(3-2a)} \ln \frac{m_b}{\mu_h} \\
& \left. + \frac{1539-3845a+3842a^2-1920a^3+480a^4-48a^5}{(2-a)^2(3-a)(3-2a)} + 4 \ln(3-2a) + \frac{2}{6} \right] : \quad (5.35)
\end{aligned}$$

When the product of T_0 with the quantity [50]

$$\begin{aligned}
H(\mu_h) = & 1 + \frac{C_F s(\mu_h)}{4} 4 \ln^2 \frac{m_b}{\mu_h} + 10 \ln \frac{m_b}{\mu_h} + 7 \frac{7}{6} + \frac{12}{m_b} \\
& 2 \ln^2 (7+4 \ln^2) \ln + 10 + \frac{2}{3} \ln^3 \\
& + \frac{C_1(\mu_h)^2}{C_7^e(\mu_h)^2} \hat{f}_{11}(\mu_h) + \frac{C_1(\mu_h)}{C_7^e(\mu_h)} \hat{f}_{17}(\mu_h) + \frac{C_1(\mu_h) C_{8g}^e(\mu_h)}{C_7^e(\mu_h)^2} \hat{f}_{18}(\mu_h) \\
& + \frac{C_{8g}^e(\mu_h)}{C_7^e(\mu_h)} \hat{f}_{78}(\mu_h) + \frac{C_{8g}^e(\mu_h)^2}{C_7^e(\mu_h)^2} \hat{f}_{88}(\mu_h) \quad (5.36)
\end{aligned}$$

from the total $B \rightarrow X_s$ decay rate is consistently expanded to $O(s(\mu_h))$, the double logarithm cancels out. Here $\mu_h = 1.2 E = m_b = 0.9$, and the functions $\hat{f}_{ij}(\mu_h)$ capture effects from operator mixing.

5.4 Numerical results

We are now in a position to explore the phenomenological implications of our results. We need as inputs the heavy-quark parameters $\mu_2 = 0.12 \text{ GeV}^2$, $\mu_1 = (0.25 \pm 0.10) \text{ GeV}^2$, and the quark masses $m_b = (4.61 \pm 0.06) \text{ GeV}$ [96], $m_s = (90 \pm 25) \text{ MeV}$ [101, 102], and $m_c/m_b = 0.222 \pm 0.027$ [50]. Here m_b is defined in the shape-function scheme at a scale $\mu_h = 1.5 \text{ GeV}$, m_s is the running mass in the $\overline{\text{MS}}$ scheme evaluated at 1.5 GeV , and m_c/m_b is a scale invariant ratio of running masses. Throughout, we use the 3-loop running coupling normalized to $\alpha_s(M_Z) = 0.1187$, matched to a 4-flavor theory at 4.25 GeV . For the matching scales, we pick the default values $\mu_h^{\text{def}} = m_b = \sqrt{2}$ and $\mu_i^{\text{def}} = \mu_h^{\text{def}} = 1.5 \text{ GeV}$, which are motivated by the underlying dynamics of inclusive processes in the shape-function region [63, 95].

In the remainder of this section we present results for the partial decay rate $\Gamma_u(\mu_h)$ computed by evaluating the right-hand side of relation (5.1). This is more informative than to focus on the value of the weight function for a particular choice

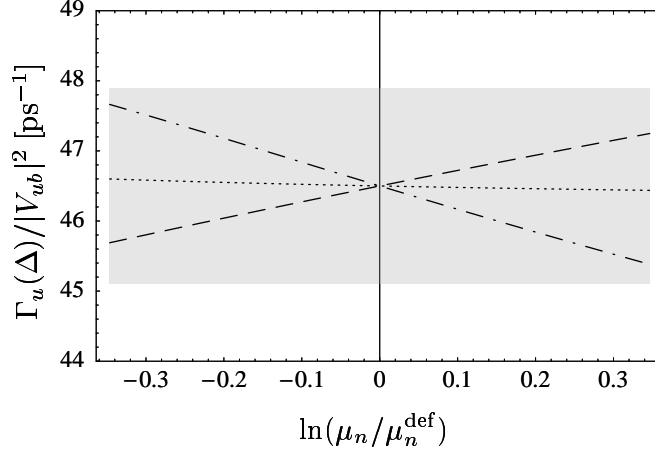


Figure 5.1: Residual scale dependence of $\Gamma_u(\Delta)$ for $\mu_p = 0.65 \text{ GeV}$. The dashed line depicts the variation of μ_h about its default value $m_b = \sqrt{2}$, the dash-dotted line the variation of μ_i about 1.5 GeV , and the dotted line the variation of μ_s also about 1.5 GeV . The highlighted area shows the combined perturbative uncertainty.

of P_+ . For the purpose of our discussion we use a simple model for the normalized photon spectrum that describes the experimental data reasonably well, namely

$$\frac{1}{s} \frac{d\sigma}{dP_+} = \frac{b^b}{(b)^b} (P_+)^{b-1} \exp \left(-\frac{P_+}{b} \right) \quad (5.37)$$

with $b = 0.77 \text{ GeV}$ and $b = 2.5$.

5.4.1 Studies of the perturbative expansion

The purpose of this section is to investigate the individual contributions to $\Gamma_u(\Delta)$ that result from the corresponding terms in the weight function, as well as their residual dependence on the matching scales. For $\mu_p = 0.65 \text{ GeV}$ we find numerically

$$\begin{aligned} \frac{\Gamma_u(0.65 \text{ GeV})}{|V_{ub}|^2 \text{ ps}^{-1}} &= 43.5 \left[1 + 0.158 [s(i)] - 0.095 [s(h)] + 0.076 [s^2(i)] \right. \\ &\quad \left. + 0.037 [s(i)s(h)] + 0.009 [\text{kin}] - 0.043 [\text{hadr}] \right] = 46.5 : \end{aligned} \quad (5.38)$$

The terms in parenthesis correspond to the contributions to the weight function arising at different orders in perturbation theory and in the $1/m_b$ expansion, as indicated by the subscripts. Note that the perturbative contributions from the intermediate scale are typically twice as large as the ones from the hard scale, which is also the naive expectation. Indeed, the two-loop $s^2(i)$ correction is numerically of comparable size to the one-loop $s(h)$ contribution. This confirms the importance of separating the scales μ_i and μ_h . The contributions from kinematical and

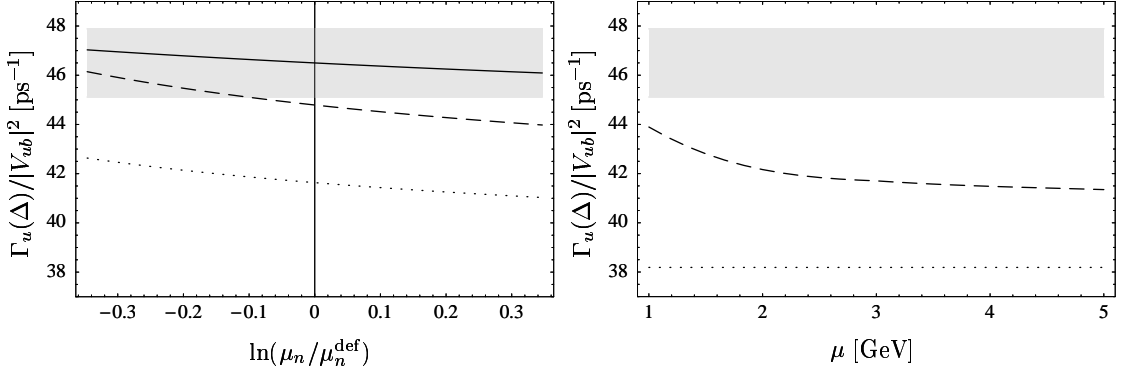


Figure 5.2: Convergence of the perturbative series and residual scale dependence. Left: RG-improved results at LO (dotted), NLO (dashed), and NNLO (solid) as a function of the scales μ_i , μ_h , μ_s , which are varied simultaneously about their default values. Right: Fixed-order results at tree-level (dotted) and one-loop order (dashed).

hadronic power corrections turn out to be numerically small, comparable to the two-loop corrections.

The weight function (5.23) is formally independent of the matching scales μ_h , μ_i , and μ_s . In Figure 5.1 we plot the residual scale dependence resulting from the truncation of the perturbative series. Each of the three scales is varied independently by a factor between $1/\sqrt{2}$ and $\sqrt{2}$ about its default value. The scale variation of μ_i is still as significant as the variation of μ_h , even though the former is known at NNLO and the latter only at NLO. We have checked analytically that the result (5.23) is independent of μ_i through two-loop order, i.e. the residual scale dependence is an $\mathcal{O}(\alpha_s^3(\mu_i))$ effect. In order to obtain a conservative estimate of the perturbative uncertainty in our predictions we add the individual scale dependencies in quadrature. This gives the gray band shown in the figure.

Figure 5.2 displays the result for $\Gamma_u(0.65 \text{ GeV})$ at different orders in RG-improved perturbation theory. At LO, we dismiss all α_s terms including the kinematical power corrections; however, leading logarithms are still resummed and give rise to a non-trivial dependence of T_0 on the coefficient a . At NLO, we include the $\mathcal{O}(\alpha_s(\mu_h))$, $\mathcal{O}(\alpha_s(\mu_i))$, and $\mathcal{O}(\alpha_s(\mu_s))$ contributions, but drop terms of order $\alpha_s^2(\mu_i)$ or $\alpha_s(\mu_i)\alpha_s(\mu_h)$. At NNLO, we include all terms shown in (5.23). In studying the different perturbative approximations we vary the matching scales simultaneously (and in a correlated way) about their default values. Compared with Figure 5.1 this leads to a reduced scale variation. The gray bands in Figure 5.2 show the total perturbative uncertainty as determined above. While the two-loop NNLO contributions are sizable, we observe a good convergence of the perturbative expansion and a reduction of the scale sensitivity in higher orders. The right-hand plot in the figure contrasts these findings with the corresponding results in fixed-order perturbation theory, which are obtained from (5.23) by setting $\mu_h = \mu_i = \mu_s =$

and truncating the series at $O(\alpha_s^2)$ for consistency. We see that the fixed-order results are also rather insensitive to the value of μ unless this scale is chosen to be small; yet, the predicted values for Γ_u are significantly below those obtained in RG-improved perturbation theory. We conclude that the small scale dependence observed in the fixed-order calculation does not provide a reliable estimator of the true perturbative uncertainty. In our opinion, a fixed-order calculation at a high scale is not only inappropriate in terms of the underlying dynamics of inclusive decay processes in the shape-function region, it is also misleading as a basis for estimating higher-order terms in the perturbative expansion.

5.4.2 Comments on the normalization of the photon spectrum

We mentioned in section 5.1 that the use of the normalized photon spectrum is advantageous because event fractions in $B \rightarrow X_s \gamma$ decay can be calculated more reliably than partial decay rates. In this section we point out another important advantage, namely that the perturbative series for the weight function $W(\mu; P_+)$ is much better behaved than that for $\tilde{W}(\mu; P_+)$. The difference of the two weight functions lies in their normalizations, which are

$$W(\mu; P_+) / m_b^3 T_0(a; \mu_h) H(\mu_h); \quad \tilde{W}(\mu; P_+) / \frac{T_0(a; \mu_h)}{[C_7^e(\mu_h)]^2 \bar{m}_b^2(\mu_h) H_s(\mu_h)^2} : \quad (5.39)$$

Here H_s is the hard function in the factorized expression for the structure function F in (5.4), which has been derived in [50]. Note that the two weight functions have a different dependence on the b -quark mass. In the case of W , three powers of m_b enter through phase-space integrations in the total decay rate $\Gamma_s(E)$, and it is therefore appropriate to use a low-scale subtracted quark-mass definition, such as the shape-function mass. In the case of \tilde{W} , on the other hand, two powers of the running quark mass $\bar{m}_b(\mu_h)$ enter through the definition of the dipole operator O_7 , and it is appropriate to use a short-distance mass definition such as that provided by the \overline{MS} scheme. In practice, we write $\bar{m}_b(\mu_h)$ as $\bar{m}_b(m_b)$ times a perturbative series in $\alpha_s(\mu_h)$.

The most pronounced effect of the difference in normalization is that the weight function \tilde{W} receives very large radiative corrections at order $\alpha_s(\mu_h)$, which range between 68% and 43% when the scale μ_h is varied between m_b and $m_b=2$. This contrasts the well-behaved perturbative expansion of the weight function W , for which the corresponding corrections vary between 11% and 7%. In other words, the hard matching corrections for \tilde{W} are about six times larger than those for W . Indeed, these corrections are so large that in our opinion relation (5.2) should not be used for phenomenological purposes.

The different perturbative behavior of the hard matching corrections to the weight functions is mostly due to the mixing of the dipole operator O_7 with other operators in the effective weak Hamiltonian for $B \rightarrow X_s \gamma$ decay. In order to

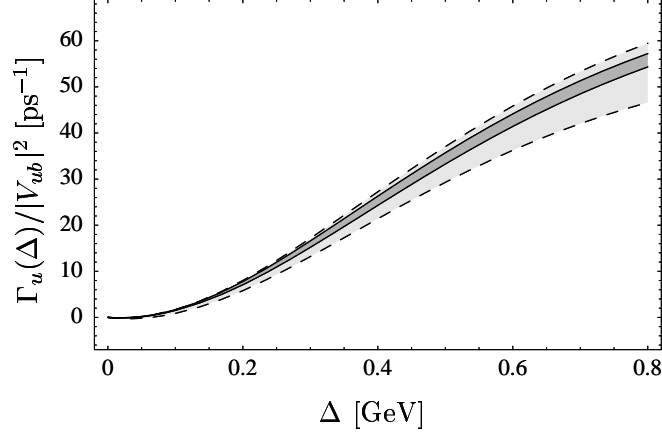


Figure 5.3: Perturbative uncertainties on $\Gamma_u(\Delta)$ encountered when using the weight function $W(\mu; P_+)$ (dark gray) or $\tilde{W}(\mu; P_+)$ (light gray). In the latter case, the normalization of the photon spectrum is chosen such that the two predictions agree at $\Delta = 0.65 \text{ GeV}$ for central values of the matching scales.

illustrate this fact, consider the one-loop hard matching coefficients defined as

$$W \sim 1 + k \frac{s(\mu_h)}{\mu_b^2} + \dots; \quad \tilde{W} \sim 1 + \mathbb{K} \frac{s(\mu_h)}{\mu_b^2} + \dots \quad (5.40)$$

With our default scale choices we have $k = 2.32 + 1.13i = 1.19$, where the second contribution ($+1.13i$) comes from operator mixing, which gives rise to the terms in the last two lines in (5.36). For the weight function W , this contribution has the opposite sign than the other terms, so that the combined value of k is rather small. For the weight function \tilde{W} , on the other hand, we find $\mathbb{K} = 1.58 - 5.52i = 7.10$. Here the contribution from operator mixing is dominant and has the same sign as the remaining terms, thus yielding a very large value of \mathbb{K} . Such a large $\mathcal{O}(s)$ correction was not observed in [94], because these authors chose to omit the contribution from operators mixing. Note that at a higher scale $\mu_h = m_b$, as was adopted in this reference, the situation is even worse. In that case we find $k = 2.81 + 1.19i = 1.62$ and $\mathbb{K} = 0.66 - 9.13i = 9.79$.

A visualization of the perturbative uncertainty is depicted in Figure 5.3, where predictions for $\Gamma_u(\Delta)$ are shown using either (5.1) or (5.2). In each case, the error band is obtained by varying the different scales about their default values, $\mu_n \in [\mu_n^{\text{def}}/2, 2\mu_n^{\text{def}}]$, and adding the resulting uncertainties in quadrature. The dark-gray band bordered by solid lines denotes the perturbative uncertainty of predictions when using the normalized photon spectrum, as in (5.1). (At the point $\Delta = 0.65 \text{ GeV}$ this uncertainty is identical to the gray band depicted in Figures 5.1 and 5.2). The light-gray band bordered by dashed lines corresponds to the use of the absolute photon spectrum, as in (5.2). The difference in precision between the two methods would be even more pronounced if we used the higher default value

$\mu_h = m_b$ for the hard matching scale. Obviously, the use of the normalized photon spectrum will result in a more precise determination of $\langle V_{ub} \rangle$.

5.4.3 Comments on α_s^2 terms and scale separation

The separation of different momentum scales using RG techniques, which is one of the key ingredients of our approach, is well motivated by the dynamics of charm-less inclusive B decays in the shape-function region. Factorized expressions for the B-decay spectra involve hard functions renormalized at μ_h multiplied by jet and shape functions defined at a lower scale. While physics at or below the intermediate scale is very similar for $B \rightarrow X_u l$ and $B \rightarrow X_s$ (as is manifested by the fact that the leading shape and jet functions are universal), the physics at the hard scale in $B \rightarrow X_s$ decay is considerably more complicated than in semileptonic decay, and it might even contain effects of New Physics. Therefore it is natural to respect the hierarchy $\mu_h \gg \mu_i$ and disentangle the various contributions, as done in this chapter. In fact, our ability to calculate the dominant two-loop corrections is a direct result of this scale separation. Nevertheless, at a technical level we can reproduce the results of a fixed-order calculation by simply setting all matching scales equal to a common scale, $\mu_h = \mu_i = \mu_s = \mu$. In this limit, the expressions derived in this chapter smoothly reduce to those obtained in conventional perturbation theory. While factorized expressions for the decay rates are superior to fixed-order results whenever there are widely separated scales in the problem, they remain valid in the limit where the different scales become of the same order.

In [94], the $O(\alpha_s^2)$ BLM corrections [103] to the weight function $\tilde{W}(\mu; P_+)$ in (5.2) were calculated in fixed-order perturbation theory. For simplicity, only the contribution of the operator O_7 to the $B \rightarrow X_s$ decay rate was included in this work. We note that without the contributions from other operators the expression for \tilde{W} is not renormalization-scale and -scheme invariant. Neglecting operator mixing in the calculation of \tilde{W} is therefore not a theoretically consistent approximation. However, having calculated the exact NNLO corrections at the intermediate scale allows us to examine some of the terms proportional to $\alpha_s^2(\mu_i)$ and compare them to the findings of [94]. In this way we confirm their results for the coefficients multiplying the logarithms $\ln^n[m_b(\mu_s/P_+) = \frac{2}{\mu_i}]$ with $n = 1, 2$ in (5.23). While the α_s^2 terms approximate the full two-loop coefficients of these logarithms arguably well, we stress that the two-loop constant at the intermediate scale is not dominated by terms proportional to α_s . Numerically we find

$$c_0^{(2)} = -47.4 + 39.6 \frac{\alpha_s}{25=3} + a \left(-31.8 + 38.8 \frac{\alpha_s}{25=3} + O(a^2) \right); \quad (5.41)$$

which means that the approximation of keeping only the BLM terms would overestimate this coefficient by almost an order of magnitude and give the wrong sign. This shows the importance of a complete two-loop calculation, as performed in this chapter.

We believe that the perturbative approximations adopted in this chapter, i.e. working to NNLO at the intermediate scale and to NLO at the hard scale, are sufficient for practical purposes in the sense that the residual perturbative uncertainty is smaller than other uncertainties encountered in the application of relation (5.1). Still, one may ask what calculations would be required to determine the missing $\mathcal{O}_7(\mu_h)$ terms in the normalization of the weight function in (5.23), or at least the terms of order $\mathcal{O}_7(\mu_h)$. For the case of $B \rightarrow X_s \gamma$ decay, the contribution of the operator \mathcal{O}_7 to the normalized photon spectrum was recently calculated at two-loop order [104], while the contributions from other operators are known to $\mathcal{O}(\alpha_s^2)$ [105]. What is still needed are the two-loop corrections to the double differential (in P_+ and y) $B \rightarrow X_u \gamma$ decay rate in (5.3).

5.4.4 Subleading corrections from hadronic structures

Due to the fact that different linear combinations of the subleading shape functions $\hat{f}(\mu)$, $\hat{u}(\mu)$, and $\hat{v}(\mu)$ enter the theoretical description of radiative and semileptonic decays starting at order $\alpha_{\text{QCD}} = m_b$, the weight function cannot be free of such hadronic structure functions. Consequently, we found in (5.23) all of the above subleading shape functions, divided by the leading shape function $\hat{S}(\mu)$. Our default model (5.32) for the subleading shape functions was chosen such that the combined effect of all hadronic power corrections could be absorbed into a single hadronic parameter α_{SSF}^2 . More generally, we define a function $\mathcal{h}_{\text{hadr}}(\mu)$ via (a factor 2 is inserted for later convenience)

$$\mathcal{u}(\mu) = [\mathcal{u}(\mu)]_{\text{def}} [1 + 2 \mathcal{h}_{\text{hadr}}(\mu)]; \quad (5.42)$$

where $[\mathcal{u}(\mu)]_{\text{def}}$ denotes the result obtained with the default model for the subleading shape functions. From (5.23), one finds that

$$\begin{aligned} \mathcal{h}_{\text{hadr}}(\mu) = & \int_0^Z dP_+ (M_B - P_+)^4 \left[2(4 - 3a) h_t(P_+) + (4 - a) h_b(P_+) + \right. \\ & \left. + (8 - 13a + 4a^2) h_v(P_+) \right] - 4(1 - a)(3 - a) \int_0^Z dP_+ (M_B - P_+)^5 \hat{S}(P_+) \quad ; \end{aligned} \quad (5.43)$$

where we have used that, at leading order in α_s and $\alpha_{\text{QCD}} = m_b$, the $B \rightarrow X_s \gamma$ photon spectrum is proportional to $(M_B - P_+)^3 \hat{S}(P_+)$. In the relation above, $h_t(\mu) = \hat{f}(\mu) - [\hat{f}(\mu)]_{\text{def}}$ etc. denote the differences between the true subleading shape functions and the functions adopted in our default model. By construction, these are functions with vanishing normalization and first moment.

The above expression for $\mathcal{h}_{\text{hadr}}(\mu)$ is exact to the order we are working; however, in practice we do not know the precise form of the functions $h_i(\mu)$. Our goal is then to find a conservative bound, $|\mathcal{h}_{\text{hadr}}(\mu)| < \mathcal{h}_{\text{hadr}}(\mu)$, and to interpret the function $\mathcal{h}_{\text{hadr}}(\mu)$ as the relative hadronic uncertainty on the value of \mathcal{J}_{ub} extracted using

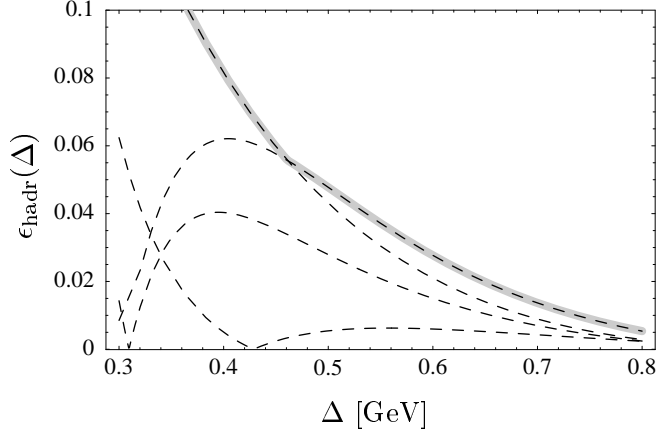


Figure 5.4: Estimates for the hadronic uncertainty $\epsilon_{\text{hadr}}(\Delta)$ obtained from a scan over models for the subleading shape functions. The dashed lines correspond to the individual results for the four $h_i(\Delta)$ functions suggested in [95]. The thick solid line, which covers one of the dashed lines, shows the maximum effect.

relation (5.1). To obtain the bound we scan over a large set of realistic models for the subleading shape functions. In [95], four different functions $h_i(\Delta)$ were suggested, which can be added or subtracted (in different combinations) to each of the subleading shape functions. Together, this provides a large set of different models for these functions. To be conservative, we pick from this set the model which leads to the largest value of $|\mathcal{J}_{\text{hadr}}(\Delta)|$. The integrand in the numerator in (5.43) is maximized if all three $h_i(\Delta)$ functions are equal to a single function, whose choice depends on the value of Δ . In the denominator, we find it convenient to eliminate the shape function $\hat{S}(P_+)$ in favor of the normalized photon spectrum. Working consistently to leading order, we then obtain

$$\epsilon_{\text{hadr}}(\Delta) = \frac{5}{(1-a)(3-a)} \frac{5a + a^2}{a} \frac{U(h_i; \mu_i)}{m_b^3} \max_i \int_0^Z \frac{dP_+ (M_B - P_+)^4 h_i(P_+)}{dP_+ (M_B - P_+)^2 \frac{1}{s(E)} \frac{d_s}{dP_+}}; \quad (5.44)$$

where as before $a = a(h_i; \mu_i) = 0.12$ for the default choice of matching scales, and $U(h_i; \mu_i) = 1.11$ [95].

The result for the function $\epsilon_{\text{hadr}}(\Delta)$ obtained this way is shown in Figure 5.4. We set the matching scales to their default values and use the model (5.37) for the photon spectrum, which is a good enough approximation for our purposes. From this estimate it is apparent that the effects of subleading shape functions are negligible for large values $\sqrt{s} \gg Q_{\text{CD}}$ and moderate for $\sqrt{s} \sim Q_{\text{CD}}$, which is the region of interest for the determination of \mathcal{J}_{ubj} . In the region $\sqrt{s} < 0.3 \text{ GeV}$ the accuracy of the calculation deteriorates. For example, we find $\epsilon_{\text{hadr}} = 2.0\%$ for

$= 0.65 \text{ GeV}$, $\delta_{\text{hadr}} = 4.8\%$ for $\mu = 0.5 \text{ GeV}$, and $\delta_{\text{hadr}} = 8.2\%$ for $\mu = 0.4 \text{ GeV}$.

5.5 Conclusions

Model-independent relations between weighted integrals of $B \rightarrow X_s$ and $B \rightarrow X_{u1}$ decay distributions, in which all reference to the leading non-perturbative shape function is avoided, offer one of the most promising avenues to a high-precision determination of the CKM matrix element $|V_{ub}|$. In order to achieve a theoretical precision of better than 10%, it is necessary to include higher-order corrections in μ_s and $\mu_{\text{QCD}} = m_b$ in this approach.

In this chapter, we have calculated the weight function $W(\mu; P_+)$ in the relation between the hadronic $P_+ = E_X - |P_X|$ spectra in the two processes, integrated over the interval $0 \leq P_+ \leq \mu_s$. Based on QCD factorization theorems for the differential decay rates, we have derived an exact formula (5.15) that allows for the calculation of the leading-power weight function to any order in perturbation theory. We have calculated the μ_s - and P_+ -dependent terms in the weight function exactly at next-to-next-to-leading order (NNLO) in renormalization-group improved perturbation theory, including two-loop matching corrections at the intermediate scale $\mu_i = m_b$ and three-loop running between the intermediate scale and the hard scale $\mu_h = m_b$. The only piece missing for a complete prediction at NNLO is the two-loop hard matching correction to the overall normalization of the weight function. A calculation of the $\mu_s^2(\mu_h)$ term would require the knowledge of both decay spectra at two-loop order, which is currently still lacking. We also include various sources of power corrections. Power corrections from phase-space factors are treated exactly. The remaining hadronic and kinematical power corrections are given to first order in $\mu_{\text{QCD}} = m_b$ and to the order in perturbation theory to which they are known.

A dedicated study of the perturbative behavior of our result for the weight function has been performed for the partial $B \rightarrow X_{u1}$ decay rate $\Gamma_u(\mu)$ as obtained from the right-hand side of relation (5.1). It exhibits good convergence of the expansion and reduced scale sensitivity in higher orders. We find that corrections of order $\mu_s^2(\mu_i)$ at the intermediate scale are typically as important as first-order $\mu_s(\mu_h)$ corrections at the hard scale. We have also seen that next-order perturbation theory significantly underestimates the value of $\Gamma_u(\mu)$, even though the apparent stability with respect to scale variations would suggest a good perturbative convergence. In order to obtain a wellbehaved expansion in powers of $\mu_s(\mu_h)$, it is important to use the normalized photon spectrum in relation (5.1). A similar relation involving the differential $B \rightarrow X_s$ decay rate receives uncontrollably large matching corrections at the hard scale and is thus not suitable for phenomenological applications. At next-to-leading order in the $1/m_b$ expansion, the weight function receives terms involving non-perturbative subleading shape functions, which cannot be eliminated. Our current ignorance about the functional forms of these functions leads to a hadronic uncertainty, which we have estimated

by scanning over a large set of models. We believe that a reasonable estimate of the corresponding relative uncertainty δ_{hadr} on \mathcal{B}_{ub} is given by the solid line in Figure 5.4.

Let us summarize our main result for the partial $B \rightarrow X_u \gamma$ decay rate with a cut $P_+ = 0.65 \text{ GeV}$, which is close to the charm threshold $M_D^2 = M_B$, and present a detailed list of the various sources of theoretical uncertainties. We find

$$\begin{aligned} \mathcal{B}_{\text{ub}}(0.65 \text{ GeV}) &= \\ &= (46.5 \pm 1.4_{\text{[pert]}} \pm 1.8_{\text{[hadr]}} \pm 1.8_{\text{[m]}} \pm 0.8_{\text{[pars]}} \pm 2.8_{\text{[norm.]}}) \mathcal{B}_{\text{ub}}^2 \text{ ps}^{-1} \\ &= (46.5 \pm 4.1) \mathcal{B}_{\text{ub}}^2 \text{ ps}^{-1}; \end{aligned} \quad (5.45)$$

where the central value is derived assuming that the $B \rightarrow X_s \gamma$ photon spectrum can be accurately described by the function (5.37). The errors refer to the perturbative uncertainty as estimated in Section 5.4.1, the uncertainty due to the ignorance about subleading shape functions as discussed in Section 5.4.4, the error in the value of the b-quark mass, other parametric uncertainties from variations of m_c , m_s , and α_s , and finally a 6% uncertainty in the calculation of the normalization of the photon spectrum [50]. To a good approximation the errors scale with the central value. The above numbers translate into a combined theoretical uncertainty of 4.4% on \mathcal{B}_{ub} when added in quadrature.

Chapter 6

Conclusions

Inclusive charmless B decays offer the most precise methods for measuring $|V_{ub}|$. The physics of these decays is rich and involves a delicate interplay of theory and experiment. In this work we have developed and described an elaborate theoretical machinery that can be applied to these decays.

We have started our discussion by explaining how to relate the differential decay rates of $B \rightarrow X_s$ and $B \rightarrow X_{u1}$ to the hadronic tensor. We have reviewed the traditional (approximate) methods of calculating the hadronic tensor, namely, an expansion in the strong coupling constant and HQET based OPE. We have explained the problems that arise from the use of these methods, and argued that they can be overcome by the use of SCET, the appropriate effective field theory for charmless inclusive B decays. We therefore reviewed some of its basic elements. Using SCET one can prove that the hadronic tensor factorizes, at each order in $1/m_b$, as a sum of products of a calculable hard function multiplied by a calculable jet function convoluted with a non perturbative shape function.

At leading order in $1/m_b$ all these functions are unique. We have calculated the leading order hard and jet function by performing a two-step matching calculation $QCD \rightarrow SCET \rightarrow HQET$. We have resummed large logarithms that arise in the calculation at next-to-leading order in renormalization-group improved perturbation theory. We have employed the operator product expansion to relate moments of the renormalized shape function with HQET parameters such as m_b , and μ^2 defined in a new physical subtraction scheme, called the "shape function scheme". We have obtained an analytic expression for the asymptotic behavior of the shape function, which reveals that it is not positive definite.

Having analyzed the leading power terms we have considered the contributions of subleading shape functions. At tree-level, the results can be expressed in terms of forward matrix elements of bi-local light-cone operators. Four-quark operators, which arise at $O(1/m_b)$, were also included. We have shown that at tree level only three independent subleading shape functions are needed.

Based on these calculations we turned, in the second part of this work, to applications. In the first application, we have presented "state-of-the-art" theoretical expressions for the triple differential $B \rightarrow X_{u1}$ decay rate and for the $B \rightarrow X_s$ photon spectrum, which incorporate all known contributions and smoothly interpolate between the "shape-function region" of large hadronic energy and small invariant mass, and the "OPE region" in which all hadronic kinematical variables scale with M_B . The differential rates are given in a form which has no explicit reference to the mass of the b quark, avoiding the associated uncertainties. Dependence on m_b enters indirectly through the properties of the leading shape function, which can be determined by fitting the $B \rightarrow X_s$ photon spectrum. This eliminates the dominant theoretical uncertainties from predictions for $B \rightarrow X_{u1}$ decay distributions, allowing for a precise determination of $|V_{ub}|$. In the shape-function region, we have factorized short-distance and long-distance contributions

at next-to-leading order in renormalization-group improved perturbation theory. The higher-order power corrections include effects from subleading shape functions where they are known. When integrated over sufficiently large portions in phase space, our results would reduce to standard OPE expressions up to yet unknown $O(\frac{2}{s})$ terms. We have presented predictions for partial $B \rightarrow X_u \gamma$ decay rates with various experimental cuts. The elaborate error analysis that we have performed contains all significant theoretical uncertainties, including weak annihilation effects. We have suggested that the latter can be eliminated by imposing a cut on high leptonic invariant mass.

In the second application we have derived a shape-function independent relation between the partial $B \rightarrow X_u \gamma$ decay rate with a cut on $P_+ = E_X - \not{E}_X$ and a weighted integral over the normalized $B \rightarrow X_s$ photon-energy spectrum. We have calculated the leading-power contribution to the weight function at next-to-next-to-leading order in renormalization-group improved perturbation theory, including exact two-loop matching corrections at the scale $\mu = m_b$. The overall normalization of the weight function is obtained up to yet unknown corrections of order $\frac{2}{s}(m_b)$. We have included power corrections from phase-space factors exactly, while the remaining subleading contributions have been included at first order in $\alpha_{\text{QCD}} = m_b$. At this level unavoidable hadronic uncertainties enter, which we have estimated in a conservative way. The combined theoretical accuracy in the extraction of $\langle V_{ub} \rangle$ is at the level of 5% if a value of β near the charm threshold can be achieved experimentally.

The work presented here was already implemented by the "B-factories": Babar and Belle. As of June 2006, Babar has measured $\langle V_{ub} \rangle$ using a combined s_H and E_1 cut [106], combined M_X and q^2 cut [107], and E_1 cut [108]. Babar has also extracted the M_X spectrum for $B \rightarrow X_s \gamma$ [5]. As of June 2006, Belle has measured $\langle V_{ub} \rangle$ using an E_1 cut [109], M_X cut, combined M_X and q^2 cut, and P_+ cut [110].

We would like to conclude this work with an outlook. The reduction of the experimental errors encourages theorists to improve the theoretical predictions. As of June 2006, what theoretical developments are feasible? In general the formalism developed in this work can be extended to higher orders in $1/m_b$ and $1/s$.

At leading power the jet function [97] and the partonic shape function [111] have already been calculated to second order in α_s . For $B \rightarrow X_s \gamma$ a next-to-next-to-leading order QCD calculation is underway, where the contribution of O_7 is already known [104, 112]. Once the complete result is known, one could extract the hard function for $B \rightarrow X_s \gamma$ from it. An "easier" calculation is to find the leading power hard function for $B \rightarrow X_u \gamma$. Having these ingredients would allow to extend the analysis of chapters 4 and 5 to a complete two loop order.

Beyond leading power one would like to find a way to extract the subleading shape functions from experiment, or at least to constrain them. This would help to reduce a large source of uncertainty in the extraction of $\langle V_{ub} \rangle$. Another possible improvement is to find the subleading shape function beyond tree level. The analysis performed in [75, 76] indicates that beyond tree level more subleading shape functions would arise. This calculation is related to the long overdue OPE calcula-

tion of the $O(\alpha_s)$ power corrections corrections to $B \rightarrow X_c l$ decays. The latter calculation would allow to check the results of the former, once it is performed.

Finally, as a result of the better control of the charm background, the experimental cuts are being pushed away from the shape function region and into the OPE region. In this intermediate region a multi scale OPE calculation, like the one performed in [50], is more appropriate. This calculation is yet to be done for semileptonic decays.

To summarize, despite the impressive progress achieved in our understanding of charm less inclusive B decays, much is left to be done. Hopefully the research presented here would help make this progress possible.

Appendix A

The hadronic tensor

In chapter 1 we defined the current correlator T as:

$$T = i \int d^4x e^{iqx} T f J^Y(0); J(x)g: \quad (A.1)$$

Reinserting the complete set of hadronic states we have

$$\begin{aligned} \langle B | J^\dagger | B \rangle &= i \int d^4x e^{iqx} \sum_{X_q} \langle B | J^Y(0) | X_q \rangle \langle X_q | J(x) | B \rangle \\ &+ \sum_{X_{bbq}} \langle X^0 | \langle B | J(x) | X_{bbq} \rangle \langle X_{bbq} | J^Y(0) | B \rangle : \end{aligned} \quad (A.2)$$

Following [12] we write the steps function as:

$$\langle X^0 \rangle = \frac{1}{2} \frac{1}{i} \int_{-1}^1 d! \frac{e^{-i!x^0}}{! - i} : \quad (A.3)$$

(these identities can be proved by contour integration, or by integrating the integral representation of the delta function). Translation invariance allows us to write:

$$\begin{aligned} \langle X | J(x) | B \rangle &= e^{i(P_x - P_B) \cdot x} \langle X | J(0) | B \rangle \\ \langle B | J(x) | X \rangle &= e^{i(P_B - P_x) \cdot x} \langle B | J(0) | X \rangle : \end{aligned} \quad (A.4)$$

Integrating over x and $!$ we find that in the rest frame of the B meson:

$$\begin{aligned} \langle B | J^\dagger | B \rangle &= \sum_{X_q} \frac{\langle B | J^Y(0) | X_q \rangle \langle X_q | J(0) | B \rangle}{M_B + E_X + q^0 - i} (2)^3 (P_x + q) \\ &+ \sum_{X_{bbq}} \frac{\langle B | J(0) | X_{bbq} \rangle \langle X_{bbq} | J^Y(0) | B \rangle}{M_B - E_X + q^0 + i} (2)^3 (P_x - q) : \end{aligned} \quad (A.5)$$

Taking the imaginary part, we find using equation (1.33)

$$\begin{aligned} W &= \frac{1}{2} \text{Im} \frac{\langle B | J^\dagger | B \rangle}{2M_B} \\ &= \frac{1}{2M_B} \sum_{X_q} \langle B | J^Y(0) | X_q \rangle \langle X_q | J(0) | B \rangle (2^3)^4 (P_B - P_X - q) \\ &+ \frac{1}{2M_B} \sum_{X_{bbq}} \langle B | J(0) | X_{bbq} \rangle \langle X_{bbq} | J^Y(0) | B \rangle (2^3)^4 (P_B - P_X + q) \end{aligned} \quad (A.6)$$

For B decays the second sum does not contribute, since the energy of X_{bbq} is always large than M_B .

Using this expression for the hadronic tensor, it is easy to prove the following symmetry of the hadronic tensor:

$$W_{\mu\nu} = (W_{\nu\mu})^* : \quad (\text{A.7})$$

Using the definition of the Hermitian conjugate, we have for each term in the first sum in (A.6):

$$\langle B | j^\nu | X_q \rangle \langle X_q | j^\mu | B \rangle = \langle X_q | j^\mu | B \rangle^* \langle B | j^\nu | X_q \rangle = \langle B | j^\nu | X_q \rangle \langle X_q | j^\mu | B \rangle \quad (\text{A.8})$$

A similar relation holds for the second sum in (A.6). Combining them gives us (A.7).

Appendix B

Perturbative Expressions

B.1 Anomalous dimensions

Here we list the known perturbative expansions of the γ -function and relevant anomalous dimensions. We work in the \overline{MS} scheme and define

$$\begin{aligned} \gamma(s) &= \frac{d_s(\gamma)}{d \ln \mu} = \sum_{n=0}^{\infty} \gamma_n \left(\frac{s}{4} \right)^{n+1}; \\ \text{cusp}(\gamma) &= \sum_{n=0}^{\infty} \gamma_n^{\text{cusp}} \left(\frac{s}{4} \right)^{n+1}; \quad \gamma_0^0(s) = \sum_{n=0}^{\infty} \gamma_n^0 \left(\frac{s}{4} \right)^{n+1}; \end{aligned} \quad (\text{B.1})$$

as the expansion coefficients for the γ -function, the leading-order SCET current anomalous dimension, and the cusp anomalous dimension. To three-loop order, the γ -function reads [113]

$$\begin{aligned} \gamma_0 &= \frac{11}{3} C_A - \frac{2}{3} n_f; \quad \gamma_1 = \frac{34}{3} C_A^2 - \frac{10}{3} C_A n_f - 2 C_F n_f; \\ \gamma_2 &= \frac{2857}{54} C_A^3 + C_F^2 - \frac{205}{18} C_F C_A - \frac{1415}{54} C_A^2 n_f + \frac{11}{9} C_F + \frac{79}{54} C_A n_f^2; \end{aligned} \quad (\text{B.2})$$

where $n_f = 4$ is the number of light flavors, $C_A = 3$ and $C_F = 4/3$. The three-loop expression for the cusp anomalous dimension has recently been obtained in [98]. The coefficients read

$$\begin{aligned} \gamma_0^{\text{cusp}} &= 4 C_F; \quad \gamma_1^{\text{cusp}} = 8 C_F - \frac{67}{18} C_A^2 - \frac{5}{6} C_A - \frac{5}{9} n_f; \\ \gamma_2^{\text{cusp}} &= 16 C_F^2 - \frac{245}{24} C_F C_A - \frac{67}{54} C_A^3 + \frac{11}{180} C_A^4 + \frac{11}{6} C_A^3 n_f + \frac{209}{108} C_A^2 n_f + \frac{5}{27} C_A n_f^2 + \frac{7}{3} C_A n_f^3 \\ &\quad + \frac{55}{24} C_F n_f + 2 C_F n_f^2 + \frac{1}{27} n_f^3 : \end{aligned} \quad (\text{B.3})$$

The SCET anomalous dimension γ_0 is explicitly known only to one-loop order. However, the two-loop coefficient can be extracted by noting that γ_0 is related to the axial-gauge anomalous dimension in deep inelastic scattering [50]. The result is

$$\begin{aligned} \gamma_0^0 &= 5 C_F; \\ \gamma_1^0 &= 8 C_F - \frac{3}{16} C_A^2 - \frac{7}{4} C_A + 3 C_F n_f + \frac{1549}{432} C_A^2 + \frac{7}{48} C_A n_f + \frac{125}{216} C_F n_f + \frac{1}{24} n_f^2 : \end{aligned} \quad (\text{B.4})$$

B.2 Evolution factor

The exact expression for the evolution factor reads

$$\ln U(h; i) = 2S(h; i) - 2a(h; i) \ln \frac{m_b}{h} - 2a_0(h; i); \quad (\text{B.5})$$

where the functions of the right-hand side are solutions to the renormalization-group equations

$$\begin{aligned} \frac{d}{d \ln} S(h; i) &= -\gamma_{\text{cusp}}(s(h)); \\ \frac{d}{d \ln} a(h; i) &= -\gamma_{\text{cusp}}(s(h)); \quad \frac{d}{d \ln} a_0(h; i) = -\gamma_0(s(h)); \end{aligned} \quad (\text{B.6})$$

with boundary conditions $S(h; i) = 0$ etc. at $h = m_b$. These equations can be integrated using that $d \ln h = (ds/s) d \ln s$. The solutions are

$$S(h; i) = \int_{s(h)}^{s(i)} \frac{\gamma_{\text{cusp}}(s)}{s} ds; \quad a(h; i) = \int_{s(h)}^{s(i)} \frac{\gamma_{\text{cusp}}(s)}{s} ds; \quad (\text{B.7})$$

and similarly for a_0 .

Next, we give explicit results for the Sudakov exponent S and the functions a and a_0 in (B.5) at next-to-leading order in renormalization-group improved perturbation theory. We obtain

$$a(h; i) = \frac{\gamma_0}{2} \ln \frac{s(i)}{s(h)} + \frac{\gamma_1}{0} \frac{1}{0} \frac{s(i)}{4} \frac{s(h)}{4} + \dots; \quad (\text{B.8})$$

and similarly for a_0 . The next-to-leading order expressions for the Sudakov exponent S contains the three-loop coefficients γ_2 and γ_3 . With $r = s(i)/s(h)$, it reads

$$\begin{aligned} S(h; i) &= \frac{\gamma_0}{4} \frac{4}{s(h)} \left(1 - \frac{1}{r} \right) \ln r + \frac{\gamma_1}{0} \frac{1}{0} (1 - r + \ln r) + \frac{\gamma_2}{2} \ln^2 r \\ &+ \frac{\gamma_3}{4} \frac{1}{0} \frac{1}{0} \frac{2}{0} (1 - r + r \ln r) + \frac{\gamma_4}{2} \frac{1}{0} \frac{2}{0} (1 - r) \ln r \\ &+ \frac{\gamma_5}{2} \frac{1}{0} \frac{2}{0} \frac{1}{0} \frac{1}{0} + \frac{\gamma_6}{0} \frac{(1 - r)^2}{2} + \dots \end{aligned} \quad (\text{B.9})$$

The next-to-leading-logarithmic evolution factor $U(h; i)$ can be obtained by combining the above expressions according to (B.5) and expanding out terms of order

Appendix C

Partially integrated decay rates

With the exception of the combined cut on the lepton energy E_1 and the hadronic quantity s_H^{max} studied in Section 4.5.5, all other partial rates investigated in our analysis can be derived by first integrating the triple differential decay rate (4.19) over the lepton energy $E_1 = E_0$ and $P = P^{max}$ analytically, where the quantity P^{max} (and in principle even E_0) may depend on the value of P_+ . The remaining integration over P_+ is then performed numerically. In such a situation, we need to evaluate the partially integrated decay rate

$$\frac{d_u}{dP_+} = \int_{P_+}^{P^{max}} dP \int_{E_0}^{E_1} dE_1 \frac{d^3 u}{dP_1 dP dP_+} : \quad (C.1)$$

Changing variables from P to y defined in (4.21), the constraint $P = P^{max}$ translates into the integration domain $0 \leq y \leq y_{ax}$, where in analogy to (4.21) we define

$$y_{max} = \frac{P^{max} - P_+}{M_B - P_+}; \quad y_0 = \frac{P_1^{max} - P_+}{M_B - P_+} = 1 - \frac{2E_0}{M_B - P_+} : \quad (C.2)$$

From the phase-space relation (1.5) it follows that a cut on the lepton energy has no effect if $y_0 \leq y_{ax}$. The result of performing the integrations in (C.1) can be written as

$$\frac{d_u(y_{max}, y_0)}{dP_+} = \frac{A_u(y_{max})}{A_u(y_0)} + \frac{B_u}{y_0} ; \quad y_{max} \leq y_0 ; \quad (C.3)$$

where

$$\begin{aligned} A_u(y_i) &= \frac{G_F^2 J_{ub}^2}{96 \cdot 3} (M_B - P_+)^5 U(h; i) \int_{y_i}^{y_{ax}} dy y^{2-2a} [(3-2y)F_1 + 6(1-y)F_2 + yF_3]; \\ B_u &= \frac{G_F^2 J_{ub}^2}{96 \cdot 3} (M_B - P_+)^5 U(h; i) \int_{y_0}^{y_{max}} dy y^{2a} y_0 \\ &\quad + 6y(1-y)F_2 + y_0(3y-2y_0)F_3] : \end{aligned} \quad (C.4)$$

When the kinematical power corrections in (4.26) are expanded as in (4.28) and (4.29), the resulting integrals over y can be expressed in terms of the master functions $I_n(b; z)$ given in eq. (86) of [63]. The resulting expressions are used to obtain the numbers in the various tables in Section 4.5.

We now list the values of y_0 and y_{max} for the different cuts studied in Section 4.5. Whenever a cut $E_1 = E_0$ on the charged-lepton energy is applied, we have

$$y_0 = 1 - \frac{2E_0}{M_B - P_+} : \quad (C.5)$$

For an additional cut $P_+ \leq P_-$, we have $y_{\text{max}} = 1$ and $0 \leq P_+ \leq \min(P_-, M_B - 2E_0)$. For a cut on hadronic invariant mass, $M_X \leq M_0$, we have

$$y_{\text{max}} = \frac{\min(M_B; M_0^2 - P_+^2) - P_+^2}{M_B^2 - P_+^2} \quad (\text{C.6})$$

and $0 \leq P_+ \leq \min(M_0; M_B - 2E_0)$. For a cut on leptonic invariant mass, $q^2 \leq q_0^2$, we have

$$y_{\text{max}} = 1 - \frac{q_0^2}{(M_B^2 - P_+^2)^2} \quad (\text{C.7})$$

and $0 \leq P_+ \leq \min(M_B - q_0; M_B - 2E_0)$. Finally, for the combined $M_X \leq q^2$ cut we take the minimum of the previous two y_{max} values.

B I B L I O G R A P H Y

- [1] A . V . M anohar and M . B . W ise, Phys. Rev. D 49, 1310 (1994) [[hep-ph/9308246](#)].
- [2] F . D e Fazio and M . N eubert, JHEP 9906, 017 (1999) [[hep-ph/9905351](#)].
- [3] S . C hen et al. [CLEO Collaboration], Phys. Rev. Lett. 87, 251807 (2001) [[hep-ex/0108032](#)].
- [4] P . K oppenburg et al. [Belle Collaboration], Phys. Rev. Lett. 93, 061803 (2004) [[hep-ex/0403004](#)].
- [5] B . A ubert et al. [BABAR Collaboration], Phys. Rev. D 72, 052004 (2005) [[hep-ex/0508004](#)].
- [6] M . E . P eskin and D . V . S chroeder, "An Introduction to quantum field theory," Reading, U S A : A d d i s o n - W e s l e y (1995)
- [7] A . J . B uras, [[hep-ph/9806471](#)].
- [8] I M . G elfand and G E . S h i l o v "G eneralized functions", New York, U S A : A c a d e m i c P r e s s (1964)
- [9] M . J e z a b e k and J . H . K u h n, Nucl. Phys. B 320, 20 (1989).
- [10] K . G . C h e t y r k i n, M . M i s i a k and M . M u n z, Phys. Lett. B 400, 206 (1997) [Erratum -*ibid.* B 425, 414 (1998)] [[hep-ph/9612313](#)].
- [11] M . N eubert, Phys. Rept. 245, 259 (1994) [[hep-ph/9306320](#)].
- [12] A . V . M anohar and M . B . W ise, "Heavy quark physics," Cam b . M o n o g r . P a r t . Phys. Nucl. Phys. Cosm ol. 10, 1 (2000).
- [13] B . B l o k, L . K o y r a k h, M . A . S h i f m a n and A . I . V a i n s h t e i n, Phys. Rev. D 49, 3356 (1994) [Erratum -*ibid.* D 50, 3572 (1994)] [[hep-ph/9307247](#)].
- [14] J . C h a y, H . G e o r g i and B . G r i n s t e i n, Phys. Lett. B 247, 399 (1990).
- [15] M . N eubert, Phys. Rev. D 49, 3392 (1994) [[hep-ph/9311325](#)];
- [16] M . N eubert, Phys. Rev. D 49, 4623 (1994) [[hep-ph/9312311](#)].
- [17] I . I . Y . B i g i, M . A . S h i f m a n, N . G . U r a l t s e v and A . I . V a i n s h t e i n, Int. J. M o d . Phys. A 9, 2467 (1994) [[hep-ph/9312359](#)].
- [18] G . P . K o r c h e m s k y and G . S t e r m a n, Phys. Lett. B 340, 96 (1994) [[hep-ph/9407344](#)].

- [19] A . F . Falk, M . E . Luke and M . J . Savage, Phys. Rev. D 49, 3367 (1994) [[hep-ph/9308288](#)].
- [20] C . W . Bauer, S . Fleming and M . E . Luke, Phys. Rev. D 63, 014006 (2001) [[hep-ph/0005275](#)].
- [21] C . W . Bauer, S . Fleming, D . Pirjol and I . W . Stewart, Phys. Rev. D 63, 114020 (2001) [[hep-ph/0011336](#)].
- [22] C . W . Bauer, D . Pirjol and I . W . Stewart, Phys. Rev. D 65, 054022 (2002) [[hep-ph/0109045](#)].
- [23] M . Beneke, A . P . Chapovsky, M . Diehl and T . Feldmann, Nucl. Phys. B 643, 431 (2002) [[hep-ph/0206152](#)];
- [24] M . Beneke and T . Feldmann, Phys. Lett. B 553, 267 (2003) [[hep-ph/0211358](#)].
- [25] R . Akhoury and I . Z . Rothstein, Phys. Rev. D 54, 2349 (1996) [[hep-ph/9512303](#)].
- [26] S . W . Bosch, R . J . Hill, B . O . Lange and M . Neubert, Phys. Rev. D 67, 094014 (2003) [[hep-ph/0301123](#)].
- [27] G . P . Korchemsky and A . V . Radyushkin, Nucl. Phys. B 283, 342 (1987);
- [28] I . A . Korchemskaya and G . P . Korchemsky, Phys. Lett. B 287, 169 (1992).
- [29] B . O . Lange and M . Neubert, Phys. Rev. Lett. 91, 102001 (2003) [[hep-ph/0303082](#)].
- [30] A . G . Grozin and M . Neubert, Phys. Rev. D 55, 272 (1997) [[hep-ph/9607366](#)].
- [31] T . Mannel and M . Neubert, Phys. Rev. D 50, 2037 (1994) [[hep-ph/9402288](#)].
- [32] A . L . Kagan and M . Neubert, Eur. Phys. J. C 7, 5 (1999) [[hep-ph/9805303](#)].
- [33] I . Bigi and N . Ural'tsev, Int. J. Mod. Phys. A 17, 4709 (2002) [[hep-ph/0202175](#)].
- [34] T . Mannel and S . Recksiegel, Phys. Rev. D 60, 114040 (1999) [[hep-ph/9904475](#)].
- [35] T . Mannel and S . Recksiegel, Phys. Rev. D 63, 094011 (2001) [[hep-ph/0009268](#)].
- [36] A . F . Falk, M . Neubert and M . E . Luke, Nucl. Phys. B 388, 363 (1992) [[hep-ph/9204229](#)].
- [37] I . I . Y . Bigi, M . A . Shifman, N . G . Ural'tsev and A . I . Vainshtein, Phys. Rev. D 50, 2234 (1994) [[hep-ph/9402360](#)].

- [38] M .Beneke and V .M .Braun, Nucl.Phys.B 426, 301 (1994) [hep-ph/9402364].
- [39] I .I .Y .B igi, M .A .Shifm an, N .U raltsev and A .I .Vainshtein, Phys. Rev. D 56, 4017 (1997) [hep-ph/9704245].
- [40] M .Beneke, Phys. Lett. B 434, 115 (1998) [hep-ph/9804241].
- [41] I .I .Y .B igi, M .A .Shifm an and N .U raltsev, Ann. Rev. Nucl. Part. Sci. 47, 591 (1997) [hep-ph/9703290].
- [42] D .Benson, I .I .B igi, T .M annel and N .U raltsev, Nucl. Phys. B 665, 367 (2003) [hep-ph/0302262].
- [43] G .M artinelli, M .Neubert and C .T .Sachrajda, Nucl.Phys.B 461, 238 (1996) [hep-ph/9504217];
- [44] M .Neubert, Phys. Lett. B 393, 110 (1997) [hep-ph/9610471].
- [45] T .Becher, R .J .H ill and M .Neubert, Phys. Rev. D 69, 054017 (2004) [hep-ph/0308122].
- [46] R .J .H ill and M .Neubert, Nucl. Phys. B 657, 229 (2003) [hep-ph/0211018].
- [47] R .J .H ill, T .Becher, S .J .Lee and M .Neubert, JHEP 0407, 081 (2004) [hep-ph/0404217].
- [48] D .Pirip and I .W .Stewart, Phys. Rev. D 67, 094005 (2003) [Erratum -ibid. D 69, 019903 (2004)] [hep-ph/0211251].
- [49] B .O .Lange and M .Neubert, Nucl. Phys. B 690, 249 (2004) [Erratum -ibid. B 723, 201 (2005)] [hep-ph/0311345].
- [50] M .Neubert, Eur. Phys. J. C 40, 165 (2005) [hep-ph/0408179].
- [51] C .W .Bauer, M .E .Luke and T .M annel, Phys. Rev. D 68, 094001 (2003) [hep-ph/0102089].
- [52] C .W .Bauer, M .Luke and T .M annel, Phys. Lett. B 543, 261 (2002) [hep-ph/0205150].
- [53] M .E .Luke, Phys. Lett. B 252, 447 (1990).
- [54] A .F .Falk and M .Neubert, Phys. Rev. D 47, 2965 (1993) [hep-ph/9209268].
- [55] M .Neubert and C .T .Sachrajda, Nucl. Phys. B 483, 339 (1997) [hep-ph/9603202].
- [56] I .I .Y .B igi, B .B lok, M .A .Shifm an, N .U raltsev and A .I .Vainshtein, hep-ph/9401298;

- [57] I. I. Y. Bigi, hep-ph/9508408.
- [58] M. Di Pierro and C. T. Sachrajda, Nucl. Phys. B 534, 373 (1998) [hep-lat/9805028].
- [59] D. Becirevic, [hep-ph/0110124].
- [60] M. S. Baek, J. Lee, C. Liu and H. S. Song, Phys. Rev. D 57, 4091 (1998) [hep-ph/9709386].
- [61] M. B. Voloshin, Phys. Lett. B 515, 74 (2001) [hep-ph/0106040].
- [62] C. W. Bauer and A. V. Manohar, Phys. Rev. D 70, 034024 (2004) [hep-ph/0312109].
- [63] S. W. Bosch, B. O. Lange, M. Neubert and G. Paz, Nucl. Phys. B 699, 335 (2004) [hep-ph/0402094].
- [64] E. Gardi, JHEP 0404, 049 (2004) [hep-ph/0403249].
- [65] F. J. Tackmann, Phys. Rev. D 72, 034036 (2005) [hep-ph/0503095].
- [66] S. W. Bosch, M. Neubert and G. Paz, JHEP 0411, 073 (2004) [hep-ph/0409115].
- [67] A. K. Leibovich, I. Low and I. Z. Rothstein, Phys. Rev. D 61, 053006 (2000) [hep-ph/9909404].
- [68] A. K. Leibovich, I. Low and I. Z. Rothstein, Phys. Lett. B 486, 86 (2000) [hep-ph/0005124].
- [69] M. Neubert, Phys. Lett. B 513, 88 (2001) [hep-ph/0104280].
- [70] C. Greub, T. Hurth and D. Wyler, Phys. Rev. D 54, 3350 (1996) [hep-ph/9603404].
- [71] A. Ali and C. Greub, Phys. Lett. B 361, 146 (1995) [hep-ph/9506374].
- [72] T. Becher, R. J. Hill, B. O. Lange and M. Neubert, Phys. Rev. D 69, 034013 (2004) [hep-ph/0309227].
- [73] A. K. Leibovich, Z. Ligeti and M. B. Wise, Phys. Lett. B 539, 242 (2002) [hep-ph/0205148].
- [74] M. Neubert, Phys. Lett. B 543, 269 (2002) [hep-ph/0207002].
- [75] K. S. M. Lee and I. W. Stewart, Nucl. Phys. B 721, 325 (2005) [hep-ph/0409045].

- [76] M .Beneke, F .Campanario, T .M annel and B .D .Pecjak, JHEP 0506, 071 (2005) [hep-ph/0411395].
- [77] N .U raltsev, Int. J. M od. Phys. A 14, 4641 (1999) [hep-ph/9905520].
- [78] I. I. Y . Bigi and N . G . U raltsev, Nucl. Phys. B 423, 33 (1994) [hep-ph/9310285].
- [79] T .O .M eyer, "Limits on weak annihilation in inclusive charm less sem ileptonic B decays", Ph.D .Thesis, Cornell University (2005).
- [80] M .Neubert, Eur. Phys. J. C 44, 205 (2005) [hep-ph/0411027].
- [81] B .A ubert et al. [BaBar Collaboration], Phys. Rev. Lett. 93, 011803 (2004) [hep-ex/0404017].
- [82] A .H .H oang, Z .L igeti and A .V .M anohar, Phys. Rev. D 59, 074017 (1999) [hep-ph/9811239].
- [83] M .Neubert, Phys. Lett. B 612, 13 (2005) [hep-ph/0412241].
- [84] T .van R itbergen, Phys. Lett. B 454, 353 (1999) [hep-ph/9903226].
- [85] S .W .Bosch, B .O .Lange, M .Neubert and G .Paz, Phys. Rev. Lett. 93, 221801 (2004) [hep-ph/0403223].
- [86] A .F .F alk, Z .L igeti and M .B .W ise, Phys. Lett. B 406, 225 (1997) [hep-ph/9705235].
- [87] I. I. Y . Bigi, R .D .D ikem an and N .U raltsev, Eur. Phys. J. C 4, 453 (1998) [hep-ph/9706520].
- [88] C .W .Bauer, Z .L igeti and M .E .Luke, Phys. Lett. B 479, 395 (2000) [hep-ph/0002161].
- [89] C .W .Bauer, Z .L igeti and M .E .Luke, Phys. Rev. D 64, 113004 (2001) [hep-ph/0107074].
- [90] B .A ubert et al. [BaBar Collaboration], [hep-ex/0408045].
- [91] M .Neubert, JHEP 0007, 022 (2000) [hep-ph/0006068].
- [92] T .Becher and M .Neubert, Phys. Lett. B 535, 127 (2002) [hep-ph/0105217].
- [93] U .A glietti, M .C iuchini and P .G ambino, Nucl. Phys. B 637, 427 (2002) [hep-ph/0204140].
- [94] A .H .H oang, Z .L igeti and M .Luke, Phys. Rev. D 71, 093007 (2005) [hep-ph/0502134].

- [95] B. O. Lange, M. Neubert and G. Paz, Phys. Rev. D 72, 073006 (2005) [hep-ph/0504071].
- [96] M. Neubert, Phys. Rev. D 72, 074025 (2005) [hep-ph/0506245].
- [97] T. Becher and M. Neubert, Phys. Lett. B 637, 251 (2006) [hep-ph/0603140].
- [98] S. Moch, J. A. M. Vermaseren and A. Vogt, Nucl. Phys. B 688, 101 (2004) [hep-ph/0403192].
- [99] C. N. Burrell, M. E. Luke and A. R. Williamson, Phys. Rev. D 69, 074015 (2004) [hep-ph/0312366].
- [100] J. Chay, C. Kim and A. K. Leibovich, Phys. Rev. D 72, 014010 (2005) [hep-ph/0505030].
- [101] E. Gamiz, M. Jamin, A. Pich, J. Prades and F. Schwab, Phys. Rev. Lett. 94, 011803 (2005) [hep-ph/0408044].
- [102] C. Aubin et al. [HPQCD Collaboration], Phys. Rev. D 70, 031504 (2004) [hep-lat/0405022].
- [103] S. J. Brodsky, G. P. Lepage and P. B. Mackenzie, Phys. Rev. D 28, 228 (1983).
- [104] K. Melnikov and A. Mitov, Phys. Lett. B 620, 69 (2005) [hep-ph/0505097].
- [105] Z. Ligeti, M. E. Luke, A. V. Manohar and M. B. Wise, Phys. Rev. D 60, 034019 (1999) [hep-ph/9903305].
- [106] B. Aubert et al. [BABAR Collaboration], Phys. Rev. Lett. 95, 111801 (2005) [hep-ex/0506036].
- [107] B. Aubert et al. [BABAR Collaboration], [hep-ex/0507017].
- [108] B. Aubert et al. [BABAR Collaboration], Phys. Rev. D 73, 012006 (2006) [hep-ex/0509040].
- [109] A. Limosani et al. [Belle Collaboration], Phys. Lett. B 621, 28 (2005) [hep-ex/0504046].
- [110] I. Bizjak et al. [Belle Collaboration], Phys. Rev. Lett. 95, 241801 (2005) [hep-ex/0505088].
- [111] T. Becher and M. Neubert, Phys. Lett. B 633, 739 (2006) [hep-ph/0512208].
- [112] I. Blokland, A. Czarnecki, M. Misiak, M. Slusarczyk and F. Tkachov, Phys. Rev. D 72, 033014 (2005) [hep-ph/0506055].
- [113] O. V. Tarasov, A. A. Vladimirov and A. Y. Zharkov, Phys. Lett. B 93, 429 (1980).

